Mechanisms and therapeutic targeting of *NT5C2* mutations in relapsed acute lymphoblastic leukemia

Chelsea Dieck

Submitted in partial fulfillment of the
requirements for the degree of
Doctor of Philosophy
under the Executive Committee
of the Graduate School of Arts and Sciences

COLUMBIA UNIVERSITY

2019

ABSTRACT

Mechanisms and therapeutic targeting of *NT5C2* mutations in relapsed acute lymphoblastic leukemia

Chelsea Dieck

Acute lymphoblastic leukemia (ALL) is an aggressive hematologic malignancy that results from the unregulated growth of B-cell and T-cell lymphoid progenitors. Despite the implementation of risk-stratification and improved multi-agent therapeutic regimens, 20% of pediatric and 50% of adult patients fail to achieve remission and end up relapsing. *NT5C2* (5' cytosolic nucleotidase II) is the most frequently mutated gene specifically found in relapsed ALL. *NT5C2* mutations are present in 20% of relapsed T-ALLs and 3-10% of relapsed B-ALLs and present as heterozygous gain of function alleles exhibiting increased nucleotidase activity. As NT5C2 can dephosphorylate and inactivate the cytotoxic metabolites generated by 6-mercaptopurine, a chemotherapy used in the treatment of ALL, these NT5C2 activating mutations can contribute to thiopurine chemotherapy resistance (Tzoneva, Perez-Garcia et al. 2013).

Here we perform an extensive structure-function study to understand how relapse-associated *NT5C2* mutations result in increased nucleotidase activity and contribute to chemotherapy resistance in ALL. Crystallization of 15 NT5C2 WT and mutant structures as well as enzymatic, structural modeling, and genetic screens identified three regulatory mechanisms of NT5C2, which are disrupted by these gain of function alleles. Class I *NT5C2* mutations lock the protein in an active configuration through stabilization of the helixA region, which allows for substrate processing and catalysis. Class II *NT5C2* mutations disrupt an intramolecular switch off domain involving the arm region and the

intermonomeric positively charged pocket. And a single C-terminus truncating mutant creates a third class of mutations, which show increased nucleotidase activity due to the loss of the C-terminus blockade against allosteric activation. These studies provide new insight into the regulatory controls that mediate NT5C2 activity providing a framework for the development of targeted inhibitors for the treatment of relapsed ALL.

In addition to looking at relapse associated *NT5C2* mutations on a structural level, we also explored how *NT5C2* mutations shape the clonal architecture and evolutionary dynamics during tumor initiation and disease progression in ALL. To formally address these questions, we developed a murine NOTCH1-driven T-ALL with conditional knock-in of the *Nt5c2*^{R367Q} mutation, the most recurrent mutation found in relapsed ALL, from the endogenous locus. Using this model, we confirmed that *Nt5c2*$^{+/R367Q}$ lymphoblasts show increased resistance to 6-MP *in vitro* and *in vivo*. We also found that *Nt5c2*$^{+/R367Q}$ mutant lymphoblasts exhibit impaired cell fitness and decreased leukemia initiating cell capacity. Metabolomic profiling and guanosine rescue experiments show that this decrease in cell fitness is due to excess clearance of purine metabolites out of the cell as a result of deregulated Nt5c2 nucleotidase activity. However, in the context of 6-MP therapy, *Nt5c2*$^{+/R367Q}$ mutant cells are positively selected for in mixed population studies *in vitro* and *in vivo*. These results identify a clear selective advantage for *NT5C2* mutant cells in the context of 6-MP chemotherapy. In addition, *NT5C2* mutant chemoresistant cells show collateral sensitivity to inhibition of inosine monophosphate dehydrogenase (IMPDH) with mizoribine, which further disrupts guanosine production pointing to a potentially selective therapy against *NT5C2* mutant cells.

We also show here the initial development of a small molecule NT5C2 inhibitor for the treatment of relapsed ALL. Using a malachite green based NT5C2 nucleotidase assay,

we performed a small molecule high throughput assay and identified HTP_2 as a lead compound with low micromolar inhibitory activity against NT5C2 R367Q mutant recombinant protein. HTP_2 can reverse 6-MP resistance in *Nt5c2*$^{+/R367Q}$ mouse lymphoblasts and *NT5C2* R29Q mutant expressing human cell lines. Interestingly, HTP_2 treatment also results in increased sensitivity to 6-MP therapy in *NT5C2* wild-type cells, suggesting a role for wild-type NT5C2 activity in the clearance of 6-MP and supporting a potential therapeutic use for NT5C2 inhibitors in potentiating the effects of 6-MP based chemotherapy in NT5C2 wild-type cells as well. *NT5C2* knockdown cells and *Nt5c2* knockout mice show no apparent toxicities suggesting that systemic inhibition of NT5C2 could be fairly well tolerated. In all, this work presents a framework for the development of a high affinity NT5C2 inhibitor for the reversal of 6-MP resistance in relapsed ALL patients.

These studies presented here address the role of *NT5C2* mutant proteins as drivers of resistance and as therapeutic targets in relapsed ALL. Improved understanding of the molecular mechanisms responsible for increased NT5C2 nucleotidase activity and on the process of clonal evolution during disease progression provide important insight into the mechanism driving ALL resistance and relapse. The identification of IMPDH inhibition as a collateral vulnerability in *NT5C2* mutant ALL cells and the development of a first-in-class NT5C2 inhibitor serve as framework for the development of new combination therapies aimed at curtailing the emergence of these thiopurine-resistant relapse driving clones in ALL.

Table of Contents

List of Figures

Chapter 1

Chapter 2

Chapter 3

Chapter 4

List of Tables

Acknowledgements

The past five years have been an incredible learning and growing experience and I could not have achieved any of this success without the support of so many people.

I would first and foremost like to thank Dr. Adolfo Ferrando for giving me the opportunity to work on this amazing project and for taking me into his lab and providing such a nurturing environment to learn. Thank you for pushing me to be the best scientist I can be and for always believing in me. Your enthusiasm for science is contagious and I cannot thank you enough for pushing me to think bigger.

Thank you to my thesis committee Dr. Laura Pasqualucci, Dr. Shan Zha, and Dr. Raul Rabadan for their continued guidance and support over the years as well as Dr. Israel Sanchez-Fernandez for participating as an external examiner for my defense.

Thank you to all of our collaborators who have made these research projects come to fruition. In particular thank you to Farhad Forouhar for his extensive crystallographic studies and structural analysis. Thank you to Arie Zask for aiding in chemical synthesis and docking analyses on NT5C2 inhibitors. Thank you to Sergey Pompou for running the NT5C2 inhibitor high throughput screens and biacore analyses.

A huge thank you to the incredible, smart, friendly, and oh so helpful members of the Ferrando lab past and present. As a new graduate student fresh out of undergraduate research I came into the lab with so many questions. Over the years I have learned so much from all of you and cannot thank you enough for your support and friendship over the years. A special thank you is extended to the NT5C2 team – Thank you Gannie Tzoneva for teaching me everything about the NT5C2 project and for being such a great friend and mentor. Thank you Clara Reglero-Gomez for jumping onto the NT5C2 project these past few months and for being an amazing source of positive energy and new ideas.

Lastly, thank you to my friends and family for their support and love over the past five years. Thank you Dieck fam for raising me to be a strong independent woman, for pushing me to think outside the box, and showing me how to follow my dreams. Thank you grad school crew for the commiseration, wine nights, laughs, and friendship. Thank you Ethan and Winston for getting me out of the lab and being the best support system a girl could ask for.

Thank you all for your guidance, support, and help in getting me to where I am today.

Dedication

This work is dedicated to the graduate students, post-docs, technicians, and PIs who have mentored me over the years. Thank you for believing in me and never doubting what I could learn and achieve.

Chapter 1: Introduction

I. Acute Lymphoblastic Leukemia

History

Acute lymphoblastic leukemia (ALL) is an aggressive hematologic malignancy of immature lymphoid cells in the bone marrow and blood. Leukemia was first described by Rudolf Virchow and John Hughes Bennet independently in 1845 (Kampen 2012). Upon realizing that his patients had more white blood cells than red cells, Virchow named the phenomenon “weisses blut” in German (‘white blood’ in English) or “Leukemia” in Greek (Patlak 2002, Kampen 2012).

Presenting morphology

ALL patients commonly present in the clinic with neutropenia, anemia, thrombocytopenia, elevated white blood cell counts, diffuse infiltration of immature lymphoblasts in the bone marrow, and hematopoietic failure (Hunger and Mullighan 2015). Infiltration of lymph nodes, spleen, and liver are common, and in the case of ALL tumors derived from T-cell progenitors (T-ALL) patients can present with mediastinal thymic masses. In addition, some patients show meningeal infiltration in the central nervous system at diagnosis. ALL patients commonly present with infections, easy bruising and fatigue as a result of low blood cell counts (Alvarnas, Brown et al. 2015, Terwilliger and Abdul-Hay 2017). Diagnosis is confirmed by the presence of 20% or more lymphoblasts in the bone marrow, which initiates further immunophenotyping, cytogenetic testing, and in some cases DNA-sequencing to further classify and treat the malignancy (Alvarnas, Brown et al. 2015).

Epidemiology

Acute lymphoblastic leukemia is a malignancy of both children and adults with about 80% of cases occurring in pediatric patients and 20% of cases occurring in adults (Terwilliger and Abdul-Hay 2017, Siegel, Miller et al. 2018). In children, ALL is the most common cancer accounting for 26% of all cancers diagnosed before the age of 14 (Ward, DeSantis et al. 2014). In the United States there are about 30 patients diagnosed with ALL per million people ages 20 and below, with the highest incidence between ages 3 and 5 (Ries LAG Bethesda, MD, 1999.). There is a second peak of increased diagnosis for adults around 50 years of age. Overall, the age-adjusted incidence of ALL in the United States is 1.7 per 100,000 men and women per year as of 2015 (Paul, Kantarjian et al. 2016). Incidence of ALL also varies greatly depending on gender, race, and ethnicity. Hispanic and white children are at a higher risk of developing ALL than African American children, and ALL is much more frequent in boys than in girls (Lim, Bhatia et al. 2014, Hunger and Mullighan 2015, Siegel, Henley et al. 2017, Siegel, Miller et al. 2018).

Genetic Landscape of ALL

Genetic abnormalities commonly found in ALL include aneuploidy, chromosomal rearrangements, copy number alterations, and point mutations all of which work together in a coordinated multistep process contributing to lymphoid cell transformation (Harrison 2009). Common pathways altered in ALL include but are not limited to, transcriptional regulation of lymphoid development and differentiation pathways, cell-cycle regulation, tumor suppressor pathways, growth factor signaling, RAS signaling, phosphatidylinositol 3-kinase pathways, and JAK stat signaling (Ferrando, Neuberg et al. 2002, Mullighan,

Su et al. 2009, Mullighan, Zhang et al. 2009, Harvey, Mullighan et al. 2010, Zhang, Mullighan et al. 2011).

ALL can be derived from B-precursor or T-precursor lymphoid progenitors. B-precursor ALL (B-ALL) accounts for 80-85% of all cases (Tasian and Hunger 2017). B-ALL and T-ALL can be sub classified into different clinic-biological groups based on the presence of chromosomal alterations and genetic lesions associated with therapeutic response and prognosis (Table 1.1) (Vardiman, Thiele et al. 2009, Alvarnas, Brown et al. 2015, Arber, Orazi et al. 2016, Heikamp and Pui 2018).

Table 1.1 – Common chromosomal and molecular abnormalities in acute lymphoblastic leukemia.

ALL	Subgroup/ Cytogenetics	Genes Involved	Frequency in Adults	Frequency in Children
B-ALL	Hyperdiploidy (>50 chromosomes)	--	7%	25%
	Hypodiploidy (40-44 chromosomes)	--	2%	1%
	Low hyperdiploidy (30-39 chromosomes)	*TP53 (Li-Fraumeni syndrome)*	10%	20%
	t(9;22)(q34;q11) Philadelphia chromosome (Ph)	*BCR-ABL1*	25%	2-4%
	t(12;21)(p13;q22)	*ETV6-RUNX1 (TEL1-AML1)*	2%	22%
	t(1;19)(q23;p13)	*TCF-PBX1 (E2A-PBX1)*	3%	6%
	BCR-ABL1-like	*ABL2, PDGFRB, NTRK3, TYK2, CSF1R, JAK2, CRLF2, EPOR*	10-30%	15%
	iAMP 21	*RUNX1*	-	2%
	Ikaroz	*IKZF1*	50%	12-17%
B-ALL and T-ALL	t(v;11q23)	*KMT2A (MLL)*	10%	8%
T-ALL	t(1;14)(p32;q11)	*TAL-1*	12%	7%
	t(10;14)(q24;q11)	*TLX1 (HOX11), TCRα and TCRδ*	8%	1%
	t(5;14)(q35;q32)	*TLX3 (HOX11L2), BCL11B*	1%	3%
	ETP	*KRAS, FLT3, EZH2, PHF6, DNMT3A, RUNX1, GATA3*	40-50%	10-15%
	NOTCH activation	*NOTCH1*	60%	60%

B- precursor acute lymphoblastic leukemia

25% of pediatric and 7% of adult B-ALL patients show high hyperdiploidy (> 50 chromosomes), which is commonly associated with a favorable prognosis. Conversely, 1% of children and 2% of adults with B-ALL have hypodiploidy (<44 chromosomes), a feature associated with very poor prognosis (Nachman, Heerema et al. 2007, Holmfeldt, Wei et al. 2013).

In addition to altered chromosome numbers, B-ALL is grouped based on the presence of recurrent oncogene-driving chromosomal translocations. The t(12;21)(p13;q22) translocation encoding the *ETV6-RUNX1* (*TEL1-AML1*) fusion is the most common translocation in B-ALL present in 22% of pediatric and 2% of adult B-ALL patients and is associated with a good prognosis. The *ETV6-RUNX1* fusion oncogene is a typical example of transcription factor fusion oncogene and is generated by the association of two hematopoietic transcription factors *ETV6* (*TEL1*, translocation-Ets-leukemia) and *RUNX1* (*AML1*, acute myeloid leukemia-1), which together deregulate the normal activity of RUNX1 and favor the development of B-precursor ALL (Morrow, Horton et al. 2004, Fischer, Schwieger et al. 2005). A second common translocation in B-ALL is the t(9;22)(q34;q11.2) rearrangement, or the Philadelphia chromosome, which is present in 2-4% of pediatric and 25% of adult B-ALL cases. The Philadelphia chromosome encodes the BCR-ABL1 fusion protein, a deregulated and constitutively active tyrosine kinase, which drives increased cell proliferation, growth, and survival (Nagar, Hantschel et al. 2003). Another less common translocation found in B-ALL is the t(1:19)(q23;p13) *TCF3-PBX1* (*E2A-PBX1*) encoding translocation, which is present in 6% of pediatric and 3% of adult ALLs. *TCF3-PBX1* encodes a chimeric transcription factor with increased transcriptional transactivation activity resulting in aberrant expression of *PBX1* target genes (Hunger, Galili et al. 1991). Additionally, translocations involving the mixed-

lineage leukemia gene (*KMT2A*) are common in B-ALL and some T-ALLs accounting for 8% of pediatric and 10% of adult ALL cases. *KMT2A,* also known as *MLL*, encodes lysine methyltransferase 2A, a histone methyltransferase involved in the epigenetic regulation of gene expression via reading and writing of histone H3 K4 trimethylation, an active promoter-associated chromatin mark. *KMT2A* has been identified in over 70 unique chromosomal translocations leading to numerous fusion proteins with a convergent mechanism of action (Meyer, Hofmann et al. 2013). *KMT2A* translocations are particularly common in infant leukemias and can be found in 75% of patients that present with ALL before the age of 1 and are generally associated with poor prognosis (Andersson, Ma et al. 2015).

Advanced molecular cytogenetic studies have uncovered a wealth of chromosomal and gene alterations in ALL, many resulting in novel molecular categories. A recent example is the identification of a group of about 2% of pediatric B-ALLs showing an internal amplification (iAMP) of part of chromosome 21, which is commonly detected with fluorescent in situ hybridization (FISH) probes encompassing the *RUNX1* gene (Harrison, Moorman et al. 2014). Leukemias harboring the rare Robertsonian translocation rob(15;21)(q10;q10) are particularly prone to develop this iAMP 21 subset of B-ALL (Li, Schwab et al. 2014). Another recently identified category of B-ALL is BCR-ABL1-like B-ALL: BCR-ABL1-like or Ph-like ALLs have a gene expression signature related to that of BCR-ABL1 positive ALLs, but do not show the BCR-ABL1 (Philadelphia chromosome) translocation (Den Boer, van Slegtenhorst et al. 2009). Genetic alterations in Ph-like ALL are very diverse, but commonly involve signaling factors and result in constitutively active kinase activity recurrently involving ABL2, PDGFRB, NTRK3, TYK2, CSF1R, and JAK2 (Roberts, Li et al. 2014), CRLF2 and EPOR (Roberts, Morin et al. 2012).

In addition, mutations in important lymphoid developmental genes are seen across the B-ALL spectrum. The two most frequently mutated B-cell development factor genes in B-ALL are *PAX5*, presenting with mutations or deletions in 35% of pediatric cases and 35% adult ALLs, and *IKZF1*, presenting with mutations in 12-17% of pediatric ALLs and 50% adult cases. *IZKF1* mutations are commonly associated with the BCR-ABL1 rearrangements (Kuiper, Schoenmakers et al. 2007, Mullighan, Goorha et al. 2007, Familiades, Bousquet et al. 2009).

T- cell acute lymphoblastic leukemia

Clinical and biological grouping of T-ALL corresponds to the presence of chromosomal rearrangements driving the expression of developmentally important transcription factor oncogenes associated with distinct stages of T-cell development (Ferrando, Neuberg et al. 2002, Belver and Ferrando 2016).

TLX1 (HOX11) and *TLX3 (HOX11L2)* are HOX genes encoding developmental transcription factors that are commonly activated in early cortical T-ALLs with a $CD1a^{+}CD4^{+}CD8^{+}$ immunophenotype. *TLX1* activation is typically caused by the t(10;14)(q24;q11) rearrangement found in 5-10% of pediatric and 30% of adult T-ALLs. This translocation places *TLX1* under control of enhancers in the T-cell Receptor (TCR) loci TCRα or TCRδ leading to high levels of *TLX1* expression (Hatano, Roberts et al. 1991, Kennedy, Gonzalez-Sarmiento et al. 1991, Ferrando, Neuberg et al. 2002, Ferrando, Neuberg et al. 2004). Similarly, the t(5;14)(q35;q32) rearrangement found in 20-25% of pediatric and 5% of adult T-ALL cases places *TLX3* under the regulatory control of the *BCL11B* locus leading to increased *TLX3* expression and activity (Bernard, Busson-LeConiat et al. 2001).

In contrast, T-ALLs with elevated levels of *TAL1* (T-cell acute lymphocytic protein 1), a basic helix-loop-helix (bHLH) transcription factor, are considered mature thymocyte stage T-ALLs presenting with a $CD4^+$ $CD8^+$ $CD3^+$ immunophenotype (Ferrando, Neuberg et al. 2002). T-ALLs express increased levels of *TAL1* through various mechanisms such as translocations placing *TAL1* expression under the control of TCR loci, the focal 90 kb deletion (TAL1d) that relocates the TAL1 coding sequence to the nearby *STIL* locus, or somatic mutations upstream of *TAL1* that generate a neoenhancer activated by mutation-generated MYB transcription factor binding sites (Begley, Aplan et al. 1989, Chen, Yang et al. 1990, Mansour, Abraham et al. 2014). In addition, TCR enhancer-engaging activating translocations have been found to involve other TAL1-related bHLH transcription factors *TAL2*, *LYL1*, and *BHLHB1* (Mellentin, Smith et al. 1989, Xia, Brown et al. 1991, Wang, Jani-Sait et al. 2000, Homminga, Vuerhard et al. 2012).

Increased *TAL1* expression is commonly found together with increased expression of *LMO* (LIM-only domain) genes *LMO1* and *LMO2*, which form transcriptional complexes with *TAL1* and other bHLH transcription factors (Larson, Lavenir et al. 1996, Ferrando, Neuberg et al. 2002). *LMO1* and *LMO2* are commonly misexpressed in T-ALL due to t(11;14)(p15;q11) and t(11;14)(p13;q11) TCR translocations respectively (McGuire, Hockett et al. 1989, Royer-Pokora, Loos et al. 1991).

Finally, early T-cell precursor (ETP) ALL with a developmental arrest at the earliest stages of T-cell differentiation ($CD4^-$ $CD8^-$ cells) are closely related to hematopoietic stem cells and myeloid progenitors (Coustan-Smith, Mullighan et al. 2009) and account for 10-15% of childhood T-ALL and 40-50% of adult T-ALLs (Van Vlierberghe, Ambesi-Impiombato et al. 2011). ETP ALLs are are commonly associated with mutations that

activate oncogenic signaling (KRAS, FLT3, IL7R), alter epigenetic programs (DNMT3A, PHF6, EZH2, SUZ12) and disrupt important transcription factors implicated in lymphoid and T-cell development including *RUNX1*, *GATA3*, and *ETV6* (Zhang, Ding et al. 2012).

In addition to these major subgroups, T-ALLs harbor a number of genetic alterations that disrupt important T-cell developmental factors or cell cycle signaling pathways. The most prominent genetic alteration in T-ALLs is the loss of the tumor suppressors $p16^{INK4A}$ and $p14^{ARF}$, which are encoded by the *CDKN2A* locus on chromosome 9. Chromosomal deletions in the *CDKN2A* locus can be found in >70% of T-ALLs (Hebert, Cayuela et al. 1994, Ferrando, Neuberg et al. 2002). $p16^{INK4A}$ inhibits the progression of the cell cycle from the G1 to S phase and $p14^{ARF}$ inhibits MDM2, a negative regulator of p53. Therefore, these deletions allow cells to bypass signals which are critical for inducing cell cycle arrest and apoptosis in response to cellular stress (Kamijo, Weber et al. 1998).

Additionally, *NOTCH1* mutations are found in >50% of T-ALLs (Weng, Ferrando et al. 2004). NOTCH1 is a class I transmembrane protein that functions as a ligand activated transcription factor. Upon extracellular ligand binding, NOTCH1 undergoes two proteolytic cleavages by ADAM 10 and gamma secretase that release the intracellular NOTCH1 (ICN) domain, which then enters the nucleus, complexes with other transcription factors and initiates transcriptional activity (Dumortier, Wilson et al. 2005). In hematopoietic cells, *NOTCH1* is critical for early T-cell fate and thymocyte development (Radtke, Wilson et al. 1999, Wolfer, Wilson et al. 2002). *NOTCH1* mutations found in ALL disrupt the heterodimerization domain or C-terminal PEST domain leading to constitutive activation of *NOTCH1* signaling (Weng, Ferrando et al. 2004). NOTCH1 activity is similarly upregulated in another 8-30% of T-ALLs due to dominant negative mutations in *FBXW7* (F-box and WD repeat domain containing 7),

which is responsible for the degradation of activated NOTCH1 (O'Neil, Grim et al. 2007, Thompson, Buonamici et al. 2007). Activated NOTCH1 signaling has been shown to contribute to leukemic cell growth directly via increased transcription of anabolic genes, protein translation, and nucleotide and amino acid metabolism as well as promoting cell growth by inducing the expression of the *MYC* oncogene (Palomero, Lim et al. 2006, Weng, Millholland et al. 2006).

Germline predispositions:

Although most genetic alterations identified in ALL occur as somatic mutations, a number of germline genetic alterations have been linked to increased ALL occurrence. Most notably, trisomy 21 (Down Syndrome) and *TP53* mutations (Li-Fraumeni syndrome) are associated with an increased risk of ALL (Kleihues, Schauble et al. 1997, Malinge, Izraeli et al. 2009, Stieglitz and Loh 2013). Additionally, rare germline mutations in *PAX5* (Shah, Schrader et al. 2013), *ARID5B* (Xu, Cheng et al. 2012), *GATA3* (Perez-Andreu, Roberts et al. 2013), *IZKF1* (Churchman, Qian et al. 2018) and *ETV6* (Moriyama, Metzger et al. 2015) have been linked to increased risk of pre-B cell ALL occurrence.

Current Therapy for ALL

Before the introduction of combination chemotherapy, survival rates for T-ALL were only about 10% compared to 40% for patients diagnosed with B-ALL (Greaves, Janossy et al. 1981). With the introduction of multiagent chemotherapy, survival rates for patients with T-ALL have drastically improved approaching 80-90% in children (Pui and Howard 2008, Tasian and Hunger 2017) and 60% in adults (Stock, Johnson et al. 2013). In addition to multi-agent chemotherapy approaches, ALL overall survival has improved due to the

integration of central nervous system (CNS)-directed treatment and reliance on risk-based stratification to moderate treatment intensity (Figure 1.1).

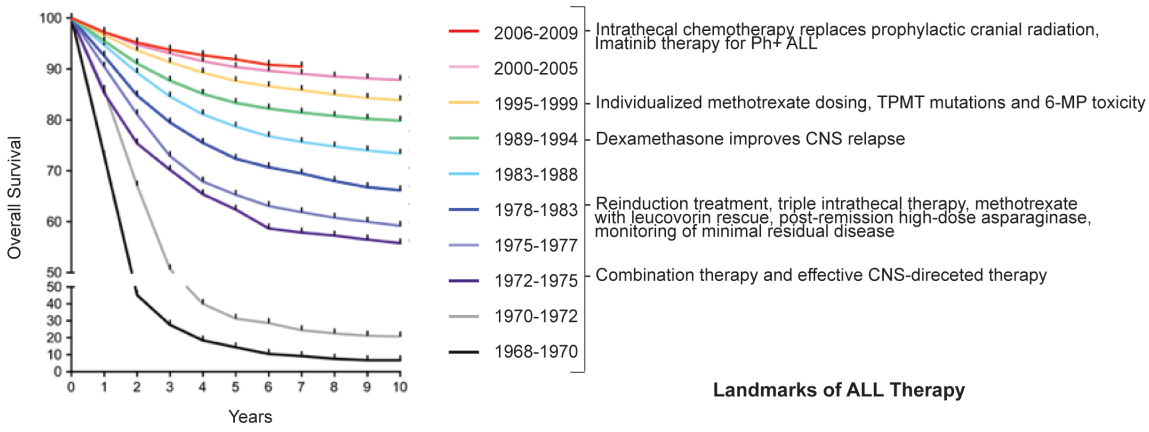

Figure 1.1 – Improved overall survival of children with acute lymphoblastic leukemia treated in cooperative group trials in North America and landmark advances in the treatment of ALL. Adapted from Tasian and Hunger 2017 and Heikamp and Pui 2018.

Upon diagnosis, patients are risk stratified based on age, white blood cell count, gender, the presence of bulky disease, T-cell lineage immunophenotype, and various chromosomal translocations (Nachman, Sather et al. 1998). For B-ALL, “standard risk’ is classified as age 1-9 years old or an initial white cell count less than 50,000 cells per cubic millimeter and “high risk” is classified as ages 10 and older or white blood cell counts greater than 50,000 cells per cubic millimeter (Smith, Arthur et al. 1996). Patients diagnosed before the age of 1 year fall into a different subgroup, often with a worse prognosis. Interestingly, age and white blood cell count are more important prognostic factors in B-ALL than in T-ALL (Pui, Yang et al. 2015). T-ALL risk stratification is largely based on CNS status, immunophenotype and early response to therapy (Schrappe, Valsecchi et al. 2011). In terms of genetic characteristics, high-risk cases include patients with Ph-like gene expression patterns, *MLL* rearrangements, intrachromosomal amplifications of chromosome 21, and hypodiploid B-ALLs and early

T-cell precursor T-ALLs. Low risk cases include hyperdiploidy and *ETV6-RUNX1* fusions in B-ALL and *NOTCH1* or *FBXW7* mutations in T-ALL (Heikamp and Pui 2018).

Although ALL is a highly heterogeneous disease and therapy is typically adapted for each patient, the standard of care therapy proceeds in three phases: (i) induction, (ii) consolidation, and (iii) maintenance. To combat central nervous system (CNS) positive leukemias, patients also receive intrathecal chemotherapy throughout treatment, but timing and schedule depend on the protocol being followed.

Induction therapy is intended to induce a rapid depletion of leukemic blasts. This phase of treatment commonly lasts between four to six weeks and consists of a glucocorticoid (dexamethasone or prednisone), vincristine, aspariginase preparation, and optional therapy with an anthracycline (doxorubicin or daunorubicin) and intrathecal chemotherapy (Table 1.2) (Pui and Evans 2006, Conter, Arico et al. 2010, Gaynon, Angiolillo et al. 2010, Schmiegelow, Forestier et al. 2010). On average 95 % of patients achieve initial remission during induction therapy (Cooper and Brown 2015).

A rapid response to initial chemotherapy is an important prognostic factor, thus minimal residual disease (MRD) levels are checked at multiple points throughout therapy to monitor leukemic burden. Patients who show slow responsiveness to induction therapy are placed on an induction intensification protocol, which greatly improves overall survival (Nachman, Sather et al. 1998). MRD is typically assessed by flow cytometry or quantitative PCR, but more recently is being assessed with next generation sequencing (NGS) which allows for enhanced sensitivity and specificity (Faham, Zheng et al. 2012, Wu, Sherwood et al. 2012).

Following remission after induction therapy, patients are treated for 2-9 months with consolidation therapy to eradicate any remaining blasts and prevent further leukemic development. Consolidation therapy incorporates a multitude of drugs different from those used in induction therapy to maximize synergistic drug combinations and minimize therapy resistance. This phase consists of intensive therapy followed by a brief low intensity maintenance-like treatment followed by a delayed intensification regimen (Tubergen, Gilchrist et al. 1993). Consolidation therapy consists of a mixture of high-dose methotrexate with folinic acid rescue, 6-mercaptopurine (6-MP), aspariginase, dexamethasone and vincristine. Cyclophosphamide and cytarabine are sometimes included for high-risk patients as well (Cooper and Brown 2015, Hunger and Mullighan 2015, Heikamp and Pui 2018).

After consolidation therapy, patients are continuously treated with a low-intensity anti-metabolite based maintenance therapy for 18-30 months. Maintenance therapy consists of daily oral 6-mercaptopurine or 6-thioguanine as well as weekly oral methotrexate. Some protocols also incorporate 5-7 day pulses of glucocorticoids and vincristine (Hunger and Mullighan 2015).

Allogeneic hematopoietic stem cell transplants (HSCT) in first remission are sometimes used in patients who fail to achieve remission or present with a very high risk of relapse or treatment failure, but there is not a well defined protocol yet for these cases (Cooper and Brown 2015).

Table 1.2 - **Chemotherapeutics used in the treatment of acute lymphoblastic leukemia**

Drug Name	Type of Drug	Mechanism of Action
Prednisone, Dexamethasone	Glucocorticoid	Glucocorticoids bind to the glucocorticoid receptor in the cytoplasm and induce localization to the nucleus leading to cell cycle arrest and apoptosis (Inaba and Pui 2010)
Vincristine	Antimitotic	Interacts with beta-tubulin and prevents the formation of spindle microtubules disrupting mitosis and cell division (Gidding, Kellie et al. 1999)
PEG asparaginase, Erwinia asparaginase	Aspariginase	Naturally occurring enzyme that depletes serum of asparagine (Muller and Boos 1998)
Daunorubicin, Doxorubicin	Anthracycline	DNA intercalating agent (Tacar, Sriamornsak et al. 2013)
Cyclophosphamide	Alkylating agent	Nitrogen mustard prodrug that induces intrastrand DNA crosslinks upon hepatic processing (Emadi, Jones et al. 2009)
6-mercaptopurine	Thiopurine	6-thioguanine nucleotides incorporate into DNA resulting in DNA base pair mismatch and subsequent apoptosis (Karran 2006)
6-thioguanine	Thiopurine	
Methotrexate	Folate analogue	Methotrexate inhibits dihydrofolate reductase blocking de novo purine biosynthesis (Longo-Sorbello and Bertino 2001)
Cytarabine	Pyrimidine analogue	Cytosine analogue with an arabinose sugar incorporates into DNA and stalls DNA replication (Kufe, Spriggs et al. 1984)

Thiopurine based maintenance therapy and germline toxicities

It was first observed in the early 1950s that combination treatment with methotrexate (MTX) and 6-mercaptopurine (6-MP) could induce temporary remissions in childhood leukemia (Farber and Diamond 1948, Burchenal, Murphy et al. 1953). Overtime and with numerous trials, this idea has now been elaborated to show that long term remission of pediatric ALL is significantly improved when patients receive post-remission maintenance therapy consisting of 6-MP and MTX treatment (Frei, Karon et al. 1965).

Although this therapy is very well established, the mechanisms for why prolonged thiopurine treatment improves ALL patient outcome are still not fully understood. Yet, multiple studies have shown that patients with higher dose intensity of 6-MP have better event free survival (Relling, Hancock et al. 1999). As maintenance therapy relies on daily

oral 6-MP administered by the patient or caregiver, compliance and therapy adherence is difficult to ensure over the 2-3 year timeline. Patients who drop below 95% 6-MP adherence are 2.5 fold more likely to relapse suggesting that 6-MP maintenance efficacy depends on chronic and continuous exposure to the drug over a long period of time (Bhatia, Landier et al. 2012).

6-MP is processed and activated by enzymes in the purine biosynthesis pathway into 2'-deoxy-6-thioguanosine triphosphate (thio dGTP) and is subsequently incorporated into DNA **(**Figure 1.2**)** (Elion 1989). The cytotoxicity of 6-MP and 6-TG treatment has a delayed effect as cytotoxicity is enacted through the post-replicative mismatch repair system. Thio dGTP leads to equal incorporation of cytosine and thymidine on the opposite strand upon DNA replication leading to DNA mismatches and subsequent mismatch repair dependent cell death (Swann, Waters et al. 1996, Waters and Swann 1997, Karran 2006). Although the majority of 6-MP is incorporate into DNA, a portion of 6-MP, which is converted to thioIMP, is also thiomethylated by TPMT (thiopurine S-methyltransferase) to MeTIMP (methylthioIMP), which inhibits purine de novo biosynthesis. Although this does not appear to play a major role in 6-MP mediated cytotoxicity as *Tpmt*$^{-/-}$ knockout mice show similar rates of de novo purine biosynthesis compared to *Tpmt*$^{+/+}$ wild type mice (Tay, Lilley et al. 1969, Hartford, Vasquez et al. 2007).

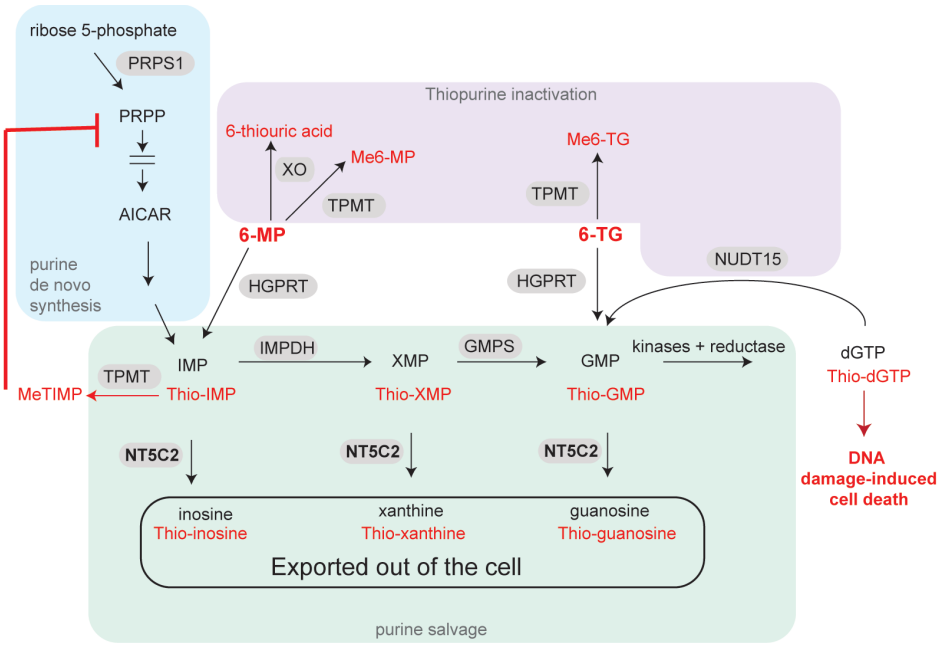

Figure 1.2 – Purine and thiopurine metabolism. NT5C2 dephosphorylates endogenous and thiopurine generated 6-hydroxypurine monophosphates before they are exported out of the cell. Abbreviations: pyrophosphate synthetase 1 gene (PRPS1), phosphoribosyl pyrophosphate (PRPP), 5-aminoimidazole-4-carboxamide ribonucleotide (AICAR), 6-mercaptopurine (6-MP), Methyl 6-MP (Me6-MP), xanthine oxidase (XO), Methyl 6-thioguanine (Me6-TG), hypoxanthine-guanine phosphoribosyltransferase (HGPRT), Nudix hydrolase 15 (NUDT15), inosine monophosphate (IMP), xanthine monophosphate (XMP), guanosine monophosphate (GMP), guanosine triphosphate (GTP), deoxy GTP (dGTP), Cytosolic 5' nucleotidase II (NT5C2), inosine monophosphate dehydrogenase (IMPDH), guanosine monophosphate synthase (GMPS), thiopurine methyltransferase (TPMT), methyl thioIMP (MeTIMP)

In addition to being converted into active cytotoxic metabolites, 6-MP is also inactivated by enzymes in the purine biosynthesis pathway creating a delicate balance between cytotoxic and inactive 6-MP metabolites. A number of toxicities have been observed due to germline mutations in these inactivating enzymes leading to inaccurate thiopurine dosing and sometimes fatal thiopurine toxicity. For example, 1 in 300 people inherit *TPMT* deficiency as an autosomal recessive trait. TPMT is an enzyme that catalyzes the S-methylation of 6-MP, decreasing the amount of thioguanine nucleotide production and incorporation into DNA (Figure 1.2) (Evans, Horner et al. 1991, McLeod, Krynetski et al. 2000). Additionally, loss of function variants in *NUDT15* (nudix hydrolase 15) are found in Asian populations and are associated with thiopurine toxicity. NUDT15 is responsible

for dephosphorylating thio-dGTP preventing its incorporation into DNA and thus minimizing the toxicity of thiopurines (Figure 1.2) (Moriyama, Nishii et al. 2016). Pretreatment screening for loss of function mutations in these critical thiopurine metabolizing enzymes is now standard of care to prevent thiopurine toxicity. Taking these mutations into account, maintenance therapy is continually adjusted on a patient-to-patient case to achieve target levels of myelosuppresion. Patients who tolerate initial 6-MP doses and are not dose escalated have a poorer outcome, thus continued monitoring and adjustment is necessary to provide effective maintenance therapy dosing (Relling, Hancock et al. 1999).

Relapsed acute lymphoblastic leukemia

Despite improved outcomes following initial therapy, overall survival of patients with primary resistant ALL who fail to achieve a complete remission and relapse remains poor. Approximately 20% of pediatric and 50% of adult patients fail to achieve remission and die as a result of disease progression (Nguyen, Devidas et al. 2008, Raetz and Bhatla 2012).

The time of relapse after therapy starts, immunophenotype of relapse, and the site of relapse are all important prognostic factors upon relapsing (Raetz and Bhatla 2012). Patients that relapse after therapy have a much better prognosis than those patients that relapse while on therapy. Additionally, patients with MRD positivity above 0.01% following induction therapy have a much higher risk of relapse (Borowitz, Wood et al. 2015). In addition, patients who relapse at extramedullary sites have a better prognosis than those who relapse in the bone marrow (Nguyen, Devidas et al. 2008).

Upon relapse, patients are treated with reinduction therapy, similar to that of induction therapy, in an attempt to induce a second remission so the patient can eventually receive a hematopoietic cell transplant. Reinduction therapy consists of the same drugs used in induction therapy but they are commonly given at increased doses or on alternate schedules (Cooper and Brown 2015, Pierro, Hogan et al. 2017). Patients who relapse within the testis tend to receive more intensive reinduction chemotherapy and testicular radiation to improve remission likelihood (Wofford, Smith et al. 1992). Patients who relapse within the CNS are treated with dexamethasone, which bypasses the blood brain barrier, low dose cranial radiation, and intensive chemotherapy administered via lumbar punctures or Ommaya ventricular reservoirs to ensure delivery to the CNS (Barredo, Devidas et al. 2006, Larson 2018).

Although the implementation of risk stratification and multi-agent chemotherapy has greatly improved the outcomes of patients treated with initial therapy over the past few decades, recent studies comparing outcomes of relapse ALL patients from 1988-94 and 1995-2002 have shown no improvement in relapsed patient survival (Nguyen, Devidas et al. 2008). Thus new therapeutic regimens and improved understanding of ALL at relapse are desperately needed for the improved treatment and survival of patients with relapsed ALL.

Genetic alterations in relapsed acute lymphoblastic leukemia

Leukemia-initiating cells capable of self-renewal (Cox, Diamanti et al. 2009, Gerby, Clappier et al. 2011), protective microenvironment safe-haven niches (Konopleva, Konoplev et al. 2002, Hawkins, Duarte et al. 2016) and clonal evolution (Mullighan, Phillips et al. 2008, Ma, Edmonson et al. 2015, Oshima, Khiabanian et al. 2016) with acquisition of secondary genetic alterations driving chemotherapy resistance (Mullighan,

Zhang et al. 2011, Meyer, Wang et al. 2013, Tzoneva, Perez-Garcia et al. 2013, Li, Li et al. 2015, Ma, Edmonson et al. 2015, Malinowska-Ozdowy, Frech et al. 2015, Oshima, Khiabanian et al. 2016) have all been implicated as drivers of ALL disease progression and relapse.

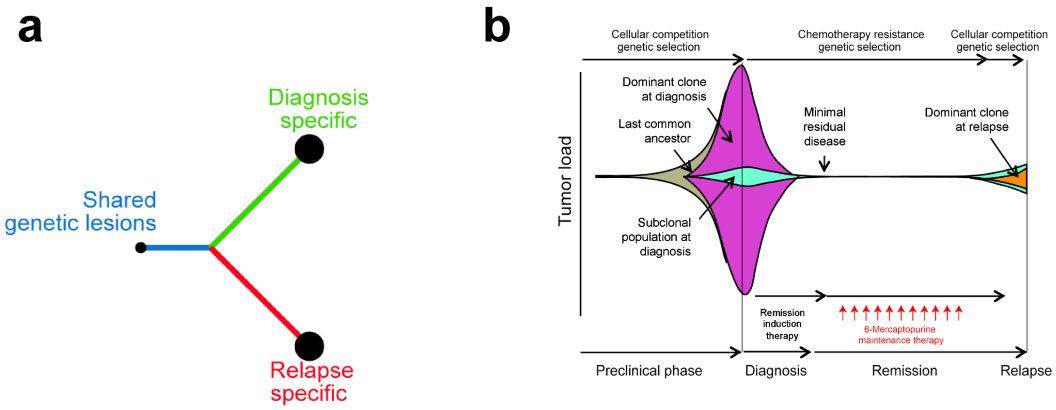

Figure 1.3 – Branched clonal evolution of relapsed leukemia. (a) Branched evolution scheme. (b) Chemotherapy driven evolution of therapy resistant clones. Adapted from Oshima et al 2016.

Recent genomic analyses of matched diagnostic and relapsed patient samples have greatly improved our understanding of the clonal evolution of relapsed ALL. These studies have shown that ALL displays branched evolution where relapse clones emerge from ancestral clones sharing some, but not all, genetic alterations with the diagnostic sample (Figure 1.3). It is postulated that multi-agent chemotherapy treatment drives this clonal evolution by suppressing prominent clones at diagnosis and simultaneously allowing for the emergence of new clones harboring resistance driving mutations (Figure 1.3) (Mullighan, Phillips et al. 2008, Ma, Edmonson et al. 2015, Oshima, Khiabanian et al. 2016). Most relapsed ALL samples preserve key genetic features from diagnosis, such as translocations and aneuploidy, but acquire additional genetic mutations and copy number alterations upon relapse. Interestingly, the frequency of somatic mutations

in ALL at diagnosis and relapse is fairly low averaging 20 or less non-silent mutations per case (Ma, Edmonson et al. 2015).

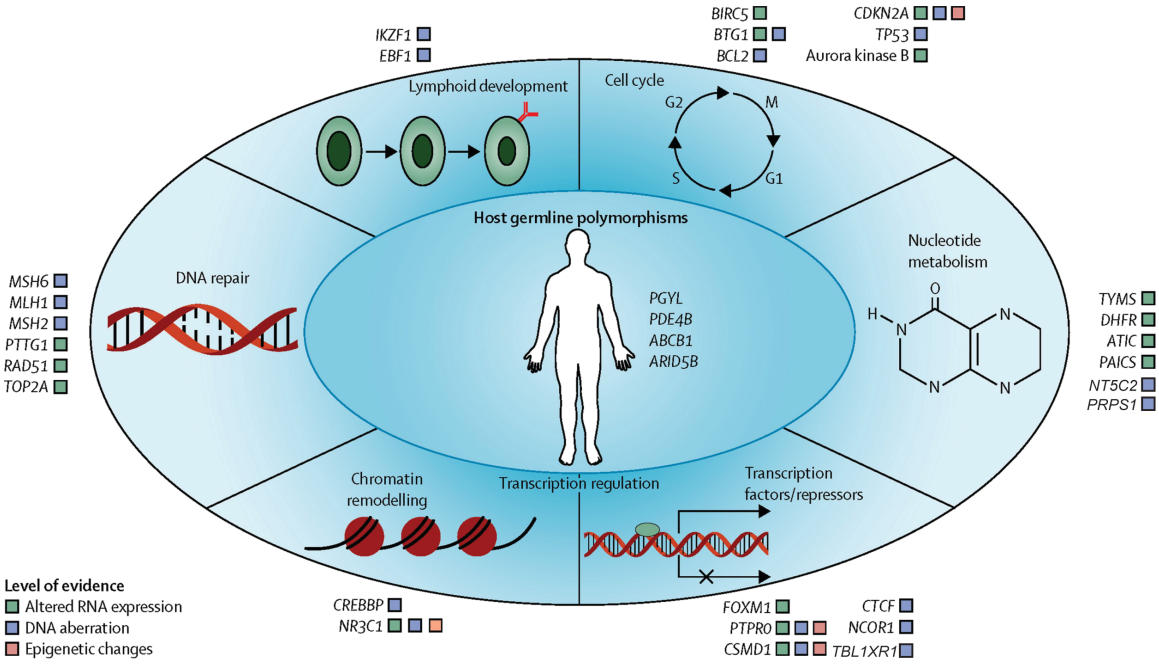

Figure 1.4. – Common genetic alterations implicated in therapy resistance and relapse in ALL. Adapted from Bhojwani and Pui 2013.

In particular, genes regulating cell cycle progression, lymphoid development, DNA repair, transcription regulation, and nucleotide metabolism have been found implicated in relapsed ALL and are summarized in Figure 1.4 (Bhojwani and Pui 2013). Some of these relapse specific genetic alterations have been directly associated with specific resistance to certain chemotherapies. For example, mutations in *CREBBP* (CREB binding protein), a transcriptional co-activator and histone acetyltransferase (HAT), are found in 20% of relapsed ALL samples and have been linked with glucocorticoid resistance. These truncating and loss of function mutations disrupt histone acetylation and thus transcriptional regulation of CREBBP targets, which include glucocorticoid responsive genes (Mullighan, Zhang et al. 2011). Additionally, mutations and deletions in

the *NR3C1* gene, which encodes the glucocorticoid receptor, and deletions in the *TBL1XR1* gene*,* which prevents repression of the glucocorticoid complex, have been associated with glucocorticoid resistance at relapse (Kuster, Grausenburger et al. 2011, Jones, Bhatla et al. 2014).

A number of genes have also been implicated in thiopurine resistance. *PRPS1 (*Pyrophosphate synthetase 1 gene) point mutations have been found in 7% of relapsed B-ALLs encoding gain of function *PRPS1* mutants and have been associated with thiopurine resistance. *PRPS1* gain of function mutations result in a build-up of hypoxanthine, which competes with 6-MP as a substrate for HPRT therefore decreasing 6-MP conversion into thio-nucleotides and minimizing the cytotoxic effects of 6-MP (Li, Li et al. 2015). Decreased expression of *MSH6* is also associated with 6-MP resistance due to the failure of MSH6 to recognize thioguanine nucleotide induced mismatches and initiate mismatch repair (Yang, Bhojwani et al. 2008, Evensen, Madhusoodhan et al. 2018). *NT5C2*, cytosolic 5' nucleotidase II, is by far the most prominent relapse ALL associated mutation accounting for 20% of relapse T-ALL and 3-10% of relapse B-ALL cases. *NT5C2* activating mutations act as gain of function alleles leading to increased processing of thiopurine metabolites and decreased cytotoxicity of these chemotherapies causing overt thiopurine chemotherapy resistance (Meyer, Wang et al. 2013, Tzoneva, Perez-Garcia et al. 2013).

New therapeutics for the treatment of ALL

With the identification of numerous genetic alterations present in diagnosis and relapsed ALL, a multitude of targeted therapeutics have been developed and implemented in clinical trials to attempt to improve patient survival. A summary of active clinical trials involving new therapies can be found in Table 1.3.

Table 1.3 – Active recruiting and non-recruiting clinical trials as of November 2018 involving new therapeutics for the treatment ALL.

Clinical Trial Identifier	Title
NCT00390793	Combination Chemotherapy and Dasatinib in Treating Participants With Philadelphia Positive or BCR-ABL Positive Acute Lymphoblastic Leukemia.
NCT01044069	Precursor B Cell Acute Lymphoblastic Leukemia (B-ALL) Treated With Autologous T Cells Genetically Targeted to the B Cell Specific Antigen CD19
NCT01683279	A Pediatric Trial of Genetically Modified Autologous T Cells Directed Against CD19 for Relapsed CD19+ Acute Lymphoblastic Leukemia
NCT01860937	T-Lymphocytes Genetically Targeted to the B-Cell Specific Antigen CD19 in Pediatric and Young Adult Patients With Relapsed B-Cell Acute Lymphoblastic Leukemia
NCT02420717	Ruxolitinib or Dasatinib With Chemotherapy in Patients With Philadelphia Chromosome (Ph)-Like Acute Lymphoblastic Leukemia (ALL)
NCT02458014	Study of Blinatumomab in Patients With B-cell Lineage Acute Lymphocytic Leukemia With Positive Minimal Residual Disease
NCT02494882	Adding Ruxolitinib to a Combination of Dasatinib Plus Dexamethasone in Remission Induction Therapy in Newly Diagnosed Philadelphia Chromosome-Positive Acute Lymphoblastic Leukemia Patients Aged 40 Years or Older
NCT02767934	Pembrolizumab in Treating Minimal Residual Disease in Patients With Acute Lymphoblastic Leukemia
NCT02819804	Nivolumab and Dasatinib in Treating Patients With Relapsed or Refractory Philadelphia Chromosome Positive Acute Lymphoblastic Leukemia
NCT02935543	CART19 in Adult Patients With Minimal Residual Disease During Upfront Treatment for ALL
NCT02981628	Inotuzumab Ozogamicin in Treating Younger Patients With Relapsed or Refractory CD22 Positive B Acute Lymphoblastic Leukemia
NCT02997761	Ibrutinib and Blinatumomab in Treating Patients With Relapsed or Refractory B Acute Lymphoblastic Leukemia
NCT03104491	Inotuzumab Ozogamicin Post-Transplant For Acute Lymphocytic Leukemia
NCT03147612	Low-Intensity Chemotherapy and Ponatinib in Treating Participants With Philadelphia Chromosome-Positive and/or BCR-ABL Positive Acute Lymphoblastic Leukemia
NCT03241940	CD19/CD22 Chimeric Antigen Receptor T Cells and Chemotherapy in Treating Children or Young Adults With Recurrent or Refractory CD19 Positive B Acute Lymphoblastic Leukemia
NCT03263572	Blinatumomab and Ponatinib in Patients With Philadelphia Chromosome (Ph)-Positive and/or BCR-ABL Positive Acute Lymphoblastic Leukemia (ALL)
NCT03472573	Palbociclib and Dexamethasone in Treating Participants With Relapsed or Refractory B-Cell Acute Lymphoblastic Leukemia
NCT03573700	Evaluation of CD19-Specific CAR Engineered Autologous T-Cells for Treatment of Relapsed/Refractory CD19+ Acute Lymphoblastic Leukemia
NCT03620058	CART22 Alone or in Combination With huCART19 for ALL

One of the most dramatic effects in overall survival has been seen with the development of tyrosine kinase inhibitors (TKIs) for the treatment of BCR-ABL1 positive ALLs (Wassmann, Pfeifer et al. 2006, Arico, Schrappe et al. 2010). The first TKI implemented in the treatment of Ph-positive ALL was Imatinib mesylate which led to complete remission rates >90% (Daver, Thomas et al. 2015). Imatinib works as a competitive inhibitor at the ATP-binding site of the ABL1 kinase, inhibiting phosphorylation and activation of downstream targets (Druker, Talpaz et al. 2001). Unfortunately, as imatinib has been implemented in the clinic, some patients have developed resistances to therapy with T315I mutations in the kinase domain, which stabilize the active kinase formation and ultimately lead to relapse. To further combat these kinase driven diseases, other TKIs such as dasatinib and ponatinib have been developed (Shah, Tran et al. 2004, Ravandi, O'Brien et al. 2015). Dasatinib is a promiscuous tyrosine kinase inhibitor known to target ABL1 as well as other Src family kinases (Zhang and Meier 2006). In contrast Ponatinib has been specifically developed to reduce the emergence of T315I resistant clones and has improved complete remission rates to 98% (Jabbour, Kantarjian et al. 2015, Sasaki, Jabbour et al. 2016). Additionally, dissection of the genetic makeup of Ph-like ALL has identified chromosomal rearrangements resulting in non *BCR-ABL1* gene fusions involving *ABL1*, *ABL2, CSF1R*, and *PDGFRB* (Pui, Roberts et al. 2017). As dasatinib targets a number of tyrosine kinases such as these, specific Ph-like ALLs similarly benefit from treatment with dasatinib (Zhang and Meier 2006, Pui, Roberts et al. 2017). Some Ph-like ALLs have also been found to have *EPOR* and *JAK2* rearrangements which contribute to increased JAK-STAT signaling making these ALLs candidates for treatment with JAK inhibitors (Roberts, Li et al. 2014). Initial experiments have confirmed increased cell death with the JAK inhibitor ruxolitinib and there are currently a number of ongoing clinical trials implementing ruxolitinib into therapy for Ph-like ALL patients.

In addition to targeted genetic treatments, immunotherapy has rapidly evolved in the treatment of acute lymphoblastic leukemia (Figure 1.5). In particular, chimeric antigen receptor T-cells or CAR T-cells have rapidly evolved over the past decade. CAR T-cells are genetically modified autologous T lymphocytes engineered to express binding sites of specific antibodies to target and eliminate cancer cells. The most common CAR T-cell strategy used for the treatment of ALL consists of an extracellular immunoglobulin domain that recognizes CD19 and an intracellular signaling domain that activates the T-cell to kill CD19 expressing B-ALL leukemic cells. Unlike chemotherapies, CAR T-cells persist in the patient for much longer and thus have lasting affects (Sabatino, Hu et al. 2016). The first clinical trial implementing CAR T-cells in the treatment of relapsed ALL induced complete remission in 93% of patients (Maude, Frey et al. 2014). This CAR T-cell therapy, Tisagenlecleucel (formerly CRL019), was designated as a “breakthrough therapy” in 2017 by the FDA and was approved for therapy in patients with relapsed B-ALL (O'Leary, Lu et al. 2018). As some patients have relapsed due to lack of persistence of CAR T-cells and emergence of CD19 negative leukemias, researchers are currently implementing a multitude of strategies to improve CAR T-cell efficacy (Maude, Frey et al. 2014, Gardner, Wu et al. 2016). These improvements include CAR T-cells targeting other antigens such as CD22, or tandem CAR T-cells that recognize CD19 and CD22 (Schneider, Xiong et al. 2017, Fry, Shah et al. 2018).

Although CAR T-cell therapeutics are an incredible new development for the treatment of B-ALL, they are not always an option as at least two weeks is needed to harvest and engineer T-cells from the patient before they are ready to use leading to a delay in therapy that is not always the best option for the patient. In these cases, monoclonal antibodies are a good alternative and have recently been implemented in the treatment

of ALL. One example in particular is the use of rituximab, a chimeric CD20 targeting antibody that induces complement-mediated cytotoxicity, which has been used extensively in the treatment of non-Hodgkins lymphoma (Cerny, Borisch et al. 2002). B-ALLs expressing high levels of CD20 were shown to have a worse prognosis and thus rituximab was added to clinical trials for these patients. Addition of rituximab to the treatment of newly diagnosed Ph-negative positive ALL has improved the 3-year complete remission duration to 70% (Thomas, O'Brien et al. 2010).

In addition to CD20 expression, many B-ALLs express CD19. As a result, Blinatumomab, a bispecific T-cell engager (BiTE) antibody construct that steers CD3-positive effector T-cells to CD19-positive leukemia cells has recently been tested in the treatment of relapsed and refractory B-cell precursor ALL. Blinatumomab has shown particular success in inducing MRD negativity in 78% of patients with positive MRD following initial therapy after just one cycle of treatment. These results lead blinatumomab to be approved for the treatment of patients with positive MRD by the FDA in March 2018 (Gokbuget, Dombret et al. 2018, Jabbour, Pui et al. 2018).

In addition to expressing CD19 and CD20, 90% of precursor B-ALLs express the cell-surface glycoprotein CD22, and thus CD22 has emerged as an attractive therapeutic target for the treatment of B-ALLs (Piccaluga, Arpinati et al. 2011, Shah, Stevenson et al. 2015). Inotuzumab ozogamicin (CMC-544) is a humanized anti-CD22 monoclonal antibody linked to the cytotoxic compound calicheamicin that has recently been added to trials to improve B-ALL therapeutic regimens (DiJoseph, Armellino et al. 2004). Upon binding to CD22, inotuzumab ozogamicin is internalized and calcheamicin is released to bind to DNA and induce double strand breaks thus inducing apoptosis (Zein, Sinha et al. 1988, Hanna, Ong et al. 1996, Kantarjian, Vandendries et al. 2016). Following success

in inducing complete remission and improving MRD negativity in patients with relapsed and refractory B-ALL, Inotuzumab ozogamicin or Besponsa was recently approved in 2017 by the FDA for the treatment of adults with relapsed or refractory B-ALL (Kantarjian, Thomas et al. 2013, DeAngelo, Stock et al. 2017, Lamb 2017).

Most immunotherapies are targeted at B-cells as they have clear antigens to target, yet it has proven difficult to identify a unique marker of T-ALL that is not present on normal T lymphocytes. The only monoclonal antibody developed for T-ALL, alemtuzumab, an anti-CD25 antibody, has shown limited success. In one study, alemtuzumab induced one complete remission out of 13 patients treated and was associated with increased toxicity (Angiolillo, Yu et al. 2009). Preclinical studies using CD5-targeted CAR T-cells to target T-cell leukemias have been fairly successful but have not yet made the move into clinical settings (Mamonkin, Rouce et al. 2015, Chen, Wada et al. 2017).

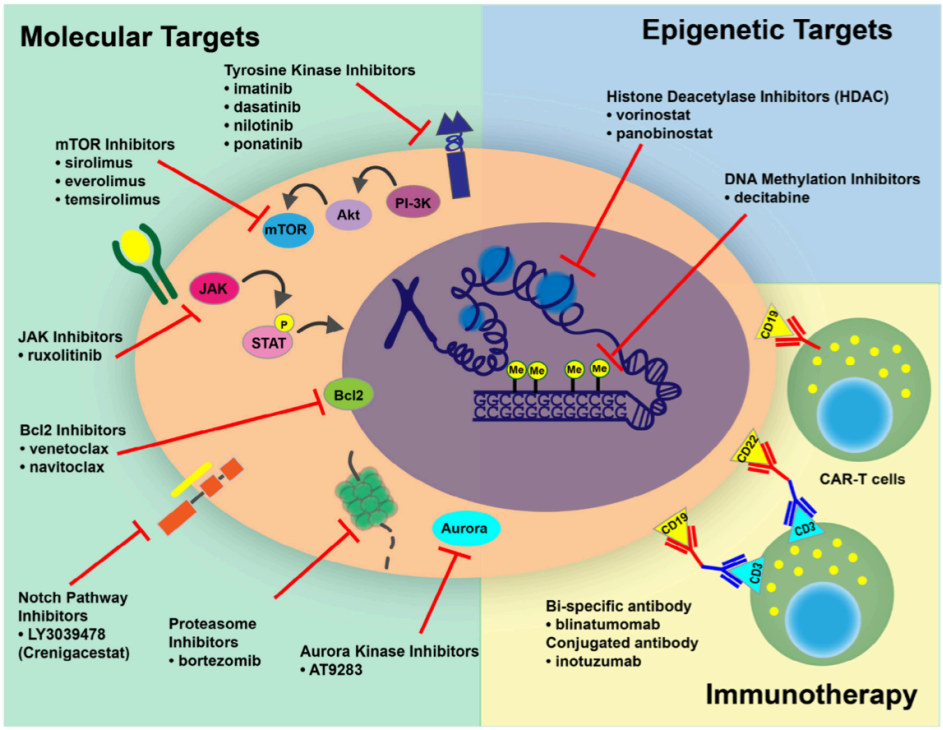

Figure 1.5 – Novel molecular, epigenetic and immunotherapeutic approaches to target relapsed and refractory disease. Adapted from Heikamp and Pui 2018.

II. Cytosolic 5' Nucleotidase II (NT5C2)

Physiologic role of NT5C2

NT5C2 (5' cytosolic nucleotidase II), also known as cN-II or high K_m 5'-nucleotidase, is one of seven mammalian 5' nucleotidases that dephosphorylates ribo and deoxyribonucleoside monophosphates. The seven nucleotidases vary in cellular localization, substrate preference and tissue specific expression, but all function to dephosphorylate nucleoside monophosphates to counterbalance the activity of nucleoside kinases as a way to regulate nucleotide pools within the cell (Table 1.4) (Bianchi and Spychala 2003, Hunsucker, Mitchell et al. 2005).

Table 1.4 – 5'-nucleotidase family member gene names and preferred substrate. Adapted from Hunsucker *et al*, 2005.

5'Nucleotidase (abbreviation)	Gene name	Protein size	Natural Substrate
Ecto-5'-nucleotidase (eN)	NT5E	574 aa	broad: purine, pyrimidine, deoxy-and ribonuceloside monophosphates
Cytosolic 5'-nucleotidase IA (cN-IA)	NT5C1B	368 aa	AMP, dTMP, dCMP, dGMP, dAMP, dIMP
Cytosolic 5'-nucleotidase IB(cN-IB)	NT5C1B	550 aa	AMP
Cytosolic 5'-nucleotidae II (cN-II)	NT5C2	561 aa	6-hydroxy purines: IMP, dIMP, GMP, dGMP, XMP
Cytosolic 5'-nucleotidae III (cN-III)	NT5C3	285 aa	Pyrimidine monophosphates: CMP, UMP, dUMP, dCMP, dTMP
Cytosolic 5′(3′)-deoxyribonucleotidase (cdN)	NT5C	201 aa	2′ and 3′ monophosphates: 3′-dUMP, 3′-dTMP, 3′-UMP and 2′-UMP; lower activity with 5′-dIMP, 5′-dUMP, 5′-dCMP, 5′-dTMP and 5′-dAMP
Mitochondrial 5′(3′)-deoxyribonucleotidase (mdN)	NT5M	228 aa	pyrimidine monophosphates with thymine or uracil bases: 5′-dUMP, 5′-dTMP, 3′-dTMP and 5′-, 3′-and 2′-UMP

NT5C2 is a ubiquitously expressed cytosolic nucleotidase that preferentially dephosphorylates the 6-hydroxypurine monophosphates inosine monophosphate (IMP), xanthine monophosphate (XMP), and guanosine monophosphate (GMP) as well as their deoxyribose forms dIMP and dGMP and with low efficiency adenosine monophosphate (AMP) into their respective purines allowing them to be exported from the cell (Itoh, Mitsui et al. 1967, Spychala, Madrid-Marina et al. 1988, Tozzi, Camici et al. 1991, Pesi, Turriani et al. 1994, Banditelli, Baiocchi et al. 1996, Allegrini, Pesi et al. 1997, Hunsucker, Mitchell et al. 2005) **(**Figure 1.6**).** In addition to its nucleotidase activity, NT5C2 also acts as a phosphotransferase to donate phosphates to acceptors such as inosine or deoxyinosine (Worku and Newby 1982, Banditelli, Baiocchi et al. 1996).

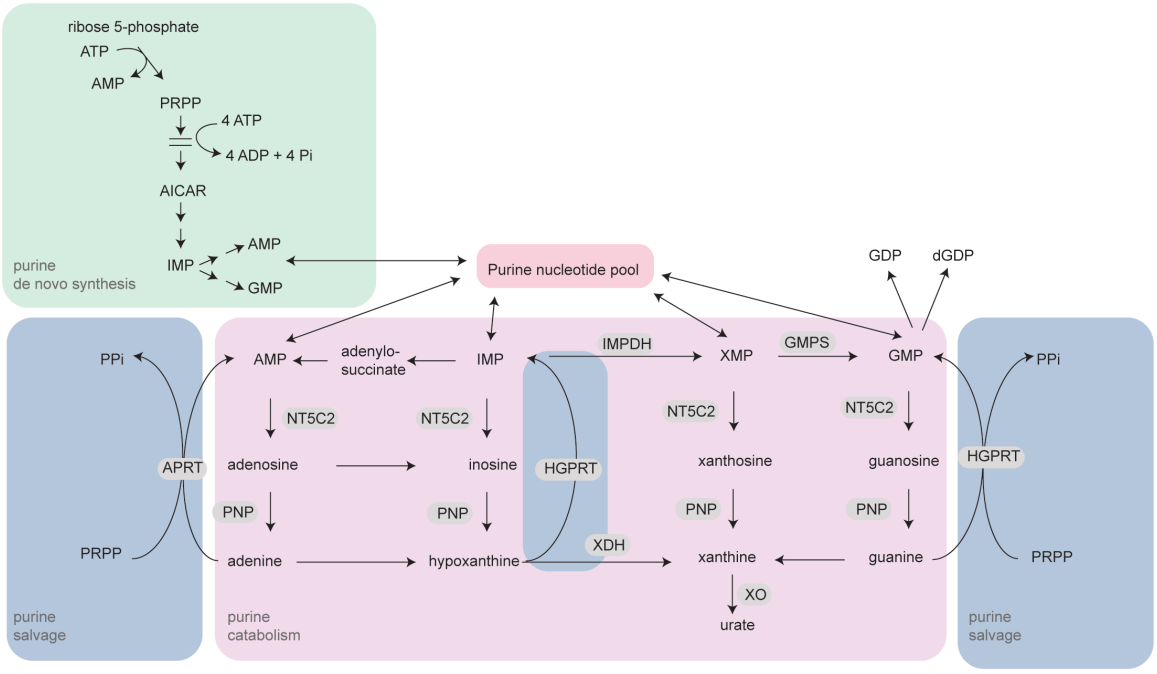

Figure 1.6 - Purine Metabolism. Abbreviations: Adenosine deaminase (ADA), Adenosine kinase (AdK), Adenylate kinase (AK), Adenine phosphoribosyltransferase (APRT), deoxyguanosine kinase (dGK),guanylate kinase (GUK), hypoxanthine-guanine phosphoribosyltransferase (HGPRT), inosine monophosphate dehydrogenase (IMPDH), nucleoside diphosphate kinase (NDPK), purine nucleoside phophorylase (PNP), ribonucleotidase reductase (RR), guanosine monophosphate synthase (GMPS), Xanthine dehydrogenase (XDH), xanthine oxidase (XO).

NT5C2 protein and structure

Structurally, NT5C2 is a member of the haloacid dehalogenase (HAD) superfamily of Mg^{2+}-dependent intracellular 5'-nucleotidases, which characteristically have an α/β-Rossman-like domain and a smaller 4-helix bundle domain (Koonin and Tatusov 1994). NT5C2 was first purified from chicken liver in 1967 (Itoh, Mitsui et al. 1967) and has now been extensively investigated in many vertebrates (Bretonnet, Jordheim et al. 2005). NT5C2 is a 561 amino acid protein and migrates to about ~57kDa as measured on an SDS-polyacrylamide gel.

NT5C2 is a homotetramer that functions as a dimer of dimers, with the dimer being the smallest functional unit with enzymatic activity (Spychala, Madrid-Marina et al. 1988, Wallden and Nordlund 2011) and is regulated by allosteric activators ATP, dATP, diadenosine tetraphosphate (Ap_4A), and 2,3-bispho-sphoglycerate (BPG) (Pinto, Canales et al. 1986, Bontemps, Van den Berghe et al. 1988, Spychala, Madrid-Marina et al. 1988, Marques, Teixeira et al. 1998) **(**Figure 1.7**)**. The physiologic activator of NT5C2 is not known, but some groups suspect Ap4A due to its ability to activate NT5C2 at lower concentrations than other activators and that Ap4A levels increase upon apoptosis, which may trigger purine catabolism and recycling for use by other cells (Pinto, Canales et al. 1986, Vartanian, Prudovsky et al. 1997).

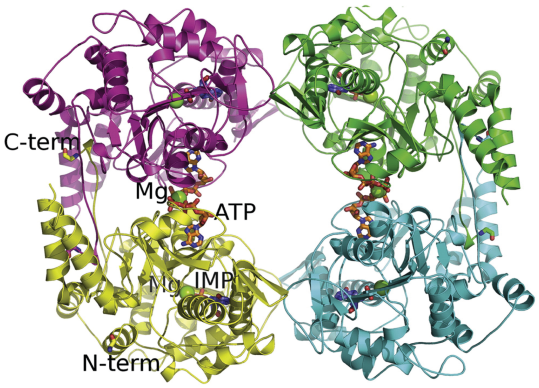

Figure 1.7- Tetrameric structure of active NT5C2 D52N 537X with IMP, Mg^{2+} and ATP bound. Adapted from Wallden and Nordlund 2011.

The allosteric binding site (also referred to as effector site 1) of NT5C2 is located close to the subunit interface, with the adenosines of two ATP molecules binding back-to-back to each subunit of the dimer with a Mg^{2+} ion coordinated between the two phosphate moieties (Figure 1.7). The adenosine moiety forms hydrogen bonds with Gln453, Asn154, and is stacked between Phe354 and Ile152 (Figure 1.8). The substrate, IMP, binds within the active site with the nucleoside stacked between Phe157, His209 and Tyr210 forming electrostatic interactions with Asp206 and Arg202 **(**Figure 1.8**).** A second effector site has been described, but its function is not yet known (Wallden, Stenmark et al. 2007).

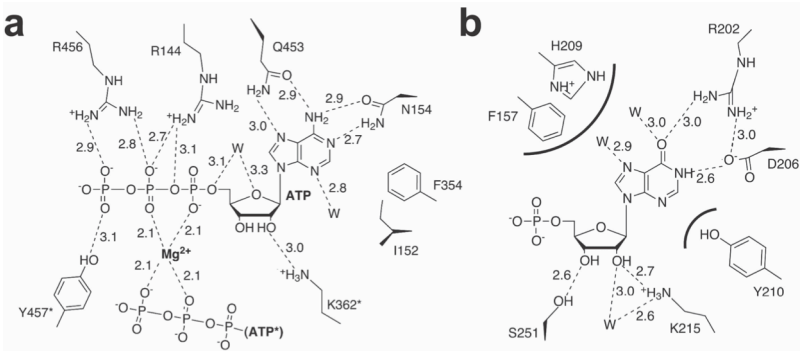

Figure 1.8 - Schematic diagrams of allosteric and active sites of NT5C2. (a) Allosteric site with activator, ATP, and Mg2+ bound. Residues marked with * are from the neighboring monomer of the dimer. (b) Active site of NT5C2 with substrate, IMP, bound. Adapted from Wallden and Nordlund 2011.

Mechanistically, the 5'-nucleotidase activity of NT5C2 proceeds via formation of a phosphoenzyme intermediate mediated by three highly conserved HAD motifs in the α/β-Rossman-like domain in the catalytic center (Figure 1.9) (Collet, Stroobant et al. 1998, Allegrini, Scaloni et al. 2001). For NT5C2, Motif I, DXDX(V/T)(L/V/I), is integral to the reaction mechanism. The first Asp (Asp52 in NT5C2) of motif I makes a nucleophilic attack on the phosphate of the substrate, while the second Asp (Asp54 in NT5C2) donates a proton to the departing nucleoside. Motif II is a (S/T) residue (Thr249 in NT5C2) which stabilizes the phosphoenzyme intermediate along with the Lys (Lys292 in NT5C2) of motif III, $K(X_x)D(X_{0-4})D$. The additional negatively charged residues in motif III (Asp351 and Asp356 in NT5C2) interact with the metallic cation, Mg^{2+}, which is essential for catalytic activity (Allegrini, Scaloni et al. 2001, Allegrini, Scaloni et al. 2004, Bretonnet, Jordheim et al. 2005). NT5C2 is also known to possess a phosphotransferase activity, but the mechanism for this has not yet been elucidated (Worku and Newby 1982).

MOTIF I:	DXDX[T/V] [L/V/I]		
cN-IA	211	DGDAVL	216
cN-IB	467	DGDAVL	472
cN-II	52	DMDYTL	57
cN-IIIA	49	DFDMTL	54
cN-IIIB	33	DFDMTL	38
cdN	10	DMDGVL	15
mdN	41	DMDGVL	46
MOTIF II:	ΦΦΦ[T/S]		
cN-IA	n/a		
cN-IB	n/a		
cN-II	246	FLAT	249
cN-IIIA	161	FIFS	164
cN-IIIB	145	FIFS	148
cdN	96	FICT	99
mdN	137	FICT	130
MOTIF III:	$K(X)_xD(X)_{0-4}D$		
cN-IA	320	$K(X)_7$ D....D	329
cN-IB	576	$K(X)_7$ D....D	585
cN-II	292	$K(X)_{58}$DHIFGD	356
cN-IIIA	213	$K(X)_{24}$DSQ.GD	242
cN-IIIB	197	$K(X)_{24}$DSI.GD	249
cdN	134	$K(X)_9$ D....D	145
mdN	165	$K(X)_9$ D....D	176

Figure 1.9 – Conserved HAD motif alignment in intracellular 5'-nucleotidase family proteins. Adapted from Monecke *et al*, 2014.

Comparison of the basal (apo) and active (allosteric effector bound) structures of NT5C2 revealed a role of the Gly355-Gln364 region in the allosteric activation of the enzyme. Upon allosteric activator binding, this region (helixA) becomes organized into an alpha helix and is stabilized by electrostatic interactions between Lys362 and the phosphate groups of the allosteric activator. This conformational change induces a rotation of Phe354 moving it out of the active site, allowing Asp356 to move in and trigger conformational changes in His352 and Lys292 of motif III, thereby transitioning the

enzyme to its active state, allowing for substrate binding and catalysis (Figure 1.10) (Wallden and Nordlund 2011).

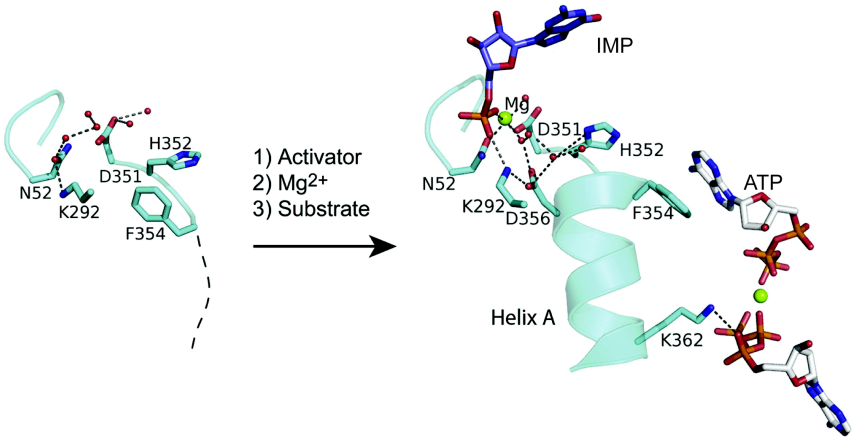

Figure 1.10- Mechanism of activation of NT5C2. (Left) Active site of apo inactive NT5C2 D52N 537X with disorganizes residues represented by a dotted line. (Right) Active, helix A, configuration of NT5C2 D52N 537X. Upon addition of activator (ATP), Mg2+, and substrate (IMP), Gly355-Glu364 becomes organized into an alpha helical configuration allowing allosteric activator, ATP, to bind and catalysis of substrate, IMP, to occur. Adapted from Wallden and Nordlund, 2011.

Additionally, NT5C2 has a striking 13 acidic-residue long C-terminus that is very well conserved in mammals which may play a role in the regulation of the enzyme. Experiments with C-terminus truncated recombinant protein have suggested that this acidic stretch may be important for the formation and stability of the tetrameric structure (Spychala, Chen et al. 1999). Additionally experiments under oxidative conditions with recombinant NT5C2 protein identified a Cys175-Cys547 disulfide bond that might play a role in enzyme regulation depending on redox states of the cell (Allegrini, Scaloni et al. 2004). Due to its acidic nature, it is suspected that the C-terminus of NT5C2 will bind in one of three positively charged regions (i) K(25)KYRR, (ii) K(359)SKKRQ, or (iii) Q(420)RRIKK (Spychala, Chen et al. 1999). As of yet, all published structures have been solved with C-terminus truncations due to solubility issues thus the regulatory capacity of this element is not yet known.

NT5C2 in relapsed leukemia

Using whole exome sequencing of matched diagnosis, remission, and relapse samples, we and other groups identified an abundance of mutations in *NT5C2* present in relapsed ALL patient samples (Meyer, Wang et al. 2013, Tzoneva, Perez-Garcia et al. 2013). Mutations in *NT5C2* occur in 20% of relapsed T-ALL and 3-10% of relapsed early precursor B-ALL cases and are particularly common amongst early relapse patients accounting for 35-45% of these cases (Meyer, Wang et al. 2013, Tzoneva, Perez-Garcia et al. 2013, Ma, Edmonson et al. 2015, Tzoneva, Dieck et al. 2018). Recently, *NT5C2* mutations have also been identified in acute promyelocytic leukemia (APL) relapse samples from patients who have been treated with 6-MP (Lehmann-Che, Bally et al. 2018). So far in the literature, our group and others have reported 32 independent *NT5C2* mutant alleles consisting of 27 single amino acid substitutions, four in frame indel mutations and a C-terminal truncating mutation (Figure 1.11) (Meyer, Wang et al. 2013, Tzoneva, Perez-Garcia et al. 2013, Kunz, Rausch et al. 2015, Ma, Edmonson et al. 2015, Oshima, Khiabanian et al. 2016, Richter-Pechanska, Kunz et al. 2017, Dieck, Tzoneva et al. 2018, Lehmann-Che, Bally et al. 2018, Tzoneva, Dieck et al. 2018). All *NT5C2* relapse associated mutations present as heterozygous mutations and are only found in relapse samples. Extensive deep sequencing efforts have failed to detect *NT5C2* mutations at the time of diagnosis, or at least at the level of detection available with current deep sequencing technologies (Tzoneva, Dieck et al. 2018).

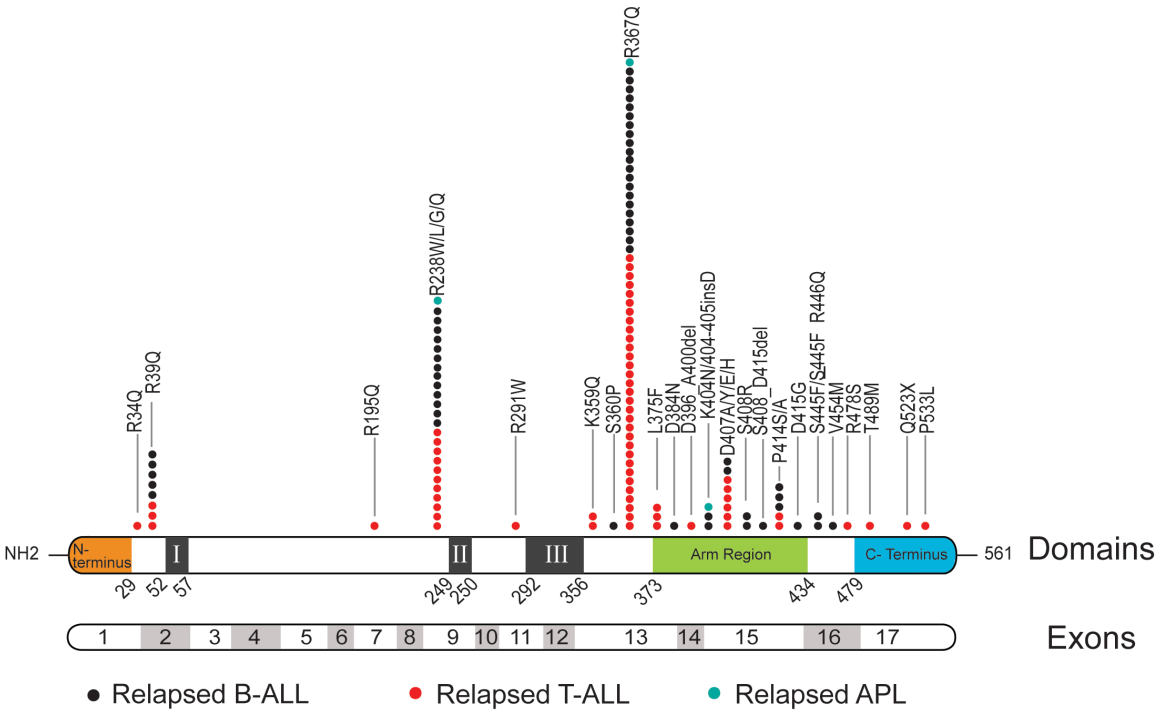

Figure 1.11 – NT5C2 relapse associated mutations. Adapted from Dieck and Tzoneva *et al*, 2018.

NT5C2 in health and disease

As NT5C2 regulates purine metabolism and levels within the cell, *NT5C2* expression and activity has been implicated in a number of human malignancies and diseases. Most notably, familial germline loss of function *NT5C2* mutations have been identified in spastic paraplegia (SPG45) (Novarino, Fenstermaker et al. 2014, Darvish, Azcona et al. 2017). Spastic paraplegia is a neurodegenerative disease resulting in upper motor neuron degeneration and lower limb spasticity. Researchers have suggested that homozygous loss of NT5C2 function obstructs the development of central white matter structures in the brain leading to this devastating disease (Elsaid, Ibrahim et al. 2017). Additionally, in genome wide association studies, schizophrenia risk alleles have been associated with altered *NT5C2* expression (Duarte, Troakes et al. 2016, Hauberg, Holm-Nielsen et al. 2016). Increased NT5C2 activity levels have also been associated with Lesch-Nyhan syndrome, an X-linked deficiency of the purine salvage enzyme

hypoxanthine-guanine phosphoribosyltransferase (HGPRT) (Pesi, Micheli et al. 2000). NT5C2 was found to dephosphorylate 5'-amino-4-imidazolecarboxamide riboside 5'-monophosphate (ZMP), a byproduct that accumulates in Lesch-Nyhan syndrome, into Z-riboside, which promotes apoptosis of neuroblastoma cell lines in culture. Thus it is postulated that increased NT5C2 activity in Lesch-Nyhan syndrome contributes to neurologic impairment in this disease as well.

In the context of chemotherapy, NT5C2 can also dephosphorylate and inactivate the cytotoxic thiopurine monophosphate nucleotides 6-thioinosine monophosphate (6-tIMP), 6-thioxanthine monophosphate (6-tXMP) and 6-thioguanosine monophosphate (6-tGMP) which are generated by the incorporation of 6-thioguanine (6-TG) and 6-mercaptopurine (6-MP), two thiopurine nucleoside analogs used in the treatment of acute lymphoblastic leukemia, into the salvage pathway of purine biosynthesis (Figure 1.2) (Brouwer, Vogels-Mentink et al. 2005). Thus, *NT5C2* mutations have been identified in relapsed ALL patient samples following thiopurine based maintenance therapy. Additionally, increased expression of *NT5C2* is correlated with worse disease-free survival in acute myeloid leukemia (Galmarini, Cros et al. 2005) and increased NT5C2 activity has also been associated with resistance to 2-chlorodeoxyadenosine (2-CdA) treatment in patients with hairy cell leukemia (HCL) and in refractory chronic lymphocytic leukemia (CLL) (Kawasaki, Carrera et al. 1993).

III. NT5C2 inhibitors

As NT5C2 plays a crucial role not only in regulating endogenous purine levels in the cell, but also in the efficacy of thiopurine therapy within the cell, NT5C2 is a relevant clinical target for developing therapeutics to decrease therapy resistance and regulate purine catabolism in patients with altered nucleotide metabolism.

Small molecule drug screening

Ideally, the first step in drug development is identifying a clear, druggable, target. In terms of screening, it is best to have a target that the biologic response can be measured *in vitro* and *in vivo* (Hughes, Rees et al. 2011). With these parameters, chemical library screening has become a major component of drug design. In current research trends, there are four common compound screening strategies: (i) Virtual library screening (ii) high throughput screening of natural and synthetic chemical libraries with no prior chemotype knowledge, (iii) screening of fragment based chemical libraries and (iv) screening for physiologic activity with follow up mechanism of action studies.

Virtual screening, which originated in the 1970s, is based around using computational models and algorithms to identify potential bioactive molecules (Shoichet 2004, Schneider 2010). Virtual screening relies on *in silico* interrogation of a crystal structure with a library of chemical compounds in attempts to identify ligands that bind to targetable pockets. Although virtual screening is a fairly cost effective method of screening chemicals, it relies heavily on assumptions of binding energies in an aqueous environment and sampling of various conformations of flexible compounds and thus results in fairly high rates of false-negative and false-positive predictions (Shoichet 2004).

In recent years, high throughput large library screening of natural compounds and synthetically designed compounds has become the standard for identifying novel therapeutics (Mayr and Bojanic 2009, Connor, Beckmann et al. 2012, Lachance, Wetzel et al. 2012). These screens typically proceed with a large initial screen of hundreds of thousands of compounds followed by secondary synthesis and verification of top hits,

testing for dose dependent activity in the screening assay, and finally secondary assay analyses to avoid off-target compounds that directly interfere with screening assay (Figure 1.12). These high throughput based library screens are particularly important when no prior knowledge is know about the chemotype likely to show activity against the target of interest and provide an unbiased approach to drug design. If virtual screening has been done or if previous lead compounds have been identified, screening of more focused libraries in a similar manner is particularly useful for a more knowledge-based screening library. These more targeted library screens are normally used and designed to parse out structure-activity relationships of the lead compound or to improve medicinal chemistry properties such as solubility, cell permeability, and increased potency.

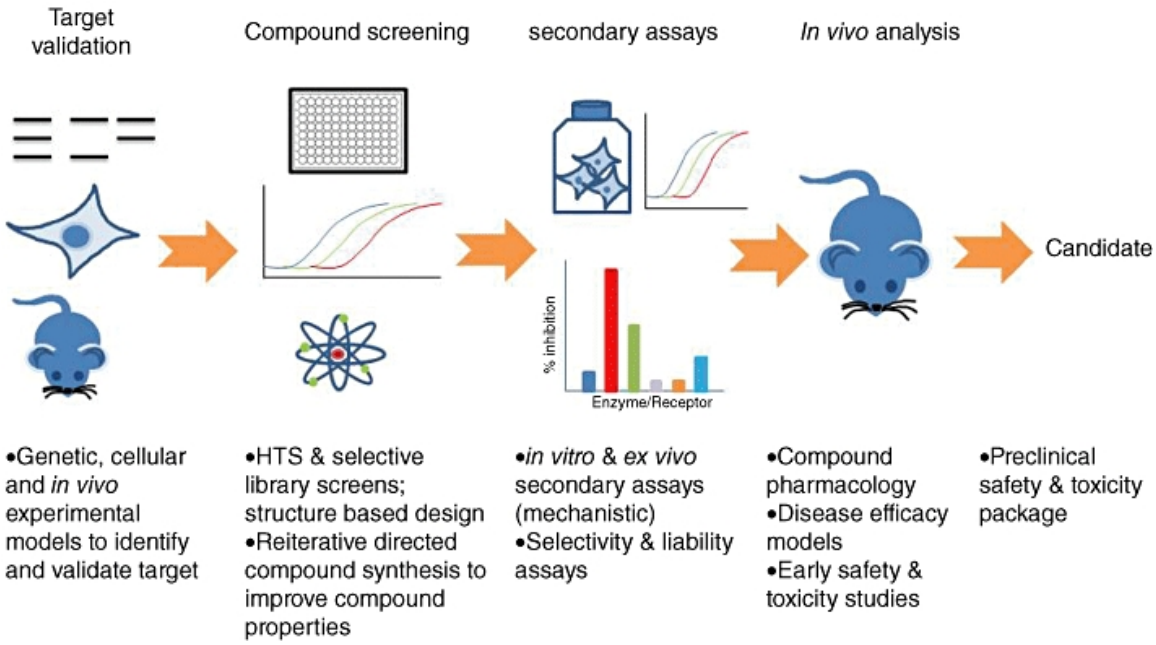

Figure 1.12 – Overview of drug discovery screening assays. Adapted from Hughes *et al* 2011.

In contrast to high throughput screens, fragment-based drug discovery (FBDD) screening consists of screening smaller libraries of very small molecular weight compounds at high concentrations. FBBD relies on low affinity interactions and allows

for screening of low-complexity and diverse chemicals to use as building blocks in the development of a more potent inhibitor (Hajduk and Greer 2007).

In addition to these targeted chemical library screens against recombinant protein, some screens are also performed in a cellular or organism based model to retain endogenous protein function (Swinney and Anthony 2011). These screens come with the advantage of maintaining a physiologic setting for drug activity, but require follow up studies to identify the direct target of the compound of interest and have the potential for unacknowledged off-target effects (Schenone, Dancik et al. 2013).

Importantly, as more and more academic and industry groups perform large-scale compound activity screens, chemical databases cataloguing compounds and their bioactivity such as ChEMBL (Gaulton, Hersey et al. 2017) and PubChem (Wang, Bryant et al. 2017) have been developed to aid researchers as they move through the drug development pipeline. In addition to these useful tools and resources for improved small molecule designs, a number of rules and guidelines have been established for developing inhibitor screens and ideal chemical qualities for new drugs:

High throughput screen assay development

The majority of chemical screening assays rely on robust activity based screens on recombinant protein or in cellular based systems. Most assays used routinely in basic lab settings need to be optimized and adapted for high throughput screening due to the large scale capacity of these screens. With increasingly large library sizes, researchers need to consider speed, efficiency, and low reagent consumption as well as ensuring the assay is robust, sensitive, reproducible and accurate in order to ensure quality results over a long period of time with batch and reagent variability. A lot of these parameters

are met with the use of high capacity 384 or 1536-well plates as well as robotics and automated liquid handling systems (Zhang, Chung et al. 1999, Hughes, Rees et al. 2011).

Most importantly, as most assays are run in singlet or duplicate to minimize reagent costs, the assay must be accurate and sensitive in its ability to identify a 'hit'. This quality is assessed by the Z-score of the assay. As high throughput assays have a high level of variability including random instrumental and human-based error, the Z-score takes these factors into account to ensure accurate differential readings regardless of variability in the assay (Figure 1.13) (Zhang, Chung et al. 1999). To ensure a large enough separation of control and sample wells, the ideal high throughput assay should have a Z-score equal to or higher than 0.5.

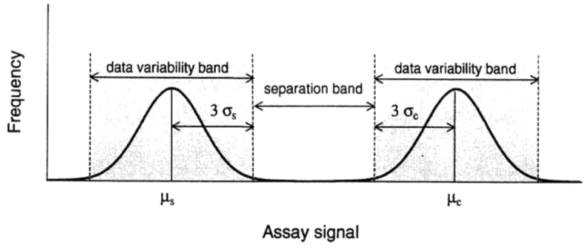

$$Z = 1 - \frac{3SD \text{ of sample} + 3SD \text{ of control}}{|\text{mean of sample} - \text{mean of control}|}$$

Figure 1.13 – Z-score for assessing high throughput assay variability and reliability. (Left) Illustration of the defined data variation band and separation band in an HTS assay. (Right) Z-score formula. Adapted from Zhang et al 1999.

In particular, for enzyme assays in high throughput conditions, additional parameters should be considered. In order to identify competitive inhibitors of an enzymatic reaction, it is essential to perform the assay under initial velocity conditions at or below the substrate K_m of the reaction. Performing the assay at initial velocity minimizes chances of reaction saturation and ensures that the reverse enzymatic reaction does not take place and interfere with the final readout (Brooks, Geeganage et al. 2004).

Small molecule screen chemical guidelines

With many chemical based screens, researchers have learned to design libraries around certain physiochemical properties to aid in a smoother transition from hit identification to use in pre-clinical and clinical settings. In 1997 Lipinski and colleagues established the Rule of Five to estimate solubility and permeability of chemical compounds used in drug discovery screens: poor absorption or permeation compounds have (i) greater than 5 H-bonds, (ii) 10 H-bond acceptors, (iii) a molecular weigh over 500 or (iv) a calculated LogP (Partition-coefficient) greater than 5 and should not be included in chemical screens (Lipinski, Lombardo et al. 2001). In addition to considering these rules when designing libraries, chemists have also begun to avoid chemicals with known toxicophores or reactive groups, which may interfere with synthesis and lead optimization down the line (Gribbon and Sewing 2005).

NT5C2 inhibitors updates and progress

As NT5C2 activity and expression levels have been implicated in chemotherapy resistance, a number of groups have begun the process of developing NT5C2 inhibitors for the treatment of these patients.

Virtual screening of small a targeted ribonucleoside phosphonates library with follow up enzymatic assays identified two β-hydroxyphosphonate analogues which inhibited NT5C2 activity at low millimolar concentrations isolating a chemotype for further improvement studies (Gallier, Lallemand et al. 2011). Follow up studies with screening of 32 analogues based on these two lead compounds identified two slightly more potent analogues (Figure 1.14): These studies showed that only modest modifications in the sugar were tolerated and that nucleobase modifications were possible but ultimately

showed no increase in inhibitory capacity. Of note these lead β-hydroxyphosphonate compounds are too polar to bypass the cell membranes and thus require further prodrug like modifications before use in preclinical models (Meurillon, Marton et al. 2014). Additionally, *in silico* screening of freely available chemical databases yielded an anthraquinone derivative (AdiS) that was shown to block nucleotidase activity by binding to the allosteric site (Figure 1.14). AdiS showed cytotoxicity in a number of human cell lines at very high micromolar concentrations highlighting the need for further optimization for a more potent and clinically accessible inhibitor (Jordheim, Marton et al. 2013).

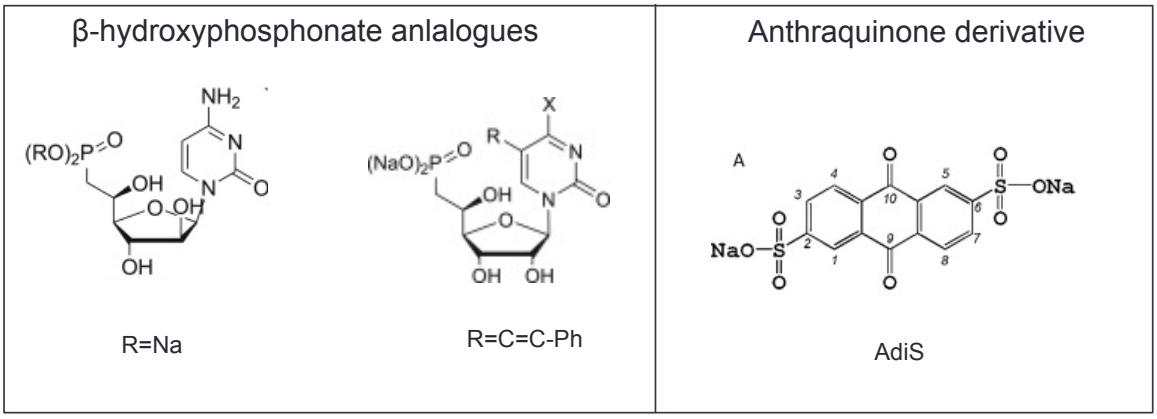

Figure 1.14 – NT5C2 inhibitory compounds identified in the literature. Adapted from Meurillon *et al* 2014 and Jordheim *et al* 2013.

These studies have made great strides in identifying chemical compounds that may bind to and inhibit NT5C2 activity, but further medicinal chemistry is needed in these lead compounds to improve their potency, cytotoxicity, and cell accessibility. Additional high throughput screens and drug development strategies may highlight additional chemotypes and lead molecules for further development of a potent inhibitor of NT5C2.

IV. Specific Aims

Acute lymphoblastic leukemia is the leading cause of cancer in children and adolescents. Although outcomes for these patients has drastically improved over the past 50 years, still 20% of these patients fail to achieve a complete remission, relapse, and succumb to the disease. *NT5C2* has been identified as the most recurrently mutated gene at relapse. There is a clear need to better understand how these *NT5C2* mutations drive clonal evolution and chemotherapy resistance in relapsed ALL in order to better treat these patients and improve overall survival. Thus, my central goal was to perform structure-function and genetic studies to better understand the role of these variants in relapsed ALL and to identify new therapeutics to curtail the emergence of these mutations in relapsed ALL.

Towards this goal, I proposed the following aims:

Aim 1: Perform an in-depth structure-function analysis of *NT5C2* relapse associated mutations.

Aim 2: Understand the role of *NT5C2* mutations in the clonal evolution of chemotherapy resistant relapse.

Aim 3: Therapeutically target *NT5C2* mutant leukemias.

Chapter 2: Structure and Mechanisms of NT5C2 Mutations Driving Thiopurine Resistance in Relapsed Lymphoblastic

Cancer Cell
Article

Structure and Mechanisms of NT5C2 Mutations Driving Thiopurine Resistance in Relapsed Lymphoblastic Leukemia

Chelsea L. Dieck,[1,12] Gannie Tzoneva,[1,9,12] Farhad Forouhar,[2,3,12] Zachary Carpenter,[4] Alberto Ambesi-Impiombato,[1,10] Marta Sánchez-Martín,[1,11] Renate Kirschner-Schwabe,[5] Scott Lew,[3] Jayaraman Seetharaman,[6] Liang Tong,[3,*] and Adolfo A. Ferrando[1,4,7,8,13,*]

[1]Institute for Cancer Genetics, Columbia University, New York, NY 10032, USA
[2]Hervert Irving Comprehensive Cancer Center, Columbia University, New York, NY 10032, USA
[3]Department of Biological Sciences, Northeast Structural Genomics Consortium, Columbia University, 1212 Amsterdam Avenue, 701 Fairchild Center, New York, NY 10027, USA
[4]Department of Systems Biology, Columbia University, New York, NY 10032, USA
[5]Department of Pediatric Oncology/Hematology, Charité-Universitätsmedizin Berlin, Berlin 10117, Germany
[6]New York Structural Biology Center, New York, NY 10027, USA
[7]Department of Pediatrics, Columbia University Medical Center, 1130 St. Nicholas Avenue, ICRC 402, New York, NY 10032, USA
[8]Department of Pathology and Cell Biology, Columbia University Medical Center, New York, NY 10032, USA
[9]Present address: Regeneron Pharmaceuticals, 777 Old Saw Mill River Road, Tarrytown, NY 10591, USA
[10]Present address: PsychoGenics, 215 College Road, Paramus, NJ 07652, USA
[11]Present address: IBM Watson Health, 75 Binney Street, Cambridge, MA 02142, USA
[12]These authors contributed equally
[13]Lead Contact
*Correspondence: ltong@columbia.edu (L.T.), af2196@columbia.edu (A.A.F.)
https://doi.org/10.1016/j.ccell.2018.06.003

SUMMARY

Activating mutations in the cytosolic 5′-nucleotidase II gene *NT5C2* drive resistance to 6-mercaptopurine in acute lymphoblastic leukemia. Here we demonstrate that constitutively active NT5C2 mutations K359Q and L375F reconfigure the catalytic center for substrate access and catalysis in the absence of allosteric activator. In contrast, most relapse-associated mutations, which involve the arm segment and residues along the surface of the inter-monomeric cavity, disrupt a built-in switch-off mechanism responsible for turning off NT5C2. In addition, we show that the C-terminal acidic tail lost in the Q523X mutation functions to restrain NT5C2 activation. These results uncover dynamic mechanisms of enzyme regulation targeted by chemotherapy resistance-driving *NT5C2* mutations, with important implications for the development of NT5C2 inhibitor therapies.

INTRODUCTION

NT5C2 is a highly conserved and ubiquitously expressed cytosolic nucleotidase involved in the maintenance of intracellular nucleotide pool homeostasis by promoting the clearance of excess purine nucleotides from cells (Allegrini et al., 1997; Bandistelli et al., 1996; Hunsucker et al., 2005; Itoh et al., 1967; Pesi et al., 1994; Spychala et al., 1988; Tozzi et al., 1991). NT5C2 preferentially dephosphorylates the 6-hydroxypurine monophosphates inosine monophosphate (IMP), guanosine monophosphate (GMP), and xanthosine monophosphate, as well as the deoxyribose forms of IMP and GMP (dIMP and dGMP), facilitating the export of the resulting purine nucleosides out of the cell (Hunsucker et al., 2005). The importance of this activity for cell homeostasis is highlighted by the association of loss-of-function mutations in *NT5C2* with hereditary spastic paraplegia in

Significance

Gain-of-function *NT5C2* mutations are highly prevalent in high-risk early relapse leukemia making NT5C2 the most prevalent therapeutic target in relapsed acute lymphoblastic leukemia. Here we identify distinct mechanisms of NT5C2 regulation targeted by relapse leukemia-associated *NT5C2* mutations. These results support a critical role of negative regulators of allosteric activation in the control of NT5C2 activity pointing to the allosteric effector site as a potential therapeutic target for the development of NT5C2 inhibitors.

Leukemia

humans (Novarino et al., 2014). Yet, perhaps the most prominent role of NT5C2 in human disease results from the capacity of this enzyme to dephosphorylate and inactivate cytotoxic thiopurine monophosphate nucleotides—6-thioinosine monophosphate, 6-thioxanthosine monophosphate, and 6-thioguanosine monophosphate—generated by the incorporation of 6-thioguanine (6-TG) and 6-mercaptopurine (6-MP), two thiopurine nucleoside analogs used in the treatment of lymphoblastic leukemia, into the salvage pathway of purine biosynthesis (Brouwer et al., 2005). In this context, somatic gain-of-function mutations in *NT5C2* encoding proteins with increased nucleotidase activity drive selective resistance to chemotherapy with 6-MP and 6-TG and are recurrently present in acute lymphoblastic leukemia (ALL) samples at relapse, with a prevalence as high as 35%–45% in early relapse ALL cases progressing under 6-MP chemotherapy (Ma et al., 2015; Meyer et al., 2013; Tzoneva et al., 2013, 2018).

Structurally, NT5C2 is a member of the haloacid dehalogenase (HAD) superfamily of Mg^{2+}-dependent intracellular 5′-nucleotidases (Koonin and Tatusov, 1994) and functions as a homotetramer made up of a dimer of two tightly associated dimers (Wallden et al., 2007). Mechanistically, the 5′-nucleotidase activity of NT5C2 proceeds via formation of a phosphoenzyme intermediate mediated by three conserved HAD motifs in the catalytic center (Allegrini et al., 2001; Collet et al., 1998). Motif I, DXDX(V/T) (L/V), is most integral to the reaction mechanism, in which the first Asp (Asp52 in NT5C2) makes a nucleophilic attack on the phosphate of the substrate and the second Asp (Asp54 in NT5C2) donates a proton to the departing nucleoside. Motif II is a (S/T) residue (Thr249 in NT5C2) which stabilizes the phosphoenzyme intermediate, and motif III, $K(X_x)D(X_{0-4})D$, contains a highly conserved Lys (Lys292 in NT5C2), which also contributes to the stabilization of the intermediate by countering some of the negative charges. In addition, motif III contains Asp351 and Asp356 in NT5C2, which interact with an essential Mg^{2+} ion involved in the catalysis. Moreover, Asp54 in motif I also helps to coordinate the Mg^{2+} ion, while Met53 and Thr56 (motif I) are important for the correct orientation of all Asp residues. These elements define the structural components required for the catalytic activity of NT5C2.

NT5C2 functions as a dimer of dimers, with the dimer being the smallest functional unit with enzymatic activity (Spychala et al., 1988; Wallden and Nordlund, 2011) and is regulated by allosteric activators with ATP, dATP, and diadenosine tetraphosphate (Ap_4A) as the most likely activators at physiological concentrations (Marques et al., 1998; Pinto et al., 1986; Spychala et al., 1988). The effector binding site of NT5C2 is located close to the subunit interface, with two ATP molecules binding back-to-back to each subunit of the dimer. Comparison of the basal (apo) and active (allosteric effector bound) structures of NT5C2 revealed a role of the Gly355-Glu364 region in the allosteric activation of the enzyme. This segment (helix A) is disordered in the apo inactive form of the enzyme and adopts an ordered α helix conformation in the effector-bound activated state. This conformational change facilitates substrate binding and catalysis by inducing a rotation of Phe354 out of the active site and by moving Asp356 into the catalytic center (Wallden and Nordlund, 2011). The relevance of helix A in the activation of NT5C2 is supported by modeling studies implicating local conformational changes in this region as responsible for the increased nucleotidase activity of a strongly activating NT5C2 mutation mapping to this site (NT5C2 p.K359Q) (Tzoneva et al., 2013). Yet, the majority of NT5C2 mutations found in relapse ALL are located outside of this helix A region, suggesting that additional regulatory elements may be involved in the control of NT5C2 activity. However, these mutations show an apparent random spatial distribution in the structure of the enzyme and their mechanisms of action remain to be established.

RESULTS

Functional Heterogeneity of NT5C2 Mutations in Relapsed ALL

To gain further insight on the role and mechanisms of *NT5C2* in resistance to 6-MP chemotherapy we compiled allelic data on 643 relapsed ALL cases along with previously published data (Kunz et al., 2015; Ma et al., 2015; Meyer et al., 2013; Oshima et al., 2016; Richter-Pechanska et al., 2017; Tzoneva et al., 2013, 2018) identifying in all 32 independent *NT5C2* mutant alleles consisting of 27 single amino acid substitutions, four in-frame indel mutations (p. Asp396_Ala400del, p.Lys404delinsLysAsp, p. Ser408_Asp415del, and p.Ser445_Arg446delinsPhe_Gln) and a C-terminal truncating mutation (p.Gln523*) (Figure 1A; Table S1) under the supervision of the Columbia University Institutional Review Board. Gain-of-function mutations resulting in increased enzymatic activity typically cluster in defined protein domains involved in enzyme regulation (Gao et al., 2017; Tamborero et al., 2013). In this context, we identified recurrent relapsed leukemia-associated NT5C2 mutations involving Arg39, Arg238, Arg367, Leu375, Asp407, and Pro414 supporting a potentially important role of these residues in the control of NT5C2 activity. However, each of these recurrent mutations show inexplicit functional features and none of them are located in the catalytic regulatory helix A region.

To functionally explore the role of NT5C2 mutations as drivers of increased nucleotidase activity and thiopurine resistance, we tested their activity and response to ATP allosteric activation (Marques et al., 1998; Pinto et al., 1986; Spychala et al., 1988) in *in vitro* nucleotidase assays. These analyses revealed distinct patterns of enzymatic activity and responses to ATP. Purified recombinant NT5C2 K359Q and NT5C2 L375F (class I mutations) showed markedly increased basal nucleotidase activity with reduced response to allosteric activation (~1.5-fold increase over basal at 0.3 mM ATP), below that observed in wild-type (WT) recombinant NT5C2 (2.6-fold over basal at 0.3 mM ATP) (Figure 1B). In contrast, most relapse-associated activating NT5C2 alleles (R39Q, R238W, R367Q, D407A, S408R, S445F, and R478S) (class II mutations) showed increased nucleotidase activity with retained or increased dynamic response to ATP allosteric regulation (2.3- to 4.6-fold over basal at 0.3 mM ATP) (Figure 1C). Finally, a C-terminal truncated mutant protein, NT5C2 Q523X, showed nucleotidase activity levels similar to those of the WT NT5C2 in basal conditions but was hyper-responsive (6.5-fold over basal at 0.3 mM ATP) to allosteric activation (class III mutation) (Figure 1D).

NT5C2 Structure and Activation-Associated Conformational Changes

To investigate the molecular basis mediating the heterogeneous patterns of activity of NT5C2 activating mutations, we

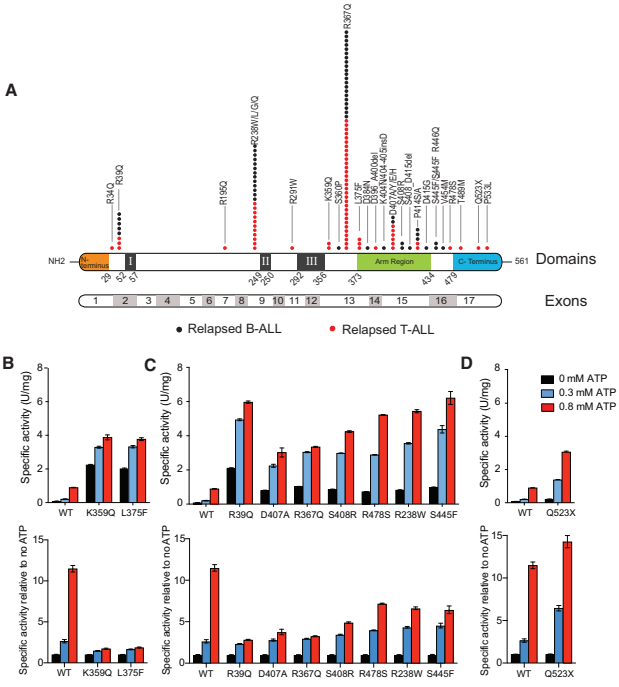

Figure 1. Distribution and Activity Profile of NT5C2 Mutations in Human-Relapsed Acute Lymphoblastic Leukemia

(A) Graphical representation of relapse-associated mutations in B-ALL (black) and T-ALL (red). HAD core motifs are shown in black rectangles with roman numerals.

(B–D) *In vitro* nucleotidase assays assessing the enzymatic activity of class I (B), class II (C), and class III (D) NT5C2 mutations in the presence of increased concentrations of ATP represented as specific activity (top) and specific activity relative to no ATP (bottom). Data in (B–D) are shown as mean ± SD. See also Table S1.

determined crystal structures of the basal and active states of relapse-associated mutants and WT full-length human NT5C2 proteins at up to 1.8 Å resolution (Figures S1A–S1D; Tables S2 and S3). The structure of the full-length human NT5C2 monomer revealed a HAD core (residues 30–372 and 435–478) with three extensions consisting of the N-terminal (residues 1–29), helical arm (residues 373–434), and C-terminal (residues 479–561) regions (Figures 2A–2F). Moreover, analysis of the structures of WT human NT5C2 in the basal (Apo) and the activated (P_i bound in the effector site) state show marked conformational and functional changes in the monomer (Figures 2A and 2B), dimer (Figures 2C and 2D), and tetramer (Figures 2E and 2F) of the enzyme upon activation, which were selectively altered by each class of NT5C2 mutations. Moreover, analysis of the buried surface area at the interface of two different (strong and weak) dimers, forming the NT5C2 tetramer showed that the strong dimer in each basal structure appears to bury twice as much area at its dimer interface compared with its active counterpart, supporting that the NT5C2 dimer and tetramer adopt a more open configuration upon allosteric activation (Figures S1E and S1F; Table S4).

Mechanism of NT5C2 Class I Mutations

In agreement with previous studies (Wallden and Nordlund, 2011), we observed residues 353–363 in the HAD core of NT5C2 change from a loop structure to a helix (helix A) upon activation. This conformational change is triggered by electrostatic interactions between Lys362 and the phosphate moieties of the ATP effector and mediates the activation of the enzyme by moving Phe354 out of and Asp356 into the active site, enabling it for substrate binding and catalysis (Figure S2) (Wallden and Nordlund, 2011). Of note, this active structure is stabilized by ionic interactions between Lys361 in helix A and Asp459, which is also positioned between Arg39 and Arg367 (Figure S2). Notably, analysis of the crystal structures of NT5C2 K359Q (Figure 3A) and NT5C2 L375F (Figures 3B and 3C), showed that this mechanism is hijacked by these class I NT5C2 mutants, which adopt an active conformation even without ATP or P_i bound in the effector site. Thus, and consistent with modeling analyses (Tzoneva et al., 2013), in NT5C2 K359Q, a mutation located within the helix A region of NT5C2, the Gln359 side chain contacts both the backbone and the side chain of Phe354, thereby promoting the formation of an active helix A configuration (Figure 3A). In addition, the presence of Gln at position 359 alters the neighboring network of interactions between Lys361 and Asp459 by abolishing one of two hydrogen bonds between Arg367 and Asp459, thereby allowing for increased stabilization of helix A (Figure 3A). Notably, the helix A region in the second class I mutant protein NT5C2 L375F is also organized in an active helical conformation in the absence of ATP or P_i (Figure 3B), as observed previously (Hnizda et al., 2016, 2018). Yet, the specific mechanisms driving this active conformation were not directly apparent as Leu375 is located away from the helix A region (Figure 3C). Mechanistically, detailed inspection of the NT5C2 L375F full-length structure revealed that the extra bulk of the Phe side chain forces a shift of ~1 Å in the Cα position of L375F and displaces the underlying helical arm (Figure 3C). As a result, Arg98, which makes two salt bridges with Glu373, and one hydrogen bond with the backbone of Asn154 in basal and active WT NT5C2 and NT5C2 K359Q, makes only one salt bridge with Glu374 in NT5C2 L375F, which, in turn, favors the interaction of Phe450 with Ile353 and an active conformation of helix A

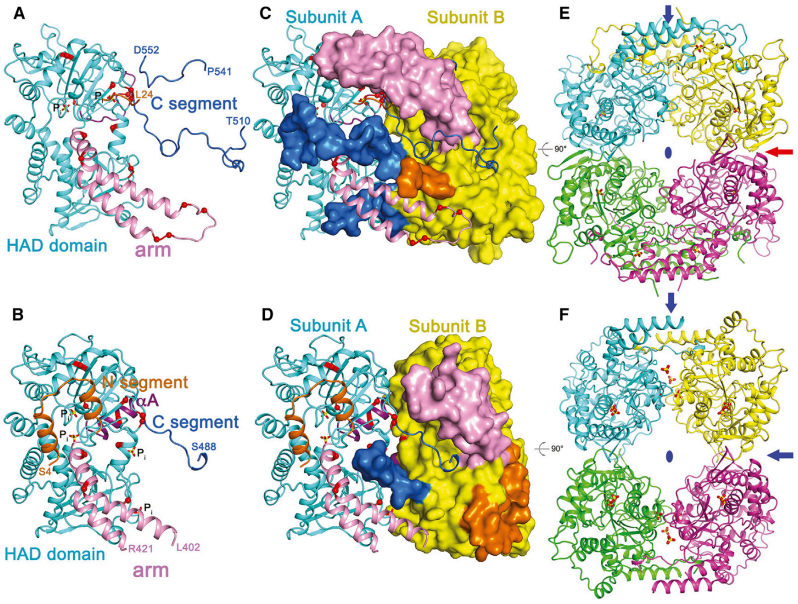

Figure 2. Crystal Structure of Basal and Activated WT Human NT5C2

(A) A Ribbon diagram of the basal structure of the full-length WT NT5C2, displaying the HAD domain (cyan) and its three extensions: N-terminal segment (orange), arm region (pink), and C-terminal segment (marine). The mutation sites are depicted as red solid spheres for Cα of each mutated amino acid. The phosphate (yellow for phosphorus) ions are depicted as stick models and labeled as P_i. The N and C termini amino acids (L24 and D552), and the termini amino acids (T510 and P541) of the disordered region in the C segment are also labeled.

(B) A ribbon diagram of the active structure of NT5C2 WT, in which the allosteric helix A (αA) is shown in dark purple. The N and C termini amino acids (S4 and S488), and the termini amino acids (L402 and R421) of the disordered region in the arm segment are also labeled.

(C and D) Ribbon and surface (for subunit B) depictions of basal (C) and active (D) dimers of WT.

(E and F) Ribbon diagrams of the basal (E) and active (F) WT tetramers, respectively. Solid blue oval and blue arrows represent crystallographic 2-fold, while solid red arrow represents non-crystallographic 2-fold. See also Figure S1 and Tables S2, S3, and S4.

(Figure 3B). In addition, the Phe side chain introduced by the L375F mutation also engages in enhanced interactions with hydrophobic residues Phe36, Leu379, Phe441, Tyr461, and His486 from the neighboring NT5C2 subunit through favorable π-stacking (Figure 3C). These results demonstrate that an active conformational state of the helix A region in the absence of allosteric modulator mediates the gain-of-function properties of NT5C2 K359Q and NT5C2 L375F class I mutants.

Although the underlying mechanisms mediating the increased activity of non-class I NT5C2 mutant proteins did not became directly apparent in the analyses of the conformational changes in the helix A segment, it did not escape our attention that activation-associated changes in NT5C2 also involve shifts in the position of the helical arm and the C-terminal segments (Figures 2A–2F). We hypothesized that despite their distant location from the catalytic site, these elements could also have a regulatory role with potentially important implications for understanding the mechanisms of action of class II and class III NT5C2 mutant proteins.

Mechanism of NT5C2 Class II Mutations

Close inspection of the distribution of class II NT5C2 mutations revealed a group of NT5C2 alleles (R39Q, R238W/L/G/Q, R367Q, S445F_R446Q, and R478S) located in a positively charged pocket at the interface of the tightly associated dimer (Figures 2A–2D and S3A), while a second group of class II mutations (K404N, 404-405insD, D407A/Y/E/H, S408R, P414S/A, and D415G) locate in the tip region of the arm segment (Figures 2A–2D). Notably, all class II NT5C2 mutant variants characterized in our enzymatic assays localize in these two regions. Based on this observation we proposed that class II mutants located in the positively charged pocket region (R39Q, R367Q, S445F, R238W, and R478S) and loop segment (D407A and S408R) could share a common mechanism of action. Consistently, the crystal structures (Table S2) of a recurrent mutation (R238W) involving the R238 residue located in the protein surface adjacent to the entrance of the inter-subunit pocket (Figure S3B), the structure of a representative allele (D407A) involving the D407 residue in the tip region of the arm segment (Figure S3C),

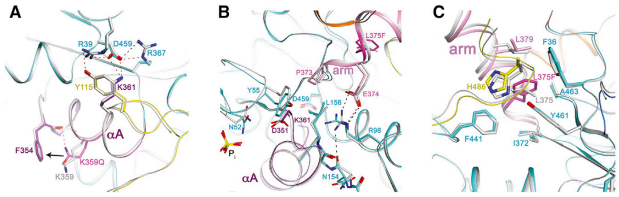

Figure 3. Crystal Structures of Class I NT5C2 Mutants

(A) Structure overlay of the active full-length WT NT5C2 (gray for Cα atoms) and the constitutively active K359Q NT5C2-537X (K359Q-537X) (color), in which the interaction between K359Q and F354 is shown. The hydrogen bonds are shown in red dashed lines and black, the latter of which is present only in the structure of WT.

(B) Structure overlay of L375F (color) with the active WT (gray). The residues affected by the L375F mutation are shown with stick models and colored accordingly.

(C) Structure overlay of WT (gray) and the constitutively active full-length NT5C2 L375F (L375F) (color), shows the mutation site L375F at the base of the arm extension. The hydrophobic residues surrounding L375F are shown as stick models and labeled. See also Figure S2.

and that of two recurrent class II pocket mutations (R39Q and R367Q) involving basic amino acids at the bottom of the positively charged inter-subunit pocket (Figure S3D), showed a common conformation in which the helix A region adopted an active structure similar to that of WT NT5C2 in the presence of allosteric activator (Figures 4A–4D). These results support that the positively charged pocket and the tip of the arm segment could form a single functional unit.

In considering the potential mechanism mediating the effects of NT5C2 class II mutants it is worth noting that NT5C2 activation results in dynamic configuration changes of the tip region of the arm segment. Specifically, the loop at the tip of the helical arm segment of NT5C2 establishes intimate contacts with the other monomer in the basal structure, yet these contacts are lost upon activation, with the helical arm pivoting away from the other monomer and the tip region becoming disordered upon allosteric activation, supporting a role for this element in NT5C2 regulation (Figures 2A–2F).

To evaluate the regulatory capacity of the tip of the helical arm segment we performed a CRISPR/Cas9 gain-of-function screen. While CRISPR/Cas9-induced frameshifts and in-frame indels targeting critical enzymatic domains are likely to be loss-of-function, in-frame alleles involving negative regulatory domains can produce protein variants with increased enzymatic activity (Donovan et al., 2017; Ipsaro et al., 2017). Such gain-of-function alleles are selectable in functional screens by their capacity to confer resistance to specific inhibitors (Donovan et al., 2017; Ipsaro et al., 2017). Here we aimed to test the potential role of the tip region of the arm segment as a potential negative regulator of NT5C2 activity following this strategy. Toward this goal we expressed Cas9 and gRNAs targeting two sites in the *Nt5c2* locus at codons H405 and I416 in the tip segment of the arm domain in mouse leukemia lymphoblast cells and then selected potential gain-of-function CRISPR-directed non-homologous end joining generated mutations resulting in increased NT5C2 nucleotidase activity for their capacity to confer resistance to 6-MP (Figure S4A). Deep sequencing analysis of CRISPR/Cas9-induced mutations treated with 6-MP revealed a positive selection of *Nt5c2* in-frame indels and point mutations compared with vehicle-treated controls (Figures 5A and 5B). Characterization of a selection of positively selected in-frame alleles demonstrated gain-of-function effects with increased nucleotidase activity (Figure S4B; Table S5). Consistently, extended targeted mutation analysis of the tip region of the arm segment of *NT5C2* in relapsed ALL patient samples identified an in-frame *NT5C2* deletion removing much of this element (delS408-D415) (Figure S4C). Notably, this mutation behaved as a class II gain-of-function allele in enzymatic assays and conferred resistance to 6-MP chemotherapy when expressed in ALL cell lines (Figures S4D and S4E). In all, these results support that local disruption of the tip region of the arm segment of NT5C2 leads to deregulated enzymatic activity, and point to this segment as a negative regulatory element disrupted by a subset of class II *NT5C2* mutations in relapsed ALL.

Should the tip of the arm segment and the positively charged inter-monomeric pocket targeted by class II NT5C2 mutations form a bipartite regulatory unit, then we predicted that these two regions could physically interact. In support of this possibility, the tip region of the arm segment of NT5C2 (Ser408) contacts the neighbor subunit (Arg238) in the absence of allosteric activator, which places Asp407, a recurrently mutated residue in the tip region, at the entrance of the positively charged dimer interface (Figure S4F). Moreover, molecular modeling analyses of the arm segment of NT5C2 revealed that, following allosteric stimulation, the NT5C2 Glu401-Asp415 segment can invade the positively charged inter-subunit pocket, which opens up upon activation (Figures 5C and S4G). Notably, the Asp407 residue targeted by recurrent mutations in the arm segment plays an important role in this transition by interacting with positively charged residues along the surface of the inter-subunit pocket (Figure S4G). Markedly, the most favorable (lowest potential energy) conformation for Asp407 in the activated state of NT5C2 places this residue interacting via hydrogen bonding with Lys361 on the helix A segment of the neighboring protomer (Figure S4H). This contact, in turn, would destabilize the interaction between Lys361 and Asp459 responsible for maintaining the enzyme in the activated state (Figure 5D) and return NT5C2 to its basal inactive conformation. Based on these results we propose that class II mutations would disrupt the dynamic movement of the tip region of the arm domain through this inter-monomeric cavity (Figure S4).

To formally test this model, we blocked the dynamic movement of the tip region of the arm segment loop containing Asp407 in WT NT5C2 using two independent antibodies against this element and tested the effects of this perturbation in NT5C2 activity. In these experiments, incubation of WT NT5C2 recombinant protein with tip region antibodies resulted in increased NT5C2 nucleotidase activity in basal conditions and, upon

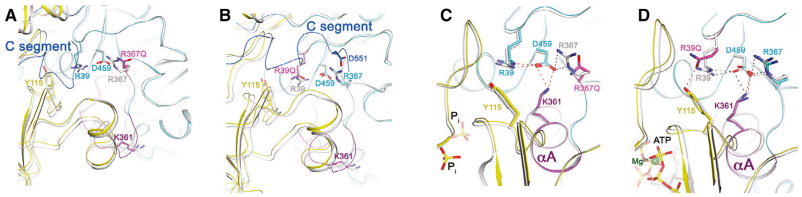

Figure 4. Crystal Structure of NT5C2 Class II Mutations

(A) Structure overlay of the basal full-length NT5C2 R367Q (R367Q) (color) and the basal full-length WT NT5C2 (gray for Cα atoms), displaying the side chains of important residues near effector binding site.

(B) Structure overlay of the basal full-length NT5C2 R39Q (color) and the basal WT NT5C2 (gray for C atoms), displaying the side chains of important residues near effector binding site. A salt bridge between R367 (in cyan) and D551 (in marine) from the C-terminal segment is shown with a red dashed line.

(C) Structure overlay of the active R367Q (color) and the active WT (gray), showing the mutant R367Q does not form a hydrogen bond with D459. The two phosphate ions, present in the active WT are depicted as stick models.

(D) Structure overlay of the active full-length NT5C2 R39Q (R39Q) (color) and the active WT (gray). ATP and Mg^{2+} ion, present in the R39Q structure, are depicted as a stick model and a dark green solid sphere, respectively. The hydrogen bonds in the R39Q structure are shown as red dash lines, while the black dash lines represent the hydrogen bonds in the active WT structure. See also Figure S3.

allosteric activation, phenocopying the effect of class II mutations (Figure 5E). Importantly, the activating effect of these NT5C2 antibodies was reversed by pre-incubation with a tip region peptide (Figure 5E). In all, these results identify a dynamic switch-off NT5C2 auto-regulatory mechanism mediated by the interplay of the tip of the arm segment and the positively charged inter-monomeric pocket targeted by class II relapsed-associated NT5C2 mutations.

Mechanism of the Class III NT5C2 Q523X Mutation

Distinct from class I and class II mutations, the Q523X C-terminal truncating mutant shows nucleotidase activity levels similar to that of WT NT5C2 but a more dynamic response to allosteric activation, in support of a third mechanism of NT5C2 regulation (Figure 6A). Of note, the C-terminal region of NT5C2 is highly conserved in vertebrates and contains a stretch of acidic residues at its end (Figure 6B). Moreover, this segment undergoes major conformation changes in the context of NT5C2 activation, suggesting a regulatory role for this region (Figures 2A–2F).

In the absence of an allosteric regulator, the C-terminal segment of one NT5C2 subunit (residues 479–510 and 537–553) folds over the base of the arm segment of the neighboring protomer so that the acidic C-terminal tail introduces itself into the positively charged inter-subunit pocket promoting a compact dimer and a tightly associated NT5C2 tetramer conformation (Figures 6C, 6D, and S5A). Of note, this tightly closed conformation is released in the allosterically activated structure of NT5C2 in which the C-terminal is no longer visible at the dimer interface and is also displaced from the surface of the neighboring subunit by the N-terminal segment (Figure S5B). These results support that the acidic tail of NT5C2 may provide a hindrance toward NT5C2 activation by stabilizing the closed inactive conformation of the enzyme. To functionally evaluate the role of the C-terminal segment of NT5C2 and its interaction with the positively charged inter-subunit pocket in the control of NT5C2 activation we tested the effects of incubating WT NT5C2 protein with polyclonal antibodies recognizing the C-terminal acidic tail in nucleotidase assays. In these experiments two independent antibodies recognizing the C-terminal acidic tail of NT5C2 induced increased enzymatic activity in response to allosteric activation (Figure 6E). Moreover, the activating effect of these antibodies was reversed by pre-incubation with a NT5C2 C-terminal tail blocking peptide, indicating that disrupting the interaction of the C-terminal acidic tail of NT5C2 with the positively charged inter-subunit pocket by antibody binding can reproduce the effects of the class III NT5C2 Q523X mutation (Figure 6E). Finally, and as predicted by this model, the apo crystal structure of NT5C2 Q523X (Table S2) revealed a dimer structure more open than that present in the apo form of NT5C2 full-length crystals (Table S4), and its active structure showed a helix A conformation similar to that of active WT NT5C2 (Figures 6F and S1). In heterozygous NT5C2 mutant cells, both homotypic and heterotypic dimers should be present (Figure S5C). In cells harboring the *NT5C2* Q523X mutant allele, homotypic (Q523X/Q523X or WT/WT) and heterotypic (WT/Q523X) dimers can be combined in six different tetramer configurations (WT/WT + WT/WT; WT/WT + WT/Q523X; WT/Q523X + WT/Q523X; Q523X/Q523X + Q523X/WT; Q523X/Q523X + WT/WT; and Q523X/Q523X + Q523X/Q523X). In this context we predict that the "opening" effect of the Q523X truncating mutation would be most prominent in homotypic mutant dimer (Q523X/Q523X) containing tetramers compared with complexes containing heterotypic (WT/Q523X) protein pairs. Yet, in all, our results support that loss of the C-terminal tail of NT5C2 in the Q523X class III mutation decreases the threshold for allosteric NT5C2 activation by promoting a more relaxed dimer and tetramer configuration.

DISCUSSION

Detailed functional understanding of the action of biological molecules involved in disease is essential for the development of rational therapeutic strategies, yet deciphering the underlying role of dynamic components based on structural information remains a daunting task. The structural and biochemical studies of NT5C2 presented here provide significant insights into the mode

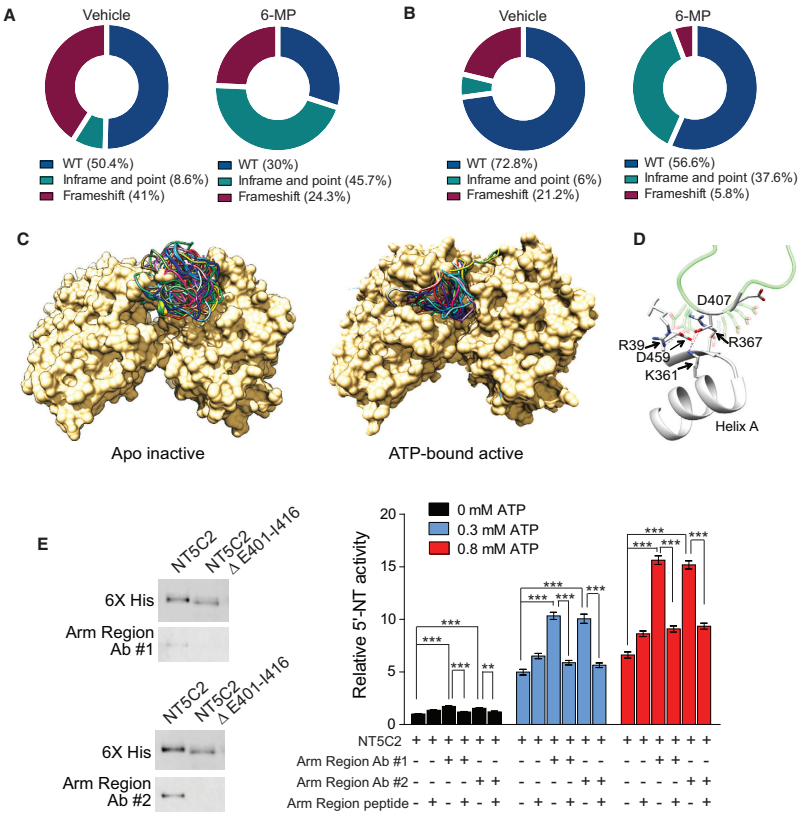

Figure 5. Functional Characterization and Modeling of the Arm Segment Region Targeted by Class II NT5C2 Mutations

(A and B) Graphical representation of mutations selected for in murine leukemic cells infected with a gRNA targeting H405 (A) or I416 (B) after treatment with vehicle or 2 μM 6-MP.

(C) Modeling analysis of the top 20 preferred conformations of the flexible arm segment in the inactive and allosterically activated NT5C2.

(D) A close-up view of the proposed interaction between Asp407 and Lys361 causing disruption of the α helix stabilizing the Asp459-Lys361 interaction.

(E) Western blot showing the specificity of antibodies generated against the tip region of the arm domain for NT5C2 (left) and *in vitro* nucleotidase assays of purified WT NT5C2 recombinant protein incubated with two unique arm segment antibodies or the arm segment peptide in the presence of increasing doses of ATP (right). Data in (E) are shown as mean ± SD. The p values were calculated using two-tailed Student's t test, $^{**}p < 0.001$, $^{***}p < 0.0001$. See also Figure S4 and Table S5.

of action and regulation of this nucleotidase, elucidating specific mechanisms responsible for stabilizing the basal inactive configuration of the enzyme, for triggering allosteric activation, and for returning the enzyme to its basal inactive state. Most critically, these findings shed light on the mechanisms of activating mutations in *NT5C2* responsible for driving resistance to 6-MP chemotherapy in relapsed ALL, setting the stage for the development of small-molecule NT5C2 inhibitors for the reversal of chemotherapy resistance in human leukemia.

Enzymatic analyses of recombinant proteins representative of NT5C2 mutations distributed in different regions of the protein in basal conditions and in response to allosteric activation confirmed the gain-of-function nature of relapse-associated NT5C2 alleles. Yet, these analyses revealed diversity in the enzymatic properties of these mutations. We distinguished three groups of mutations based on their enzymatic profile. Class I mutations encompass alleles K359Q and L375F, which show a strong increase in nucleotidase activity in the absence of

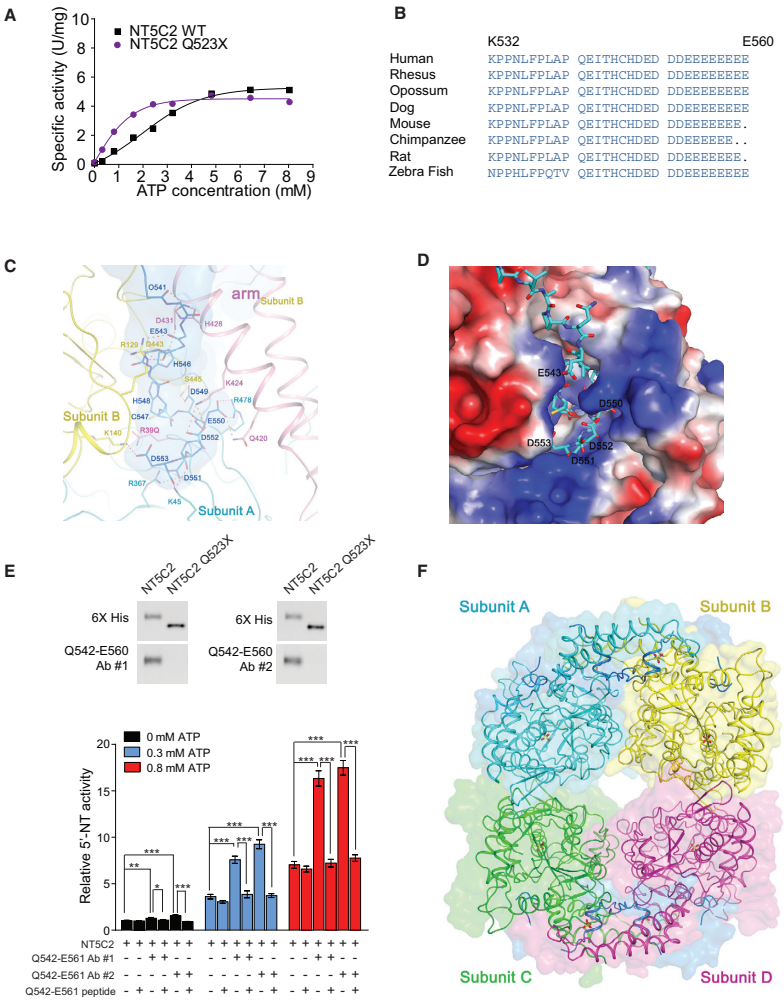

Figure 6. Functional Characterization of the NT5C2 C Terminus and Class III Mutation

(A) *In vitro* nucleotidase assays assessing the enzymatic activity of class III NT5C2 Q523X mutation in the presence of increased concentrations of ATP.

(B) Protein sequence alignment of the C-terminal of NT5C2 in vertebrate species.

(C) Basal structure of the full-length NT5C2 R39Q (R39Q), displaying the interactions of predominantly acidic region of the C-terminal segment with the positively charged residues at the dimer interface. Red dashed lines depict hydrogen bonds. The side chains of residues that are involved in polar interactions are shown by stick models. The side chain of R39Q is colored with light magenta, while others are colored accordingly.

(D) A surface potential depiction of the dimer interface in the basal structure of the full-length R39Q (R39Q). The acidic tail of the protomer A is shown with a stick model in which several acidic residues are labeled.

(E) Western blot showing the specificity of antibodies generated against the C terminus of NT5C2 (top) and *in vitro* nucleotidase assays of WT NT5C2-purified recombinant protein incubated with two unique C terminus targeted antibodies or the C terminus peptide in the presence of increasing doses of ATP (bottom).

(legend continued on next page)

allosteric activation. Class II alleles, which account for >95% of relapse-associated NT5C2 mutations, show increased levels of nucleotidase activity in basal conditions, yet their enzymatic activity is still dynamically increased in response to allosteric effector. Finally, the class III group of NT5C2 mutations is defined by the C-terminal truncating NT5C2 Q523X allele, which shows nucleotidase activity similar to that of WT NT5C2 in basal conditions but is hyper-responsive to allosteric activation.

Two distinct selection pressures influence the clonal evolution of NT5C2 mutations in ALL. In the absence of 6-MP chemotherapy, depletion of the intracellular nucleoside pool as a result of increased activity of this enzyme normally involved in purine degradation, can negatively impact the growth of NT5C2 gain-of-function bearing leukemia clones (Tzoneva et al., 2018). However, increased clearance of thiopurine metabolites during 6-MP therapy confers a selective advantage to cells harboring activating NT5C2 alleles. Class II NT5C2 mutations, by far the most prevalent group in relapsed ALL, balance these two opposing selective pressures by conferring increased nucleotidase activity, yet retaining control by allosteric regulation. It is possible that the rare, yet stronger, class I alleles are less frequently found because of a higher fitness cost in the absence of 6-MP chemotherapy, and that weaker class III NT5C2 mutations are poorly selected as result of a more limited capacity to confer resistance to 6-MP.

NT5C2 is kept in an inactive state in the absence of allosteric activators binding to the effector site. This inactive basal conformation is secured by the C-terminal acidic tail, which inserts itself in between the two NT5C2 dimer subunits establishing multiple interactions with positively charged residues. In this, the C-terminal segment of NT5C2 functions as a fastener securing a tight closed inactive configuration of the enzyme. As a result, NT5C2 must undergo structural rearrangement in order to switch to an active configuration. This transition to an active state, involves the organization of the N-terminal segment of the protein in a helical configuration. This displaces the C terminus from the surface of the neighboring subunit and removes it from the inter-monomeric space, now favoring a more open dimer conformation. In addition, binding of ATP to the effector site induces allosteric activation by inducing the helical conformation of the helix A segment, which reconfigures the catalytic center for substrate accessibility and catalysis. Yet, the transition to an activated state is coupled with a mechanism that returns the enzyme back to its inactive basal configuration. As the inter-subunit space opens, Asp407 in the tip segment of the arm domain is mobilized from its location next to the opening of this cavity and is pulled into the inter-monomeric space via interactions with multiple positively charged residues lining the surface of this pocket. In this way, the negatively charged Asp407 ultimately reaches and destabilizes the helix A segment, located at the bottom of the inter-subunit pocket. In this, a mechanistic parallel can be seen between NT5C2 and Marvin Minsky's "ultimate machine" design, a self-inactivating device consisting of a box with a switch which, when turned "on," activates a lever that appears from inside the box and turns the switch back "off."

Activating gain-of-function mutations driving oncogenic transformation involving multiple different mechanisms are recurrently found in human cancer. Mutations in the PEST domains of MYC (Salghetti et al., 1999) and NOTCH1 (Weng et al., 2004) result in increased protein stability via disruption of degron motifs responsible for protein turnover via proteasomal degradation. Activating mutations in RAS signaling factors lock these proteins in their active GTP-bound configuration by interfering with their intrinsic GTPase activity (Scheffzek et al., 1997). In addition, kinase oncoproteins are frequently activated by mutations that interfere with intramolecular interactions responsible for keeping them inactive in basal conditions. For example, lymphoma-associated activating mutations involving the SH2 domain and the C-terminal region of FYN kinase disrupt the inhibitory interaction of these elements induced by CSK phosphorylation of the FYN C-terminal region Y531 (Palomero et al., 2014). At other times, activating mutations favor activation by interfering with allosteric inhibitory feedback mechanisms, as is the case in PFK1 mutations, which drive increased glycolytic activity in some tumor cells (Webb et al., 2015). In this regard, and of relevance to 6-MP resistance, activating mutations in PRPS1 found in leukemia interfere with allosteric feedback inhibition of this enzyme by purine metabolites resulting in increased nucleotide biosynthesis and consequent inhibition of 6-MP activation (Li et al., 2015). Some aspects of NT5C2 activation by relapsed leukemia-associated mutations, such as the disruption of intramolecular interactions responsible for maintaining the enzyme in an inactive configuration (class III mutations), or the mimicry of the effects of allosteric regulation with the catalytic center (class I mutations), relate to some of those found in other proteins with cancer-associated activating mutations. Yet, to our knowledge, the dynamic switch-off of the activated helix A mediated by the tip region of the arm domain and the positively charged inter-monomeric unit targeted by class II mutations represents a self-regulatory mechanism distinct from those present in other enzymes harboring gain-of-function mutations.

Large-scale cancer-sequencing efforts have uncovered a complex landscape of somatic mutations associated with malignant transformation (Cancer Genome Atlas Research Network et al., 2013). However, the interpretation of individual mutations can be challenging in the absence of mechanistic information, thus highlighting the need for in-depth functional analyses. This imperative is particularly pressing in the case of mutations potentially driving clinically relevant phenotypes such as response or resistance to therapy. The results reported here demonstrate a functional and structural diversity of leukemia-associated *NT5C2* mutations and provide a framework for the functional interpretation of these genetic lesions in the clinic. Thus, mutations involving the tip segment of the arm region and residues located in the inter-subunit space, particularly those involving positively charged residues, and truncating

(F) Structure overlay of the basal NT5C2 Q523X (Q523X) (ribbon) and the basal full-length NT5C2 R39Q (R39Q) (surface), showing the lack of the C terminus (marine) in Q523X results in a more open tetramer as compared with that of R39Q.

Data in (A and E) are shown as mean ± SD. The p values were calculated using two-tailed Student's t test, *p < 0.05, **p < 0.001, ***p < 0.0001. See also Figure S5.

mutations involving the C-terminal segment of NT5C2, should be considered highly likely activating alleles. Finally, the dependence of NT5C2 class II and class III mutant proteins, which encompasses >95% of relapse-associated NT5C2 mutations, on allosteric activation points to the allosteric effector site as a potentially attractive target for the design of small-molecule NT5C2 inhibitors for the reversal of 6-MP resistance in relapsed ALL.

STAR★METHODS

Detailed methods are provided in the online version of this paper and include the following:

- KEY RESOURCES TABLE
- CONTACT FOR REAGENT AND RESOURCE SHARING
- EXPERIMENTAL MODEL AND SUBJECT DETAILS
  - Patient Samples
  - Mice
  - Cell Culture
- METHOD DETAILS
  - Drugs
  - Site-Directed Mutagenesis
  - Plasmids and Vectors
  - Retroviral and Lentiviral Production and Infection
  - *In Vitro* Cell Viability and Chemotherapy Response Assays
  - CRISPR Guided Generation and 6-MP Selection of Arm Domain Mutant NT5C2 Lymphoblasts
  - Deep Sequencing
  - Recombinant Protein Production and Purification
  - 5′-Nucleotidase Assays
  - Immunoprecipitation
  - Antibody Generation
  - Structural Modeling Analyses
  - Crystallization and Structure Determination
  - Crystallization of the Basal Forms of NT5C2
  - Crystallization of the Active Form of NT5C2
- QUANTIFICATION AND STATISTICAL ANALYSIS
- DATA AND SOFTWARE AVAILABILITY

SUPPLEMENTAL INFORMATION

Supplemental Information includes five figure and five tables and can be found with this article online at https://doi.org/10.1016/j.ccell.2018.06.003.

ACKNOWLEDGMENTS

We thank Juan Alvarez Ferrando and Carlos Alvarez Ferrando for their insightful comments and suggestions on mechanic devices and circuit models with analogous logic to that of NT5C2 regulation. This work was supported by a Leukemia & Lymphoma Society Translational Research grant TRP2181-14 (to A.A.F.), the NIH grants CA206501 (to A.A.F.), P30CA013696 and S10OD012018 (to L.T.), a grant from the Protein Structure Initiative of the NIH (U54 GM074958) to L.T., and an Innovative Research Award from the Alex Lemonade Stand Foundation (to A.A.F.). G.T. was supported by a Howard Hughes Medical Institute International Student Research Fellowship. M.S.-M. was supported by a Rally Foundation Fellowship. C.L.D. was supported by the NIH/National Cancer Institute T32-CA09503 training grant. We thank the National Synchrotron Light Source-Stanford Synchrotron Radiation Lightsource user transition program supported jointly by the Life Science Biomedical Technology Research, National Synchrotron Light Source II and Structural Molecular Group at Stanford Synchrotron Radiation Lightsource under National Institute of General Medical Sciences grants P41GM111244 and P41GM103393, and Department of Energy Biological and Environmental Research contracts DE-SC0012704. Stanford Synchrotron Radiation Lightsource is operated under Department of Energy Basic Energy Sciences contract no. DE-AC02-76SF00515.

AUTHOR CONTRIBUTIONS

C.L.D., G.T., F.F., Z.C., A.A-I., M.S.-M, R.K.-S., S.L., and J.S. performed research. A.A.-I. analyzed deep sequencing data. F.F., J.S., S.L., and L.T. performed structural studies. A.A.F. designed the study, supervised research. A.A.F. and L.T. wrote the paper with C.L.D., F.F., and G.T.

DECLARATION OF INTERESTS

The authors declare no competing interests.

Received: December 18, 2017
Revised: April 6, 2018
Accepted: June 6, 2018
Published: July 9, 2018

REFERENCES

Adams, P.D., Afonine, P.V., Bunkoczi, G., Chen, V.B., Davis, I.W., Echols, N., Headd, J.J., Hung, L.W., Kapral, G.J., Grosse-Kunstleve, R.W., et al. (2010). PHENIX: a comprehensive Python-based system for macromolecular structure solution. Acta Crystallogr. D Biol. Crystallogr. *66*, 213–221.

Allegrini, S., Pesi, R., Tozzi, M.G., Fiol, C.J., Johnson, R.B., and Eriksson, S. (1997). Bovine cytosolic IMP/GMP-specific 5′-nucleotidase: cloning and expression of active enzyme in *Escherichia coli*. Biochem. J. *328* (Pt 2), 483–487.

Allegrini, S., Scaloni, A., Ferrara, L., Pesi, R., Pinna, P., Sgarrella, F., Camici, M., Eriksson, S., and Tozzi, M.G. (2001). Bovine cytosolic 5′-nucleotidase acts through the formation of an aspartate 52-phosphoenzyme intermediate. J. Biol. Chem. *276*, 33526–33532.

Banditelli, S., Baiocchi, C., Pesi, R., Allegrini, S., Turriani, M., Ipata, P.L., Camici, M., and Tozzi, M.G. (1996). The phosphotransferase activity of cytosolic 5′-nucleotidase; a purine analog phosphorylating enzyme. Int. J. Biochem. Cell Biol *28*, 711–720.

Brouwer, C., Vogels-Mentink, T.M., Keizer-Garritsen, J.J., Trijbels, F.J., Bokkerink, J.P., Hoogerbrugge, P.M., van Wering, E.R., Veerman, A.J., and De Abreu, R.A. (2005). Role of 5′-nucleotidase in thiopurine metabolism: enzyme kinetic profile and association with thio-GMP levels in patients with acute lymphoblastic leukemia during 6-mercaptopurine treatment. Clin. Chim. Acta *361*, 95–103.

Cancer Genome Atlas Research Network, Weinstein, J.N., Collisson, E.A., Mills, G.B., Shaw, K.R., Ozenberger, B.A., Ellrott, K., Shmulevich, I., Sander, C., and Stuart, J.M. (2013). The Cancer Genome Atlas Pan-Cancer analysis project. Nat. Genet. *45*, 1113–1120.

Cingolani, P., Platts, A., Wang le, L., Coon, M., Nguyen, T., Wang, L., Land, S.J., Lu, X., and Ruden, D.M. (2012). A program for annotating and predicting the effects of single nucleotide polymorphisms, SnpEff: SNPs in the genome of *Drosophila melanogaster* strain w1118; iso-2; iso-3. Fly (Austin) *6*, 80–92.

Collet, J.F., Stroobant, V., Pirard, M., Delpierre, G., and Van Schaftingen, E. (1998). A new class of phosphotransferases phosphorylated on an aspartate residue in an amino-terminal DXDX(T/V) motif. J. Biol. Chem. *273*, 14107–14112.

Donovan, K.F., Hegde, M., Sullender, M., Vaimberg, E.W., Johannessen, C.M., Root, D.E., and Doench, J.G. (2017). Creation of novel protein variants with CRISPR/Cas9-mediated mutagenesis: turning a screening by-product into a discovery tool. PLoS One *12*, e0170445.

Eswar, N., Eramian, D., Webb, B., Shen, M.Y., and Sali, A. (2008). Protein structure modeling with MODELLER. Methods Mol. Biol. *426*, 145–159.

Fiser, A., Do, R.K., and Sali, A. (2000). Modeling of loops in protein structures. Protein Sci. *9*, 1753–1773.

Gao, J., Chang, M.T., Johnsen, H.C., Gao, S.P., Sylvester, B.E., Sumer, S.O., Zhang, H., Solit, D.B., Taylor, B.S., Schultz, N., et al. (2017). 3D clusters of somatic mutations in cancer reveal numerous rare mutations as functional targets. Genome Med. *9*, 4.

Heckl, D., Kowalczyk, M.S., Yudovich, D., Belizaire, R., Puram, R.V., McConkey, M.E., Thielke, A., Aster, J.C., Regev, A., and Ebert, B.L. (2014). Generation of mouse models of myeloid malignancy with combinatorial genetic lesions using CRISPR-Cas9 genome editing. Nat. Biotechnol. *32*, 941–946.

Herranz, D., Ambesi-Impiombato, A., Palomero, T., Schnell, S.A., Belver, L., Wendorff, A.A., Xu, L., Castillo-Martin, M., Llobet-Navas, D., Cordon-Cardo, C., et al. (2014). A NOTCH1-driven MYC enhancer promotes T cell development, transformation and acute lymphoblastic leukemia. Nat. Med. *20*, 1130–1137.

Herranz, D., Ambesi-Impiombato, A., Sudderth, J., Sanchez-Martin, M., Belver, L., Tosello, V., Xu, L., Wendorff, A.A., Castillo, M., Haydu, J.E., et al. (2015). Metabolic reprogramming induces resistance to anti-NOTCH1 therapies in T cell acute lymphoblastic leukemia. Nat. Med. *21*, 1182–1189.

Hnizda, A., Fabry, M., Moriyama, T., Pachl, P., Kugler, M., Brinsa, V., Ascher, D.B., Carroll, W.L., Novak, P., Zaliova, M., et al. (2018). Relapsed acute lymphoblastic leukemia-specific mutations in NT5C2 cluster into hotspots driving intersubunit stimulation. Leukemia *32*, 1393–1403.

Hnizda, A., Skerlova, J., Fabry, M., Pachl, P., Sinalova, M., Vrzal, L., Man, P., Novak, P., Rezacova, P., and Veverka, V. (2016). Oligomeric interface modulation causes misregulation of purine 5-nucleotidase in relapsed leukemia. BMC Biol. *14*, 91.

Holm, L., and Laakso, L.M. (2016). Dali server update. Nucleic Acids Res. *44*, W351–W355.

Hunsucker, S.A., Mitchell, B.S., and Spychala, J. (2005). The 5'-nucleotidases as regulators of nucleotide and drug metabolism. Pharmacol. Ther. *107*, 1–30.

Ipsaro, J.J., Shen, C., Arai, E., Xu, Y., Kinney, J.B., Joshua-Tor, L., Vakoc, C.R., and Shi, J. (2017). Rapid generation of drug-resistance alleles at endogenous loci using CRISPR-Cas9 indel mutagenesis. PLoS One *12*, e0172177.

Itoh, R., Mitsui, A., and Tsushima, K. (1967). 5'-Nucleotidase of chicken liver. Biochim. Biophys. Acta *146*, 151–159.

Jogl, G., Tao, X., Xu, Y., and Tong, L. (2001). COMO: a program for combined molecular replacement. Acta Crystallogr. D Biol. Crystallogr. *57*, 1127–1134.

Koonin, E.V., and Tatusov, R.L. (1994). Computer analysis of bacterial haloacid dehalogenases defines a large superfamily of hydrolases with diverse specificity. Application of an iterative approach to database search. J. Mol. Biol. *244*, 125–132.

Kunz, J.B., Rausch, T., Bandapalli, O.R., Eilers, J., Pechanska, P., Schuessele, S., Assenov, Y., Stutz, A.M., Kirschner-Schwabe, R., Hof, J., et al. (2015). Pediatric T-cell lymphoblastic leukemia evolves into relapse by clonal selection, acquisition of mutations and promoter hypomethylation. Haematologica *100*, 1442–1450.

Li, B., Li, H., Bai, Y., Kirschner-Schwabe, R., Yang, J.J., Chen, Y., Lu, G., Tzoneva, G., Ma, X., Wu, T., et al. (2015). Negative feedback-defective PRPS1 mutants drive thiopurine resistance in relapsed childhood ALL. Nat. Med. *21*, 563–571.

Li, H., and Durbin, R. (2009). Fast and accurate short read alignment with Burrows-Wheeler transform. Bioinformatics *25*, 1754–1760.

Ma, X., Edmonson, M., Yergeau, D., Muzny, D.M., Hampton, O.A., Rusch, M., Song, G., Easton, J., Harvey, R.C., Wheeler, D.A., et al. (2015). Rise and fall of subclones from diagnosis to relapse in pediatric B-acute lymphoblastic leukaemia. Nat. Commun. *6*, 6604.

Marques, A.F., Teixeira, N.A., Gambaretto, C., Sillero, A., and Sillero, M.A. (1998). IMP-GMP 5'-nucleotidase from rat brain: activation by polyphosphates. J. Neurochem. *71*, 1241–1250.

McRee, D.E. (1999). XtalView/Xfit – a versatile program for manipulating atomic coordinates and electron density. J. Struct. Biol. *125*, 156–165.

Meyer, J.A., Wang, J., Hogan, L.E., Yang, J.J., Dandekar, S., Patel, J.P., Tang, Z., Zumbo, P., Li, S., Zavadil, J., et al. (2013). Relapse-specific mutations in NT5C2 in childhood acute lymphoblastic leukemia. Nat. Genet. *45*, 290–294.

Novarino, G., Fenstermaker, A.G., Zaki, M.S., Hofree, M., Silhavy, J.L., Heiberg, A.D., Abdellateef, M., Rosti, B., Scott, E., Mansour, L., et al. (2014). Exome sequencing links corticospinal motor neuron disease to common neurodegenerative disorders. Science *343*, 506–511.

Oshima, K., Khiabanian, H., da Silva-Almeida, A.C., Tzoneva, G., Abate, F., Ambesi-Impiombato, A., Sanchez-Martin, M., Carpenter, Z., Penson, A., Perez-Garcia, A., et al. (2016). Mutational landscape, clonal evolution patterns, and role of RAS mutations in relapsed acute lymphoblastic leukemia. Proc. Natl. Acad. Sci. USA *113*, 11306–11311.

Otwinowski, Z., and Minor, W. (1997). Presessing of X-ray diffraction data collected in oscillation mode. Mehods Enzymol. *276*, 307–326.

Palomero, T., Couronne, L., Khiabanian, H., Kim, M.Y., Ambesi-Impiombato, A., Perez-Garcia, A., Carpenter, Z., Abate, F., Allegretta, M., Haydu, J.E., et al. (2014). Recurrent mutations in epigenetic regulators, RHOA and FYN kinase in peripheral T cell lymphomas. Nat. Genet. *46*, 166–170.

Pesi, R., Turriani, M., Allegrini, S., Scolozzi, C., Camici, M., Ipata, P.L., and Tozzi, M.G. (1994). The bifunctional cytosolic 5'-nucleotidase: regulation of the phosphotransferase and nucleotidase activities. Arch. Biochem. Biophys. *312*, 75–80.

Pettersen, E.F., Goddard, T.D., Huang, C.C., Couch, G.S., Greenblatt, D.M., Meng, E.C., and Ferrin, T.E. (2004). UCSF Chimera – a visualization system for exploratory research and analysis. J. Comput. Chem. *25*, 1605–1612.

Pinto, R.M., Canales, J., Gunther Sillero, M.A., and Sillero, A. (1986). Diadenosine tetraphosphate activates cytosol 5'-nucleotidase. Biochem. Biophys. Res. Commun. *138*, 261–267.

Richter-Pechanska, P., Kunz, J.B., Hof, J., Zimmermann, M., Rausch, T., Bandapalli, O.R., Orlova, E., Scapinello, G., Sagi, J.C., Stanulla, M., et al. (2017). Identification of a genetically defined ultra-high-risk group in relapsed pediatric T-lymphoblastic leukemia. Blood Cancer J. *7*, e523.

Rost, B., Yachdav, G., and Liu, J. (2004). The PredictProtein server. Nucleic Acids Res. *32*, W321–W326.

Roy, A., Kucukural, A., and Zhang, Y. (2010). I-TASSER: a unified platform for automated protein structure and function prediction. Nat. Protoc. *5*, 725–738.

Salghetti, S.E., Kim, S.Y., and Tansey, W.P. (1999). Destruction of Myc by ubiquitin-mediated proteolysis: cancer-associated and transforming mutations stabilize Myc. EMBO J. *18*, 717–726.

Scheffzek, K., Ahmadian, M.R., Kabsch, W., Wiesmuller, L., Lautwein, A., Schmitz, F., and Wittinghofer, A. (1997). The Ras-RasGAP complex: structural basis for GTPase activation and its loss in oncogenic Ras mutants. Science *277*, 333–338.

Schnell, S.A., Ambesi-Impiombato, A., Sanchez-Martin, M., Belver, L., Xu, L., Qin, Y., Kageyama, R., and Ferrando, A.A. (2015). Therapeutic targeting of HES1 transcriptional programs in T-ALL. Blood *125*, 2806–2814.

Schroder, G.F., Levitt, M., and Brunger, A.T. (2010). Super-resolution biomolecular crystallography with low-resolution data. Nature *464*, 1218–1222.

Schroeter, E.H., Kisslinger, J.A., and Kopan, R. (1998). Notch-1 signalling requires ligand-induced proteolytic release of intracellular domain. Nature *393*, 382–386.

Shalem, O., Sanjana, N.E., Hartenian, E., Shi, X., Scott, D.A., Mikkelsen, T.S., Heckl, D., Ebert, B.L., Root, D.E., Doench, J.G., et al. (2014). Genome-scale CRISPR-Cas9 knockout screening in human cells. Science *343*, 84–87.

Spychala, J., Madrid-Marina, V., and Fox, I.H. (1988). High Km soluble 5'-nucleotidase from human placenta. Properties and allosteric regulation by IMP and ATP. J. Biol. Chem. *263*, 18759–18765.

Tamborero, D., Gonzalez-Perez, A., and Lopez-Bigas, N. (2013). OncodriveCLUST: exploiting the positional clustering of somatic mutations to identify cancer genes. Bioinformatics *29*, 2238–2244.

Tozzi, M.G., Camici, M., Pesi, R., Allegrini, S., Sgarrella, F., and Ipata, P.L. (1991). Nucleoside phosphotransferase activity of human colon carcinoma cytosolic 5'-nucleotidase. Arch. Biochem. Biophys. *291*, 212–217.

Trifonov, V., Pasqualucci, L., Tiacci, E., Falini, B., and Rabadan, R. (2013). SAVI: a statistical algorithm for variant frequency identification. BMC Syst. Biol. *7* (*Suppl 2*), S2.

Tzoneva, G., Dieck, C.L., Oshima, K., Ambesi-Impiombato, A., Sanchez-Martin, M., Madubata, C.J., Khiabanian, H., Yu, J., Waanders, E., Iacobucci, I., et al. (2018). Clonal evolution mechanisms in NT5C2 mutant-relapsed acute lymphoblastic leukaemia. Nature *553*, 511–514.

Tzoneva, G., Perez-Garcia, A., Carpenter, Z., Khiabanian, H., Tosello, V., Allegretta, M., Paietta, E., Racevskis, J., Rowe, J.M., Tallman, M.S., et al. (2013). Activating mutations in the NT5C2 nucleotidase gene drive chemotherapy resistance in relapsed ALL. Nat. Med. *19*, 368–371.

Unni, S., Huang, Y., Hanson, R.M., Tobias, M., Krishnan, S., Li, W.W., Nielsen, J.E., and Baker, N.A. (2011). Web servers and services for electrostatics calculations with APBS and PDB2PQR. J. Comput. Chem. *32*, 1488–1491.

Wallden, K., and Nordlund, P. (2011). Structural basis for the allosteric regulation and substrate recognition of human cytosolic 5′-nucleotidase II. J. Mol. Biol. *408*, 684–696.

Wallden, K., Stenmark, P., Nyman, T., Flodin, S., Graslund, S., Loppnau, P., Bianchi, V., and Nordlund, P. (2007). Crystal structure of human cytosolic 5′-nucleotidase II: insights into allosteric regulation and substrate recognition. J. Biol. Chem. *282*, 17828–17836.

Webb, B.A., Forouhar, F., Szu, F.E., Seetharaman, J., Tong, L., and Barber, D.L. (2015). Structures of human phosphofructokinase-1 and atomic basis of cancer-associated mutations. Nature *523*, 111–114.

Weng, A.P., Ferrando, A.A., Lee, W., Morris, J.P.t., Silverman, L.B., Sanchez-Irizarry, C., Blacklow, S.C., Look, A.T., and Aster, J.C. (2004). Activating mutations of NOTCH1 in human T cell acute lymphoblastic leukemia. Science *306*, 269–271.

STAR★METHODS

KEY RESOURCES TABLE

REAGENT or RESOURCE	SOURCE	IDENTIFIER
Antibodies		
NT5C2 arm region antibody	Covance	CG111 and CG112
NT5C2 C-terminus antibody	Covance	CG109 and CG110
6x His Epitope Tag Antibody (HisH8)	Thermo Fisher Scientific	Cat# MA1-21315, RRID:AB_557403
DYKDDDDK Tag Antibody	Cell Signaling Technology	Cat # 2368S, RRID:AB_2217020
Anti-HA High Affinity	Roche	Cat# 11867431001, RRID:AB_390919
Bacterial and Virus Strains		
Rosetta 2(DE3) *Escherichia coli*	Millipore Sigma	Cat# 71397-4
Chemicals, Peptides, and Recombinant Proteins		
6-Mercaptopurine monohydrate	Fisher Scientific	Cat# AC226520050
Adenosine 5′-triphosphate disodium salt hydrate	Sigma Aldrich	Cat# A3377
JetPEI	Polyplus	Cat # 101-10N
Polybrene Infection/Transfection Reagent	Fisher Scientific	Cat# NC9515805
Doxycycline	Clontech	Cat# 631311
IPTG	Life Technologies	Cat# 15529019
Lysozyme from chicken egg white	Sigma Aldrich	Cat# L3790-10X1ML
Imidazole	Sigma Aldrich	Cat# I2399-100G
TCEP	Sigma Aldrich	Cat# 646547-10X1ML
Critical Commercial Assays		
QuikChange II XL Site-Directed Mutagenesis Kit	Agilent Technologies	Cat # 200522
Cell Proliferation Kit I	Sigma Aldrich	Cat# 11465007001
DNEasy Blood & Tissue Kit	Qiagen	Cat# 69506
MiSeq Reagent Kit v2 (500 cycle)	Illumina Inc.	Cat# MS-102-2003
5′-NT Enzymatic Test Kit	Diazyme Laboratories	Cat# DZ123A-K
5′-NT Control Set	Diazyme Laboratories	Cat# DZ123A-CON
NextSeq 500 Mid Output Kit (300 cycles)	Illumina Inc.	Cat # FC-404-1003
Deposited Data		
Coordinates of NT5C2 WT 537X (Basal)	This paper	PDB: 6DDC
Coordinates of NT5C2 R367Q 537X (Basal)	This paper	PDB: 6DDB
Coordinates of NT5C2 Q523X (Basal)	This paper	PDB: 6DDL
Coordinates of NT5C2 WT (Basal)	This paper	PDB: 6DDO
Coordinates of NT5C2 R367Q (Basal)	This paper	PDB: 6DDK
Coordinates of NT5C2 R39Q (Basal)	This paper	PDB: 6DDQ
Coordinates of NT5C2 L375F 537X (Active)	This paper	PDB: 6DDX
Coordinates of NT5C2 K359Q 537X (Active)	This paper	PDB: 6DDY
Coordinates of NT5C2 R367Q 537X (Active)	This paper	PDB: 6DDH
Coordinates of NT5C2 R238W 537X (Active)	This paper	PDB: 6DDZ
Coordinates of NT5C2 D407A 537X (Active)	This paper	PDB: 6DD3
Coordinates of NT5C2 Q523X (Active)	This paper	PDB: 6DE0
Coordinates of NT5C2 WT (Active)	This paper	PDB: 6DE1
Coordinates of NT5C2 L375F (Active)	This paper	PDB: 6DE2
Coordinates of NT5C2 R39Q (Active)	This paper	PDB: 6DE3
Experimental Models: Cell Lines		
Human: HEK293T	ATCC	ATCC # CRL-3216, RRID:CVCL_0063
Human: JURKAT	ATCC	ATCC # TIB-152™, RRID:CVCL_0367
Human: JURKAT-TET3G	Clontech	Cat# 631181

(*Continued on next page*)

Continued

REAGENT or RESOURCE	SOURCE	IDENTIFIER
Experimental Models: Organisms/Strains		
Mouse: C57BL/6	Jackson Labs	Stock No: 000664
Oligonucleotides		
Primer: Nt5c2_H405_gRNA_Forward: CACCGtcctcttgttcccagGCACC	This paper	N/A
Primer: Nt5c2_H405_gRNA_Reverse: AAACGGTGCctgggaacaagaggaC	This paper	N/A
Primer: Nt5c2_I416_gRNA_Forward: CACCGCAGCAGTAGCAATGAGCGCC	This paper	N/A
Primer: Nt5c2_I416_gRNA_Reverse: AAACGGCGCTCATTGCTACTGCTGC	This paper	N/A
Recombinant DNA		
Plasmid: pLOC-NT5C2	Open Biosystems	
Plasmid: pET28aLIC	Cheryl Arrowsmith	Addgene Cat #26094
Plasmid: pL-CRISPR.efs.gfp	Heckl et al., 2014	Addgene Cat #57818
Plasmid: pLVXTRE3GZsGreen1	Clontech	Cat# 631361
Plasmid: pMSCV-pBabeMCS-IRES-RFP	Martine Roussel & Charles Sherr	Addgene Cat #33337
Software and Algorithms		
R	https://www.r-project.org/	N/A
Matlab	https://www.mathworks.com/products/matlab.html	N/A
Chimera Suite	Pettersen et al., 2004	N/A
I-TASSER	Roy et al., 2010	N/A
Modeller Software Suite	Eswar et al., 2008	N/A
SAVI	Trifonov et al., 2013	N/A
Burrows–Wheeler Aligner (BWA aln)	Li and Durbin, 2009	N/A
SnpEFF	Cingolani et al., 2012	N/A
Other		
Ni Sepharose 6 Fast Flow	GE Healthcare	Cat# 17-5318-01
COLUMN PD 10	VWR	Cat# 95017-001

CONTACT FOR REAGENT AND RESOURCE SHARING

Further information and requests for resources and reagents should be directed to and will be fulfilled according to institutional rules by the Lead Contact, Adolfo Ferrando (af2196@columbia.edu).

EXPERIMENTAL MODEL AND SUBJECT DETAILS

Patient Samples

DNAs from leukemic ALL blasts at relapse were provided by the Department of Pediatric Oncology/Hematology at the Charité-Universitätsmedizin Berlin in Berlin, Germany. Informed consent was obtained at study entry and samples were collected under the supervision of local Institutional Review Boards for participating institutions (Charité-Universitätsmedizin and Columbia University Medical Center) and analyzed under the supervision of the Columbia University Medical Center Institutional Review Board.

Mice

We maintained all animals in specific pathogen-free facilities at the Irving Cancer Research Center at Columbia University Medical Campus. The Columbia University Institutional Animal Care and Use Committee (IACUC) approved all animal procedures. To generate NOTCH1-induced T-ALL tumors in mice, we performed retroviral transduction of bone marrow cells (C57BL/6) enriched in Lineage negative cells isolated using magnetic beads (Lineage Cell Depletion Kit, Miltenyi Biotec) with retroviruses expressing

an activated form of the *NOTCH1* oncogene (ΔE-NOTCH1) (Schroeter et al., 1998) and the red fluorescent protein (RFP) and transplanted them via intravenous injection into lethally irradiated isogenic recipients (6-8 week old C57BL/6 females, Jackson Labs) as previously described (Herranz et al., 2014, 2015).

Cell Culture

We performed cell culture in a humidified atmosphere at 37°C under 5% CO_2. We purchased 293T cells for viral production from American Type Culture Collection and grew them in DMEM media supplemented with 10% fetal bovine serum (FBS), 100 U ml^{-1} penicillin G and 100 μg ml^{-1} streptomycin for up to two weeks. We purchased JURKAT TET3G cells from Clontech and cultured them in RPMI-1640 media supplemented with 10% tet-approved FBS, 100 U ml^{-1} penicillin G and 100 μg ml^{-1} streptomycin. Cell lines were regularly authenticated and tested for mycoplasma contamination. We cultured ΔE-NOTCH1 driven mouse leukemic cells in OptiMEM media supplemented with 10% FBS, 100 U ml^{-1} penicillin G, 100 μg ml^{-1} streptomycin, 55 μM β-mercaptoethanol and 10 ng ml^{-1} mouse IL7.

METHOD DETAILS

Drugs

We purchased 6-mercaptopurine (6-MP) and ATP from Sigma-Aldrich. For *in vitro* assays we dissolved 6-MP in DMSO and ATP in Reagent 2 of the 5′-NT Enzymatic Test Kit (Diazyme).

Site-Directed Mutagenesis

We generated the *NT5C2* mutations by site-directed mutagenesis on the mammalian expression pLOC-NT5C2 vector (Open Biosystems) using the QuikChange II XL Site-Directed Mutagenesis Kit (Stratagene) according to the manufacturer's instructions.

Plasmids and Vectors

We obtained the pET28aLIC (Plasmid #26094) and pL-CRISPR.efs.gfp (plasmid # 57818) plasmids from Addgene and the pLVXTRE3GZsGreen1 vector from Clontech. We amplified the coding sequence of the NT5C2 cDNA from pLOC-NT5C2 (Tzoneva et al., 2013) and cloned it into the pET28aLIC vector using In-fusion cloning using the In-Fusion HD Cloning Kit (Clonetch) following manufacturer guidelines. We cloned the NT5C2 S408-D415 loop deletion mutation into the pET28aLIC and pLVXTRE3GZsgreen1 vector using Gibson Assembly using the Gibson Assembly Master Mix (New England Biolabs) following manufacturer guidelines. We cloned a truncated active form of NOTCH1 ΔE-NOTCH1 (Schroeter et al., 1998) into the pMSCV-pBabeMCS-IRES-RFP retroviral vector (Addgene plasmid # 33337). We generated lentiviral vectors expressing CAS9 and gRNAs targeting the arm segment of mouse *Nt5c2* by cloning the corresponding gRNA oligonucleotides (Sigma-Aldrich) into pL-CRISPR.efs.gfp as reported (Shalem et al., 2014).

Retroviral and Lentiviral Production and Infection

We transfected lentiviral plasmids together with gag-pol (pCMV ΔR8.91) and V-SVG (pMD.G VSVG) expressing vectors into 293T cells using JetPEI transfection reagent (Polyplus). We collected viral supernatants after 48 h and used them to infect JURKAT Tet-On human cell lines by spinoculation with 4 μg mL^{-1} Polybrene Infection/Transfection Reagent (Fisher Scientific). We selected infected human cell lines with 1 mg ml^{-1} puromycin (Sigma Aldrich) for 5 days.

In Vitro Cell Viability and Chemotherapy Response Assays

We analyzed chemotherapy responses of human leukemia cell lines expressing wild-type NT5C2 or NT5C2 S408-D415 deletion following 72-hour incubation with increasing concentrations of 6-mercaptopurine by measurement of the metabolic reduction of the tetrazolium salt MTT using the Cell Proliferation Kit I (Roche) following the manufacturer's instructions. We analyzed human cell lines with inducible expression of wild-type or mutant NT5C2 after 48 hours of doxycycline treatment (1 mg ml^{-1}).

CRISPR Guided Generation and 6-MP Selection of Arm Domain Mutant NT5C2 Lymphoblasts

We generated NOTCH1-induced mouse T-ALL tumors via retroviral transduction of mouse hematopoietic progenitors with lentiviral particles expressing a constitutively active truncated NOTCH1 allele (ΔE-NOTCH1) as before (Herranz et al., 2014; Herranz et al.; Schnell et al., 2015). We infected ΔE-NOTCH1 mouse lymphoblasts with lentivirus particles expressing CAS9 and gRNAs targeting *Nt5c2* at codons H405 or I416, or with CAS9 only control lentiviral particles. We sorted infected cells based on GFP expression using a SONY SH800S cell sorter (SONY). We treated sorted gRNA expressing cells with 2 μM 6-MP or DMSO control for 72 hours. Following 6-MP treatment, cells were washed and placed in fresh media. Upon complete recovery from treatment, cells were harvested and DNA was isolated using DNEasy Blood &Tissue Kit (Qiagen).

Deep Sequencing

CRISPR Mutagenesis Deep Sequencing

We amplified by PCR genomic DNA sequences encompassing exon16 of mouse *Nt5c2* from 50 ng of genomic DNA extracted from mouse NOTCH1-induced T-ALL lymphoblast cells with primers designed according to Fluidigm recommendations and containing

Fluidigm-specific adapter sequences at the 5' ends. We barcoded the resulting amplified PCR products using Illumina –Fluidigm specific barcodes so that each sample carried a unique barcode. We pooled all indexed amplicons and quantified the resulting library with Qbit and BioANalyzer analysis. To increase library diversity we spiked the library with 50% PhiX genomic library and sequenced in a MiSeq instrument to generate 2x251 bp paired end reads.

We combined each read pair into a single sequence by finding the optimal alignment allowing up to 0 mismatches and without gaps. We aligned merged pairs as single-end reads to the mouse mm10 genome build using BWA (Li and Durbin, 2009). We classified non-synonymous SNPEFF (Cingolani et al., 2012) variant calls as either in-frame and point mutations (disruptive inframe deletion, disruptive inframe insertion, inframe deletion, inframe insertion, missense variant, and inframe insertion and splice region variant) or frameshift (disruptive inframe deletion and splice region variant, frameshift variant, frameshift variant and splice acceptor variant and splice region variant and intron variant, frameshift variant and splice donor variant and splice region variant and intron variant, frameshift variant and splice region variant, frameshift variant and stop gained, inframe deletion and splice region variant, splice acceptor variant and inframe deletion and splice region variant and intron variant, stop gained and disruptive inframe insertion, stop gained and inframe insertion, stop gained), and relative counts over the total reads of each class were compared across samples.

Patient Sample Deep Sequencing

We identified *NT5C2* variants that differed from the reference genome in targeted resequencing data, containing the *NT5C2* gene, generated using the Access Array system from Fluidigm and analyzed them by paired-end sequencing (2 × 150 bp) in a NextSeq500 instrument (Illumina) using the SAVI algorithm (Trifonov et al., 2013).

Recombinant Protein Production and Purification

For 5'-nucleotidase assays in the absence and presence of allosteric activators we cloned, expressed and purified recombinant wild-type and mutant NT5C2 proteins as previously described (Tzoneva et al., 2013). Briefly, we cloned full-length complementary DNA constructs encoding wild-type or mutant NT5C2 with an N-terminal hexahistidine (His_6) tag in the pET28a-LIC expression vector. We expressed recombinant proteins from Rosetta 2(DE3) *Escherichia coli* cells by induction with 0.5 mM isopropyl-β-D-thiogalactopyranoside for 3 h at 37°C. We harvested cells and lysed them in lysis buffer (50 mM sodium phosphate, pH 7.4, 100 mM NaCl, 10% glycerol, 5 mM β-mercaptoethanol, 1% Triton X-100, 0.5 mg ml^{-1} lysozyme and 20 mM imidazole) supplemented with Complete EDTA-free protease inhibitor (Roche). We purified His_6-tagged NT5C2 proteins by binding them to nickel-Sepharose beads and eluting them with 50 mM sodium phosphate, pH 7.4, 100 mM NaCl, 10% glycerol, 5 mM β-mercaptoethanol and 300 mM imidazole. We removed imidazole by buffer exchange using PD-10 desalting columns (GE Healthcare). We assessed protein expression and purity by SDS-PAGE and Coomassie staining.

For X-ray crystallography analyses we cloned full-length (561 amino acids) or C-terminally truncated (amino acids 1-536) complementary DNA constructs encoding wild-type or mutant NT5C2 with an N-terminal hexahistidine (His_6) tag in the pET28a-LIC expression vector. We expressed recombinant proteins from Rosetta 2(DE3) *Escherichia coli* cells by induction with 0.5 mM isopropyl-β-D-thiogalactopyranoside overnight at 16°C. We resuspended harvested cells in lysis buffer (50 mM sodium phosphate pH 7.4, 500 mM sodium chloride, 10% glycerol, 0.5 mM TCEP, 20 mM imidazole) supplemented with Complete EDTA-free protease inhibitor (Roche) and lysed cells by sonication. We purified recombinant proteins using an ÄKTA fast protein liquid chromatography system (GE Healthcare) using a 2-step protocol adapted from one previously described (Wallden et al., 2007). We first performed affinity chromatography using a 1 ml Ni^{2+}-charged His-Trap HP column (GE Healthcare) equilibrated in lysis buffer. We eluted NT5C2 proteins from the His-Trap column in a step-wise method with elution buffer (lysis buffer with 500mM imidazole) by first setting the buffer ratio to 25% elution buffer for 8 column volumes and then switching to a linear gradient to 100% elution buffer over 10 column volumes. We pooled NT5C2-containing fractions and purified further by size exclusion chromatography using a HiLoad 16/60 Superdex 200 gel filtration column (GE Healthcare) equilibrated in 50 mM sodium phosphate, pH 7.4, 100 mM NaCl, 10% glycerol and 0.5 mM TCEP. We assessed protein expression and purity by SDS-PAGE and Coomassie staining and concentrated protein samples to 4-9 mg/ml.

For 5'-nucleotidase assays of NT5C2 proteins incubated with arm region or C-terminal polyclonal antibodies in presence or absence of their corresponding specific blocking peptides, we expressed proteins as described for standard 5'-nucleotidase assays (Tzoneva et al., 2013). We purified His_6-tagged NT5C2 proteins in a 2-step process. First we bound proteins to nickel-Sepharose beads and eluted them with 50 mM sodium phosphate, pH 7.4, 100 mM NaCl, 10% glycerol, 5 mM β-mercaptoethanol and 300 mM imidazole. We then further purified NT5C2 protein eluates by size exclusion using a HiLoad 16/60 Superdex 200 gel filtration column (GE Healthcare) equilibrated in 50 mM sodium phosphate, pH 7.4, 100 mM NaCl, 10% glycerol and 0.5 mM TCEP.

5′-Nucleotidase Assays

We assessed 5′-NT activity of purified recombinant wild-type and mutant NT5C2 proteins using the 5′-NT Enzymatic Test Kit (Diazyme) according to the manufacturer's instructions as described previously (Tzoneva et al., 2013). We calculated 5′-NT activity levels using a calibrator of known 5′-NT activity as standard. We performed assays in triplicate in an Infinite M200 Tecan plate reader.

For assays with allosteric activators ATP, was dissolved directly in Reagent 2 of the test kit (containing the substrate IMP) and made serial dilutions to achieve a range of concentrations. For assays with antibodies and peptides (custom-generated by Covance), both antibodies and peptides were resuspended in phosphate buffered saline (PBS) and all corresponding samples and controls were diluted with PBS accordingly. We performed statistical analysis by Student's *t*-test.

Immunoprecipitation

293T cells transfected with FLAG-tagged wild-type NT5C2 and HA-tagged NT5C2 R367Q were collected in lysis buffer (50 mM Tris-HCl, 150 mM NaCl, 1 mM EDTA, 5% Glycerol, 5 mM β-ME, 0.1% Triton). We incubated cell lysates with EZview™ Red ANTI-FLAG® M2 Affinity Gel clone M2 beads (Sigma) or EZview™ Red Anti-HA Affinity Gel beads (Sigma) for 2 hours at 4°C. Following four washes with lysis buffer and one wash with PBS, we boiled the beads in 2x SDS-loading buffer, separated them by SDS PAGE and transfered them to a nitrocellulose membrane for western blot analysis. We detected Flag-tagged proteins by immunoblot with a DYKDDDDK Tag Antibody (Cell Signaling Technology Cat # 2368) and HA-tagged proteins with an Anti-HA High Affinity antibody (Roche Cat #11867431001).

Antibody Generation

We generated rabbit polyclonal antisera directed against Keyhole Limpet Hemocyanin-conjugated NT5C2 peptides corresponding to the tip of the arm segment (E399-I414) or the C-terminus segment (Q542-E561) of the wild-type NT5C2 protein. Specific immunoglobulins were purified from rabbit sera by positive affinity purification using the corresponding immobilized peptide columns (Covance).

Structural Modeling Analyses

Computational modeling analyses and images were generated using Chimera suite (Pettersen et al., 2004). Additional modeling was conducted using Modeller (Eswar et al., 2008) and I-TASSER webserver (Roy et al., 2010). Tip region of the arm domain models were built, refined and scored using Modeller Software suite (Eswar et al., 2008; Fiser et al., 2000). Top models for figures were selected by ranking 5,000 iterations by DOPE score as described elsewhere (Fiser et al., 2000). All secondary structure prediction was conducted using the PredictProtein platform and webserver (Rost et al., 2004). Path prediction and molecular dynamics of NT5C2 models were predicted using UCSF Chimera software (Pettersen et al., 2004). Electrostatics of NT5C2 molecular surfaces were investigated with APBS and PDB2PQR software packages. PDB2PQR submission was run with a PARSE force field, optimal hydrogen bonding network. PROPKA was utilized to assign protonation states for each structure at their respective crystallization pH (Unni et al., 2011). Charge mapping method utilized was cubic Bspline discretization. Mobile ions were not included and Poisson-Boltzmann was run with linearized (lpbe) setting. Supplementary electrostatics analysis and visualization was conducted through use of the Columbic surface coloring algorithm provided in Chimera software package (Pettersen et al., 2004).

Crystallization and Structure Determination

All crystals of the human NT5C2 were grown using the microbatch under oil method. In all cases, 1-4 μl of the protein solution was mixed with 1-2 μl of the precipitant solution. The truncated wild-type (WT-537X) and its corresponding mutants were grown at 18°C, whereas all of the full-length wild-type NT5C2 and its corresponding mutants were grown at 4°C for the first week, and then transferred to 18°C for the next 3 weeks. All protein samples contain a mutation at position 52 (D52N), and the protein concentration ranges from 3-12 mg/ml in a buffer consisting of 50 mM Na_3PO_4 (pH 7.4), 100 mM NaCl, 10% glycerol, and 0.5 mM TCEP. Beam lines X4C of the National Synchrotron Light Source (NSLS), BL14-1 and BL12-2 of Stanford National Accelerator Laboratory (SLAC), BL501 and BL502 of Berkeley Advanced Light Source (ALS), and SER-CAT of Advance Photon Source (APS) were used for collecting a single-wavelength native data set for each of fifteen crystal structures presented in this study. All of the diffraction images were processed with the HKL2000 package (Otwinowski and Minor, 1997). For the sake of clarity, the crystallization experiments are described below in two parts for basal and active forms of NT5C2. All of the chemicals for crystallization purposes were purchased from Sigma-Aldrich and the paraffin oil for micro batch method was purchased from Hampton Inc.

Crystallization of the Basal Forms of NT5C2

A: Crystallization of the Basal WT-537X, R367Q-537X, and Q523X

The basal form of WT-537X was crystallized using a crystallization reagent comprising 100 mM sodium acetate trihydrate (pH 4.6) and 2 M ammonium sulfate. In contrast, R367Q-537X was crystallized using a crystallization reagent comprising sodium acetate trihydrate (pH 4.6) and 30% (v/v) 2-Methyl-2, 4-pentanediol (MPD), 20 mM calcium chloride dihydrate, and 5 mM $MnCl_2$. The crystals of the basal form of Q523X were obtained by microseeding method using crystals of the basal form of the full-length R39Q (see below) and using the same crystallization condition as that for R367Q-537X, except $MnCl_2$ was not added into the crystallization mixture. All crystals were cryoprotected by supplementing the crystallization solution with 20% (v/v) glycerol and flash-freezing in liquid nitrogen for data collection at 100 K. Crystals of the three basal forms WT-537X, R367Q-537X and Q523X diffracted X-rays to 2.91 Å, 2.80 Å, and 2.26 Å resolution respectively, and they belong to space group C2, and there are two protomers in the asymmetric unit (ASU) of the crystals.

The structure of the active form of WT-537X NT5C2 in complex with ATP, Mg^{2+}, and IMP (PDB id: 2XCW) was used as a search model to determine the structure of the basal form of WT-537X NT5C2 using the molecular replacement method with the program COMO (Jogl et al., 2001). The entire loop at the tip of the arm segment and four additional residues (489-492) of the C-terminal segment were manually built with the program XtalView (McRee, 1999). Most stages of the structure refinement were performed using CNS 1.3 (Schroder et al., 2010), and PHENIX was used at the final stage of refinement for this and other structures reported in this study (Adams et al., 2010). Crystal structure of the basal R367Q-537X was subsequently determined using the basal structure of WT-537X using a similar methodology.

B: Crystallization of the Basal Full-Length WT, R567Q, and R39Q

The basal forms of the three full-length enzymes, WT, R367Q, and R39Q, were crystallized using a crystallization condition consisting of 100 mM HEPES (pH 7.5), 10% (w/v) PEG 3350, and 200 mM L-proline. Whereas crystals of the full-length R367Q (R367Q) were grown without microseeding, those of the full-length WT (WT) and R39Q (R39Q) were obtained by microseeding method. A few large crystals of R367Q were used as seeds for growing crystals of R39Q, while seeds from R39Q crystals were used for growing crystals of WT. All crystals were cryoprotected by supplementing the crystallization solution with 20% (v/v) ethylene glycol and flash-freezing in liquid nitrogen for data collection at 100 K. Crystals of WT, R367Q, and R39Q, respectively, diffracted X-rays to 2.48 Å, 2.50 Å, 2.31 Å resolution, and they all belong to space group $C222_1$ with two protomers in ASU of each crystal. These structures were subsequently determined using the structure of basal form of WT-537X as the search model in the molecular replacement method. These structures revealed mostly ordered C-terminal segment, which was reported for the first time in this study.

Crystallization of the Active Form of NT5C2

A: Crystallization of the Active Forms of L375F-537X, K359Q-537X, R367Q-537X, R238W-537X, D407A-537X, and Q523X

Crystals of L375F-537X were grown using the crystallization cocktail consisting of 1.8 M ammonium citrate tribasic (pH 7), while those of K359Q-537X were grown in presence of ATP, Mg^{2+}, and IMP and by using the crystallization cocktail comprising 0.1 M HEPES (pH 7.5), 20% (w/v) PEG 1000, and 0.1 M ammonium bromide. In both cases, the structures were in active form, and in the latter case no detectable electron density was observed for ATP, Mg^{2+} or IMP. The crystals, respectively, diffracted X-rays to 2.9 Å and 1.8 Å resolution. Crystals of R367Q-537X were grown in presence of ATP, Mg^{2+}, and IMP using the crystallization reagent consisting of 0.1 M HEPES (pH 7.5), 20% (w/v) PEG 1000, and 0.1 M ammonium nitrate. Crystals diffracted X-ray to resolution 2.35 Å. Whereas IMP has well-defined electron density, there is no interpretable electron density for ATP or Mg^{2+}.

Crystals of R238W-537X were grown in presence of ATP, Mg^{2+}, and IMP using the crystallization cocktail consisting of 35% (w/v) tascimate (pH 7). Clear electron density was observed for both ATP and Mg^{2+} ion. Seeds from crystals of the full-length L375F (see below), in complex with ATP and Mg^{2+}, were used to grow crystals of D407A-537X in presence of ATP, Mg^{2+}, and IMP using the crystallization reagent consisting of 2M ammonium sulfate and 5% (v/v) 2-proponal. A similar methodology was used to grow crystals of Q523X in presence of ATP, Mg^{2+}, and IMP. No electron density was detected for ATP, Mg^{2+}, or IMP in either structure of D407A-537X or 537X. All crystals were cryoprotected by supplementing the crystallization solution with 20% (v/v) glycerol and flash-freezing in liquid nitrogen for data collection at 100 K. Crystals of R238W-537X, D407A-537X, and 537X diffracted X-rays to 1.97 Å. 1.98 Å, and 2.05 Å resolution, respectively. All crystals of the active form of NT5C2-537X, wild-type and mutant, belong to space group *I*222 with one protomer in ASU.

B: Crystallization of Active Form of Three Full-Length Proteins: WT, L375F, and R39Q

The full length WT (WT) enzyme in presence of ATP, Mg^{2+}, and IMP was crystallized using seeds from crystals of the full length L375F (see below) and the crystallization reagent comprising 0.1 M HEPES (pH 7.5), and 20% (w/v) PEG 1000, and 0.1 M ammonium nitrate. The full length L375F (L375F) was crystallized in presence of ATP, Mg^{2+}, and IMP, and by using a crystallization reagent consisting of 2M ammonium sulfate and 5% (v/v) 2-proponal. The full length R39Q (R39Q) was crystallized in presence of ATP, Mg^{2+}, IMP, and by using the crystallization reagent consisting of 100 mM HEPES (pH 7.5) and 12% (w/v) PEG 3350. While crystals of WT were cryoprotected by supplementing the crystallization solution with 20% (v/v) glycerol, those of L375F and R39Q were cryoprotected with 20% (v/v) ethylene glycol and all the crystals were flash-frozen in liquid nitrogen for data collection at 100 K.

Whereas neither ATP, Mg^{2+}ion nor IMP was observed in the structure of WT, there were well-defined electron densities for both ATP and Mg^{2+}ion in the structures of L375F and R39Q. Crystals of the full length active forms of NT5C2, WT, L375F, and R39Q, diffracted X-ray to 2.15 Å. 2.10 Å, and 3.06 Å resolution, respectively.

All nine structures of the active form of NT5C2 belong to space group *I*222 with one protomer in ASU. The data quality and refinement statistics are shown in Table S2.

QUANTIFICATION AND STATISTICAL ANALYSIS

We performed statistical analysis by Student's *t*-test. We considered results with $P < 0.05$ as statistically significant.

DATA AND SOFTWARE AVAILABILITY

The atomic coordinates reported in this paper are deposited in PDB:6DDC, 6DDB, 6DDL, 6DDO, 6DDK, 6DDQ, 6DDX, 6DDY, 6DDH, 6DDZ, 6DD3, 6DE0, 6DE1, 6DE2, 6DE3.

Table S1. Related to Figure 1 *NT5C2* mutations identified in relapsed ALL patient samples.

Sample ID	Diagnosis	Exon	Predicted amino acid change	Reported in
Relapse T-ALL B63	T-ALL	15	D407Y	This paper
Relapse T-ALL B63	T-ALL	2	R39Q	This paper
Relapse B-ALL 1	B-ALL	13	R367Q	This paper
Relapse B-ALL 2	B-ALL	13	R367Q	This paper
Relapse B-ALL 3	B-ALL	13	R367Q	This paper
Relapse B-ALL 284	B-ALL	15	K404N	This paper
Relapse B-ALL 4	B-ALL	15	D407Y	This paper
Relapse B-ALL 240	B-ALL	15	P414S	This paper
Relapse B-ALL 5	B-ALL	9	R238L	This paper
Relapse B-ALL 6	B-ALL	15	P414S	This paper
Relapse B-ALL 7	B-ALL	15	del_S408_D415	This paper
Relapse B-ALL 326	B-ALL	13	R367Q	This paper
Relapse B-ALL 8	B-ALL	9	R238L	This paper
Relapse B-ALL 9	B-ALL	13	R367Q	This paper
Relapse B-ALL 396	B-ALL	15	D407H	This paper
Relapse B-ALL 396	B-ALL	15	D415G	This paper
Relapse B-ALL 403	B-ALL	9	R238W	This paper
Relapse B-ALL 403	B-ALL	13	R367Q	This paper
Relapse B-ALL 371	B-ALL	13	R367Q	This paper
Relapse B-ALL 377	B-ALL	13	R367Q	This paper
Relapse B-ALL 376	B-ALL	13	D384N	This paper
Relapse B-ALL 265	B-ALL	2	R39Q	This paper
Relapse B-ALL 427	B-ALL	2	R39Q	This paper
Relapse B-ALL 304	B-ALL	16	V454M	This paper
Relapse B-ALL 287	B-ALL	9	R238W	This paper
Relapse B-ALL 315	B-ALL	9	R238W	This paper
Relapse B-ALL 10	B-ALL	13	R367Q	This paper
Relapse B-ALL 11	B-ALL	13	R367Q	This paper
Relapse B-ALL 234	B-ALL	13	R367Q	This paper
Relapse B-ALL 12	B-ALL	13	R367Q	This paper
Relapse B-ALL 243	B-ALL	13	R367Q	This paper
Relapse B-ALL 244	B-ALL	13	R367Q	This paper
Relapse T-ALL 4	T-ALL	13	R367Q	Tzoneva et al. 2013
Relapse T-ALL 11	T-ALL	13	K359Q	Tzoneva et al. 2013
Relapse T-ALL 17	T-ALL	13	R367Q	Tzoneva et al. 2013
Relapse T-ALL 17	T-ALL	9	R238L	Tzoneva et al. 2013
Relapse T-ALL 22	T-ALL	9	R238W	Tzoneva et al. 2013
Relapse T-ALL 29	T-ALL	11	R291W	Tzoneva et al. 2013
Relapse T-ALL 35	T-ALL	13	R367Q	Tzoneva et al. 2013
Relapse T-ALL 37	T-ALL	15	D407A	Tzoneva et al. 2013
Relapse T-ALL 30	T-ALL	17	Q523*	Tzoneva et al. 2013
Relapse pre-B ALL 16	pre-B ALL	13	R367Q	Tzoneva et al. 2013
Relapse T-ALL B11	T-ALL	13	R367Q	Tzoneva et al. 2013
Relapse T-ALL B15	T-ALL	13	R367Q	Tzoneva et al. 2013
Relapse T-ALL B30	T-ALL	13	R367Q	Tzoneva et al. 2013
Relapse T-ALL B37	T-ALL	13	R367Q	Tzoneva et al. 2013
Relapse T-ALL B39	T-ALL	13	R367Q	Tzoneva et al. 2013

Relapse T-ALL B44	T-ALL	13	R367Q	Tzoneva et al. 2013
Relapse T-ALL B48	T-ALL	13	R367Q	Tzoneva et al. 2013
Relapse T-ALL B52	T-ALL	13	R367Q	Tzoneva et al. 2013
Relapse T-ALL B53	T-ALL	13	R367Q	Tzoneva et al. 2013
Relapse T-ALL B9	T-ALL	9	R238W	Tzoneva et al. 2013
Relapse T-ALL B29	T-ALL	9	R238W	Tzoneva et al. 2013
Relapse T-ALL B64	T-ALL	9	R238W	Tzoneva et al. 2013
Relapse T-ALL B9	T-ALL	13	L375F	Tzoneva et al. 2013
Relapse T-ALL B64	T-ALL	13	L375F	Tzoneva et al. 2013
T-ALL C4	T-ALL	13	R367Q	Tzoneva et al. 2018
T-ALL C5	T-ALL	9	R238W	Tzoneva et al. 2018
T-ALL C7	T-ALL	13	R367Q	Tzoneva et al. 2018
T-ALL C10	T-ALL	9	R238W	Tzoneva et al. 2018
T-ALL C11	T-ALL	13	R367Q	Tzoneva et al. 2018
T-ALL C14	T-ALL	15	D407E	Tzoneva et al. 2018
T-ALL C17	T-ALL	13	R367Q	Tzoneva et al. 2018
T-ALL C18	T-ALL	13	R367Q	Tzoneva et al. 2018
T-ALL C20	T-ALL	13	R367Q	Tzoneva et al. 2018
T-ALL N1	T-ALL	13	R367Q	Tzoneva et al. 2018
SJBALL192	B-ALL	15	P414A	Tzoneva et al. 2018
SJBALL192	B-ALL	2	R39Q	Tzoneva et al. 2018
SJTALL001	T-ALL	2	R39Q	Tzoneva et al. 2018
n/a	B-ALL	9	R238W	Meyer et al. 2013
n/a	B-ALL	9	R238W	Meyer et al. 2013
n/a	B-ALL	9	R238W	Meyer et al. 2013
n/a	B-ALL	13	R367Q	Meyer et al. 2013
n/a	B-ALL	15	K404ins	Meyer et al. 2013
n/a	B-ALL	15	S408R	Meyer et al. 2013
n/a	B-ALL	16	S445F	Meyer et al. 2013
PANTSM	B-ALL	2	R39Q	Ma et al. 2015
PAPAGK	B-ALL	9	R238G	Ma et al. 2015
PAPJIB	B-ALL	13	R367Q	Ma et al. 2015
PAPJIB	B-ALL	9	R238Q	Ma et al. 2015
PAPSPG	B-ALL	9	R238W	Ma et al. 2015
PAPSPN	B-ALL	15	S408R	Ma et al. 2015
PAPZNK	B-ALL	13	R367Q	Ma et al. 2015
PAPZNK	B-ALL	13	S360P	Ma et al. 2015
PARFTR	B-ALL	9	R238G	Ma et al. 2015
PARFTR	B-ALL	2	R39Q	Ma et al. 2015
PARFTR	B-ALL	9	R238W	Ma et al. 2015
PARFTR	B-ALL	13	R367Q	Ma et al. 2015
PARJZZ	B-ALL	13	R367Q	Ma et al. 2015
PASKAY	B-ALL	13	R367Q	Ma et al. 2015
11	T-ALL	13	R367Q	Richter-Pechanska et al. 2017
11	T-ALL	15	P414S	Richter-Pechanska et al. 2017
15	T-ALL	13	R367Q	Richter-Pechanska et al. 2017
23	T-ALL	14	396_400del	Richter-Pechanska et al. 2017
24	T-ALL	9	R238W	Richter-Pechanska et al. 2017
76	T-ALL	17	T489M	Richter-Pechanska et al. 2017
29	T-ALL	9	R238W	Richter-Pechanska et al. 2017
29	T-ALL	15	D407H	Richter-Pechanska et al. 2017

30	T-ALL	13	R367Q	Richter-Pechanska et al. 2017
37	T-ALL	13	R367Q	Richter-Pechanska et al. 2017
39	T-ALL	13	R367Q	Richter-Pechanska et al. 2017
78	T-ALL	9	R238G	Richter-Pechanska et al. 2017
44	T-ALL	13	R367Q	Richter-Pechanska et al. 2017
48	T-ALL	13	R367Q	Richter-Pechanska et al. 2017
48	T-ALL	2	R39Q	Richter-Pechanska et al. 2017
59	T-ALL	7	R195Q	Richter-Pechanska et al. 2017
63	T-ALL	15	D407Y	Richter-Pechanska et al. 2017
64	T-ALL	9	R238W	Richter-Pechanska et al. 2017
64	T-ALL	13	L375F	Richter-Pechanska et al. 2017
5376	T-ALL	2	R34Q	Richter-Pechanska et al. 2017
S20	T-ALL	17	P533L	Richter-Pechanska et al. 2017
A61	T-ALL	13	R367Q	Kunz et al. 2015
T92	T-ALL	15	D407Y	Kunz et al. 2015
S00285	T-ALL	13	R367Q	Kunz et al. 2015
S00456	T-ALL	15	P414S	Kunz et al. 2015
S00207	T-ALL	13	R367Q	Kunz et al. 2015
T92	T-ALL	13	R367Q	Kunz et al. 2015
19	T-ALL	16	R478S	Oshima et al. 2016
19	T-ALL	13	R367Q	Oshima et al. 2016
29	T-ALL	13	K359Q	Oshima et al. 2016
41	B-precursor ALL	16	S445F_R446Q	Oshima et al. 2016

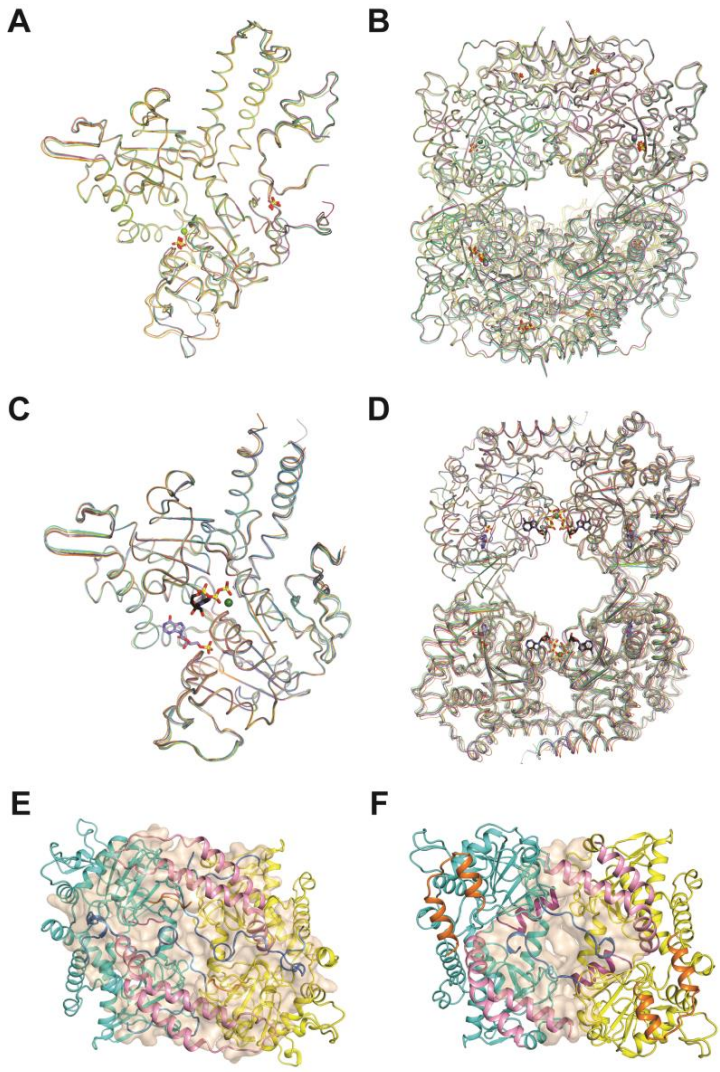

Figure S1. Related to Figure 2 Structural overlay and buried surface area of basal and active monomers and tetramers. (**A**) An overlay of 5 basal NT5C2 monomers: cyan, orange, yellow, green, and magenta for Cα atoms of the full-length WT (WT), R367Q-537X, Q523X, the full-length R367Q (R367Q) and the full-length R39Q (R39Q), respectively. Phosphates (yellow for phosphate) and Mg^{2+} ions are depicted as stick models and solid dark-green spheres, respectively. (**B**) An overlay of 5 basal NT5C2 tetramers. The color schemes are the same as (**A**) and Mn^{2+} ions are shown with solid purple spheres. (**C**) An overlay of 9 active NT5C2 monomers: cyan, blue, orange, yellow, salmon, grey, purple, green, magenta, for Cα atoms of WT, L375F, R39Q, Q523X, K359Q-537X, L375F-537X, R367Q-537X, D407A-537X and R238W-537X, respectively. ATP (black and yellow for C and P atoms), IMP (purple for C atoms) are represented as stick models and a Mg^{2+} ion as a solid dark-green sphere. (**D**) An overlay of 9 active NT5C2 tetramers. Color schemes are as in (**C**). (**E**) Cartoon representation of the strong dimer in the full-length WT basal structure, in which the buried surface area at the dimer interface is depicted with wheat color. (**F**) Cartoon representation of the strong dimer in the full-length WT active structure, in which the buried surface area at the dimer interface is depicted with wheat color. Views of the dimers in A and B are similar to those in **Fig1 C** and **D**.

Table S2. Related to Figure 2. Data collection and refinement statistics.

NT5C2	**WT-537X**	**R367Q-537X**	**Q523X**	**WT**	**R367Q**
State	**Basal**	**Basal**	**Basal**	**Basal**	**Basal**
Ligands	P_i, Mg^{2+}	P_i, Mn^{2+}	P_i	P_i	P_i
Data collection					
Space group	*C*2	*C*2	*C*2	$C222_1$	$C222_1$
Cell dimensions					
a, *b*, *c* (Å)	144.5, 124.1, 90.7	143.1, 123.1, 90.3	143.4, 123.6, 91.3	122.1, 173.1, 123.3	121.9, 171.4, 122.4
α, β, γ (°)	90, 116.2, 90	90, 115.5, 90	90, 115.5, 90	90, 90, 90	90, 90, 90
Resolution (Å)	39.42-2.91 (3.03-2.91)*	49.1-2.80 (2.91-2.80)*	49.44-2.26 (2.31-2.26)*	48.05-2.48 (2.53-2.48)*	49.81-2.50 (2.55-2.50)*
R_{merge} (%)	11.5 (58.1)	9.1 (38.7)	12.1 (53.7)	12.2 (55.1)	13.1 (55.4)
$CC_{1/2}$	0.94 (0.80)	0.98 (0.93)	0.95 (0.86)	0.96 (0.98)	0.97 (0.93)
I/σI	8.9 (1.9)	24.4 (5.7)	21.4 (3.2)	19.7 (2.4)	20.4 (4.3)
Completeness (%)	96.6 (96.5)	98.9 (98.2)	99.9 (100)	100 (100)	100 (100)
Redundancy	3.2 (2.9)	6.1 (6.1)	7.5 (7.1)	7.4 (7.5)	12.5 (12.6)
Refinement					
Resolution (Å)	39.42-2.91 (2.96-2.91)*	49.1-2.80 (2.84-2.80)	49.4-2.26 (2.29-2.26)	48.05-2.48 (2.51-2.48)*	49.81-2.50 (2.53-2.50)*
No. reflections	30,410 (1,227)	34,385 (1220)	67,084 (2,003)	46,552 (1,395)	44,609 (1,987)
R_{work} / R_{free} (%)	17.8 (25.0)/ 25.6 (37.1)	21.7 (26.3)/ 29.1 (38.5)	19.5 (24.3)/ 21.9 (27.5)	18.3 (23.1)/ 22.4 (28.1)	16.0 (19.9)/ 21.7 (28.6)
No. atoms					
Protein	7,741	7,624	7,630	8,160	8,030
Ligand/ion	22	22	20	20	10
Water	279	168	677	550	516
B-factors					
Protein	43.0	42.0	34.6	33.6	31.6
Ligand/ion	35.2	42.5	40.9	26.4	16.4
Water	31.5	35.6	41.2	34.1	33.1
RMSD					
Bond lengths (Å)	0.008	0.009	0.007	0.002	0.007
Bond angles (°)	1.0	1.2	0.9	0.5	0.9
PDB code	6DDC	6DDB	6DDL	6DDO	6DDK

NT5C2	**R39Q**	**L375F-537X**	**K359Q-537X**	**R367Q-537X**	**R238W-537X**
State	**Basal**	**Active**	**Active**	**Active**	**Active**
Ligands	P_i, EDO	P_i	P_i, GOL	IMP	ATP, Mg^{2+}, P_i, GOL
Data collection					
Space group	*C*222$_1$	*I*222	*I*222	*I*222	*I*222
Cell dimensions					
a, *b*, *c* (Å)	121.5, 171.1, 122.2	92.2, 127.1, 130.6	91.5, 126.8, 130.2	91.9, 127.8, 130.3	92.68, 127.3, 131.1
α, β, γ (°)	90, 90, 90	90, 90, 90	90, 90, 90	90, 90, 90	90, 90, 90
Resolution (Å)	42.76-2.31 (2.37-2.31)*	45.5-2.9 (2.95-2.90)*	45.4-1.8 (1.86-1.80)*	48.66-2.35 (2.39-2.35)*	33.6-1.97 (1.97-2.05)*
R_{merge} (%)	11.3 (56.2)	9.6 (39.6)	7.4 (51.0)	8.9 (47.6)	7.6 (58.8)
$CC_{1/2}$	0.98 (0.93)	0.99 (0.97)	0.98 (0.92)	0.98 (0.89)	0.98 (0.88)
$I/\sigma I$	16.2 (4.0)	23.9 (4.4)	44.1 (2.7)	28.0 (4.0)	30.9 (2.9)
Completeness (%)	99.9 (100)	98.8 (100)	99.4 (100)	100 (99.9)	99.8 (100)
Redundancy	13.7 (13.8)	7.0 (7.0)	13.3 (13.5)	7.4 (6.8)	10.1 (6.6)
Refinement					
Resolution (Å)	42.76-2.31 (2.34-2.31)	45.5-2.9 (2.99-2.90)	45.4-1.80 (1.82-1.80)	48.66-2.35 (2.39-2.35)	33.6-1.97 (1.99-1.97)
No. reflections	55,925 (1,700)	16,680 (1,082)	69,296 (1817)	32,292 (1,239)	54,413 (1,622)
R_{work} / R_{free} (%)	14.9 (16.7)/ 20.2 (23.5)	21.7 (25.3)/ 29.5 (35.0)	18.2 (23.8)/ 20.3 (27.6)	17.4 (21.6)/ 22.2 (27.7)	17.6 (22.5)/ 20.2 (27.6)
No. atoms					
Protein	8,158	3,859	3,780	3,863	3,856
Ligand/ion	28	5	29	23	51
Water	782	26	346	127	340
B-factors					
Protein	32.4	51.6	35.1	37.7	28.5
Ligand/ion	37.2	78.1	49.2	62.6	58.1
Water	40.3	41.4	45.8	45.4	33.5
RMSD					
Bond lengths (Å)	0.007	0.008	0.007	0.008	0.007
Bond angles (°)	0.9	1.1	1.0	1.0	1.0
PDB code	6DDQ	6DDX	6DDY	6DDH	6DDZ

NT5C2	**D407A-537X**	**Q523X**	**WT**	**L375F**	**R39Q**
State	**Active**	**Active**	**Active**	**Active**	**Active**
Ligands	P_i, GOL	P_i, GOL	P_i, GOL	ATP, Mg^{2+}, P_i, EDO	ATP, Mg^{2+}, P_i
Data collection					
Space group	*I*222	*I*222	*I222*	*I*222	*I*222
Cell dimensions					
a, *b*, *c* (Å)	90.9, 126.5, 130.2	91.1, 126.6, 130.6	90.7, 126.3, 130.7	91.5, 126.7, 130.2	92.4, 129.1, 131.0
α, β, γ (°)	90, 90, 90	90, 90, 90	90, 90, 90	90, 90, 90	90, 90, 90
Resolution (Å)	38.25-1.98 (2.03-1.98)*	48.94-2.05 (2.09-2.05)*	48.88-2.15 (2.18-2.15)*	48.94-2.10 (2.15-2.10)*	46.18-3.06 (3.12-3.06)*
R_{merge} (%)	9.1 (53.4)	6.7 (42.7)	5.7 (24.5)	9.7 (55.0)	14.5 (49.8)
$CC_{1/2}$	0.98 (0.95)	0.98 (0.94)	0.99 (0.98)	0.98 (0.95)	0.96 (0.86)
$I/\sigma I$	25.1 (3.6)	36.6 (4.3)	43.1 (8.5)	35.2 (4.9)	9.8 (2.9)
Completeness (%)	99.9 (100)	100 (100)	100 (100)	100 (100)	99.2 (99.9)
Redundancy	12.1 (11.8)	7.4 (7.4)	7.4 (7.4)	14.7 (14.8)	4.7 (4.7)
Refinement					
Resolution (Å)	38.25-1.98 (2.00-1.98)	48.94-2.05 (2.07-2.05)	48.88-2.15 (2.18-2.15)	48.94-2.10 (2.12-2.10)*	46.18-3.06 (3.16-3.06)
No. reflections	52,385 (1,558)	47,644 (1,455)	40,999 (1,233)	44,471 (1,304)	14,798 (1,077)
R_{work} / R_{free} (%)	16.6 (20.8)/ 20.1 (27.1)	16.6 (19.5)/ 19.9 (22.5)	17.0 (19.7)/ 21.0 (25.4)	15.3 (18.1)/ 18.4 (23.7)	16.0 (20.9)/ 22.1 (31.6)
No. atoms					
Protein	3,837	3,784	3,809	3,848	3,846
Ligand/ion	32	26	26	48	38
Water	445	356	284	439	77
B-factors					
Protein	29.1	33.3	31.6	30.4	50.7
Ligand/ion	45.9	55.1	44.8	32.8	46.5
Water	26.2	39.6	43.2	29.4	36.2
RMSD					
Bond lengths (Å)	0.006	0.006	0.007	0.006	0.007
Bond angles (°)	0.8	0.8	1.0	0.8	1.0
PDB code	6DD3	6DE0	6DE1	6DE2	6DE3

*Highest resolution shell is shown in parenthesis. P_i, EDO, and GOL represent phosphate ion, ethylene glycol, and glycerol.

Table S4. Related to Figure 2. Buried surface area (Å^2) in the basal versus active state.

Basal	**Strong dimer**	**Weak dimer**
WT-537X	9,783	1,799
R367Q-537X	8,438	1,973
Q523X	9,783	1,757
WT	14,469	2,423
R367Q	14,625	2,500
R39Q	15,699	2,512
Active	**Strong dimer**	**Weak dimer**
K359Q-537X	3,783	1,728
L375F-537X	4,442	1,719
R367Q-537X	4,057	1,693
D407A-537X	4,414	1,767
R238W-537X	4,052	1,651
Q523X	3,825	1,739
WT	4,187	1,852
L375F	4,184	1,710
R39Q	4,204	1,694

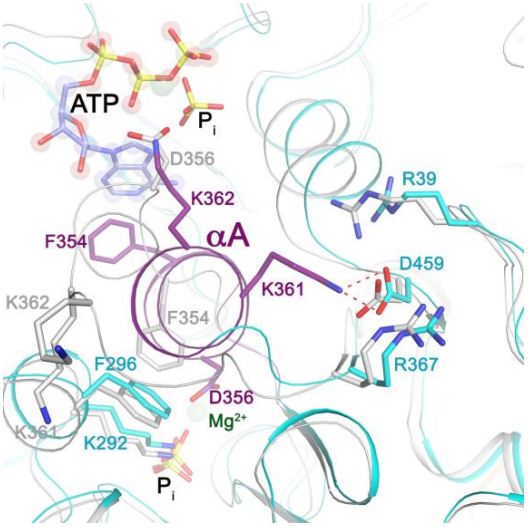

Figure S2. Related to Figure 3. Topology of the helix A (αA) region in basal vs active form of the full-length WT structures. A close-up view of helix A region (deep purple) in activated full-length wild-type NT5C2 as compared with that of basal structure (grey). The side chain of important residues on and near the helix A region are shown with stick models, and the Red dash lines represent H-bonds. Phosphate ions (P_i) and the metal ion are also shown. The stick model of ATP from the active structure of the full-length R39Q NT5C2 (R39Q) is also shown as a reference for the position of Pi in the active structure of the full-length wild-type NT5C2 (WT).

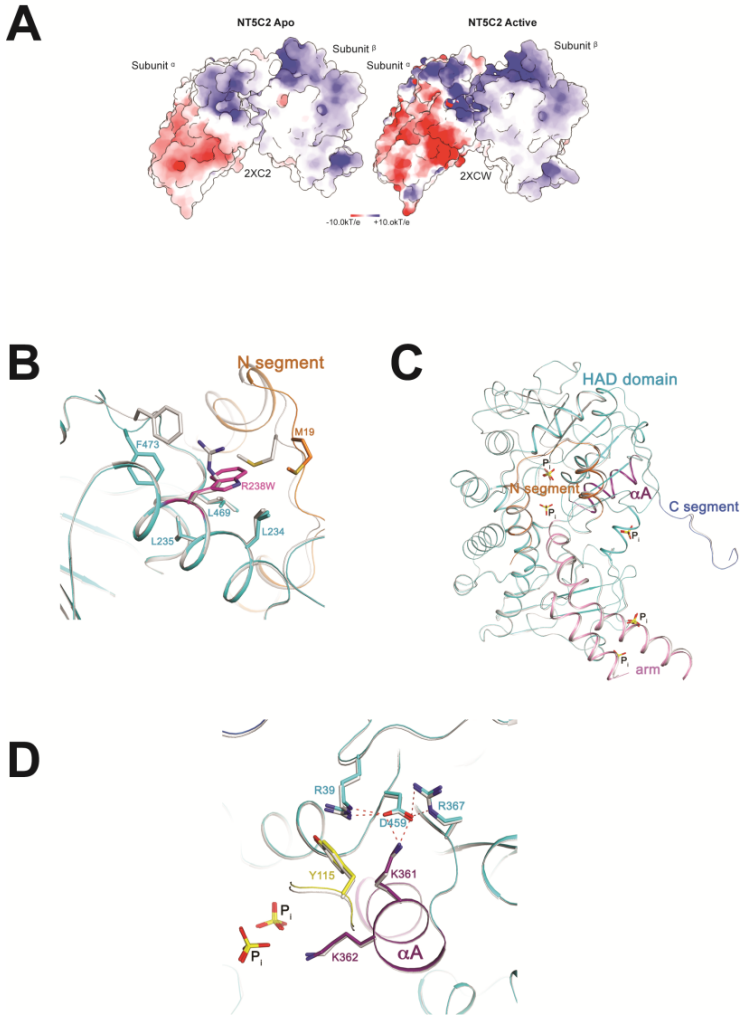

Figure S3. Related to Figure 4 Electrostatic Surface visualization of NT5C2 and close-up view of R238W mutation site and structural overlay of active NT5C2 D407A-537X and the full-length wild-type NT5C2 (WT). (**A**) Electrostatics comparison between apo (left) and active (right) wild-type NT5C2. Ambient Surface Representation of active NT5C2 with Adaptive Poisson-Boltzmann Solver values mapped and color-coded representing negativity (red) and positivity (blue). Scale shown is normalized to -10kT/e-10kT/e. (**B**) Structural overlay of NT5C2 R238W-537X (colored) and WT (grey). The side chains R238 (grey) and R238W (light magenta) and the residues surrounding are shown with stick models, labeled and colored accordingly. A hydrophobic tryptophan residue at position 238 is a much better fit for the local hydrophobic pocket comprising a number of hydrophobic residues (L234, L235, L469, F473, M19, L24). Substitution of R238 with Trp results in displacement of Cα of Met19 and Phe473 by ~1.5 Å, yet this has little effect in the overall conformation of the enzyme. (**C**) A Ribbon diagram showing the superposition of the active D407A-537X (colored) and WT (grey). The helix A (αA, deep purple), HAD domain and the three segments are colored and labeled for the structure of D407A. Phosphate ions are shown with stick models and labeled. (**D**) A close-up view of αA, depicting the essential hydrogen bonds (red dash lines) between D459 with the three basic residues R39, R367 and K361.

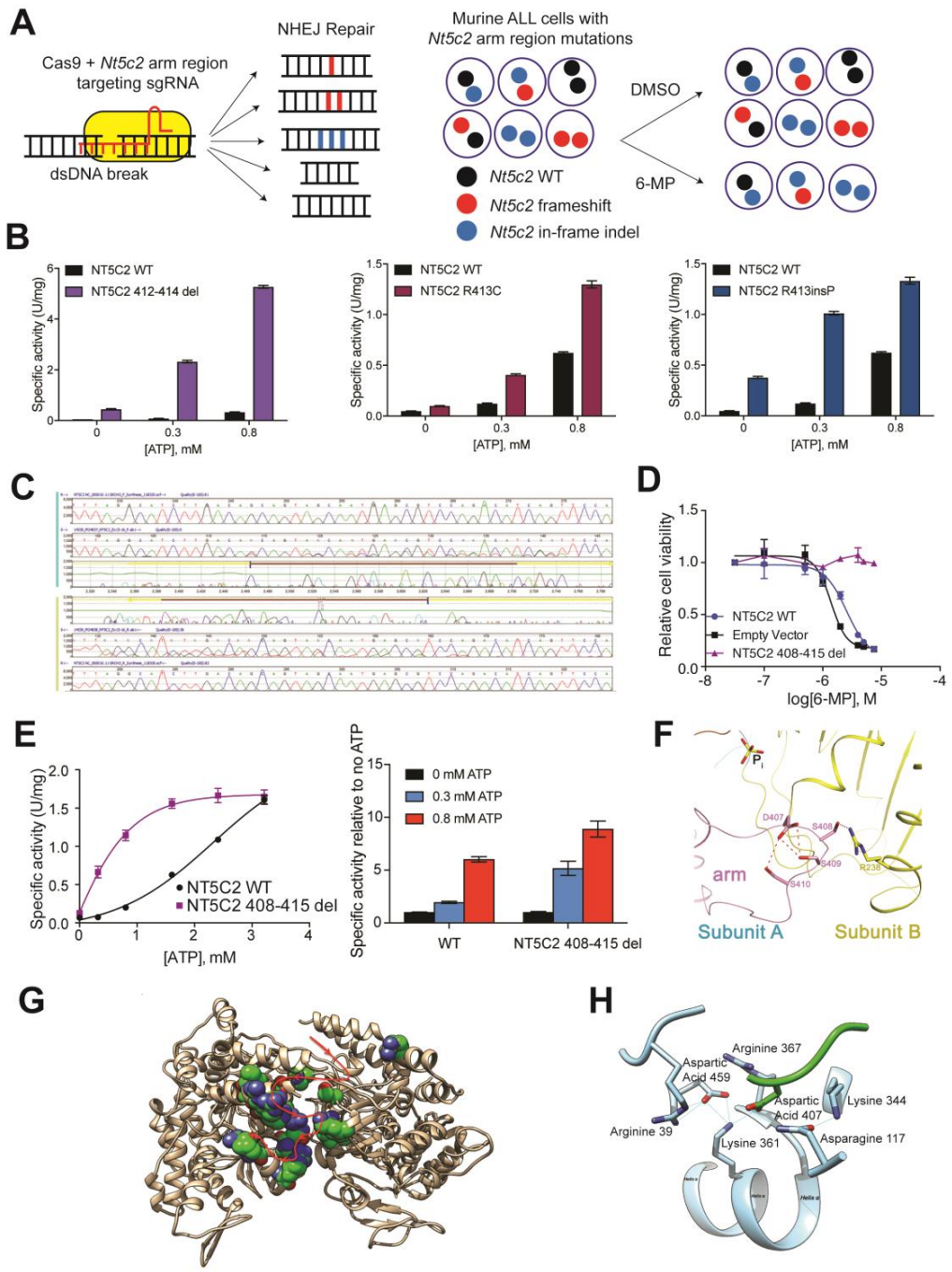

Figure S4. Related to Figure 5. Functional characterization of the NT5C2 arm region. (**A**) Schematic representation of CRISPR/CAS9 screen to identify gain-of-function NT5C2 alleles with inframe indels in the arm region of NT5C2. (**B**) *In vitro* nucleotidase assays of recombinant protein of inframe indel NT5C2 mutants identified as gain of function alleles in the CRISPR/Cas9 screen compared to NT5C2 wild-type protein. (**C**) Chromatogram of Relapse B-ALL 7 patient sample sanger sequencing of NT5C2 exon 15 showing the *NT5C2* p.S408-D415del mutation. (**D**) Cell viability assay showing drug response of JURKAT TET3G cell line

infected with doxycycline inducible wild-type or NT5C2 S408-D415 deletion expressing lentiviruses to increasing doses of 6-MP. (**E**) *In vitro* nucleotidase assays of NT5C2 S408-D415 deletion purified recombinant protein compared to NT5C2 wild-type. (**F**) Interaction of the tip region of the arm segment from one protomer with R238 of another protomer at the dimer interface. A close-up view of the hydrogen bonding network of the residues at the tip of the arm segment (pink) in subunits A and the side chain of R238 in subunit B. The red dashlines depict hydrogen bonds. (**G**) Utilizing molecular dynamics morphing between top ranked conformations in active NT5C2, the path of Asp407 was assessed for interactions. Dynamic register of electrostatic potential of different predicted conformations of Asp407 in the arm region reveals a distinct positive track into the inter-monomer cavity. Displayed residues are depicted in spherical atomic surface and colored by charge (blue=positive, red=negative, green=neutral). All atoms revealed show distance potential for electrostatic interaction with Asp407 as it passes through highest DOPE scoring models. Atoms reveal a positive track through which Asp407 and other loop residues may bind in a fleeting stepwise fashion (shown with red arrow). (**H**) Lowest energy prediction conformation of arm region showing interactions between Lys361 and Asp407 (green) via hydrogen bonding (teal lines). Data in **B**, **D** and **E** are shown as mean ± s.d.

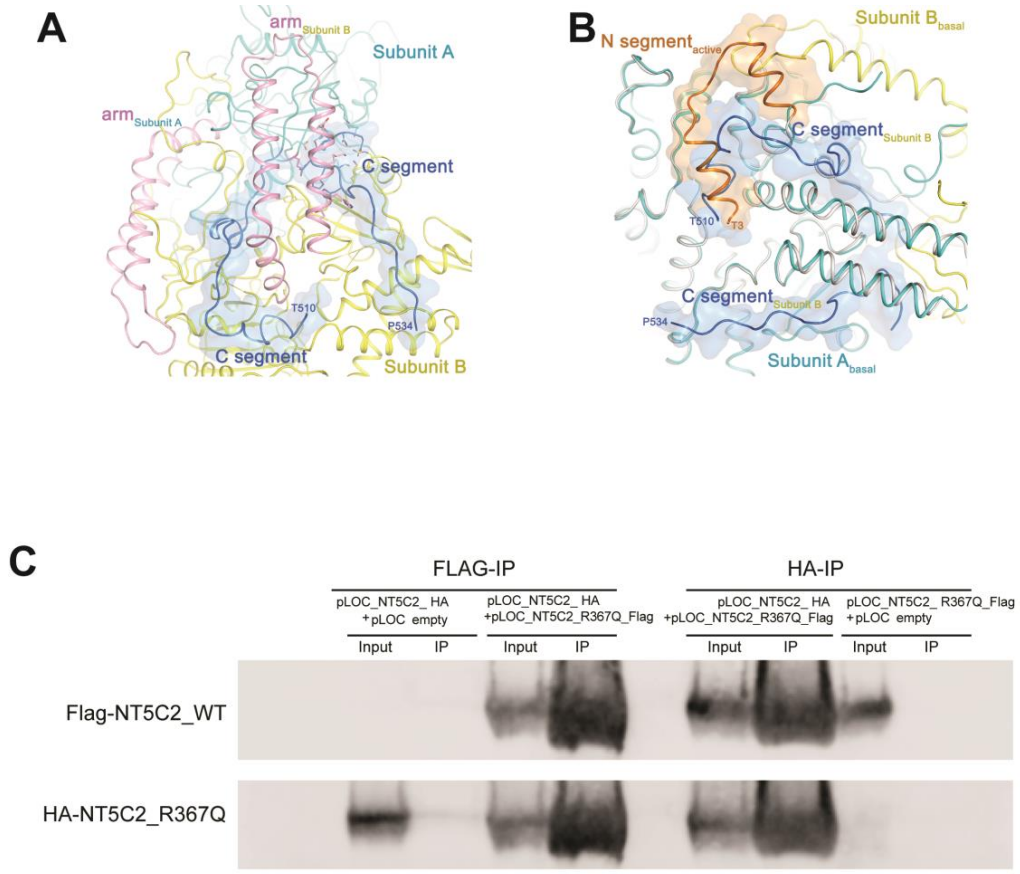

Figure S5. Related to Figure 6. The location of the C-terminal and N-terminal segments in the basal structure of the full-length R39Q and hetero-tetramer analysis. (**A**) A Ribbon diagram displaying the C-terminal segment (marine) of the full-length R39Q (R39Q) (cyan for Cα atoms) from subunit A (cyan), which wraps around the base of the arm segment (pink) of subunit B (yellow), where the acidic tail of the subunit A interacts with the positively-charged amino acids at the dimer interface. The arm segment of both subunit A and B is shown in pink, while the C-terminal segment of subunit A is colored marine and is also represented by surface so as to accentuate its location. Residues 511-535 of the C-terminal segment are disordered. (**B**) A Ribbon diagram showing an overlay of the active ATP-bound full-length R39Q dimer (orange for C atoms of the N segment and gray for the rest of Cα atoms) and the basal structure of the same enzyme, in which subunits A and B are shown in cyan and yellow, respectively. The C-segment of subunit B of the basal structure is colored in marine. The N-segment and the C-segment of the active and the basal structures are also depicted as transparent orange and marine surfaces, respectively. (**C**) Mutant-wild-type NT5C2 complex detection via Flag and HA immunoprecipitations from 293T cells expressing Flag-tagged NT5C2 wild-type and HA-tagged NT5C2 R367Q protein or empty vector controls.

Chapter 3: Clonal evolution mechanisms in *NT5C2* mutant-relapsed acute lymphoblastic leukaemia.

LETTER

doi:10.1038/nature25186

Clonal evolution mechanisms in *NT5C2* mutant–relapsed acute lymphoblastic leukaemia

Gannie Tzoneva[1]†*, Chelsea L. Dieck[1]*, Koichi Oshima[1], Alberto Ambesi-Impiombato[1]†, Marta Sánchez-Martín[1], Chioma J. Madubata[2], Hossein Khiabanian[3], Jiangyan Yu[4,5], Esme Waanders[4], Ilaria Iacobucci[6], Maria Luisa Sulis[7], Motohiro Kato[8], Katsuyoshi Koh[8], Maddalena Paganin[9], Giuseppe Basso[9], Julie M. Gastier-Foster[10,11,12,13], Mignon L. Loh[14,15], Renate Kirschner-Schwabe[16], Charles G. Mullighan[6], Raul Rabadan[2,17] & Adolfo A. Ferrando[1,2,7,18]

Relapsed acute lymphoblastic leukaemia (ALL) is associated with resistance to chemotherapy and poor prognosis[1]. Gain-of-function mutations in the 5′-nucleotidase, cytosolic II (*NT5C2*) gene induce resistance to 6-mercaptopurine and are selectively present in relapsed ALL[2,3]. Yet, the mechanisms involved in *NT5C2* mutation-driven clonal evolution during the initiation of leukaemia, disease progression and relapse remain unknown. Here we use a conditional-and-inducible leukaemia model to demonstrate that expression of NT5C2(R367Q), a highly prevalent relapsed-ALL *NT5C2* mutation, induces resistance to chemotherapy with 6-mercaptopurine at the cost of impaired leukaemia cell growth and leukaemia-initiating cell activity. The loss-of-fitness phenotype of $NT5C2^{+/R367Q}$ mutant cells is associated with excess export of purines to the extracellular space and depletion of the intracellular purine-nucleotide pool. Consequently, blocking guanosine synthesis by inhibition of inosine-5′-monophosphate dehydrogenase (IMPDH) induced increased cytotoxicity against *NT5C2*-mutant leukaemia lymphoblasts. These results identify the fitness cost of *NT5C2* mutation and resistance to chemotherapy as key evolutionary drivers that shape clonal evolution in relapsed ALL and support a role for IMPDH inhibition in the treatment of ALL.

Improved support and intensified chemotherapy regimens have increased the overall survival rates of newly diagnosed paediatric ALL to over 80%[1]. However, the outcomes of patients with relapsed or refractory ALL remain poor, with cure rates of only about 40%[1]. Leukaemia-initiating cells capable of self-renewal[4,5], protective microenvironment safe-haven niches[6,7] and clonal evolution[8–10] with acquisition of secondary genetic alterations driving chemotherapy resistance[2,3,9–13] have all been implicated as drivers of ALL disease progression and relapse. In this context, heterozygous activating mutations in the *NT5C2* nucleotidase gene are present in about 20% of relapsed paediatric T-cell ALL (T-ALL) cases[2] and 3–10% of relapsed B-precursor ALLs[2,3]. NT5C2 (Enzyme Commission (EC) number 3.1.3.5) is a highly conserved and ubiquitously expressed enzyme responsible for catalysing the 5′-dephosphorylation of the purine nucleotides inosine monophosphate, xanthine monophosphate and guanosine monophosphate[14]. This activity controls the intracellular levels of 6-hydroxypurine monophosphate nucleotides via their dephosphorylation to nucleosides, which are subsequently exported out of the cell[14,15]. In addition, NT5C2 metabolizes and inactivates the active metabolites that mediate the cytotoxic activity of 6-mercaptopurine (6-MP), a purine analogue chemotherapy drug that is broadly used in the treatment of ALL[16] (Extended Data Fig. 1). Expression of gain-of-function relapse-associated mutant forms of NT5C2 can therefore induce resistance to 6-MP *in vitro*[2,3].

Genomic profiling of matched samples from the time of ALL diagnosis and after relapse supports the hypothesis that cellular competition and chemotherapy resistance work as dynamic evolutionary forces that shape the clonal architecture of ALL[8–10]. To test this hypothesis we generated a knock-in mouse model ($Nt5c2^{+/co\text{-}R367Q}$) for conditional expression of Nt5c2(R367Q) (Extended Data Fig. 2), the most common *NT5C2* mutation found in relapsed ALL[2,3], and generated primary NOTCH1-induced $Rosa26^{+/CreERT2}Nt5c2^{+/co\text{-}R367Q}$ T-ALL tumours[17,18] (Extended Data Fig. 2) with conditional tamoxifen-inducible expression of Nt5c2(R367Q) (Fig. 1a and Extended Data Fig. 2). Treatment of isogenic *Nt5c2* wild-type ($Nt5c2^{+/co\text{-}R367Q}$, vehicle-treated) and $Nt5c2^{+/R367Q}$ mutant ($Nt5c2^{+/co\text{-}R367Q}$, 4-hydroxy-tamoxifen-treated) leukaemia cells with increasing concentrations of 6-MP showed overt resistance to thiopurine chemotherapy specifically in $Nt5c2^{+/R367Q}$ mutant cells (Fig. 1b). Moreover, $Nt5c2^{+/R367Q}$ mutant cells were positively selected in a dose-dependent manner over isogenic wild-type $Nt5c2^{+/co\text{-}R367Q}$ tumour cells under 6-MP treatment *in vitro* (Fig. 1c). Treatment of mice harbouring isogenic $Nt5c2^{+/co\text{-}R367Q}$ (vehicle treated, wild-type group) or $Nt5c2^{+/R367Q}$ (tamoxifen treated, mutant group) leukaemias with 6-MP produced a dose-dependent response in $Nt5c2^{+/co\text{-}R367Q}$ wild-type tumours and overt resistance with progression in $Nt5c2^{+/R367Q}$ mutant leukaemias (Fig. 1d, e and Extended Data Fig. 2g). Moreover, 6-MP treatment of mixed tumour populations of isogenic wild-type $Nt5c2^{+/co\text{-}R367Q}$ and mutant $Nt5c2^{+/R367Q}$ lymphoblasts demonstrated positive selection *in vivo* of cells harbouring the Nt5c2(R367Q)-encoding mutant allele (Extended Data Fig. 2h). These results support a direct role for NT5C2(R367Q) as a driver of 6-MP resistance *in vivo* and are concordant with the strong association of *NT5C2* mutations with early relapse and progression during 6-MP maintenance therapy in the clinic[2,3].

Recent genomic studies of matched diagnostic and relapsed ALL samples support the hypothesis that relapsed leukaemia emerges from the expansion of pre-existing resistant populations present as minor

[1]Institute for Cancer Genetics, Columbia University, New York, New York 10032, USA. [2]Department of Systems Biology, Columbia University, New York, New York 10032, USA. [3]Rutgers Cancer Institute, Rutgers University, New Brunswick, New Jersey 08903, USA. [4]Princess Maxima Center for Pediatric Oncology, Utrecht, 3584 CT, the Netherlands. [5]Department of Human Genetics, Radboud University Medical Center and Radboud Institute for Molecular Life Sciences, Nijmegen, 6525 GA, the Netherlands. [6]Department of Pathology, St. Jude Children's Research Hospital, Memphis, Tennessee 38105, USA. [7]Department of Pediatrics, Columbia University Medical Center, New York, New York 10032, USA. [8]Department of Hematology-Oncology, Saitama Children's Medical Center, Saitama 339-8551, Japan. [9]Onco-Hematology Division, Department, Salute della Donna e del Bambino (SDB), University of Padua, 35128 Padua, Italy. [10]Department of Pathology and Laboratory Medicine, Nationwide Children's Hospital, Columbus, Ohio 43205, USA. [11]Department of Pathology, Ohio State University School of Medicine, Columbus, Ohio 43210, USA. [12]Department of Pediatrics, Ohio State University School of Medicine, Columbus, Ohio 43210, USA. [13]Children's Oncology Group, Arcadia, California 91006, USA. [14]Department of Pediatrics, University of California, San Francisco, California 94143, USA. [15]Helen Diller Family Comprehensive Cancer Center, San Francisco, California 94115, USA. [16]Department of Pediatric Oncology/Hematology, Charité-Universitätsmedizin Berlin, Berlin, 10117, Germany. [17]Department of Biomedical Informatics, Columbia University, New York, New York 10032, USA. [18]Department of Pathology and Cell Biology, Columbia University Medical Center, New York, New York 10032, USA. †Present addresses: Regeneron Pharmaceuticals, Tarrytown, New York, New York 10591, USA (G.T.); PsychoGenics, Paramus, New Jersey 07652, USA (A.A.-I.).
*These authors contributed equally to this work.

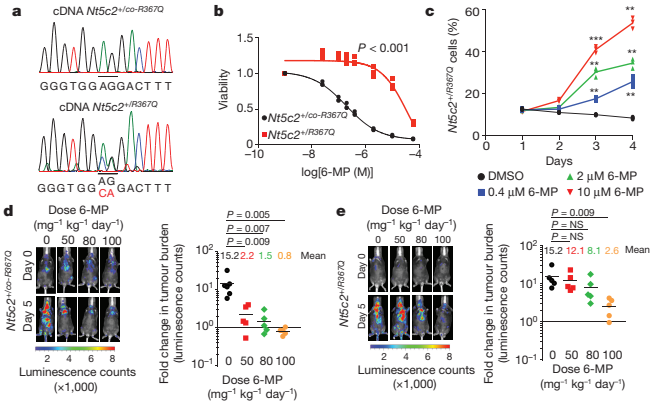

Figure 1 | Expression of Nt5c2(R367Q) in a NOTCH1-induced mouse model of ALL induces resistance to 6-MP. a, cDNA sequencing chromatograms of *Nt5c2*$^{+/co\text{-}R367Q}$ wild-type and *Nt5c2*$^{+/R367Q}$ isogenic T-ALL cells. Data are representative of results from more than two experiments. **b**, Cell viability of isogenic *Nt5c2*$^{+/co\text{-}R367Q}$ and *Nt5c2*$^{+/R367Q}$ T-ALL cells treated with increasing concentrations of 6-MP ($n = 3$ biological replicates). **c**, Change in the percentage of *Nt5c2*$^{+/R367Q}$ T-ALL cells over time in a mixed culture with isogenic *Nt5c2*$^{+/co\text{-}R367Q}$ cells treated with 6-MP ($n = 3$ biological replicates). DMSO, dimethylsulfoxide. **d**, **e**, Tumour burden in mice allografted with *Nt5c2*$^{+/co\text{-}R367Q}$ (**d**) or isogenic *Nt5c2*$^{+/R367Q}$ (**e**) leukaemia cells and treated with 6-MP. Data for the vehicle groups are from 6 (**d**) or 5 (**e**) mice and from 5 mice for the treatment groups. $^{**}P \leq 0.01$, $^{***}P \leq 0.001$, two-tailed Student's *t*-test. NS, not significant.

subclones at the time of diagnosis[19]. To evaluate further the role of NT5C2 as a driver of clonal progression and relapse in ALL, we used ultra-deep sequencing with unique-molecular-identifier barcoding (4,100× coverage) to analyse the presence of *NT5C2* mutations in 14 diagnostic DNA samples from cases showing acquired *NT5C2* mutations at relapse. Notably, these analyses (1:1,000 sensitivity) failed to detect the corresponding relapse-associated *NT5C2* mutant allele at the time of diagnosis (Extended Data Table 1). NT5C2(R367Q) allele-specific quantitative PCR (qPCR) ($n = 9$) (1:1,000 sensitivity) yielded similar negative results (Extended Data Table 1). Moreover, in one case bearing the NT5C2(R39Q) mutation at the time of relapse, droplet PCR analysis (1:20,000 sensitivity) detected the presence of this mutation during complete remission 37 days prior to the emergence of clinical relapse (Extended Data Table 1). Before then, and at the time of diagnosis, the signal for this mutation (0.00064%) was below the established sensitivity of the assay (0.005%). In a separate case we detected a NT5C2(P414A) mutation in first relapse and a second NT5C2(R39Q) variant in second relapse. In this patient, the NT5C2(P414A) mutation was not detectable by droplet PCR analysis at the time of diagnosis, whereas the mutant allele encoding NT5C2(R39Q) was detected below the 0.005% detection threshold at 0.0024–0.0031% frequency. However, analysis of bone marrow at the time of first relapse detected a NT5C2(R39Q) subclonal population (0.0058%) in addition to the NT5C2(P414A) clone. These NT5C2(R39Q) mutant cells expanded (0.0224%) in a serial sample obtained during a second complete remission 60 days later, while the NT5C2(P414A) mutant clone decreased, becoming clonal at the time of second relapse 50 days later (Extended Data Table 1). These results suggest that *NT5C2* mutations can be detected in complete-remission samples before relapse, yet, if present in the clonal repertoire at the time of diagnosis, they represent quantitatively minor populations below the sensitivity of molecular assays.

Resistance-driving mutations have been linked to enhanced leukaemia growth and proliferation, clonal expansion at early stages of tumour development and increased leukaemia stem-cell activity[20–22]. However, studies of resistance to bacterial antibiotics have uncovered frequent examples of evolutionary trade-offs in which the acquisition of drug resistance is coupled with a reduced-fitness phenotype[23]. In this context, we noted that in the absence of chemotherapy, *Nt5c2*$^{+/R367Q}$ mouse tumour cells showed decreased proliferation *in vitro*, a delayed entry into the S phase of the cell cycle (Fig. 2a, b) and delayed tumour progression *in vivo* compared with wild-type *Nt5c2*$^{+/co\text{-}R367Q}$ isogenic controls (Fig. 2c). Moreover, limiting dilution transplantation assays demonstrated a 17-fold reduction of leukaemia-initiating cell activity in mutant *Nt5c2*$^{+/R367Q}$ tumour cells (Fig. 2d–e and Extended Data Table 2). Of note, allele expression analysis of tumours recovered from mice transplanted with *Nt5c2*$^{+/R367Q}$ leukaemia lymphoblasts showed decreased expression of the mutant *Nt5c2* transcripts, suggesting downregulation of the mutant allele encoding Nt5c2(R367Q) during tumour progression in the absence of 6-MP (Extended Data Fig. 3). These results support the hypothesis that Nt5c2(R367Q) imposes a notable fitness cost to leukaemia lymphoblasts.

Given the role of NT5C2 in the degradation and export of purine nucleotides[15], we examined whether imbalances in the intracellular purine-nucleotide pool could mediate the loss-of-fitness phenotype observed in *Nt5c2*$^{+/R367Q}$ mutant leukaemia cells. Broad-based metabolomic analysis showed that NT5C2 activation in *Nt5c2*$^{+/R367Q}$ ALL lymphoblasts leads to decreased intracellular levels of NT5C2 substrates (inosine monophosphate, xanthine monophosphate and guanosine monophosphate) and accumulation of downstream nucleotide products and their metabolites (inosine, hypoxanthine, xanthosine, xanthine, guanine and uric acid) in conditioned media (Fig. 3 and Supplementary Tables 1, 2). Similarly, expression of NT5C2(R367Q)

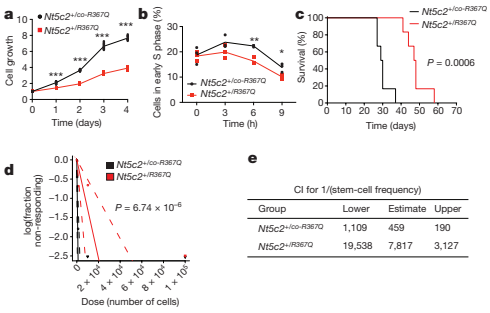

Figure 2 | Nt5c2(R367Q) expression impairs proliferation and leukaemia-initiating cell activity in ALL. a, *In vitro* growth (fold change) of isogenic *Nt5c2*$^{+/co\text{-}R367Q}$ wild-type and *Nt5c2*$^{+/R367Q}$ mutant mouse T-ALL cells. **b**, Cell cycle progression of *Nt5c2*$^{+/co\text{-}R367Q}$ and *Nt5c2*$^{+/R367Q}$ mouse T-ALL cells. **c**, Kaplan–Meier survival curve of mice harbouring *Nt5c2*$^{+/co\text{-}R367Q}$ and *Nt5c2*$^{+/R367Q}$ isogenic leukaemias ($n = 6$ per group). **d**, Leukaemia-initiating cell analysis in mice bearing *Nt5c2*$^{+/co\text{-}R367Q}$ or isogenic *Nt5c2*$^{+/R367Q}$ leukaemia cells ($n = 6$ mice per group). **e**, Confidence intervals (CI) showing 1/(stem-cell frequency) based on **d**. **a**, **b**, Data are from three biological replicates. $^{*}P \leq 0.05$, $^{**}P \leq 0.005$, $^{***}P \leq 0.001$, two-tailed Student's *t*-test (**a**, **b**) or two-sided log-rank test (**c**).

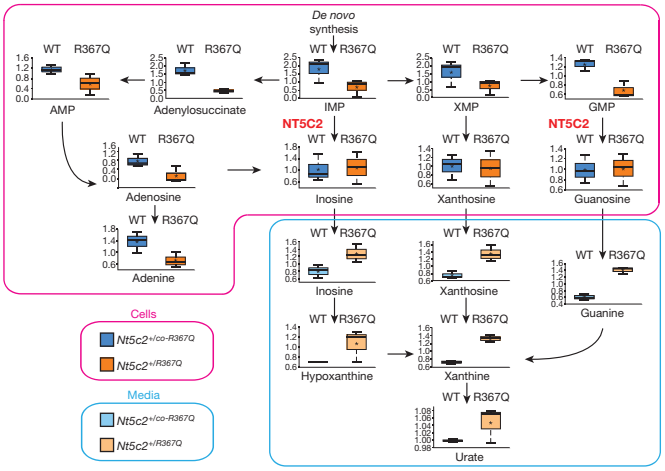

Figure 3 | Nt5c2(R367Q) decreases the intracellular purine nucleoside pool and increases secretion of purines in ALL cells. Diagram of the purine *de novo* biosynthesis and salvage pathways, showing gas chromatography–mass spectrometry and liquid chromatography–tandem mass spectrometry metabolic profiles (mass spectrometry scaled intensity, arbitrary units) of wild-type $Nt5c2^{+/co\text{-}R367Q}$ (WT) and $Nt5c2^{+/R367Q}$ mutant (R367Q) isogenic primary mouse T-ALL cells and their corresponding conditioned media ($n = 3$ biological replicates). Box plots represent the upper quartile to lower quartile distribution. Asterisks indicate mean values, horizontal lines indicate median values and whiskers indicate the maximum and minimum values.

in human T-ALL (CUTLL1) and B precursor ALL (REH) cell lines resulted in depletion of intracellular purine nucleotides and increased levels of purine metabolites in the culture media (Extended Data Fig. 4 and Supplementary Tables 3, 4). Increased extracellular purine metabolites are consistent with the described activity of NT5C2 in promoting the export of purine nucleotides[15] and might result in potential non-cell autonomous satellite effects modulating nucleotide metabolism and the response to 6-MP in by-standing wild-type *NT5C2* cells.

A corollary of these findings is that because of this metabolic imbalance, gain-of-function *NT5C2* mutations could be negatively selected during ALL tumour initiation and early disease progression, a time when clonal evolution is driven primarily by competition for microenvironment resources with normal haematopoietic stem and progenitor cells first, and then between different leukaemia clones[24]. Consistent with this model, integrated sequential network (ISN)[25] analysis of mutation dynamics from diagnostic and relapse mutation data identified *NT5C2* mutations as late events in the clonal evolution of ALL (Extended Data Fig. 5).

We hypothesized that gain-of-function relapse-associated *NT5C2* mutations could result in increased leukaemia dependence on purine synthesis, rendering leukaemia lymphoblasts more sensitive to drugs targeting this pathway. Indeed, acquired drug resistance in bacteria can be accompanied by collateral sensitivity to an alternative antibiotic agent[23]. To test this possibility, we analysed the response of $Nt5c2^{+/co\text{-}R367Q}$ wild-type and isogenic $Nt5c2^{+/R367Q}$ mutant ALL lymphoblasts to mizoribine, an inhibitor of inosine-5′-monophosphate dehydrogenase (IMPDH), a rate-limiting enzyme required for the synthesis of guanine nucleotides[26]. Notably, these experiments demonstrated significantly increased sensitivity to mizoribine in $Nt5c2^{+/R367Q}$ mutant leukaemia cells *in vitro* compared to $Nt5c2^{+/co\text{-}R367Q}$ wild-type isogenic controls (Fig. 4a and Extended Data Fig. 6). Moreover, guanosine supplementation in the media rescued the effects of mizoribine in

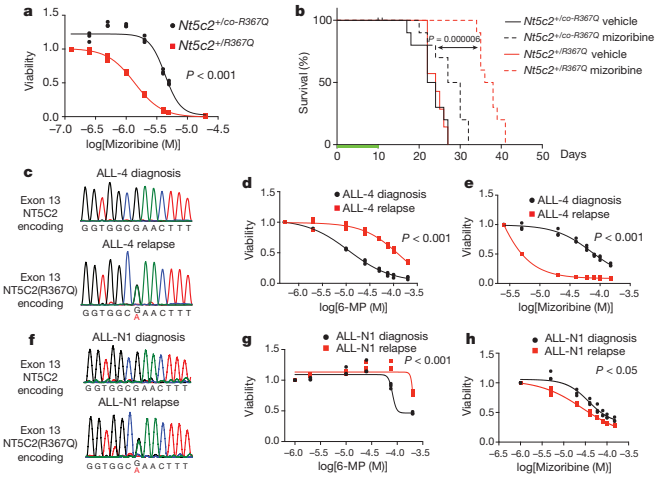

Figure 4 | Collateral sensitivity to IMPDH inhibition in NT5C2(R367Q) mutant tumour cells. a, Cell viability of isogenic $Nt5c2^{+/co\text{-}R367Q}$ and $Nt5c2^{+/R367Q}$ T-ALLs treated with mizoribine. **b**, Kaplan–Meier survival curve of mice harbouring $Nt5c2^{+/co\text{-}R367Q}$ and $Nt5c2^{+/R367Q}$ isogenic leukaemias ($n = 10$ mice per group) after initial treatment with mizoribine or vehicle (green bar). **c**, **f**, DNA sequencing chromatograms corresponding to two matched primary human T-ALL xenografts obtained from samples taken at the time of diagnosis (wild-type NT5C2) and after relapse (NT5C2(R367Q)) (matched pairs are labelled as ALL-4 (**c**–**e**) and ALL-N1 (**f**–**h**)). **d**, **g**, Cell viability of samples evaluated in **c** and **f** showing resistance to 6-MP in relapsed T-ALL xenograft cells. **e**, **h**, Cell viability in samples analysed in **c**, **f**, **d** and **g** showing collateral sensitivity to mizoribine in relapsed T-ALL xenograft cells. Data in **a**, **d**, **e**, **g** and **h** are from three biological replicates and *P* values were calculated using two-tailed Student's *t*-test. *P* value in **b** was calculated with a two-sided log-rank test.

Nt5c2$^{+/co\text{-}R367Q}$ wild-type and *Nt5c2*$^{+/R367Q}$ mutant lymphoblasts, supporting a mechanistic role for nucleotide depletion in the activity of this drug and its synthetic lethal interaction with the mutant allele encoding Nt5c2(R367Q) (Extended Data Fig. 6). Similar differential responses to mizoribine in wild-type *Nt5c2*$^{+/co\text{-}R367Q}$ cells and in *Nt5c2*$^{+/R367Q}$ mutant cells were observed *in vivo* in a subcutaneous lymphoma model (Extended Data Fig. 6). Furthermore, treatment of *Nt5c2*$^{+/R367Q}$ leukaemia-bearing mice with mizoribine induced a marked *in vivo* anti-leukaemic response, with significantly improved survival compared with isogenic *Nt5c2*$^{+/co\text{-}R367Q}$ wild-type controls ($P < 0.0001$) (Fig. 4b). Similarly, expression of gain-of-function NT5C2 mutations (R238W, K359Q, R367Q and D407A) associated with relapse in CUTLL1 and REH ALL cells induced resistance to 6-MP and increased their sensitivity to mizoribine (Extended Data Figs 7, 8). As before, guanosine supplementation ameliorated the anti-leukaemic effects of mizoribine in this experiment, providing evidence that depletion of nucleotides is the mechanism of action for this drug (Extended Data Figs 7, 8). Additionally, knockdown of *IMPDH2*, the gene encoding the main IMPDH isoform expressed in proliferating tissues and tumour cells, led to decreased growth in NT5C2(R367Q)-expressing REH and CUTLL1 cells compared to wild-type *NT5C2*-expressing lymphoblasts (Extended Data Figs 7, 8). We also observed resistance to 6-MP with increased sensitivity to mizoribine in leukaemia cells from two human primary xenografts harbouring the mutant NT5C2(R367Q)-encoding allele compared to matched wild-type NT5C2 ALL blasts derived from samples obtained at the time of diagnosis (Fig. 4c–h). Moreover, immunodeficient mice transplanted with an NT5C2(R367Q) xenograft derived from a relapsed patient showed decreased tumour burden and tumour infiltration following mizoribine treatment compared to mice transplanted with matched wild-type *NT5C2* xenograft cells derived from samples taken at the time of diagnosis (Extended Data Fig. 6).

These results document fitness cost and acquired resistance to 6-MP as evolutionary forces that drive the clonal evolution dynamics and selection of relapse-associated *NT5C2* mutations in ALL, highlight the relevance of nucleotide export in the control of nucleotide homeostasis[27] and in the context of antimetabolite therapy[28], and identify collateral sensitivity to IMPDH inhibition as a potentially relevant vulnerability in *NT5C2*-mutant leukaemia.

Online Content Methods, along with any additional Extended Data display items and Source Data, are available in the online version of the paper; references unique to these sections appear only in the online paper.

Received 7 December 2016; accepted 30 November 2017.
Published online 17 January 2018.

1. Hunger, S. P. & Mullighan, C. G. Acute lymphoblastic leukemia in children. *N. Engl. J. Med.* **373,** 1541–1552 (2015).
2. Tzoneva, G. *et al.* Activating mutations in the *NT5C2* nucleotidase gene drive chemotherapy resistance in relapsed ALL. *Nat. Med.* **19,** 368–371 (2013).
3. Meyer, J. A. *et al.* Relapse-specific mutations in *NT5C2* in childhood acute lymphoblastic leukemia. *Nat. Genet.* **45,** 290–294 (2013).
4. Gerby, B. *et al.* Expression of CD34 and CD7 on human T-cell acute lymphoblastic leukemia discriminates functionally heterogeneous cell populations. *Leukemia* **25,** 1249–1258 (2011).
5. Cox, C. V., Diamanti, P., Evely, R. S., Kearns, P. R. & Blair, A. Expression of CD133 on leukemia-initiating cells in childhood ALL. *Blood* **113,** 3287–3296 (2009).
6. Konopleva, M. *et al.* Stromal cells prevent apoptosis of AML cells by up-regulation of anti-apoptotic proteins. *Leukemia* **16,** 1713–1724 (2002).
7. Hawkins, E. D. *et al.* T-cell acute leukaemia exhibits dynamic interactions with bone marrow microenvironments. *Nature* **538,** 518–522 (2016).
8. Mullighan, C. G. *et al.* Genomic analysis of the clonal origins of relapsed acute lymphoblastic leukemia. *Science* **322,** 1377–1380 (2008).
9. Ma, X. *et al.* Rise and fall of subclones from diagnosis to relapse in pediatric B-acute lymphoblastic leukaemia. *Nat. Commun.* **6,** 6604 (2015).
10. Oshima, K. *et al.* Mutational landscape, clonal evolution patterns, and role of RAS mutations in relapsed acute lymphoblastic leukemia. *Proc. Natl Acad. Sci. USA* **113,** 11306–11311 (2016).
11. Li, B. *et al.* Negative feedback-defective PRPS1 mutants drive thiopurine resistance in relapsed childhood ALL. *Nat. Med.* **21,** 563–571 (2015).
12. Mullighan, C. G. *et al. CREBBP* mutations in relapsed acute lymphoblastic leukaemia. *Nature* **471,** 235–239 (2011).
13. Malinowska-Ozdowy, K. *et al. KRAS* and *CREBBP* mutations: a relapse-linked malicious liaison in childhood high hyperdiploid acute lymphoblastic leukemia. *Leukemia* **29,** 1656–1667 (2015).
14. Spychała, J., Madrid-Marina, V. & Fox, I. H. High K_m soluble 5′-nucleotidase from human placenta. Properties and allosteric regulation by IMP and ATP. *J. Biol. Chem.* **263,** 18759–18765 (1988).
15. Gazziola, C., Ferraro, P., Moras, M., Reichard, P. & Bianchi, V. Cytosolic high K_m 5′-nucleotidase and 5′(3′)-deoxyribonucleotidase in substrate cycles involved in nucleotide metabolism. *J. Biol. Chem.* **276,** 6185–6190 (2001).
16. Brouwer, C. *et al.* Role of 5′-nucleotidase in thiopurine metabolism: enzyme kinetic profile and association with thio-GMP levels in patients with acute lymphoblastic leukemia during 6-mercaptopurine treatment. *Clin. Chim. Acta* **361,** 95–103 (2005).
17. Schroeter, E. H., Kisslinger, J. A. & Kopan, R. Notch-1 signalling requires ligand-induced proteolytic release of intracellular domain. *Nature* **393,** 382–386 (1998).
18. Herranz, D. *et al.* A NOTCH1-driven MYC enhancer promotes T cell development, transformation and acute lymphoblastic leukemia. *Nat. Med.* **20,** 1130–1137 (2014).
19. Ferrando, A. A. & López-Otín, C. Clonal evolution in leukemia. *Nat. Med.* **23,** 1135–1145 (2017).
20. Clappier, E. *et al.* Clonal selection in xenografted human T cell acute lymphoblastic leukemia recapitulates gain of malignancy at relapse. *J. Exp. Med.* **208,** 653–661 (2011).
21. Wong, T. N. *et al.* Rapid expansion of preexisting nonleukemic hematopoietic clones frequently follows induction therapy for *de novo* AML. *Blood* **127,** 893–897 (2016).
22. Shlush, L. I. *et al.* Tracing the origins of relapse in acute myeloid leukaemia to stem cells. *Nature* **547,** 104–108 (2017).
23. Andersson, D. I. & Hughes, D. Antibiotic resistance and its cost: is it possible to reverse resistance? *Nat. Rev. Microbiol.* **8,** 260–271 (2010).
24. Greaves, M. & Maley, C. C. Clonal evolution in cancer. *Nature* **481,** 306–313 (2012).
25. Wang, J. *et al.* Tumor evolutionary directed graphs and the history of chronic lymphocytic leukemia. *eLife* **3,** (2014).
26. Gan, L. *et al.* The immunosuppressive agent mizoribine monophosphate forms a transition state analogue complex with inosine monophosphate dehydrogenase. *Biochemistry* **42,** 857–863 (2003).
27. Reaves, M. L., Young, B. D., Hosios, A. M., Xu, Y. F. & Rabinowitz, J. D. Pyrimidine homeostasis is accomplished by directed overflow metabolism. *Nature* **500,** 237–241 (2013).
28. Ser, Z. *et al.* Targeting one carbon metabolism with an antimetabolite disrupts pyrimidine homeostasis and induces nucleotide overflow. *Cell Reports* **15,** 2367–2376 (2016).

Supplementary Information is available in the online version of the paper.

Acknowledgements We are grateful to R. Kopan for the ΔE-NOTCH1 construct and T. Ludwig for the *ROSA26*$^{Cre\text{-}ERT2/+}$ mouse. This work was supported by the Leukemia & Lymphoma Society Quest for Cures (R0749-14) and Translational Research (6455-15; 6531-18) awards (A.A.F.), an Innovative Research Award from the Alex Lemonade Stand Foundation (A.A.F.), the Chemotherapy Foundation (A.A.F.), National Institutes of Health (NIH) grants R35 CA210065 (A.A.F.), R01 CA206501 (A.A.F.), U54 CA193313 (R.R.), R01 CA185486 (R.R.), U54 CA209997 (R.R.), U10 CA98543 (J.M.G., M.L.L.), P30 CA013696, the Human Specimen Banking Grant U24 CA114766 (J.M.G.), the Stewart Foundation (R.R.) and the American Lebanese Syrian Associated Charities of St Jude Children's Research Hospital. G.T. was supported by a HHMI International Student Research Fellowship. M.S.M. was supported by a Rally Foundation fellowship. C.L.D. was supported by NIH/NCI T32-CA09503. J.Y. was supported by the China Scholarship Council (CSC 201304910347) and the Ter Meulen Grant of the Royal Netherlands Academy of Arts and Sciences. E.W. was supported by the Dutch Cancer Society (KUN2012-5366).

Author Contributions G.T. and C.L.D. performed biochemical, cellular and animal studies. M.S.-M. and K.O. helped in experimental therapeutic experiments. A.A.-I. and H.K. analysed deep sequencing data. C.J.M. performed ISN analysis. M.L.S., M.K., K.K., M.P., G.B., J.M.G.-F. and M.L.L. provided clinical specimens. J.Y., E.W. and I.I. performed and analysed droplet PCR analyses. R.K.-S. provided clinical samples and correlative analyses of clinical data. C.G.M. supervised droplet PCR analyses; R.R. supervised deep sequencing and ISN analyses. A.A.F. designed the study, supervised the research and wrote the manuscript with G.T. and C.L.D.

Author Information Reprints and permissions information is available at www.nature.com/reprints. The authors declare no competing financial interests. Readers are welcome to comment on the online version of the paper. Publisher's note: Springer Nature remains neutral with regard to jurisdictional claims in published maps and institutional affiliations. Correspondence and requests for materials should be addressed to A.A.F. (af2196@columbia.edu).

METHODS

Patient samples. DNA samples from leukaemic ALL blasts obtained at diagnosis and after relapse and matched remission lymphocytes were provided by the Hemato-Oncology Laboratory at University of Padua, Italy; the Children's Oncology Group in the Department of Hematology/Oncology at Saitama Children's Medical Center, Saitama, Japan and St Jude Children's Research Hospital. Informed consent was obtained at study entry and samples were collected under the supervision of local Institutional Review Boards for participating institutions and analysed under the supervision of the Columbia University Medical Center Institutional Review Board (Protocol Number: IRB-AAAB3250). Research was conducted in compliance with ethical regulations.

Cell lines and cell culture procedures. We performed cell culture in a humidified atmosphere at 37 °C under 5% CO_2. We harvested primary mouse tumour cells from the spleens of leukaemic mice by processing spleens through a 70-μm mesh to obtain single-cell suspensions and incubated cells with red blood cell lysis buffer. Tumour cells were then placed in culture in Opti-MEM media supplemented with 10% fetal bovine serum (FBS), 100 U ml^{-1} penicillin G, 100 μg ml^{-1} streptomycin, 55 μM β-mercaptoethanol, 10 ng ml^{-1} mouse IL-7 and 10 ng ml^{-1} human IL-2. Subsequent passages of tumour cells did not include IL-2. We passaged and harvested primary human xenograft T-ALL cells from the spleens of NRG (NOD.Cg-*Rag1*^{tm1Mom}*Il2rg*^{tm1Wjl}/SzJ, Jackson Laboratory) mice and cultured them in RPMI media supplemented with 20% FBS, 100 U ml^{-1} penicillin G, 100 μg ml^{-1} streptomycin and 10 ng ml^{-1} human IL-7. We purchased HEK293T cells for viral production and REH cells from American Type Culture Collection. The CUTLL1 cell line, which was generated by continuous culture of T-cell lymphoblastic pleural effusion cells from a patient in relapse, has been characterized and reported previously[29]. We grew HEK293T cells in DMEM media supplemented with 10% FBS, 100 U ml^{-1} penicillin G and 100 μg ml^{-1} streptomycin for up to two weeks. We cultured CUTLL1 and REH cells in RPMI-1640 media supplemented with 10% FBS, 100 U ml^{-1} penicillin G and 100 μg ml^{-1} streptomycin. Cell lines were regularly authenticated and tested for mycoplasma contamination.

Drugs. We purchased tamoxifen, guanosine, 4-hydroxytamoxifen, 6-mercaptopurine (6-MP) and mizoribine from Sigma-Aldrich. For *in vitro* assays we dissolved 4-hydroxytamoxifen in 100% ethanol, guanosine in DMSO, 6-MP in DMSO and mizoribine in PBS. For *in vivo* studies we resuspended 100 mg tamoxifen in 100 μl of ethanol and added corn oil to reach a final concentration of 3 mg 100 μl^{-1}. We then rotated the tamoxifen suspension for 1 h at 55 °C and froze it in aliquots at −20 °C. We administered tamoxifen as a single 100 μl intraperitoneal injection per mouse. For intraperitoneal injections of 6-MP we prepared frozen aliquots of 5 mg ml^{-1} 6-MP in 0.1 M NaOH and immediately before each round of treatment we prepared fresh final solutions of 6-MP by buffering the stock solution down to pH 8 with 0.2 M NaH_2PO_4. This resulted in a 6-MP concentration of 3.48 mg ml^{-1}, which we diluted to various final concentrations using a solution made from 0.05 M NaOH and 0.2 M NaH_2PO_4 adjusted to pH 8. We administered 6-MP as 25 mg kg^{-1}. 40 mg kg^{-1} and 50 mg kg^{-1} all twice a day. We prepared vehicle by dissolving 0.254 g NaCl in 50 ml 0.05 M NaOH and adjusting the pH to 8 with 0.2 M NaH_2PO_4. For intraperitoneal injections we dissolved mizoribine (TCI America and Toronto Research Chemicals) in PBS at 10 mg ml^{-1} or 15 mg ml^{-1} and froze aliquots to be thawed before treatment. We adjusted injection volume to correct for any differences in weight between individual mice.

Plasmid and vectors. We obtained MigR1_Δ-E NOTCH1_GFP from R. Kopan, sh-TURBOGFP and pLKO.1_IMPDH2_shRNA (clone ID: NM_000884.1-360s1c1) from Sigma Aldrich's Mission shRNA library and FUW-mCherry-Puro-Luc from ref. 30. We generated the NT5C2 R238W, K359Q, R367Q and D407A mutations in the pLOC-NT5C2 plasmid[2] by site-directed mutagenesis using the QuikChange II XL Site-Directed Mutagenesis kit (Stratagene) according to the manufacturer's instructions.

Retroviral and lentiviral infections. We transfected retroviral or lentiviral plasmids together with *gag-pol* (pCMV ΔR8.91) and V-SVG (pMD.G VSVG) expressing vectors into HEK293T cells using JetPEI transfection reagent (Polyplus). We collected viral supernatants after 48 h and used them to infect mouse bone marrow progenitors, human cell lines, or primary tumour cells by spinoculation with 4 μg ml^{-1} Polybrene Infection/Transfection Reagent (Fisher Scientific). We selected infected primary mouse tumour cells or human cell lines with 1 mg ml^{-1} blasticidin (InvivoGen) for 14 days.

Mice and animal procedures. We maintained all animals in specific pathogen-free facilities at the Irving Cancer Research Center at Columbia University Medical Campus. The Columbia University Institutional Animal Care and Use Committee (IACUC) approved all animal procedures. Animal experiments were conducted in compliance with all relevant ethical regulations. Animals were euthanized upon showing symptoms of clinically overt disease (do not feed, lack of activity, abnormal grooming behaviour, hunch back posture) or excessive weight loss (10–15% body weight loss over a week) and before reaching the maximum permitted tumour burden of 90% blasts in the bone marrow. To generate conditional Nt5c2(R367Q) knock-in mice we used homologous recombination in C57BL/6 embryonic stem cells to introduce a point mutation (AG→CA) in exon 14 that caused the R367Q substitution (two nucleotide changes were introduced to replace the mouse R367 codon (AGA) with a glutamine-coding codon (CAA)) as well as a loxP-flanked wild-type mini-gene cassette (1958 bp, inserted 233 bp upstream of exon 14) composed of the fusion of exons 14–18 and flanking genomic sequences upstream of exon 14 and downstream of exon 18. Immediately downstream of the mini-gene we introduced a FRT-flanked neomycin selection cassette. We generated chimaeras in C57BL/6 albino blastocysts using three independent knock-in embryonic stem-cell clones identified by PCR analysis and verified by Southern blot. We verified germ-line transmission in the offspring of highly chimaeric male mice crossed with C57BL/6 females. To remove the neomycin selection cassette we crossed mice harbouring the targeting construct with a Flp germ line deleter line (B6;SJL-Tg(ACTFLPe)9205Dym/J, Jackson Laboratory) and crossed the resulting mice with wild-type C57BL/6 to breed out the Flp allele. To generate inducible knock-in mice we bred animals harbouring the *Nt5c2*$^{co\text{-}R367Q}$ allele with *Rosa26*$^{+/creERT2}$ mice, which express a tamoxifen-inducible form of the Cre recombinase from the ubiquitous *Rosa26* locus[31].

To generate NOTCH1-induced T-ALL tumours in mice, we performed retroviral transduction of bone marrow cells (from *Rosa26*$^{+/creERT2}$*Nt5c2*$^{+/co\text{-}R367Q}$ mice) enriched in lineage negative cells isolated using magnetic beads (Lineage Cell Depletion Kit, Miltenyi Biotec) with retroviruses expressing an activated form of the *NOTCH1* oncogene (ΔE-NOTCH1)[17] and the green fluorescent protein (GFP) and transplanted them via intravenous injection into lethally irradiated isogenic recipients (6–8-week-old C57BL/6 females, Taconic Farms) as previously described[18,32].

We assessed T-ALL tumour development by monitoring $CD4^+CD8^+GFP^+$ cells in peripheral blood by flow cytometry. In brief, we incubated blood samples with red blood cell lysis buffer (155 mM NH_4Cl, 10 mM $KHCO_3$, 0.1 mM EDTA) for 5 min at room temperature three times before staining with APC–Cy7-conjugated antibodies against mouse CD4 (BD Pharmingen-552051) and PE–Cy7-conjugated antibodies against mouse CD8a (eBioscience-25-0081-82). Flow cytometry analyses were performed in a FACSCanto flow cytometer (BD Biosciences) and analysed with Flowjo software (FlowJo LLC).

For all subsequent *in vivo* studies, we harvested fresh *Rosa26*$^{+/creERT2}$*Nt5c2*$^{+/co\text{-}R367Q}$ T-ALL tumour cells from the spleens of donor mice and transplanted them into sublethally irradiated (4 Gy) secondary recipients (C57BL/6 females, 6–8 weeks old, Taconic Farms). Animals were randomly assigned to different treatment groups and no blinding was done. For survival and leukaemia-initiating cell experiments, we treated mice with tamoxifen (3 mg via intraperitoneal injection) two days after transplantation to induce mini-gene-cassette deletion and expression of the *Nt5c2* allele encoding the R367Q mutation in the leukaemic cells, or with corn oil vehicle in the control group ($n = 6$ mice per group). Mice were then observed for incidence and time of onset of leukaemia.

To detect tamoxifen-inducible mini-gene deletion, we purified DNA from primary Rosa26$^{+/creERT2}$*Nt5c2*$^{+/co\text{-}R367Q}$ mouse tumour cells treated with 1 μM 4-hydroxytamoxifen or ethanol vehicle (*in vitro* experiments) and tamoxifen or corn oil vehicle (*in vivo* experiments) and then performed PCR-amplification with a three-primer reaction: (i) the minigene cassette (primer immediately upstream of proximal loxP site and reverse primer in exon 17) and (ii) the deleted mini-gene and wild-type alleles (primer immediately upstream of proximal loxP site and reverse primer in intron 14). The deleted and wild-type alleles differ by the size of the remaining loxP site (49 bp). We visualized PCR products resolved by electrophoresis in a 1.5% agarose gel with ethidium bromide.

To detect tamoxifen-inducible expression of mRNA corresponding to the *Nt5c2* allele encoding the R367Q mutation, we purified total RNA from mouse tumour cells with the RNeasy kit (Qiagen), prepared complementary DNA (cDNA) by reverse transcription using the SuperScript First-Strand Synthesis System for RT–PCR (Invitrogen) and PCR amplified the *Nt5c2* exon 14 cDNA region using primers spanning neighbouring exons following standard procedures. We analysed the resulting PCR products by dideoxy DNA sequencing to verify the expression of the engineered nucleotide substitutions in the *Nt5c2* allele encoding the R367Q mutation.

For experimental therapeutics treatment studies, we used *Rosa26*$^{+/creERT2}$ *Nt5c2*$^{+/co\text{-}R367Q}$ T-ALL tumour cells infected with lentiviral particles expressing the red cherry fluorescent protein and luciferase (FUW-mCherry-Luc-puro). We transplanted luciferased *Rosa26*$^{+/creERT2}$*Nt5c2*$^{+/co\text{-}R367Q}$ T-ALL tumour cells into C57BL/6 recipients by intravenous injection and monitored tumour development by *in vivo* luminescence bioimaging with the *In vivo* Imaging System (IVIS, Xenogen) and by flow cytometry using analysis of GFP^+ cells in peripheral blood. Once mice had 50% GFP positive cells in the peripheral blood and a detectable baseline tumour burden by bioluminescence, we treated them with tamoxifen

(3 mg, intraperitoneal injection) or corn oil vehicle as described above. Two days later we initiated treatment with a range of doses of 6-MP (0, 50, 80, 100 mg kg^{-1} per day) via intraperitoneal injection for five consecutive days ($n = 5$ mice per group). We monitored disease progression and response to chemotherapy by bioluminescence imaging on days 0, 3 and 6 after the start of 6-MP treatment. We euthanized mice on day 6 and analysed GFP$^+$ tumour infiltration in the spleen by flow cytometry. To assess mizoribine response *in vivo* we treated *Rosa26*$^{+/creERT2}$ *Nt5c2*$^{+/co\text{-}R367Q}$ leukaemia bearing mice 48 h following tamoxifen or corn oil vehicle treatment (as described above) with 40 mg kg^{-1} mizoribine or PBS vehicle ($n = 10$ per group) via intraperitoneal injection for ten consecutive days. Mice were then observed for incidence and time of onset of leukaemia.

For experimental therapeutic treatment studies in a subcutaneous setting, *Rosa26*$^{+/creERT2}$ *Nt5c2*$^{+/co\text{-}R367Q}$ T-ALL tumour cells infected with lentiviral particles expressing the red cherry fluorescent protein and luciferase (FUW-mCherry-Luc-puro) were treated with 1 μM 4-hydroxytamoxifen or ethanol vehicle *in vitro*, mixed with an equal volume of Corning Matrigel Membrane Matrix (Fisher Scientific) and injected (10^6 cells) into the flanks of female C57BL/6 mice. Upon detectable baseline tumour burden by bioluminescence, mice were treated intraperitoneally with PBS vehicle or mizoribine (20, 40, 75 or 100 mg kg^{-1} per day, $n = 4$ per dose) for 5 consecutive days. We monitored tumour progression and response to mizoribine by bioluminescence imaging on days 0 and 6 after the start of mizoribine treatment. Subcutaneous tumours were not allowed to exceed 20 mm in diameter.

To evaluate the competitive selection of *Nt5c2*$^{+/R367Q}$ cells *in vivo* we mixed wild-type *Nt5c2*$^{+/co\text{-}R367Q}$ and *Nt5c2*$^{+/R367Q}$ mutant mouse tumour cells at a 1:10, 1:100 and 1:1,000 *Nt5c2*$^{+/R367Q}$:*Nt5c2*$^{+/co\text{-}R367Q}$ ratios and transplanted into C57BL/6 recipients by intravenous injection. Ten days after transplant, mice were treated with vehicle or 50 mg kg^{-1} 6-MP per day for 5 days, then allowed to recover for ten days and given a second round of treatment for 1–3 days. Following this second cycle of treatment, mice were euthanized and lymphoblasts were recovered from spleen samples for quantitative evaluation of *Nt5c2*$^{+/R367Q}$ mutant cells.

We generated primary human leukaemia xenografts by intravenous injection of cryopreserved leukaemia lymphoblasts from diagnostic and relapsed acute lymphoblastic leukaemia patient samples into immunodeficient NRG mice.

We infected primary leukaemia xenograft cells with lentiviral particles expressing the red cherry fluorescent protein and luciferase (FUW-mCherry-Luc-puro) and transplanted matched ALL-4 diagnosis and ALL-4 relapse tumour cells into NRG immunodeficient recipients by intravenous injection and monitored tumour development by *in vivo* luminescence bioimaging with the *In vivo* Imaging System (IVIS, Xenogen) and by analysis of human CD45$^+$ cells in peripheral blood by flow cytometry with an APC conjugated antibody (eBioscience 17-0459-42). Upon tumour establishment, mice were treated intraperitoneally with PBS vehicle or mizoribine (100 mg kg^{-1} administered twice a day) for 3 consecutive days. Four animals in the relapse-xenograft mizoribine treatment group did not tolerate the full course of therapy presumably because of tumour lysis syndrome and were not included in the analysis. We euthanized mice on day 4 and analysed spleen weight and CD45$^+$ tumour infiltration in the bone marrow by flow cytometry.

***In vitro* cell viability and chemotherapy response assays.** We measured cell growth and chemotherapy responses of primary mouse tumours, patient-derived xenografts, and human ALL cell lines *in vitro* by measurement of the metabolic reduction of the tetrazolium salt MTT using the Cell Proliferation Kit I (Roche) following the manufacturer's instructions. We analysed chemotherapy responses following 72-h incubation with increasing concentrations of 6-mercaptopurine or mizoribine.

For the mixed culture experiment of isogenic wild-type *Nt5c2*$^{+/co\text{-}R367Q}$ and *Nt5c2*$^{+/R367Q}$ mouse tumour cells, we treated uninfected tumour cells (expressing GFP) with vehicle and treated the same tumour cells previously infected with a mCherry-expressing vector (FUW-mCherry-Luc-puro) with 4-hydroxytamoxifen and quantified proportions of the two cell populations by FACS analysis using a Fortessa flow cytometer (BD Biosciences) and analysed data with FlowJo software (FlowJo LLC). All experiments were performed in triplicate.

Cell synchronization and cell cycle analysis. We synchronized isogenic wild-type *Nt5c2*$^{+/co\text{-}R367Q}$ and *Nt5c2*$^{+/R367Q}$ mouse tumour cells using a double thymidine block procedure. In brief, we incubated cells with 2 mM thymidine (Sigma Aldrich) for 16 h, allowed cells to recover for 14 h in regular media, and incubated a second time with 2 mM thymidine for 16 h. We harvested cells at 0, 3, 6 and 9 h time points and stained them with propidium iodide (Sigma Aldrich) for cell cycle progression analysis. FACS analysis was performed using a FACSCanto flow cytometer (BD Biosciences) and we analysed data with FlowJo software (FlowJo LLC).

Quantitative allele-specific qPCR assay. We quantitatively assessed the presence of the allele encoding NT5C2(R367Q) in matching DNA specimens obtained at diagnosis and during remission using a custom Mutation Detection Competitive Allele-Specific TaqMan PCR (castPCR) Assay (Life Technologies) using 30 ng of DNA in a reaction volume of 20 μl in a 7500 real-time PCR system (Applied Biosystems) following the manufacturer's instructions and recommended cycling conditions. We determined a detection ΔC_t cut-off value for the assay by running the wild-type and mutant *NT5C2* assays on genomic DNA samples from three wild-type cell lines and calibrated both assays by spiking in increasing concentrations of wild-type *NT5C2* or of the plasmid containing the *NT5C2* allele encoding the R367Q mutation. We determined the assay sensitivity for the allele encoding NT5C2(R367Q) by analysing *NT5C2* wild-type genomic DNA samples spiked with decreasing concentrations of the plasmid containing the *NT5C2* allele encoding the R367Q mutation. We analysed experimental data using the Mutation Detector Software (Life Technologies) to calculate the ΔC_t value between the wild-type *NT5C2* and the NT5C2(R367Q)-encoding allele assay reads for each sample, and comparing these to the predetermined ΔC_t cut-off value.

To quantitatively assess the presence of *Nt5c2*$^{+/R367Q}$ mutant cells in mixed tumour populations of wild-type *Nt5c2*$^{+/co\text{-}R367Q}$ and *Nt5c2*$^{+/R367Q}$ mutant lymphoblasts, we performed a quantitative analyses of mutant transcripts normalizing tumour content by quantitative PCR with reverse transcription (RT–PCR) analysis of GFP. In this experiment we isolated RNA from lymphoblasts with the RNeasy kit (Qiagen) and prepared complementary DNA (cDNA) by reverse transcription using the SuperScript First-Strand Synthesis System for RT–PCR (Invitrogen). *Nt5c2* exon 14 was amplified using TaqMan Gene Expression Master Mix (TaqMan) and the allele encoding Nt5c2(R367Q) was detected using a mutant-specific TaqMan probe (5′ FAM-AGGGTGGCAGACTTT-MGBNFQ 3′, ThermoFisher). *Actb* (β-actin) and GFP were amplified using FastStart Universal SYBR Green Master (ROX) (Roche) following standard protocols. Quantitative PCR reactions were run in a 7500 Real Time PCR System (Applied Biosystems). C_t values of the allele encoding Nt5c2(R367Q) and GFP were normalized to *Actb* C_t values and a ratio was taken of Nt5c2(R367Q) expression over GFP expression to represent the percentage of *Nt5c2*$^{+/R367Q}$ mutant cells present in mixed tumour populations.

Digital droplet PCR. Targeted ultra-deep mutation screening was performed using the digital droplet PCR technique (RainDance Technologies) as described previously[33]. In brief, TaqMan assay primers and probes were custom designed for the allele encoding NT5C2(P414A) using PrimerExpress 3.0 (Thermo Fisher Scientific). Primers and probes for the allele encoding NT5C2(R39Q) were designed through the Custom TaqMan Assay Design Tool (CADT) (Life Technologies) with the support of RainDance Technologies. Probes matching the wild-type allele were labelled with VIC fluorescent reporter dye and probes matching the mutant allele were labelled with FAM dye. Amplicon sizes ranged from 75 bp to 120 bp. Genomic DNA was sheared to 3 kb using the M220 instrument (Covaris) and a total of 500–1,000 ng of fragmented DNA was used in each 50 μl ddPCR reaction. The digital droplet PCR reaction further contained 1× TaqMan Genotyping Master Mix (Applied Biosystems), 1× digital PCR droplet stabilizer (RainDance Techonologies), and 1× TaqMan primers and probes mix (Integrated DNA Technologies). In line with the manufacturer's instructions, an average of 7×10^6 droplets were generated by the RainDrop Source instrument and emulsion PCR was performed using the C1000 Thermal Cycler (BioRad). Droplet fluorescence of the amplified product was detected by the RainDrop Sense instrument and data analysis was carried out using the RainDrop Analyst II Software (RainDance Techonolgies).

To determine the detection limit of the assays, we constructed dilution curves of patient tumour cells and cells from the REH cell line. The REH cell line was confirmed to be wild type after Sanger sequencing for the locations targeted in the digital droplet PCR. We collected pure populations of tumour cells by flow cytometric sorting of the relapse samples of patients SJBALL192 (containing cells heterozygous for the allele encoding NT5C2(R39Q)). We made serial dilutions of tumour cells with wild-type cells (REH cell line) to generate final mutant allele frequency (MAF) levels of 50%, 5%, 0.5%, 0.05%, 0.005%, and 0.0005% and isolated DNA using phenol–chloroform. With an input of 500 ng DNA in the digital droplet PCR assay the MAFs correspond to 70,000, 7,000, 700, 70, 7, and 0.7 copies, respectively. A frequency of >0.005% (>7 copies) could be consistently detected.

Duplex sequencing of diagnostic patient samples. Duplex sequencing was carried out by TwinStrand Biosciences under fully blinded conditions using methods previously described[34,35]. In brief, 400 ng of extracted genomic DNA was ultrasonically sheared, A-tailed and ligated to degenerate tag-containing Duplex adapters. The library was amplified and subjected to two successive rounds of hybrid capture with 120 bp biotinylated oligonucleotide probes tiled across exons 9, 11, 13, 15, 16 and 17 of the human *NT5C2* gene and flanking sequences. Indexed libraries were pooled and sequenced on an Illumina NextSeq 500. Duplex consensus sequences were generated after alignment to hg38 using the requirement that error-corrected bases be supported by at least three independent reads from each original strand. The variant calls for each sample were filtered against known single nucleotide polymorphisms in the Phase 3 build of the 1000 genomes database and tabulated

versus all reference base calls at the eight codons of interest. Variant allele frequency was calculated as the number of variants per total number of error-corrected bases at each nucleotide position. The average error-corrected molecular depth at codons of interest was approximately 4,100× (1,840–8,530×), yielding an average power for detecting variants at a level of 1/1,000 of ~98%.

Metabolomic analyses. To analyse metabolic differences between *Nt5c2*$^{+/co\text{-}R367Q}$ and *Nt5c2*$^{+/R367Q}$ primary mouse tumours, we treated tumour cells in triplicate with 1 μM 4-hydroxytamoxifen for 48 h *in vitro* to induce expression of the allele encoding Nt5c2(R367Q) or with vehicle for wild-type controls, after which we diluted out the 4-hydroxytamoxifen or vehicle with media. After 72 h, we harvested cells into packed 50–100-μl size pellets and collected conditioned media for analyses ($n = 3$, cell pellets and media). We flash-froze cell pellet and media samples, which were then extracted using standard solvent extraction methods and analysed on the gas chromatography–mass spectrometry and liquid chromatography–tandem mass spectrometry platforms by Metabolon. Analysed metabolites consisted of a total of 459 named biochemicals in cells and 252 named biochemicals in media. We first normalized results to protein concentration, log transformed and imputed any missing values with the minimum observed value for each compound. We then used Welch's two-sample *t*-test to identify biochemicals that differed significantly between experimental groups. To account for the multiple comparisons that occur in metabolomics studies we also calculated an estimate of the false discovery rate (*q*-value), which indicates the fraction of biochemicals that would meet a given *P*-value cut-off by random chance. Similar processing and analyses were performed on CUTLL1 and REH ALL cell lines expressing wild-type NT5C2 or NT5C2(R367Q). Analysed metabolites in these cell lines consisted of a total of 596 named biochemicals in cells and 347 in media.

ISN of relapsed ALL. We illustrated the sequential order of somatic mutations in relapsed ALL using the ISN[25] that pools evolutionary paths across all patients. We selected recurrently mutated genes that were previously defined as drivers of paediatric ALL[36–38] and relapse-genes[10,11]. Only non-synonymous single nucleotide variants were used in analysis. For each patient, we generated a sequential network that defined early events as mutations observed in both the primary tumour and the relapsed tumour, whereas late events were mutations only observed in the relapsed tumour. Each node represented a gene, and each arrow pointed from a gene with an early event to a gene with a late event. The ISN then pooled sequential networks across all patients. To test whether a gene within the ISN was significantly early or late, we used the binomial test based on the in-degree and out-degree of each node. Somatic mutation data used to generate ISN were aggregated from previously published studies (refs 9–11).

Statistical analyses. We performed statistical analysis by Student's *t*-test. We considered results with $P < 0.05$ as statistically significant. Survival in mouse experiments was represented with Kaplan–Meier curves and significance was estimated with the log-rank test (GraphPad Prism). We analysed serial limited dilution leukaemia-initiating cell data using the ELDA software[39]. No outlier data points were excluded in the analyses.

Data availability. All data generated or analysed during this study are included in this published article and its Supplementary Information.

29. Palomero, T. *et al.* CUTLL1, a novel human T-cell lymphoma cell line with t(7;9) rearrangement, aberrant NOTCH1 activation and high sensitivity to gamma-secretase inhibitors. *Leukemia* **20,** 1279–1287 (2006).
30. Kimbrel, E. A. *et al.* Systematic *in vivo* structure-function analysis of p300 in hematopoiesis. *Blood* **114,** 4804–4812 (2009).
31. Guo, K. *et al.* Disruption of peripheral leptin signaling in mice results in hyperleptinemia without associated metabolic abnormalities. *Endocrinology* **148,** 3987–3997 (2007).
32. Herranz, D. *et al.* Metabolic reprogramming induces resistance to anti-NOTCH1 therapies in T cell acute lymphoblastic leukemia. *Nat. Med.* **21,** 1182–1189 (2015).
33. Iacobucci, I. *et al.* Truncating erythropoietin receptor rearrangements in acute lymphoblastic leukemia. *Cancer Cell* **29,** 186–200 (2016).
34. Schmitt, M. W. *et al.* Detection of ultra-rare mutations by next-generation sequencing. *Proc. Natl Acad. Sci. USA* **109,** 14508–14513 (2012).
35. Kennedy, S. R. *et al.* Detecting ultralow-frequency mutations by Duplex Sequencing. *Nat. Protoc.* **9,** 2586–2606 (2014).
36. Futreal, P. A. *et al.* A census of human cancer genes. *Nat. Rev. Cancer* **4,** 177–183 (2004).
37. Van Vlierberghe, P. & Ferrando, A. The molecular basis of T cell acute lymphoblastic leukemia. *J. Clin. Invest.* **122,** 3398–3406 (2012).
38. Zhang, J. *et al.* Key pathways are frequently mutated in high-risk childhood acute lymphoblastic leukemia: a report from the Children's Oncology Group. *Blood* **118,** 3080–3087 (2011).
39. Hu, Y. & Smyth, G. K. ELDA: extreme limiting dilution analysis for comparing depleted and enriched populations in stem cell and other assays. *J. Immunol. Methods* **347,** 70–78 (2009).

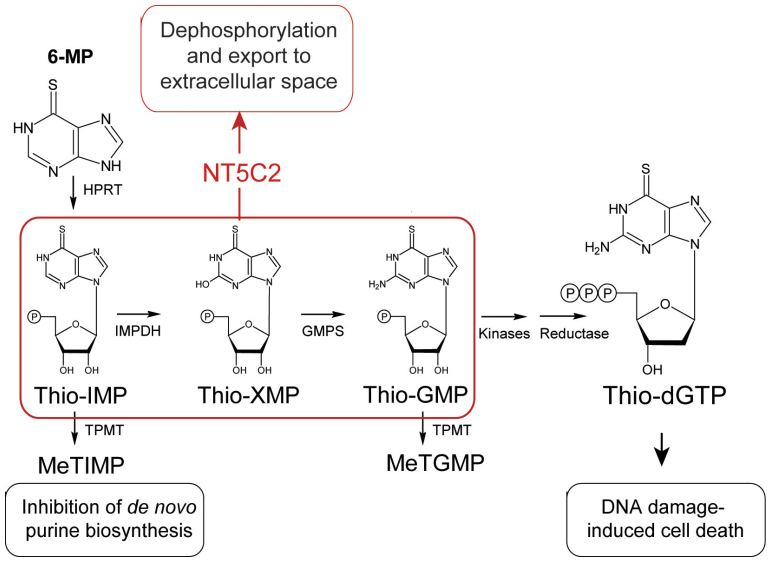

Extended Data Figure 1 | Schematic representation of 6-MP activation and mechanism of action. The hypoxanthine-guanine phosphoribosyl transferase enzyme (HPRT) processes 6-MP to thio-IMP, which is then converted to thio-XMP and thio-GMP. Subsequent metabolism of thio-GMP by kinases and reductases yields thio-dGTP which is incorporated into replicating DNA strands and triggers the DNA mismatch-repair machinery, leading to cell cycle arrest and apoptosis. The anti-leukaemic effects of 6-MP are in part also attributed to a second metabolic pathway in which thiopurine *S*-methyl transferase (TPMT) methylates thio-IMP to form methylthio-IMP (MeTIMP), which is a potent inhibitor of amidophosphoribosyltransferase (ATase), an enzyme catalysing the committed step of *de novo* purine biosynthesis.

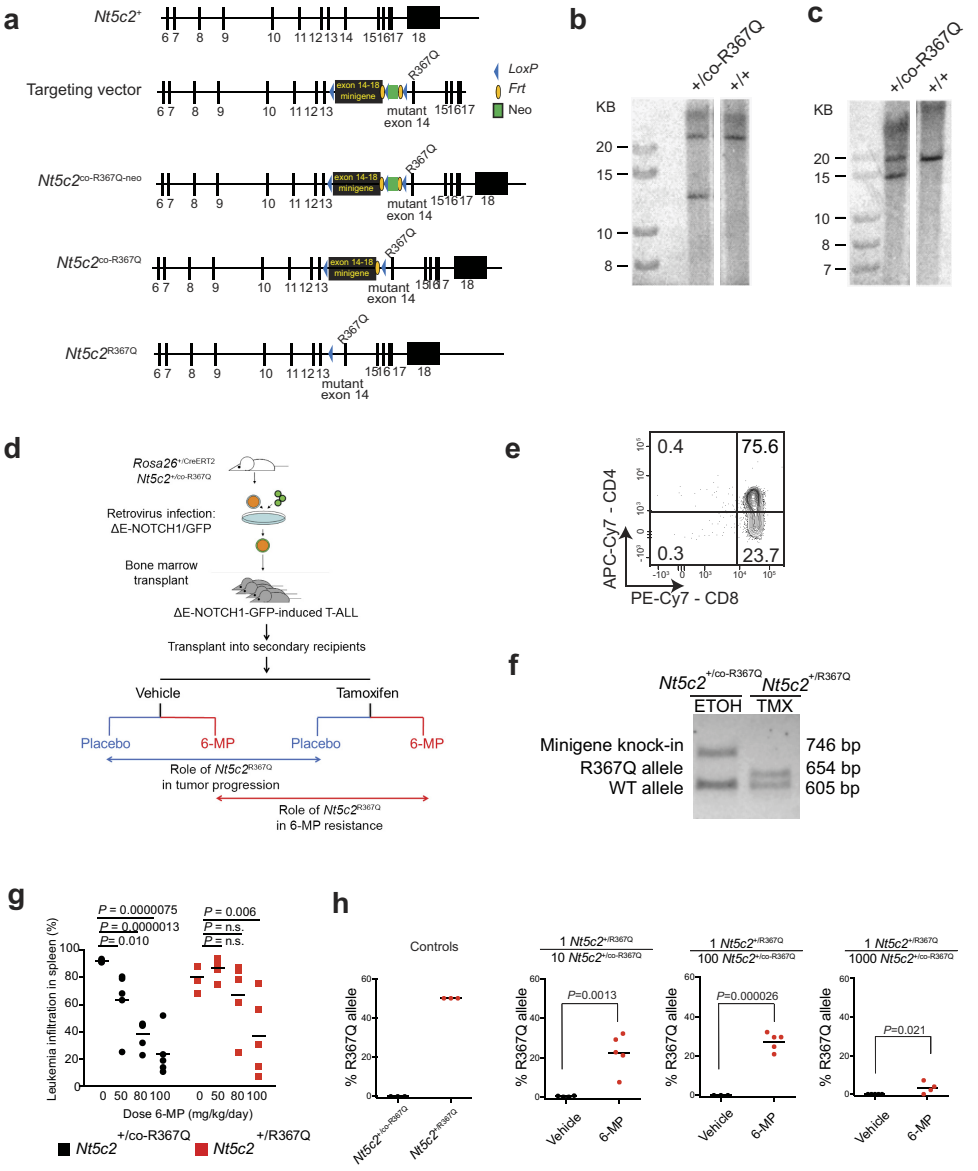

Extended Data Figure 2 | See next page for caption.

Extended Data Figure 2 | Conditional knock-in targeting of *Nt5c2*, generation and analysis of a Nt5c2(R367Q) conditional inducible T-ALL model. a, Schematic representation of the targeting strategy for the generation of $Nt5c2^{+/co\text{-}R367Q}$ conditional knock-in mice. **b**, Southern blot analysis of DNA samples from $Nt5c2^{+/+}$ and targeted $Nt5c2^{+/co\text{-}R367Q}$ embryonic stem cells after digestions with BamHI restriction enzyme and hybridization of a DNA probe external to the long arm. **c**, Southern blot analysis of DNA samples from $Nt5c2^{+/+}$ and targeted $Nt5c2^{+/co\text{-}R367Q}$ embryonic stem cells after digestion with ApaI restriction enzyme and hybridization of a DNA probe to the short arm. **d**, Schematic depiction of the strategy for developing conditional inducible $Nt5c2^{+/co\text{-}R367Q}$ primary mouse T-ALL tumours and for assessing the role of $Nt5c2^{+/R367Q}$ on leukaemia progression and response to chemotherapy. **e**, Representative FACS plot of a $Rosa26^{+/creERT2}Nt5c2^{+/co\text{-}R367Q}$ ΔE-NOTCH1-induced primary T-ALL tumour with a $CD4^{+}CD8^{+}$ immunophenotype. **f**, Representative genotyping PCR results from genomic DNA of a $Rosa26^{+/CreERT2}$ $Nt5c2^{+/co\text{-}R367Q}$ ΔE-NOTCH1-induced primary T-ALL tumour treated with 4-hydroxytamoxifen (TMX) or vehicle only (ethanol, ETOH) *in vitro* showing Cre-mediated deletion of the exon 14–18 *Nt5c2* wild-type mini-gene. **g**, Tumour burden assessed in the spleen (percentage of GFP^{+} cells) in mice allografted with *NOTCH1*-induced $Nt5c2^{+/co\text{-}R367Q}$ and isogenic $Nt5c2^{+/R367Q}$ primary leukaemia cells treated with a range of 6-MP doses ($n = 5$ per group). **h**, Analysis of selection for the mutant allele encoding Nt5c2(R367Q) by qPCR in mice allografted with $Nt5c2^{+/co\text{-}R367Q}$ and $Nt5c2^{+/R367Q}$ primary mouse T-ALL cells at a 1:10, 1:100 and 1:1,000 $Nt5c2^{+/R367Q}$:$Nt5c2^{+/co\text{-}R367Q}$ dilution and treated with vehicle or 6-MP ($n = 5$ mice per group and $n = 3$ technical replicates for the controls). The horizontal bar represents mean values. *P* values were calculated using two-tailed Student's *t*-test (**g**) or a one-tailed Student's *t*-test (**h**). Data in **e** and **f** show representative results from more than two experiments.

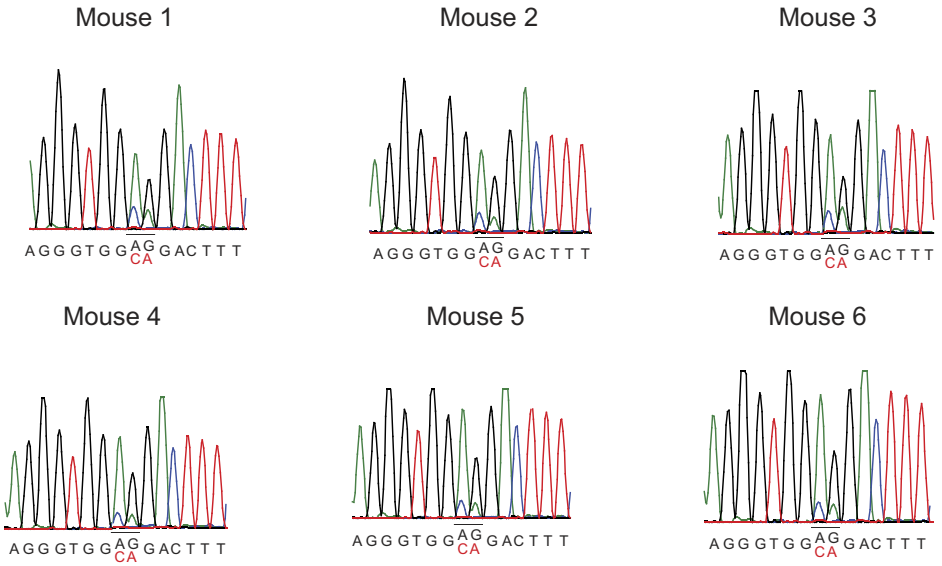

Extended Data Figure 3 | Decreased expression of the allele encoding Nt5c2(R367Q) allele upon leukaemia progression *in vivo*. Sanger sequencing chromatograms of cDNA from tumours in Fig. 2c show decreased expression of the Nt5c2(R367Q)-encoding allele over the wild-type *Nt5c2* allele compared with recently 4-hydroxytamoxifen treated $Rosa26^{+/creERT2}Nt5c2^{+/co\text{-}R367Q}$ cells (Fig. 1a). Mutant-allele deoxynucleotides are indicated in red.

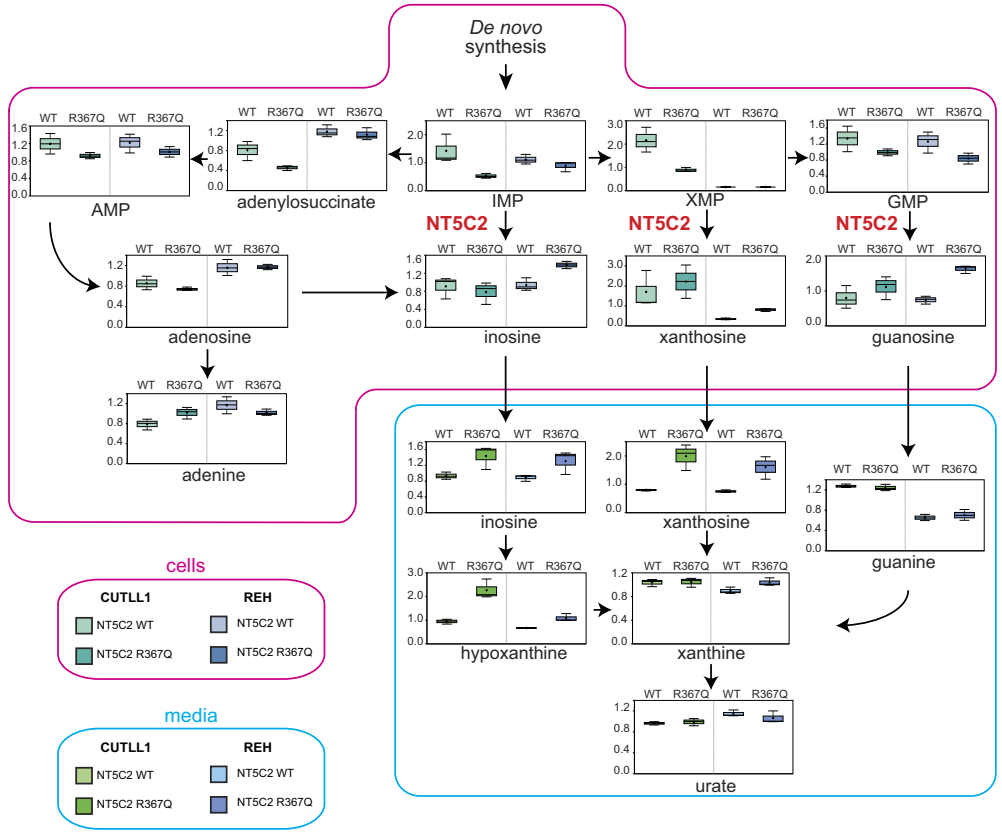

Extended Data Figure 4 | NT5C2(R367Q) expression leads to increased purine export in T-ALL and B-ALL cell lines. Diagram of the purine *de novo* biosynthesis and salvage pathways, showing gas chromatography–mass spectrometry and liquid chromatography–tandem mass spectrometry metabolic profiles (mass spectrometry scaled intensity, arbitrary units) of CUTLL1 and REH cell lines expressing wild-type NT5C2 or NT5C2(R367Q) and their corresponding conditioned media ($n = 3$ biological replicates per sample). Box plots represent the upper quartile to lower quartile distribution. Plus signs indicate mean values, horizontal lines indicate median values and whiskers indicate the maximum and minimum values of the distributions.

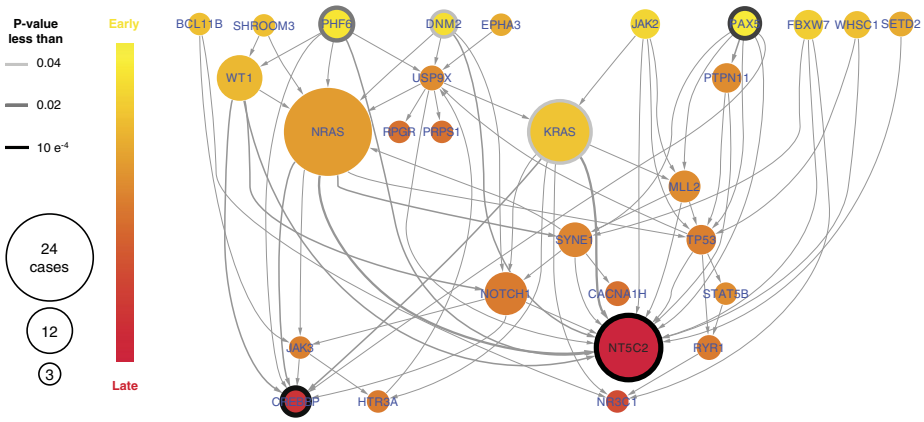

Extended Data Figure 5 | *NT5C2* mutations are late events in ALL. ISN illustrating the sequential order of somatic mutations in relapsed ALL by pooling evolutionary paths across patients. Each node represents a gene and each arrow points from a gene with an early event to a gene with a late event. To test whether a gene within the ISN was significantly early or late, we used a one-sided binomial test based on the in-degree and out-degree of each node.

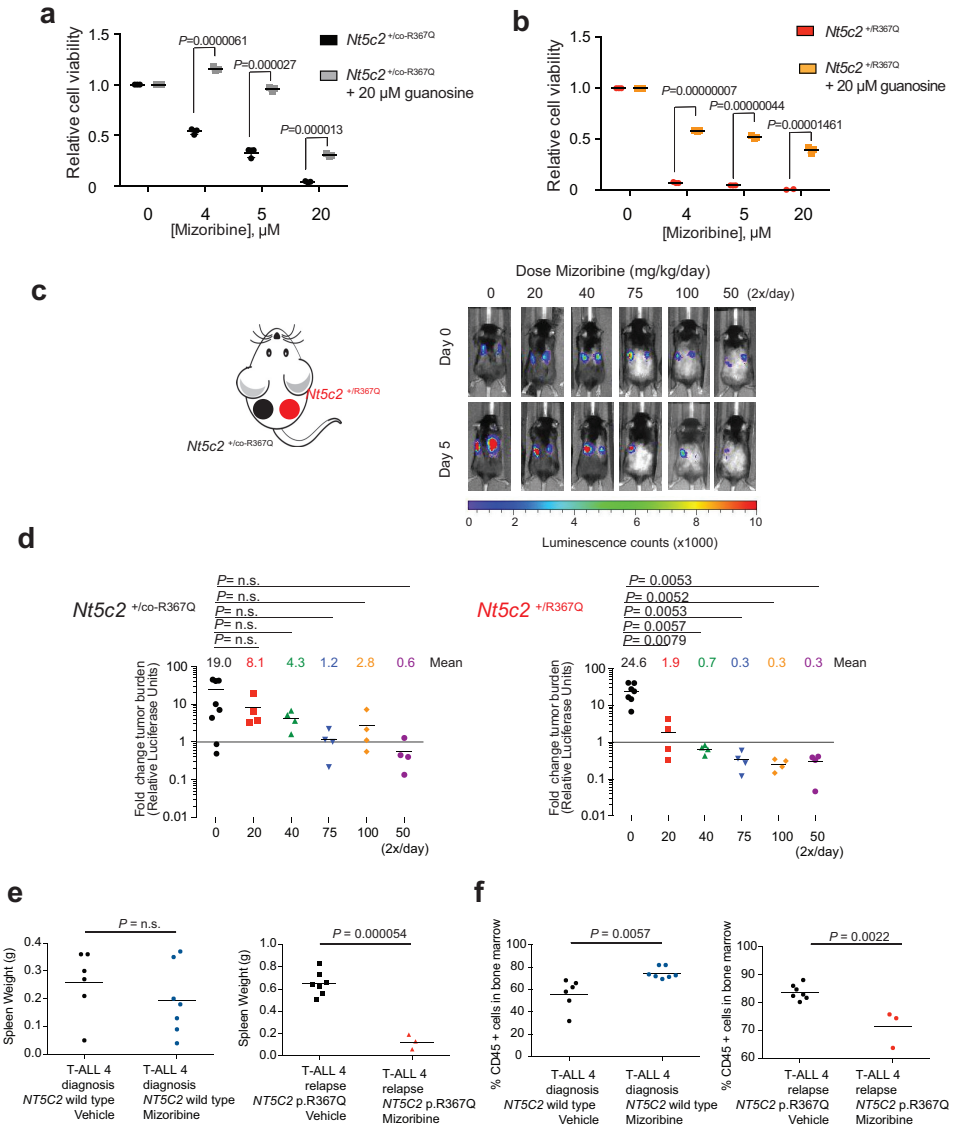

Extended Data Figure 6 | Guanosine rescue of mizoribine sensitivity *in vitro* and mizoribine activity against NT5C2(R367Q) mutant cells *in vivo*. **a**, **b**, Cell viability assays showing drug responses of wild-type *Nt5c2*$^{+/co\text{-}R367Q}$ primary mouse T-ALL cells (**a**) or mutant *Nt5c2*$^{+/R367Q}$ mouse T-ALL lymphoblasts (**b**) to increasing doses of mizoribine in the presence of 20 μM guanosine ($n = 3$ biological replicates). **c**, Analysis of tumour burden assessed by bioimaging in mice transplanted with wild-type *Nt5c2*$^{+/co\text{-}R367Q}$ leukaemia cells (left flank) or mutant *Nt5c2*$^{+/R367Q}$ leukaemia cells (right flank) treated with a range of mizoribine doses ($n = 8$ mice for the vehicle group and $n = 4$ mice per treated group). **d**, Quantification of data from **c**. **e**, Analysis of tumour burden assessed by spleen weight in mice allografted with wild-type NT5C2 ALL-4 diagnosis or NT5C2(R367Q) ALL-4 relapsed-patient derived leukaemia cells treated with 100 mg kg^{-1} mizoribine twice a day ($n = 6$ for diagnosis vehicle group, $n = 3$ for relapse treated group and $n = 7$ for diagnosis treated and relapse vehicle groups). **f**, Analysis of tumour burden assessed by percentage of CD45^{+} cells in the bone marrow of mice allografted with NT5C2 wild-type ALL-4 diagnosis or NT5C2(R367Q) ALL-4 relapsed-patient derived leukaemia cells treated with 100 mg kg^{-1} mizoribine twice daily. ($n = 3$–7 mice per group). Horizontal bars in **a**, **b**, **d**–**f** indicate mean values. *P* values were calculated using a two-tailed Student's *t*-test.

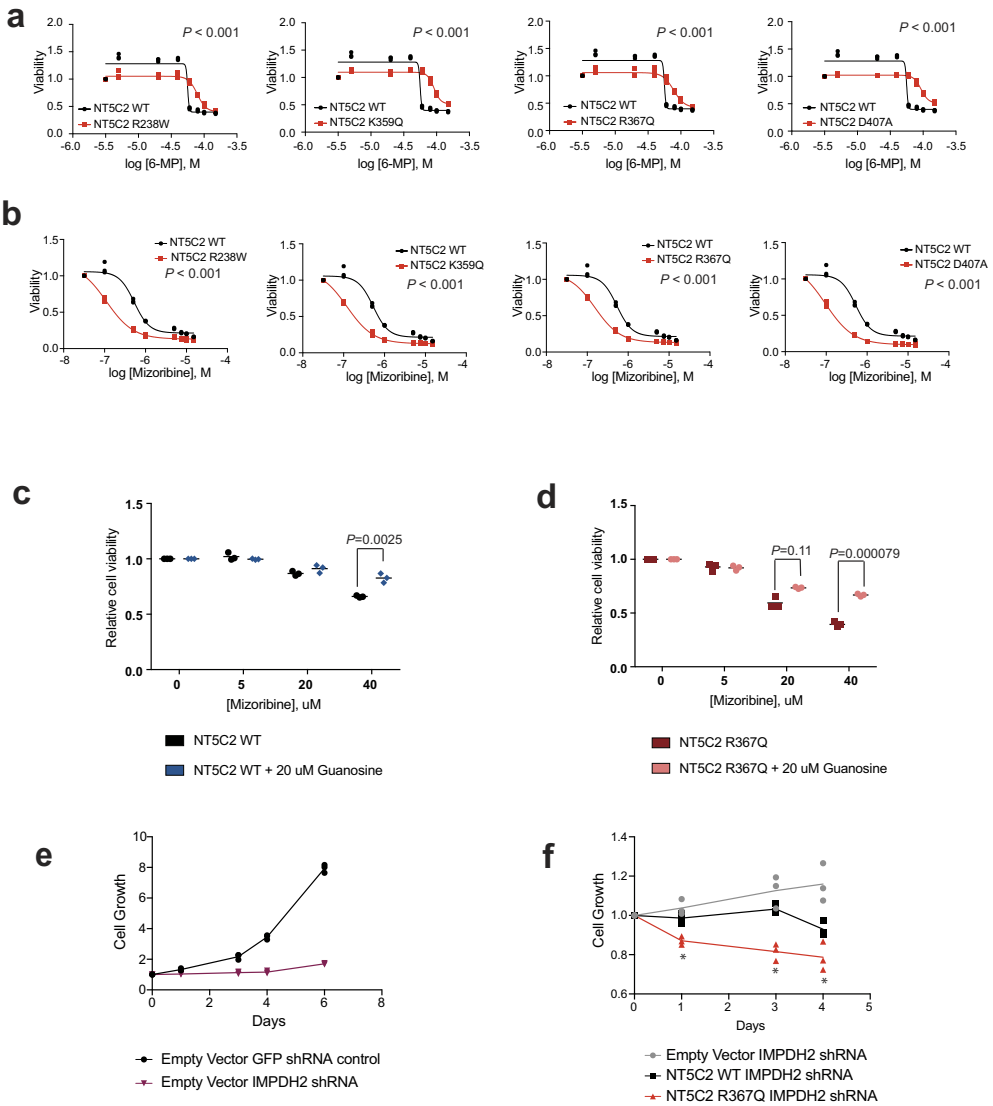

Extended Data Figure 7 | 6-MP and IMPDH inhibition response in CUTLL1 cells. a, Cell viability assays showing drug responses of the CUTLL1 cell line infected with wild-type or mutant *NT5C2*-expressing lentiviruses to increasing doses of 6-MP. **b**, Cell viability assays as in **a** documenting the response to mizoribine. **c**, **d**, Cell viability assay showing drug responses of wild-type (**c**) or NT5C2(R367Q) (**d**) CUTLL1 cells to increasing doses of mizoribine in the presence of 20 μM guanosine. **e**, Growth curve of CUTLL1 cells infected with a control short hairpin RNA (shRNA) targeting GFP or an shRNA targeting *IMPDH2*. **f**, Growth curve of wild-type or NT5C2(R367Q) CUTLL1 cells and infected with a shRNA targeting *IMPDH2*. **a**–**f**, Data are from three biological replicates. Horizontal bars in **c** and **d** indicate mean values. *P* values were calculated using a two-tailed Student's *t*-test. $^*P \leq 0.05$.

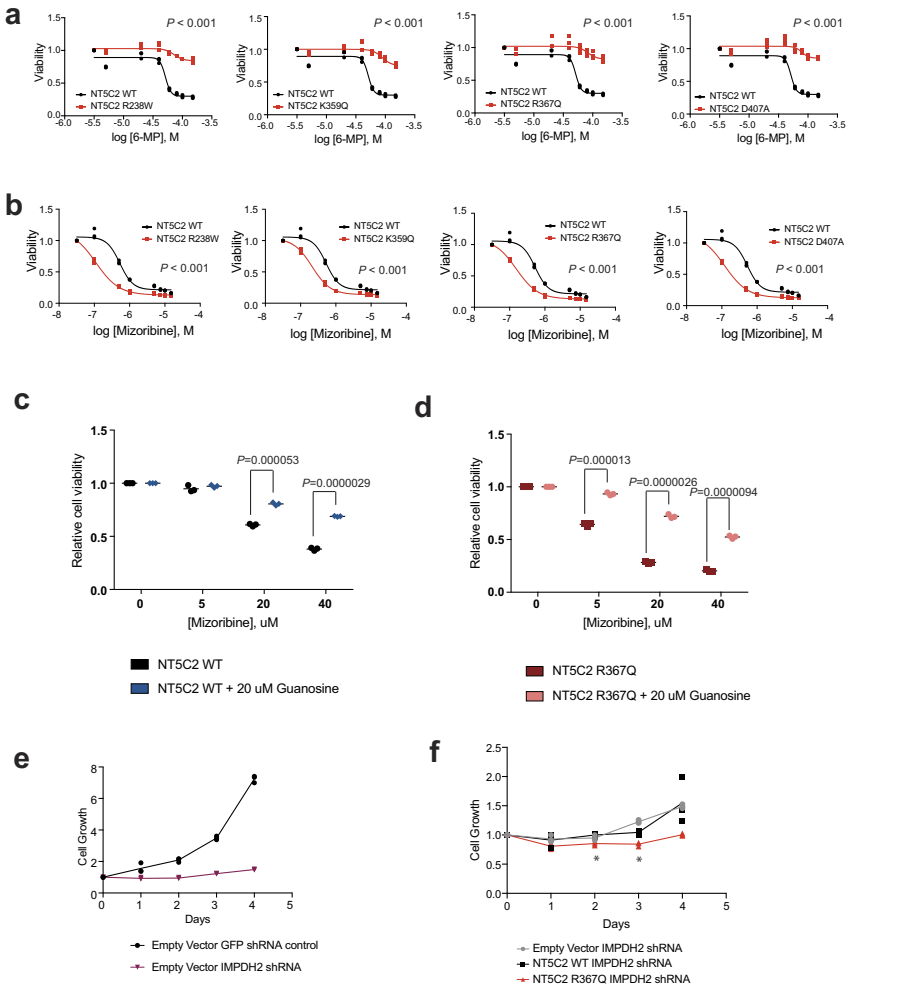

Extended Data Figure 8 | 6-MP and IMPDH inhibition response in REH B-ALL cells. a, Cell viability assay showing drug responses of the REH cell line infected with wild-type or mutant NT5C2-expressing lentiviruses to increasing doses of 6-MP. **b**, Cell viability assays as in **a** documenting the response to mizoribine. **c**, **d**, Cell viability assay showing drug responses of wild-type (**c**) or NT5C2(R367Q) (**d**) REH cells to increasing doses of mizoribine in the presence of 20 μM guanosine. **e**, Growth curve of REH cells infected with a control shRNA targeting GFP or shRNA targeting *IMPDH2*. **f**, Growth curve of wild-type or NT5C2(R367Q) REH cells and infected with an shRNA targeting *IMPDH2*. **a**–**f**, $n = 3$ biological replicates. Horizontal bars in **c** and **d** indicate mean values. *P* values were calculated using a two-tailed Student's *t*-test. $^{*}P \leq 0.05$.

Extended Data Table 1 | Deep sequencing, allele-specific PCR and droplet PCR analyses of matched diagnostic and remission DNA from patients with *NT5C2* mutations at relapse

Duplex Sequencing

Sample	Relapse Mutation	Average duplex depth	Allele load at diagnosis
T-ALL 11	K359Q	5009	Not detected
T-ALL 22	R238W	6519	Not detected
T-ALL 29	R391	3728	Not detected
T-ALL 30	Q523*	3512	Not detected
T-ALL C4	R367Q	5863	Not detected
T-ALL C5	R238W	3341	Not detected
T-ALL C7	R367Q	5134	Not detected
T-ALL C10	R238W	4299	Not detected
T-ALL C11	R367Q	3086	Not detected
T-ALL C14	D407E	3755	Not detected
T-ALL C17	R367Q	3497	Not detected
T-ALL C18	R367Q	3660	Not detected
T-ALL C20	R367Q	3693	Not detected
T-ALL N1	R367Q	3507	Not detected

NT5C2(R367Q) Allele Specific PCR

Sample	Detection threshold	Allele load at diagnosis	Allele load at remission
T-ALL 4	1/1000	Not detected	-
T-ALL 17	1/1000	Not detected	Not detected
T-ALL 35	1/1000	Not detected	-
T-ALL C4	1/1000	Not detected	Not detected
T-ALL C7	1/1000	Not detected	Not detected
T-ALL C11	1/1000	Not detected	Not detected
T-ALL C17	1/1000	Not detected	Not detected
T-ALL C18	1/1000	Not detected	Not detected
T-ALL C20	1/1000	Not detected	Not detected

Serial Patient Sample Droplet PCR

Sample	Sample Type	Days since diagnosis	Detection threshold (%)	Mutation	Mutant Allele Frequency (%)
SJBALL192	D	0	0.005	P414A	0.00000
SJBALL192	R1	170	0.005	P414A	37.73843
SJBALL192	CR	204	0.005	P414A	0.20425
SJBALL192	CR	230	0.005	P414A	0.15196
SJBALL192	R2	280	0.005	P414A	0.00064
SJBALL192	D	0	0.005	R39Q	0.00256
SJBALL192	R1	170	0.005	R39Q	0.00584
SJBALL192	CR	230	0.005	R39Q	0.02241
SJBALL192	R2	280	0.005	R39Q	48.57407
SJTALL001	D	0	0.005	R39Q	0.00238
SJTALL001	D	0	0.005	R39Q	0.00307
SJTALL001	CR	53	0.005	R39Q	0.00576
SJTALL001	CR	53	0.005	R39Q	0.00762
SJTALL001	CR	218	0.005	R39Q	0.00333
SJTALL001	CR	218	0.005	R39Q	0.00579
SJTALL001	CR	362	0.005	R39Q	0.01952
SJTALL001	R1	399	0.005	R39Q	3.70027
SJTALL001	R1	412	0.005	R39Q	3.57648
SJTALL001	CR	434	0.005	R39Q	0.00931
SJTALL001	R2	751	0.005	R39Q	37.58709
SJTALL001	R2	751	0.005	R39Q	39.23768

D = Diagnosis, CR=complete remission, R1=First Relapse, R2=Second Relapse

Extended Data Table 2 | Leukaemia-initiating cell activity of isogenic *Nt5c2*$^{+/co\text{-}R367Q}$ wild-type and *Nt5c2*$^{+/R367Q}$ primary mouse T-ALL tumours

Rosa26$^{+/CreERT2}$ *Nt5c2* R367Q $^{+/co\text{-}R367Q}$ – Vehicle treated		
Number of cells injected / mouse	**Number of mice injected**	**Number of leukemia-developing mice**
100000	6	6
10000	6	6
1000	6	5
100	6	2
10	6	0

Rosa26$^{+/CreERT2}$ *Nt5c2* R367Q $^{+/R367Q}$ – Tamoxifen treated		
Number of cells injected / mouse	**Number of mice injected**	**Number of leukemia-developing mice**
100000	6	6
10000	6	3
1000	6	3
100	5	0
10	5	0

Chapter 4: NT5C2 inhibitors for the reversal of 6-MP resistance in relapsed acute lymphoblastic leukemia

Introduction

5' Cytosolic nucleotidase II (NT5C2) is a ubiquitously expressed cytosolic enzyme that dephosphorylates 6-hydroxypurine monophosphates IMP, GMP, XMP, dGMP, and dIMP so that their purine precursors can be exported from the cell (Brouwer, Vogels-Mentink et al. 2005). Regulating nucleotide levels within the cell is a very important process as shown by the multitude of diseases associated with altered nucleotide availability such as Lesch-Nyhan syndrome and adenylosuccinate lyase deficiency (Pesi, Micheli et al. 2000, Jinnah, Sabina et al. 2013). The importance of NT5C2 activity is particularly apparent in hereditary spastic paraplegia, a rare neurodegenerative disease, which has been associated with loss of function mutations in *NT5C2* (Darvish, Azcona et al. 2017, Elsaid, Ibrahim et al. 2017).

In addition to regulating endogenous purine levels, NT5C2 also regulates metabolism of 6-mercaptopurine and 6-thioguanine, two chemotherapies commonly used in the treatment of acute lymphoblastic leukemia (ALL). NT5C2 dephosphorylates and inactivates the cytotoxic thiopurine monophosphate nucleotides 6-thioinosine monophosphate (thio-IMP), 6-thioxanthine monophosphate (thio-XMP) and 6-thioguanosine monophosphate (thio-GMP) into thiopurine nucleosides, which are then exported from the cell (Brouwer, Vogels-Mentink et al. 2005). Thus, NT5C2 plays a crucial role in regulating the efficacy of thiopurine therapy. In this context, gain of function *NT5C2* mutations have been found in 20% of relapsed T-ALL and 3-10% of relapsed B-ALL cases and drive thiopurine chemotherapy resistance (Tzoneva, Perez-Garcia et al. 2013, Tzoneva, Dieck et al. 2018). Additionally increased expression of

NT5C2 is associated with worse outcome in AML patients treated with cytarabine (Galmarini, Cros et al. 2005, Mitra, Crews et al. 2011).

Activation and regulatory mechanisms controlling NT5C2 activity have been elucidated through extensive structure function analyses of NT5C2 WT and gain-of-function relapse ALL associated NT5C2 mutant proteins in basal and active configurations (Wallden, Stenmark et al. 2007, Wallden and Nordlund 2011, Hnizda, Skerlova et al. 2016, Dieck, Tzoneva et al. 2018, Hnizda, Fabry et al. 2018). Structurally, NT5C2 is a member of the haloacid dehalogenase (HAD) superfamily of Mg^{2+}-dependent intracellular 5'-nucleotidases (Koonin and Tatusov 1994) and functions as a homotetramer made up of a dimer of two tightly-associated dimers with the dimer being the smallest functional unit with enzymatic activity (Wallden, Stenmark et al. 2007). NT5C2 is inactive in basal conditions and is allosterically activated by ATP, dATP and diadenosine tetraphosphate (Ap_4A) (Pinto, Canales et al. 1986, Spychala, Madrid-Marina et al. 1988, Marques, Teixeira et al. 1998). NT5C2 activation and inactivation is regulated by three structural regulatory elements; (i) the helix A allosteric response element (Gly355-Gln364) which is disordered in basal conditions, becomes ordered into an alpha helix (helix A) upon allosteric activation allowing for substrate binding and subsequent catalysis to occur (Wallden, Stenmark et al. 2007, Wallden and Nordlund 2011). Catalysis of the substrate proceeds via formation of a phosphoenzyme intermediate at Asp52 mediated by three conserved HAD motifs in the catalytic center (Collet, Stroobant et al. 1998, Allegrini, Scaloni et al. 2001). (ii) The second regulatory element consists of an intramolecular interaction between the tip of the arm region and inter-monomeric positively charged pocket, which work together to switch-off the enzyme: upon allosteric activation and substrate binding, the tip region of the flexible arm region of NT5C2 Glu373-Tyr434 disengages from the neighboring monomer, travels down the intermonomeric cavity,

interacts with Lys361 and disrupts the stabilization of the helixA region returning the enzyme to an inactive, off, configuration. (iii) The third regulatory element is the stretch of 13 acidic amino acids at the C-terminus of NT5C2. These negatively charged residues sit in the positively charged intermonomeric space in the basal configuration and act as a blockade against allosteric activation (Dieck, Tzoneva et al. 2018).

All three of these critical regulatory elements are coopted by relapse ALL associated NT5C2 mutant proteins to create gain-of-function enzymes that contribute to chemotherapy resistance. Class I NT5C2 mutations (NT5C2 K359Q and L375F) lock the allosterically activated helixA in a constitutively active configuration leading to continuous activation and substrate processing. Class II mutations which account for >95% of mutations (NT5C2 R39Q, R238W/L/G/Q, R367Q, S445F_R446Q, R478S, K404N, 404-405insD, D407A/Y/E/H, S408R, P414S/A and D415G) lie in the intermonomeric pocket or arm region of NT5C2 and disrupt this intramolecular NT5C2 switch-off mechanism. Additionally, a single Class III C-terminus truncating mutant, NT5C2 Q523*, favors allosteric activation of NT5C2 due to the loss of a C-terminal acidic tail (Dieck, Tzoneva et al. 2018).

As NT5C2 plays an important role in physiologic purine regulation as well as thiopurine metabolism and efficacy, it is a strong candidate for inhibitor development. Several groups have begun the process of identifying an inhibitor of NT5C2 using docking studies, virtual screening of chemical databases, and fragment based drug design (Nguyen, Devidas et al. 2008, Gallier, Lallemand et al. 2011, Jordheim, Marton et al. 2013, Meurillon, Marton et al. 2014, Marton, Guillon et al. 2015), but none have yet shown efficacy in preclinical models. Recent studies have shown that the majority of relapse associated *NT5C2* mutations which drive chemotherapy resistance retain the

ability to respond to allosteric activation, pointing to the allosteric effector site as a potentially attractive target for the design of small molecule NT5C2 inhibitors for the reversal of 6-MP resistance in relapsed ALL (Dieck, Tzoneva et al. 2018). Here we show the first stages of the development of a targeted inhibitor of NT5C2 for the reversal of 6-MP resistance in *NT5C2* mutant relapsed ALL.

Results

High-throughput inhibitor screen and HTP_2 validation

To assess NT5C2 activity and screen for small molecule inhibitors in a high throughput manner, we developed a high throughput malachite green based nucleotidase assay. Assays were performed using NT5C2 R367Q recombinant protein as it represents the most frequent relapse ALL associated *NT5C2* mutation (Tzoneva, Dieck et al. 2018). Briefly, purified recombinant NT5C2 R367Q is incubated with inosine monophosphate (IMP) as substrate for 15 minutes at 37ºC to allow the nucleotidase reaction to occur. The enzymatic reaction (IMP→ Pi +inosine) is terminated by the addition of malachite green reagent. Colorimetric analysis of the malachite green reagent reaction with free phosphate (Pi) is measured after 15 minutes. The malachite green assay was optimized to meet NIH high throughput enzyme assay guidelines (Brooks, Geeganage et al. 2004) ensuring the assay is run at a linear initial velocity with substrate concentrations at or below the K_m (Figure 4.1).

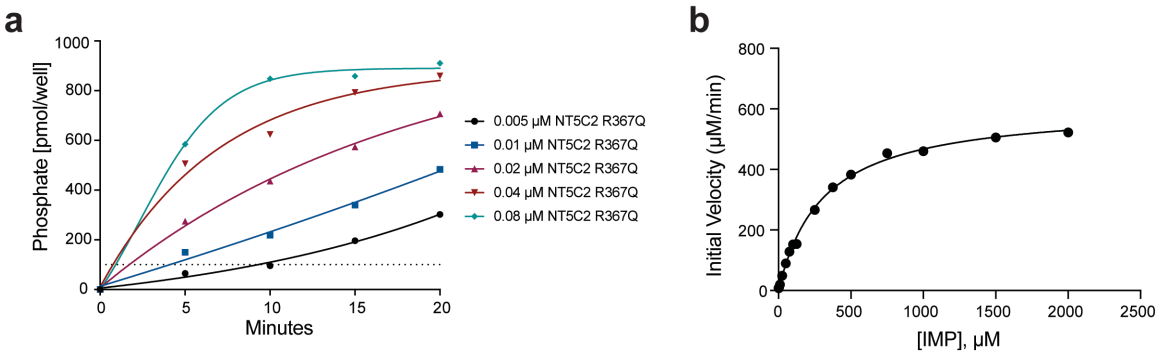

Figure 4.1 – Optimization of malachite green assay measuring NT5C2 R367Q conversion of inosine monophosphate (IMP) to inosine and phosphate. (a) Reaction progress curve of NT5C2 R367Q recombinant protein at five protein concentrations (b) Initial velocity versus substrate concentration of 0.02 μM NT5C2 R367Q recombinant protein with IMP as substrate. Vmax= 610 μM IMP/min, K_m = 308 uM IMP.

Using this optimized high throughput assay, we analyzed a diversity library of 60,640 compounds curated by the Columbia University's High Throughput Screen Facility in collaboration with Brent Stockwell. From the primary screen, 3 standard deviations away from the mean was used as a cutoff to select 225 compounds that had 33.21% inhibitory activity or higher. Following confirmatory assays and dose dependent curves, we identified a single lead compound with dose dependent NT5C2 R367Q low micromolar inhibitory activity, compound HTP_2 (Figure 4.2 a,b). To confirm the inhibitory activity of small molecule inhibitor, HTP_2 we resynthesized the compound at the Columbia University Probe Synthesis Facility and repeated malachite green nucleotidase assay analysis (Figure 4.2 c). Molecular docking analyses predict that HTP_2 binds to the active site of NT5C2 (Figure 4.2 d) and Biacore surface plasmon resonance binding studies confirm a dose dependent binding interaction of HTP_2 with NT5C2 R367Q recombinant protein (Figure 4.2 e).

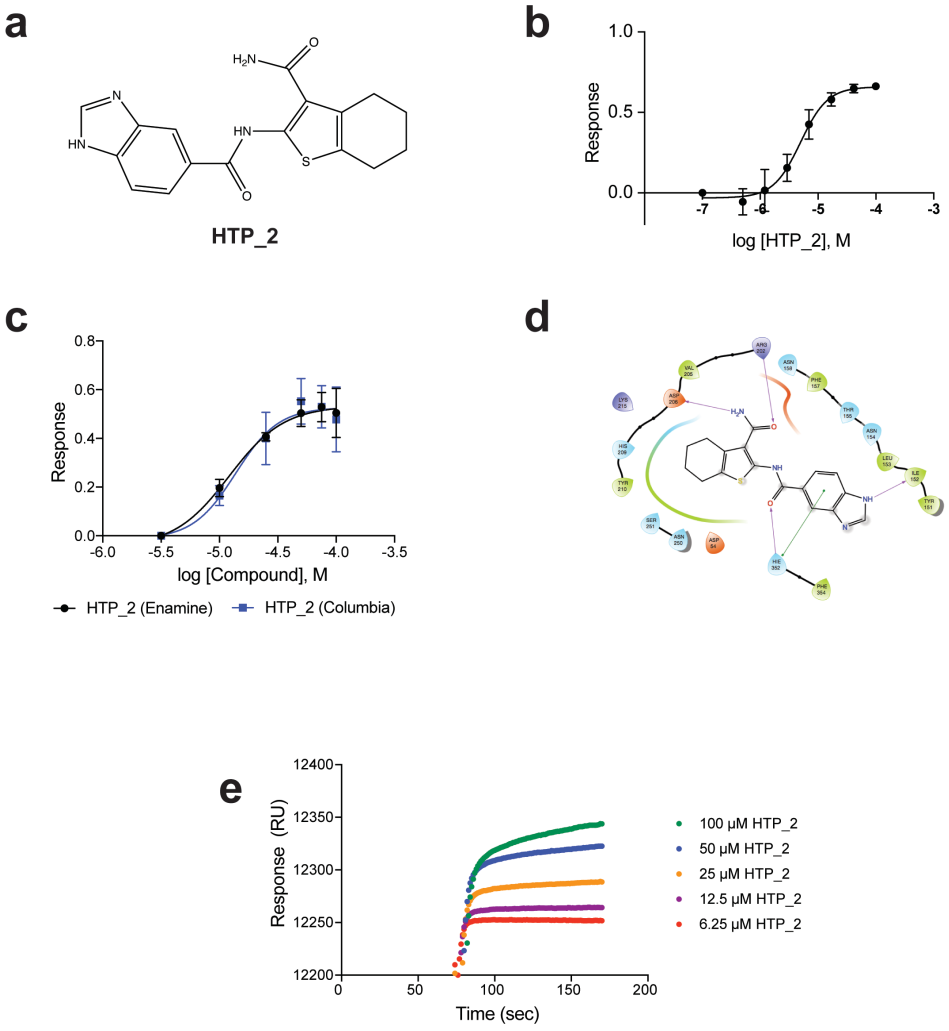

Figure 4.2 – HTP_2 binds and inhibits NT5C2 R367Q. (a) Structure of HTP_2 (b) Malachite green assay of NT5C2 R367Q recombinant protein incubated with increasing concentrations of HTP_2 (c) Malachite green assay analysis of HTP_2 provided by Enamine or synthesized in house at the Columbia Probe Synthesis facility incubated with recombinant NT5C2 R367Q protein (d) Molecular docking of HPT_2 in the active site of the NT5C2 D52N R39Q crystal structure (e) Representative sensorgram for HTP_2 binding NT5C2 R367Q recombinant protein generated with Biacore surface plasmon resonance technology. K_d = 54.5 µM HTP_2.

HTP_2 reverses 6-MP resistance in ALL lymphoblasts

Activating relapse ALL associated *NT5C2* mutations lead to increased 6-MP resistance due to increased processing and export of thiopurine cytotoxic metabolites resulting in less thioguanine nucleotide incorporation into DNA. We hypothesized that NT5C2 inhibition should reverse this resistance mechanism and make 6-MP therapy more effective in *NT5C2* mutant cells. Indeed when we treat *NT5C2* R29Q mutant PEER and

BE13 human ALL cell lines with 6-MP and increasing doses of small molecule NT5C2 inhibitor HTP_2, we see increased sensitivity to 6-MP chemotherapy (Figure 4.3 a). Interestingly, we also see similar increased 6-MP cytotoxicity in *NT5C2* wild-type JURKAT and CUTLL1 human ALL cell lines suggesting inhibition of wild type NT5C2 as well as mutant NT5C2 may improve 6-MP cytotoxicity and be a useful therapy in the treatment of all ALLs, not just those harboring activating *NT5C2* mutations (Figure 4.3 b). This increased sensitivity to 6-MP in the presence of NT5C2 inhibitor HTP_2 was also evaluated in *Nt5c2* WT (*Nt5c2*$^{+/co\text{-}R367Q}$) and *Nt5c2* mutant (*Nt5c2*$^{+/R367Q}$) murine NOTCH1 driven ALL lymphoblasts and human cell lines overexpressing relapse associated NT5C2 mutations (Figure 4.3 c and d). Isobologram analyses further show combination therapy with 6-MP and small molecule NT5C2 inhibitor HTP_2 is synergistic in both *Nt5c2* WT (*Nt5c2*$^{+/co\text{-}R367Q}$) and *Nt5c2* mutant (*Nt5c2*$^{+/R367Q}$) mouse lymphoblasts (Figure 4.3 e).

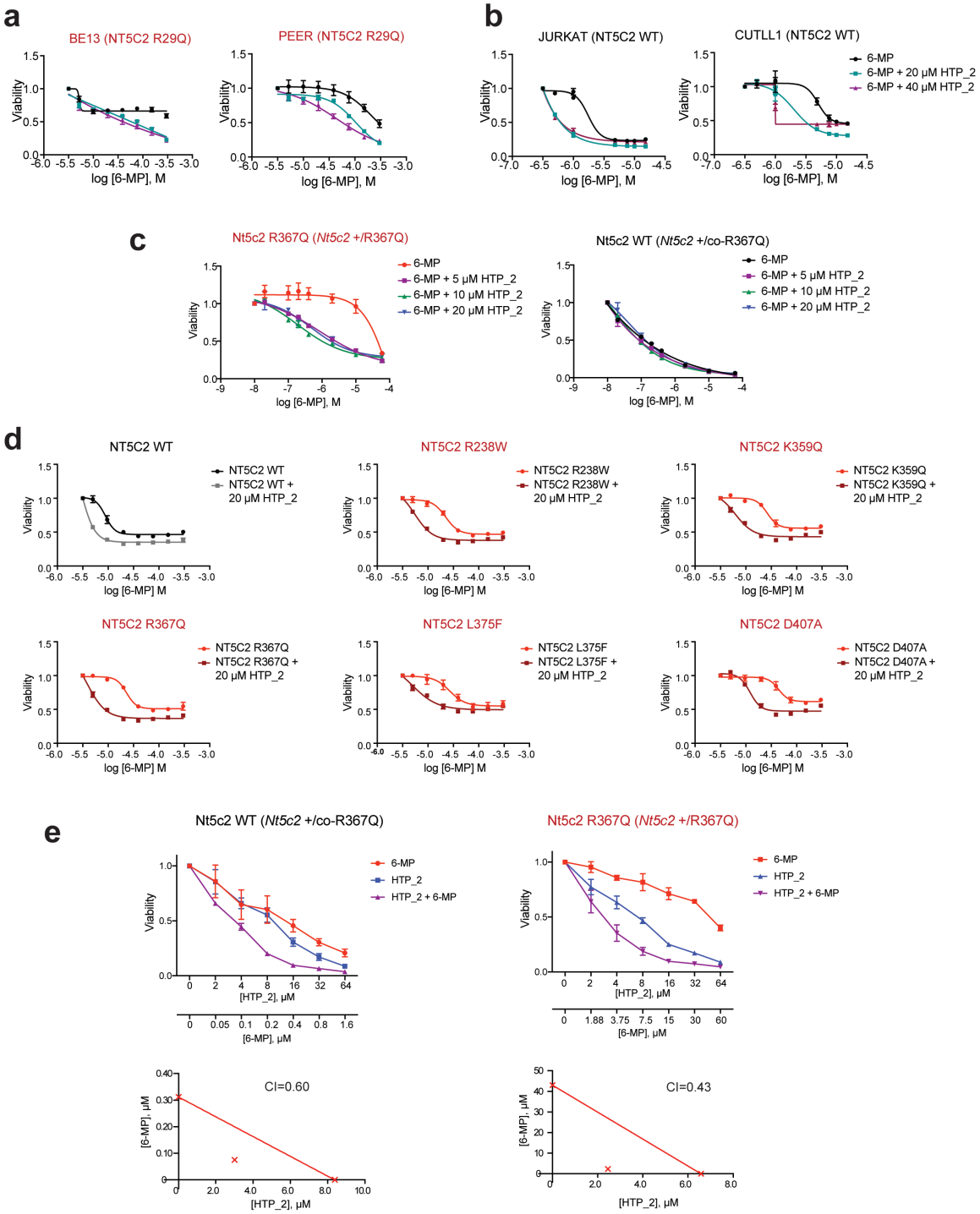

Figure 4.3 – NT5C2 inhibitor HTP_2 sensitizes human and murine NT5C2 wildtype and mutant lymphoblasts to 6-MP chemotherapy. (a, b, c, d) Cell viability of (a) PEER and BE13 NT5C2 mutant human ALL cell lines (b) JURKAT and CUTLL1 NT5C2 WT human ALL cell lines (c) *Nt5c2* WT (*Nt5c2*$^{+/co\text{-}R367Q}$) and *Nt5c2* mutant (*Nt5c2*$^{+/R367Q}$) mouse lymphoblasts and (d) CUTLL1 cell lines expressing NT5C2 WT and NT5C2 relapse associated NT5C2 mutations treated with 6-MP and increasing doses of HTP_2. (e) Isobologram analysis of *Nt5c2* WT (*Nt5c2*$^{+/co\text{-}R367Q}$) and *Nt5c2* mutant (*Nt5c2*$^{+/R367Q}$) mouse lymphoblasts treated with 6-MP, HTP_2, or a combination of 6-MP and HTP_2.

We repeated drug combination studies in *NT5C2* knockout CUTLL1 cell lines generated using CRISPR/CAS9 technology (Figure 4.4 a). Consistent with the small molecule inhibition of NT5C2 studies, *NT5C2* knockout cells showed increased sensitivity to 6-MP therapy (Figure 4.4 b). Additionally, *NT5C2* knockout cells did not show further sensitization to 6-MP therapy upon addition of HTP_2 suggesting that this phenotype is directly related to NT5C2 activity and that HTP_2 is a specific inhibitor of NT5C2 (Figure 4.4 b). Additional studies still need to be performed to assess whether HTP_2 binds to other nucleotidase protein family members to further confirm this specificity.

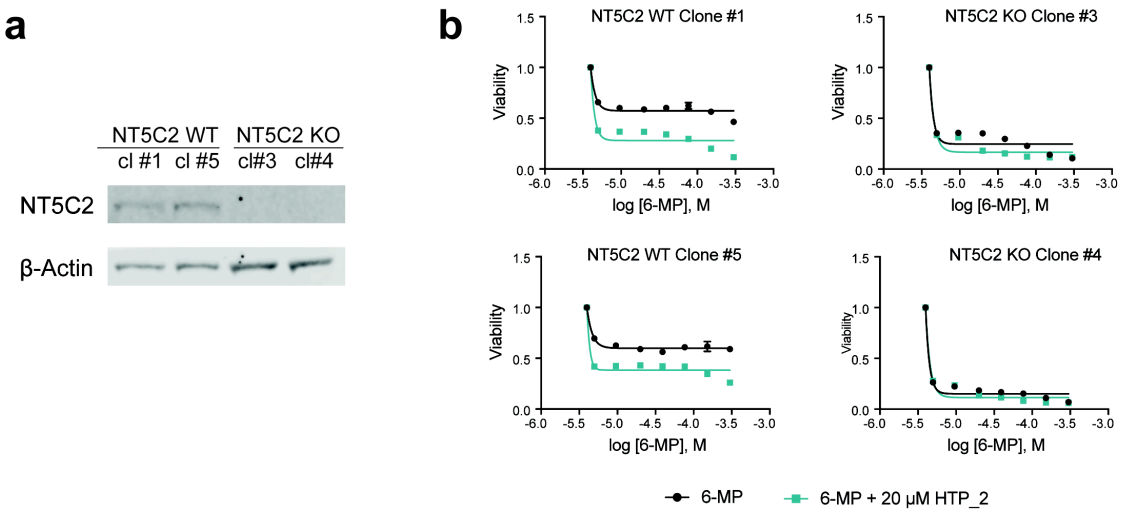

Figure 4.4 – *NT5C2* Knockout cells show increased sensitivity to 6-MP. (a) Western blot analysis of CUTLL1 cells infected with NT5C2 gRNA CAS9 targeting constructs (NT5C2 KO) or CAS9 empty vector controls (NT5C2 WT). (b) Cell viability of CUTLL1 NT5C2 WT (left) and NT5C2 knockout (right) clones treated with increasing doses of 6-MP and 20 μM HTP_2.

Toxicity evaluation of NT5C2 inhibition

In developing a new inhibitor, it is necessary to consider potential therapeutic toxicities that may occur. In particular, *NT5C2* loss of function mutations have been associated with a hereditary neurodegenerative disease, spastic paraplegia (SPG45) (Darvish, Azcona et al. 2017, Elsaid, Ibrahim et al. 2017), thus it is important to check the potential

toxicity of systemic NT5C2 inhibition. In efforts to assess NT5C2 inhibitor toxicity, we have generated *NT5C2* knockout clones in the CUTLL1 T-ALL cell line using CRISPR Cas9 technology (Figure 4.4 a). *NT5C2* wild-type and *NT5C2* KO cells show no apparent growth or proliferation disparities suggesting that systemic administration of NT5C2 inhibitors could be fairly well tolerated. To further examine the potential toxicity of NT5C2 inhibitors, we have also generated an *Nt5c2* knockout mouse line using CRISPR Cas9 technology (Figure 4.5). *Nt5c2* knockout mice are viable, fertile, and have no apparent developmental delays in agreement with previously published work using a conditional *Nt5c2* knockout mouse model (Kviklyte, Vertommen et al. 2017).

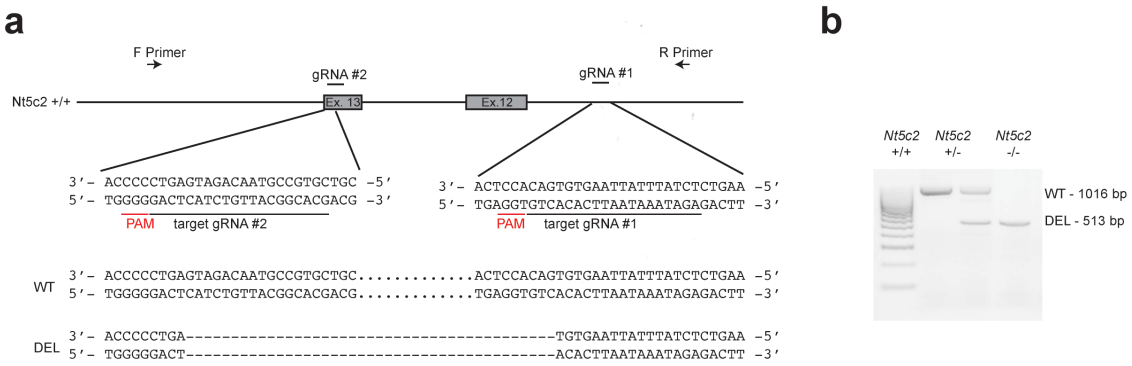

Figure 4.5 – *NT5C2* knockout mouse generation and characterization. (a) Genomic map of Nt5c2 gRNA targeting in chromosome 19 of the mouse genome (b) Genotyping of *Nt5c2* +/+, *Nt5c2* +/- and *Nt5c2* -/- mice.

Discussion

Thiopurine chemotherapy is the critical agent in a 2-3 year anti-metabolite maintenance regimen consisting of daily, oral 6-MP, given to ALL patients upon remission to prevent further leukemic growth (Pui and Evans 2006, Conter, Arico et al. 2010, Gaynon, Angiolillo et al. 2010, Schmiegelow, Forestier et al. 2010). Multiple studies have shown that patients with higher dose intensity of 6-MP have better event free survival and patients with <95% adherence to maintenance therapy are 2.5 times more likely to

relapse (Relling, Hancock et al. 1999, Bhatia, Landier et al. 2012). Thus, 6-MP maintenance therapy is critical for improving event free survival in patients with ALL and this is dependent on chronic and continuous exposure to the drug over a long period of time.

Although maintenance therapy has proven to be very successful, some patients do relapse during therapy suggesting mechanisms of resistance to 6-MP treatment. Deletions and decreased expression of *MSH6* (MutS homolog 6) as well as mutations in *PRPS1* have been associated with 6-MP resistance, yet the most frequent mechanism of thiopurine resistance in relapsed ALL cases is the presence of activating mutations in *NT5C2* (Yang, Bhojwani et al. 2008, Meyer, Wang et al. 2013, Tzoneva, Perez-Garcia et al. 2013, Li, Li et al. 2015, Evensen, Madhusoodhan et al. 2018). Activating mutations in the *NT5C2* gene are found in 20% of relapsed T-ALLs and 3-10% of relapsed B-ALLs and are particularly common amongst early relapse accounting for 35-45% of cases. As relapse associated *NT5C2* mutations act as gain-of-function alleles with increased nucleotidase activity that lead to chemotherapy resistance, NT5C2 stands as a clear therapeutic target to prevent the emergence of these thiopurine resistant clones in relapsed ALL.

Here we describe the identification of HTP_2, a small molecule inhibitor of NT5C2. HTP_2 shows low millimolar inhibitory activity against NT5C2 R367Q recombinant protein and reverses 6-MP resistance in mutant *NT5C2* lymphoblasts. Additionally, we show that small molecule NT5C2 inhibitor HTP_2 also sensitizes *NT5C2* wild-type cells to 6-MP chemotherapy. This data is consistent with unpublished work from Koichi Oshima identifying *NT5C2* as one of the top CRISPR knockout sensitizing genes for 6-MP sensitivity. This screen and the data shown here suggest that pan NT5C2 inhibition

may be effective to reverse 6-MP resistance even in the absence of *NT5C2* activating mutations and thus NT5C2 inhibitors may be useful in treating all leukemias that are at risk of developing thiopurine resistance.

We have shown promising preliminary results with small molecule NT5C2 inhibitor HTP_2 here, yet HTP_2 is fairly insoluble and therefore very difficult to move forward into *in vivo* and clinical studies. Further testing and screening of HTP_2 analogues is necessary to identify NT5C2 inhibitors with increased solubility and increased potency against NT5C2. Upon identifying more soluble and potent inhibitors, co-crystallization studies will be critical for understanding the mechanism of inhibition and ways to further improve NT5C2 specificity and targeting. Additionally, HTP_2 and other inhibitors will need to be screened against other nucleotidase family member proteins to select for compounds with minimal off target effects.

NT5C2 mutations are particularly common amongst early relapse patients still undergoing therapy suggesting that 6-MP based maintenance treatment creates an immense selective pressure towards the emergence of these mutations and subsequent relapse. The development of NT5C2 inhibitors and improved, personalized therapy regimens has the potential to improve the efficacy of ALL maintenance therapy by curtailing the emergence of *NT5C2* mutant clones responsible for relapse.

Materials and Methods

Drugs and Small-Molecule Compounds

We purchased 6-mercaptopurine (6-MP), inosine 5'-monophosphate disodium salt hydrate and ATP from Sigma-Aldrich. For *in vitro* assays we dissolved 6-MP in DMSO and ATP in Tris gel filtration buffer (50 mM Tris-HCl, 100 mM NaCl, 10% Glycerol, 5 mM β-mercaptoethanol). HTP_2 was purchased from Enamine (cat# Z27358589) and dissolved in DMSO.

Cell Culture

We performed cell culture in a humidified atmosphere at 37ºC under 5% CO_2. We purchased 293T cells for viral production from American Type Culture Collection (ATCC) and grew them in DMEM media supplemented with 10% fetal bovine serum (FBS), 100 U ml^{-1} penicillin G and 100 µg ml^{-1} streptomycin for up to two weeks. The CUTLL1 cell line, which was generated by continuous culture of a T-cell lymphoblastic pleural effusion cells from a patient at relapse, has been characterized and reported before (Palomero, Barnes et al. 2006). We obtained REH and JURKAT cells from American Type Culture Collection (ATCC) and BE13 and PEER cells from Deutsche Sammlung von Mikroorganismen und Zellkulturen (DSMZ). We cultured CUTLL1 and REH cells in RPMI-1640 media supplemented with 10% FBS, 100 U ml^{-1} penicillin G and 100 µg ml^{-1} streptomycin and BE13 and PEER cells in RPMI-1640 media supplemented with 20% FBS, 100 U ml^{-1} penicillin G and 100 µg ml^{-1} streptomycin. Cell lines were regularly authenticated and tested for mycoplasma contamination. Mouse *Rosa26*$^{+/CreERT2}$ *Nt5c2*$^{+/co\text{-}R367Q}$ T-ALL tumor cells were previously described (Tzoneva, Dieck et al. 2018), and were culture in OptiMEM media supplemented with 10% fetal bovine serum (FBS), 100 U ml^{-1} penicillin G, 100 µg ml^{-1} streptomycin, 55 µM β-mercaptoethanol, and 10 ng ml^{-1} mouse IL7.

Plasmids and vectors

We obtained the pET28aLIC (Plasmid #26094) and pL-CRISPR.efs.gfp (Plasmid #57818) plasmids from Addgene. We amplified the coding sequence of the NT5C2 cDNA from pLOC-NT5C2 (Tzoneva, Perez-Garcia et al. 2013) and cloned it into the pET28aLIC vector using In-fusion cloning using the In-Fusion HD Cloning Kit (Clontech) following manufacturer guidelines. We generated lentiviral vectors expressing CAS9 and gRNAs targeting the exon 3 of murine *Nt5c2* by cloning the corresponding gRNA oligonucleotides (Sigma-Aldrich) into pL-CRISPR.efs.gfp as reported (Shalem, Sanjana et al. 2014). *NT5C2* R238W, K359Q, L375F, R367Q, and D407A mutations were cloned into the pLOC-NT5C2 plasmid (Tzoneva, Perez-Garcia et al. 2013) by site directed mutagenesis using the QuikChange II XL Site-Directed Mutagenesis kit (Stratagene) according to manufacturer's guidelines.

Lentiviral production and infection

We transfected lentiviral plasmids together with gag-pol (pCMV ΔR8.91) and V-SVG (pMD.G VSVG) expressing vectors into 293T cells using JetPEI transfection reagent (Polyplus). We collected viral supernatants after 48 h and used them to infect the CUTLL1 human cell line by spinoculation with 4 μg mL^{-1} Polybrene Infection/Transfection Reagent (Fisher Scientific). pLOC infected cells were selected with 10 days of Blasticidin treatment.

Malachite green assay

The malachite green enzymatic assay was adapted from a previously published protocol (Gallier, Lallemand et al. 2011) and optimized for NT5C2 R367Q enzyme kinetics. To optimize the assay, initial velocity and linear reaction conditions were performed following NIH enzyme assay guidelines (Brooks, Geeganage et al. 2004).

Briefly, 0.02 μM or 2.6 ng/mL purified recombinant NT5C2 R367Q protein was incubated with 100 μM inosine monophosphate (IMP) as substrate for 15 minutes at 37ºC. Enzymatic reaction (IMP→ Pi +inosine) was terminated by addition of the malachite green reagent (Sigma Aldrich, MAK307). Colorimetric analysis of malachite green reaction with free phosphate (Pi) was measured after 15 minutes at 600 nM. Assays were performed in Tris gel filtration buffer (50 mM Tris-HCl, 100 mM NaCl, 10% Glycerol, 5 mM β-mercaptoethanol) with a final concentration of 10 mM $MgCl^{2+}$. For assays with inhibitors or small molecule compounds, compounds dissolved in DMSO were added to the protein and incubated for 10 minutes at room temperature prior to adding IMP substrate.

High-throughput inhibitor screen

Screening procedure was performed on Cell:Explorer robotic station (Perkin Elmer) using the following modules: Janus liquid handling platform with NanoHead, FlexDrop liquid dispenser, Liconic microplate hotel, Liconic 500 microplate incubator (+37C), Envision plate reader. Briefly, 20 μL of 0.4 μM NT5C2 R367Q recombinant protein in Tris Gel Filtration Buffer or buffer alone controls were plated in clear bottom low binding black 384 well microplates (Greiner, Cat No 781906). Compounds from the Enamine library (see below) were then delivered to the plates by the NanoHead from 10mM stock library microplates to a final concentration of 100 nM. Plates were then incubated at room temperature in the Liconic hotel for 10 minutes. 20 μL of 200 mM Inosine monophosphate (IMP), substrate, were added to the wells with the Flexdrop and plates were incubated at 37^{o}C in the Liconic incubator for 15 minutes. Following incubation, 5 μL of the malachite green reagent (Sigma, Cat No MAK-307) was added to all of the wells. Plates were incubated in the Liconic hotel for 15 minutes and then read on an

Envision plate reader at 650 nM. $MgCl^{2+}$ was added to all buffers for a final concentration of 10 mM in the assay.

Enamine Library

The Enamine Library consists of 60,640 compounds filtered for traditional physicochemical descriptors such as the rule of five, rotatable bond count, topological polar surface, and suitable aqueous solubility. The Enamine library was curated by assigning a score for each compound relative to the calculated value in relationship to a standard value using a method similar to Bickerton et al (Bickerton, Paolini et al. 2012). For example the number of rotatable bonds was calculated for each compound, then using a standard value of 6, deviations from that value are penalized based on distance from 6. After all criteria are calculated, the distribution of scores is then used to stratify the population with the highest scoring compounds being eliminated. The resulting compounds were clustered and two compounds from each cluster were selected for purchase.

Analysis

In screening the Enamine library, each plate had two columns for a non-treatment control containing all elements of the assay without the addition of library compounds and two columns serving as negative controls that had neither substrate nor drugs added. The raw data for all compound containing wells were normalized to the average of all the wells screened. From the primary screen, 3 standard deviations away from the mean was used as a cutoff to select 225 compounds that had 33.21% inhibitory activity or higher. Next, those 225 compounds were subject to confirmatory assay by cherry-picking them from the original library and testing again in the same assay. Out of 225 compounds 28 were confirmed. Next, we chose 6 compounds, which showed best inhibition and tested them in dose-response curves.

HTP_2 synthesis

HTP_2 was synthesized as shown in the Scheme. Compound **1** was treated with thionyl chloride in toluene at 100°C to give the corresponding acid chloride **2**. Reaction of **2** with the amine **3** in DMF in the presence of Hunig's base gave HTP_2 after purification by reverse phase HPLC.

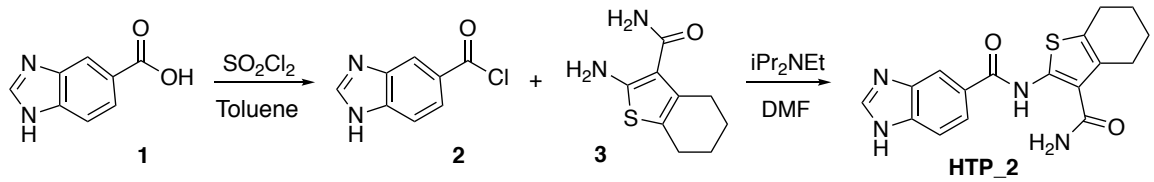

NT5C2 recombinant protein purification

For 5'-nucleotidase assays in the absence and presence of allosteric activators we cloned, expressed and purified recombinant wild-type and mutant NT5C2 proteins as previously described (Dieck, Tzoneva et al. 2018). Briefly, we cloned full-length NT5C2 cDNA constructs with an N-terminal hexahistidine (His_6) tag in the pET28a-LIC expression vector. We expressed recombinant proteins from Rosetta 2(DE3) *Escherichia coli* cells by induction with 0.5 mM isopropyl-β-D-thiogalactopyranoside overnight at 16 °C. We resuspended harvested cells in lysis buffer (50 mM Tris-HCl pH 7.4, 500 mM sodium chloride, 10% glycerol, 0.5 mM TCEP, 20 mM imidazole) supplemented with Complete EDTA-free protease inhibitor (Roche) and lysed cells by sonication. We purified recombinant proteins using an ÄKTA fast protein liquid chromatography system (GE Healthcare) using a 2-step protocol adapted from one previously described (Wallden, Stenmark et al. 2007). We first performed affinity chromatography using a 1 ml Ni^{2+}-charged His-Trap HP column (GE Healthcare) equilibrated in lysis buffer. We eluted NT5C2 proteins from the His-Trap column in a step-wise method with elution buffer (lysis buffer with 500mM imidazole) by first setting

the buffer ratio to 25% elution buffer for 8 column volumes and then switching to a linear gradient to 100% elution buffer over 10 column volumes. We pooled NT5C2-containing fractions and purified further by size exclusion chromatography using a HiLoad 16/60 Superdex 200 gel filtration column (GE Healthcare) equilibrated in 50 mM Tris-HCl, pH 7.4, 100 mM NaCl, 10% glycerol and 0.5 mM TCEP.

***In vitro* cell viability and chemotherapy response assays**

We analyzed chemotherapy responses of human leukemia cell lines or murine mouse lymphoblasts following 72-hour incubation with increasing concentrations of 6-mercaptopurine or HTP_2 by measurement of the metabolic reduction of the tetrazolium salt MTT using the Cell Proliferation Kit I (Roche) following the manufacturer's instructions. Isobologram synergy assays where performed as above with 6-MP, HTP_2 or the combination of 6-MP and HTP_2 at a consistent ratio.

Nt5c2 KO mouse generation

Nt5c2 knockout mice were generated using CRISPR-Cas9 technology (Wang, Yang et al. 2013). Single guide RNAs (sgRNAs) were designed in exon 13 and intron 11-12 of the murine *Nt5c2* on chromosome 19 (Figure 4.5), evaluated for potential off-targets using E-CRISPR (Deutsches Krebsforschungszentrum) (Heigwer, Kerr et al. 2014), and purchased (Synthego, Redwood City, CA). Fertilized eggs were collected from the oviducts of superovulated B6CBAF1 female mice that had mated with B6CBAF1 stud males. 100 ng/μL of Cas9 mRNA (TriLink Biotechnologies L-6125) and 50 ng/μL of sgRNA were mixed and injected into zygotes at the pronuclei stage in M2 medium (Sigma M7167). After injection, eggs were transferred into the oviducts of Swiss Webster foster females. Genotyping of newly generated mice was performed by *Nt5c2* PCR amplification using KAPA HiFi HotStart ReadyMix and running PCR products on a 1.5% agarose gel. The wild-type band is detected at ~1000bp and the deletion band is

detected at ~500bp (Forward primer: CTCTGGGATGAGCTGAGAGG; Reverse primer: CCACCAAAGGTACCATGACC). We maintained all animals in specific pathogen-free facilities at the Irving Cancer Research Center at Columbia University Medical Campus. The Columbia University Institutional Animal Care and Use Committee (IACUC) approved all animal procedures. Animal experiments were conducted in compliance with all relevant ethical regulations.

CRISPR/CAS9 NT5C2 Knockout in ALL cell lines

CUTLL1 cells were infected with pL-CRISPR.efs.gfp lentiviral particles containing an Nt5c2 exon 3 targeted sgRNA (GCAAAGCTGAGCAACTCCTG) or empty vector controls. We sorted infected cells based on GFP expression using a SONY SH800S cell sorter (SONY) and subsequently grew single cell clones. *NT5C2* knockout was confirmed per clone via western blot analysis.

Western blot analysis

Cells were lysed in RIPA buffer, cleared of cell debris and boiled with 1x SDS-loading buffer. BCA protein quantification was performed according to manufacturer guidelines (BCA Protein Assay Kit, Fisher Scientific) and equal amounts of lysate were loaded onto a 7% Tris-acetate gel (Life technologies), separated by SDS PAGE, and transferred to a nitrocellulose membrane for western blot analysis. We detected NT5C2 with a mouse anti-NT5C2 antibody (Sigma Aldrich # WH0022978M2) and β-actin with a mouse monoclonal anti-β-actin antibody (Sigma Aldrich # A5441).

HTP_2 Docking

Schrodinger Maestro was used for docking HTP_2 into the ligand binding site of NT5C2 R39Q (PDB: 6DDQ). LigPrep was used to generate energy minimized 3D molecular ligands of HTP_2 optimized for docking using Glide. The OPLS3 force field was used

and ionization states at pH 7.0 +/- 2.0 were generated as well as tautomers. Protein Preparation Wizard was used to convert the PDB structure NT5C2 R39Q (PDB: 6DDQ) to an all-atom, fully prepared protein models for use in Glide. HET states were generated using Epik at pH 7.0 +/- 2.0. Hydrogen bonds were assigned using PROPKA at pH 7.0. A restrained protein minimization was run using the OPLS3 force field. A receptor grid was generated in the prepared protein centered on the ligand binding site of NT5C2. Computation docking was done with Schrodinger Glide using the ligand structures from LigPrep and the receptor grid generated on the protein optimized using Protein Preparation Wizard. Standard precision docking was used with flexible ligand sampling. GlideScores were generated for each ligand-receptor docking. GlideScore is an empirical scoring function indicative of binding affinity and comprised of terms that account for lipophilic-lipophilic interactions, hydrogen bonds, rotatable bond penalties, and contributions from protein-ligand coulomb-vdW energies. Lower GlideScores indicate stronger binding.

Biacore Assay

A Biacore X100 surface plasmon resonance system (GE Healthcare) was used to test the binding kinetics of small molecule inhibitor HTP_2 with NT5C2 R367Q recombinant protein. NT5C2 R367Q protein was immobilized by covalent binding via amino group on a sensor chip, CM-5, at concentration 100 μg/ml with a final binding of 111136 RU (Response Units). Each small molecule compound was diluted in running buffer to 100 μM. Rmax was calculated based on the molecular weight of the protein and compounds, and the amount of protein we used for the binding analysis.

$$\text{Rmax} = \frac{\text{the amount of protein immobilized in RU}}{\text{MW of protein} * \text{MW of small molecule}}$$

Evaluation software was used to calculate the K_d for the small molecule: protein binding affinity.

Quantification and statistical analyses

We performed statistical analysis by Student's *t*-test. We considered results with $P < 0.05$ as statistically significant. Isobologram analysis was performed using Calcusyn software.

Chapter 5: Conclusions

Despite improved therapy regimens, 20% of pediatric and 50% of adult ALL patients fail to achieve remission and end up relapsing. Here we show an in-depth analysis of the role of *NT5C2* mutations in chemotherapy resistance and emergence of therapy resistant clones in relapsed ALL.

With extensive structure-function analyses of NT5C2 wild-type and relapse associated NT5C2 mutant proteins, we identified three critical regulatory elements that control NT5C2 activation and inactivation: (i) the helix A allosteric response element, (ii) an intramolecular, arm region mediated, switch off mechanism, and (iii) the c-terminus allosteric activation blockade. Each of these regulatory elements is disrupted in relapse associated *NT5C2* mutations leading to increased nucleotidase activity and subsequent chemotherapy resistance when expressed in ALL cells. Importantly, these analyses identified that the majority of NT5C2 relapse associated mutant proteins, retain the ability to bind and respond to allosteric activators identifying a potential therapeutic target for the development of NT5C2 inhibitors.

Moving forward, it will be important to continue to further our understanding of how NT5C2 is regulated to identify additional mechanisms of chemotherapy resistance. In addition to looking at direct structure-function relationships, it may be interesting to look at levels of *NT5C2* regulation at transcriptional and post-translational levels. Unpublished work has identified four post-translation modifications present on NT5C2. Additional studies are needed to explore the regulatory capacity of these modifications, but preliminary results suggest that a phosphorylation at Ser502 of NT5C2 leads to increased nucleotidase activity (Appendix 1.1). This identifies an additional activation

mechanism that may be altered to induce thiopurine resistance in relapsed ALL and thus should be further explored.

In addition to understanding the role of *NT5C2* mutations on a structural level, we also present here data on the clonal evolution of *NT5C2* relapse associated mutations in relapsed ALL. We generated a knock-in mouse model (*Nt5c2*$^{+/co\text{-}R367Q}$) with conditional expression of *Nt5c2*^{R367Q}, the most common *NT5C2* mutation found in relapsed ALL, and generated primary NOTCH1-induced *Rosa26*$^{+/CreERT2}$ *Nt5c2*$^{+/co\text{-}R367Q}$ T-ALL tumors. Using this model, we saw overt resistance to 6-MP in *Nt5c2*$^{+/R367Q}$ mutant leukemias, and were surprised to find that this chemotherapy resistance phenotype came at the cost of impaired cell fitness and leukemia initiating cell activity. *Nt5c2*$^{+/R367Q}$ mutant cells show increased export of purines to the extracellular space and depletion of the intracellular purine nucleotide pool, resulting in delayed cell growth and proliferation. Despite this impaired fitness, *Nt5c2*$^{+/R367Q}$ mutant cells are positively selected over isogenic *Nt5c2*$^{+/co\text{-}R367Q}$ wild type cells in mixed tumor populations in response to 6-MP chemotherapy *in vitro* and *in vivo* (Tzoneva, Dieck et al. 2018). Thus, thiopurine treatment selects for *NT5C2* gain of function mutations as key evolutionary drivers shaping the clonal evolution of relapsed ALL. This data along with the fact that 6-MP is a major component of maintenance therapy for ALL patients, that *NT5C2* mutations frequently occur in early relapse and the recent identification of *NT5C2* mutations in relapsed APL patients treated with 6-MP (Lehmann-Che, Bally et al. 2018) suggest that thiopurine therapy creates an immense selective pressure towards the emergence of these mutations and subsequent relapse.

Improving the outcomes of patients with relapsed ALL will involve further understanding of the genetic variants and mechanisms by which relapse clones acquire therapy

resistance. In discovering the fitness cost associated with relapse associated *NT5C2* mutations, we revealed a weak point in relapsed *NT5C2* mutant ALL we could use to further target mutant cells. Given their increased dependence on purine synthesis, *NT5C2* mutant cells are particularly sensitive to the inosine monophosphate dehydrogenase (IMPDH) inhibitor, mizoribine, which further blocks guanosine production in the cells leading to selective cytotoxicity in *NT5C2* mutant lymphoblasts (Tzoneva, Dieck et al. 2018). Identifying further synthetic lethalities in *NT5C2* mutant cells and other drug resistant ALL populations will aid in developing multi-agent chemotherapy regimens to target relapse ALL with specific genetic vulnerabilities.

In addition to finding collateral sensitivities to continue to target *NT5C2* mutations in relapsed ALL, the development of potent NT5C2 inhibitors may provide useful therapeutic options for the treatment of relapsed ALL and other diseases associated with increased nucleotidase activity such as Lesch-Nyhan syndrome (Pesi, Micheli et al. 2000). Here we identify a small molecule inhibitor of NT5C2, HTP_2, which shows low millimolar inhibitory activity in *in vitro* enzymatic assays on NT5C2 R367Q recombinant protein. Importantly HTP_2 synergizes with 6-MP chemotherapy working to reverse 6-MP resistance in *NT5C2* mutant cell lines. NT5C2 small molecule inhibitor HTP_2 also yields increased sensitivity to 6-MP in *NT5C2* wild-type cells suggesting that NT5C2 inhibition may prove to be a useful therapeutic for the treatment of all ALLs and not just those harboring *NT5C2* mutations. HTP_2 requires additional optimization to improve target potency and solubility to move forward in preclinical *in vivo* models.

Continued studies to identify drivers of chemotherapy resistance are integral to our understanding of relapsed ALL. Along with *NT5C2* mutations, other groups have identified mutations in *CREBBP* and *PRPS1* as relapse specific variants that drive

glucocorticoid and thiopurine resistance respectively (Mullighan, Zhang et al. 2011, Mar, Bullinger et al. 2014, Li, Li et al. 2015). Additional mechanistic analyses and further understanding of the role of *NT5C2* and these other genes in relapsed leukemia will be critical for improving the outcome of patients with relapsed ALL. Additionally, further development of the small molecule NT5C2 inhibitor HTP_2 may prove useful in treating relapse ALL patients harboring *NT5C2* mutant alleles. Many targeted and personalized therapies have shown to be successful in the treatment of diseases over the past few decades and further development of targeted NT5C2 therapeutics has the potential to improve the efficacy of ALL maintenance therapy by curtailing the emergence of *NT5C2* mutant clones responsible for relapse.

References

Allegrini, S., R. Pesi, M. G. Tozzi, C. J. Fiol, R. B. Johnson and S. Eriksson (1997). "Bovine cytosolic IMP/GMP-specific 5'-nucleotidase: cloning and expression of active enzyme in Escherichia coli." Biochem J **328 (Pt 2)**: 483-487.

Allegrini, S., A. Scaloni, M. G. Careddu, G. Cuccu, C. D'Ambrosio, R. Pesi, M. Camici, L. Ferrara and M. G. Tozzi (2004). "Mechanistic studies on bovine cytosolic 5'-nucleotidase II, an enzyme belonging to the HAD superfamily." European journal of biochemistry / FEBS **271**: 4881-4891.

Allegrini, S., A. Scaloni, L. Ferrara, R. Pesi, P. Pinna, F. Sgarrella, M. Camici, S. Eriksson and M. G. Tozzi (2001). "Bovine cytosolic 5'-nucleotidase acts through the formation of an aspartate 52-phosphoenzyme intermediate." J Biol Chem **276**(36): 33526-33532.

Alvarnas, J. C., P. A. Brown, P. Aoun, K. K. Ballen, S. K. Barta, U. Borate, M. W. Boyer, P. W. Burke, R. Cassaday, J. E. Castro, P. F. Coccia, S. E. Coutre, L. E. Damon, D. J. DeAngelo, D. Douer, O. Frankfurt, J. P. Greer, R. A. Johnson, H. M. Kantarjian, R. B. Klisovic, G. Kupfer, M. Litzow, A. Liu, A. V. Rao, B. Shah, G. L. Uy, E. S. Wang, A. D. Zelenetz, K. Gregory and C. Smith (2015). "Acute Lymphoblastic Leukemia, Version 2.2015." J Natl Compr Canc Netw **13**(10): 1240-1279.

Andersson, A. K., J. Ma, J. Wang, X. Chen, A. L. Gedman, J. Dang, J. Nakitandwe, L. Holmfeldt, M. Parker, J. Easton, R. Huether, R. Kriwacki, M. Rusch, G. Wu, Y. Li, H. Mulder, S. Raimondi, S. Pounds, G. Kang, L. Shi, J. Becksfort, P. Gupta, D. Payne-Turner, B. Vadodaria, K. Boggs, D. Yergeau, J. Manne, G. Song, M. Edmonson, P. Nagahawatte, L. Wei, C. Cheng, D. Pei, R. Sutton, N. C. Venn, A. Chetcuti, A. Rush, D. Catchpoole, J. Heldrup, T. Fioretos, C. Lu, L. Ding, C. H. Pui, S. Shurtleff, C. G. Mullighan, E. R. Mardis, R. K. Wilson, T. A. Gruber, J. Zhang and J. R. Downing (2015). "The landscape of somatic mutations in infant MLL-rearranged acute lymphoblastic leukemias." Nat Genet **47**(4): 330-337.

Angiolillo, A. L., A. L. Yu, G. Reaman, A. M. Ingle, R. Secola and P. C. Adamson (2009). "A phase II study of Campath-1H in children with relapsed or refractory acute lymphoblastic leukemia: a Children's Oncology Group report." Pediatr Blood Cancer **53**(6): 978-983.

Arber, D. A., A. Orazi, R. Hasserjian, J. Thiele, M. J. Borowitz, M. M. Le Beau, C. D. Bloomfield, M. Cazzola and J. W. Vardiman (2016). "The 2016 revision to the World Health Organization classification of myeloid neoplasms and acute leukemia." Blood **127**(20): 2391-2405.

Arico, M., M. Schrappe, S. P. Hunger, W. L. Carroll, V. Conter, S. Galimberti, A. Manabe, V. Saha, A. Baruchel, K. Vettenranta, K. Horibe, Y. Benoit, R. Pieters, G. Escherich, L. B. Silverman, C. H. Pui and M. G. Valsecchi (2010). "Clinical outcome of children with newly diagnosed Philadelphia chromosome-positive acute lymphoblastic leukemia treated between 1995 and 2005." J Clin Oncol **28**(31): 4755-4761.

Banditelli, S., C. Baiocchi, R. Pesi, S. Allegrini, M. Turriani, P. L. Ipata, M. Camici and M. G. Tozzi (1996). "The phosphotransferase activity of cytosolic 5'-nucleotidase; a purine analog phosphorylating enzyme." Int J Biochem Cell Biol **28**(6): 711-720.

Barredo, J. C., M. Devidas, S. J. Lauer, A. Billett, M. Marymont, J. Pullen, B. Camitta, N. Winick, W. Carroll and A. K. Ritchey (2006). "Isolated CNS relapse of acute lymphoblastic leukemia treated with intensive systemic chemotherapy and delayed CNS radiation: a pediatric oncology group study." J Clin Oncol **24**(19): 3142-3149.

Begley, C. G., P. D. Aplan, M. P. Davey, K. Nakahara, K. Tchorz, J. Kurtzberg, M. S. Hershfield, B. F. Haynes, D. I. Cohen, T. A. Waldmann and et al. (1989). "Chromosomal translocation in a human leukemic stem-cell line disrupts the T-cell antigen receptor delta-chain diversity region and results in a previously unreported fusion transcript." Proc Natl Acad Sci U S A **86**(6): 2031-2035.

Belver, L. and A. Ferrando (2016). "The genetics and mechanisms of T cell acute lymphoblastic leukaemia." Nat Rev Cancer **16**(8): 494-507.

Bernard, O. A., M. Busson-LeConiat, P. Ballerini, M. Mauchauffe, V. Della Valle, R. Monni, F. Nguyen Khac, T. Mercher, V. Penard-Lacronique, P. Pasturaud, L. Gressin, R. Heilig, M. T. Daniel, M. Lessard and R. Berger (2001). "A new recurrent and specific cryptic translocation, t(5;14)(q35;q32), is associated with expression of the Hox11L2 gene in T acute lymphoblastic leukemia." Leukemia **15**(10): 1495-1504.

Bhatia, S., W. Landier, M. Shangguan, L. Hageman, A. N. Schaible, A. R. Carter, C. L. Hanby, W. Leisenring, Y. Yasui, N. M. Kornegay, L. Mascarenhas, A. K. Ritchey, J. N. Casillas, D. S. Dickens, J. Meza, W. L. Carroll, M. V. Relling and F. L. Wong (2012). "Nonadherence to oral mercaptopurine and risk of relapse in Hispanic and non-Hispanic white children with acute lymphoblastic leukemia: a report from the children's oncology group." J Clin Oncol **30**(17): 2094-2101.

Bhojwani, D. and C. H. Pui (2013). "Relapsed childhood acute lymphoblastic leukaemia." Lancet Oncol **14**(6): e205-217.

Bianchi, V. and J. Spychala (2003). "Mammalian 5'-nucleotidases." J Biol Chem **278**(47): 46195-46198.

Bickerton, G. R., G. V. Paolini, J. Besnard, S. Muresan and A. L. Hopkins (2012). "Quantifying the chemical beauty of drugs." Nat Chem **4**(2): 90-98.

Bontemps, F., G. Van den Berghe and H. G. Hers (1988). "5'-Nucleotidase activities in human erythrocytes. Identification of a purine 5'-nucleotidase stimulated by ATP and glycerate 2,3-bisphosphate." Biochem J **250**(3): 687-696.

Borowitz, M. J., B. L. Wood, M. Devidas, M. L. Loh, E. A. Raetz, W. L. Salzer, J. B. Nachman, A. J. Carroll, N. A. Heerema, J. M. Gastier-Foster, C. L. Willman, Y. Dai, N. J. Winick, S. P. Hunger, W. L. Carroll and E. Larsen (2015). "Prognostic significance of minimal residual disease in high risk B-ALL: a report from Children's Oncology Group study AALL0232." Blood **126**(8): 964-971.

Bretonnet, A. S., L. P. Jordheim, C. Dumontet and J. M. Lancelin (2005). "Regulation and activity of cytosolic 5'-nucleotidase II. A bifunctional allosteric enzyme of the Haloacid Dehalogenase superfamily involved in cellular metabolism." FEBS Lett **579**(16): 3363-3368.

Brooks, H. B., S. Geeganage, S. D. Kahl, C. Montrose, S. Sittampalam, M. C. Smith and J. R. Weidner (2004). Basics of Enzymatic Assays for HTS. Assay Guidance Manual. G. S. Sittampalam, N. P. Coussens, K. Brimacombe et al. Bethesda (MD).

Brouwer, C., T. M. Vogels-Mentink, J. J. Keizer-Garritsen, F. J. Trijbels, J. P. Bokkerink, P. M. Hoogerbrugge, E. R. van Wering, A. J. Veerman and R. A. De Abreu (2005). "Role of 5'-nucleotidase in thiopurine metabolism: enzyme kinetic profile and association with thio-GMP levels in patients with acute lymphoblastic leukemia during 6-mercaptopurine treatment." Clin Chim Acta **361**(1-2): 95-103.

Burchenal, J. H., M. L. Murphy, R. R. Ellison, M. P. Sykes, T. C. Tan, L. A. Leone, D. A. Karnofsky, L. F. Craver, H. W. Dargeon and C. P. Rhoads (1953). "Clinical evaluation of a new antimetabolite, 6-mercaptopurine, in the treatment of leukemia and allied diseases." Blood **8**(11): 965-999.

Cerny, T., B. Borisch, M. Introna, P. Johnson and A. L. Rose (2002). "Mechanism of action of rituximab." Anticancer Drugs **13 Suppl 2**: S3-10.

Chen, K. H., M. Wada, K. G. Pinz, H. Liu, K. W. Lin, A. Jares, A. E. Firor, X. Shuai, H. Salman, M. Golightly, F. Lan, L. Senzel, E. L. Leung, X. Jiang and Y. Ma (2017). "Preclinical targeting of aggressive T-cell malignancies using anti-CD5 chimeric antigen receptor." Leukemia **31**(10): 2151-2160.

Chen, Q., C. Y. Yang, J. T. Tsan, Y. Xia, A. H. Ragab, S. C. Peiper, A. Carroll and R. Baer (1990). "Coding sequences of the tal-1 gene are disrupted by chromosome translocation in human T cell leukemia." J Exp Med **172**(5): 1403-1408.

Churchman, M. L., M. Qian, G. Te Kronnie, R. Zhang, W. Yang, H. Zhang, T. Lana, P. Tedrick, R. Baskin, K. Verbist, J. L. Peters, M. Devidas, E. Larsen, I. M. Moore, Z. Gu, C. Qu, H. Yoshihara, S. N. Porter, S. M. Pruett-Miller, G. Wu, E. Raetz, P. L. Martin, W. P. Bowman, N. Winick, E. Mardis, R. Fulton, M. Stanulla, W. E. Evans, M. V. Relling, C. H. Pui, S. P. Hunger, M. L. Loh, R. Handgretinger, K. E. Nichols, J. J. Yang and C. G. Mullighan (2018). "Germline Genetic IKZF1 Variation and Predisposition to Childhood Acute Lymphoblastic Leukemia." Cancer Cell **33**(5): 937-948.e938.

Collet, J. F., V. Stroobant, M. Pirard, G. Delpierre and E. Van Schaftingen (1998). "A new class of phosphotransferases phosphorylated on an aspartate residue in an amino-terminal DXDX(T/V) motif." J Biol Chem **273**(23): 14107-14112.

Connor, C. O., H. S. Beckmann and D. R. Spring (2012). "Diversity-oriented synthesis: producing chemical tools for dissecting biology." Chem Soc Rev **41**(12): 4444-4456.

Conter, V., M. Arico, G. Basso, A. Biondi, E. Barisone, C. Messina, R. Parasole, G. De Rossi, F. Locatelli, A. Pession, N. Santoro, C. Micalizzi, M. Citterio, C. Rizzari, D. Silvestri, R. Rondelli, L. Lo Nigro, O. Ziino, A. M. Testi, G. Masera and M. G. Valsecchi (2010). "Long-term results of the Italian Association of Pediatric Hematology and

Oncology (AIEOP) Studies 82, 87, 88, 91 and 95 for childhood acute lymphoblastic leukemia." Leukemia **24**(2): 255-264.

Cooper, S. L. and P. A. Brown (2015). "Treatment of pediatric acute lymphoblastic leukemia." Pediatr Clin North Am **62**(1): 61-73.

Coustan-Smith, E., C. G. Mullighan, M. Onciu, F. G. Behm, S. C. Raimondi, D. Pei, C. Cheng, X. Su, J. E. Rubnitz, G. Basso, A. Biondi, C. H. Pui, J. R. Downing and D. Campana (2009). "Early T-cell precursor leukaemia: a subtype of very high-risk acute lymphoblastic leukaemia." Lancet Oncol **10**(2): 147-156.

Cox, C. V., P. Diamanti, R. S. Evely, P. R. Kearns and A. Blair (2009). "Expression of CD133 on leukemia-initiating cells in childhood ALL." Blood **113**(14): 3287-3296.

Darvish, H., L. J. Azcona, A. Tafakhori, M. Ahmadi, A. Ahmadifard and C. Paisan-Ruiz (2017). "Whole genome sequencing identifies a novel homozygous exon deletion in the NT5C2 gene in a family with intellectual disability and spastic paraplegia." NPJ Genom Med **2**.

Daver, N., D. Thomas, F. Ravandi, J. Cortes, R. Garris, E. Jabbour, G. Garcia-Manero, G. Borthakur, T. Kadia, M. Rytting, M. Konopleva, H. Kantarjian and S. O'Brien (2015). "Final report of a phase II study of imatinib mesylate with hyper-CVAD for the front-line treatment of adult patients with Philadelphia chromosome-positive acute lymphoblastic leukemia." Haematologica **100**(5): 653-661.

DeAngelo, D. J., W. Stock, A. S. Stein, A. Shustov, M. Liedtke, C. A. Schiffer, E. Vandendries, K. Liau, R. Ananthakrishnan, J. Boni, A. D. Laird, L. Fostvedt, H. M. Kantarjian and A. S. Advani (2017). "Inotuzumab ozogamicin in adults with relapsed or refractory CD22-positive acute lymphoblastic leukemia: a phase 1/2 study." Blood Adv **1**(15): 1167-1180.

Den Boer, M. L., M. van Slegtenhorst, R. X. De Menezes, M. H. Cheok, J. G. Buijs-Gladdines, S. T. Peters, L. J. Van Zutven, H. B. Beverloo, P. J. Van der Spek, G. Escherich, M. A. Horstmann, G. E. Janka-Schaub, W. A. Kamps, W. E. Evans and R. Pieters (2009). "A subtype of childhood acute lymphoblastic leukaemia with poor treatment outcome: a genome-wide classification study." Lancet Oncol **10**(2): 125-134.

Dieck, C. L., G. Tzoneva, F. Forouhar, Z. Carpenter, A. Ambesi-Impiombato, M. Sanchez-Martin, R. Kirschner-Schwabe, S. Lew, J. Seetharaman, L. Tong and A. A. Ferrando (2018). "Structure and Mechanisms of NT5C2 Mutations Driving Thiopurine Resistance in Relapsed Lymphoblastic Leukemia." Cancer Cell **34**(1): 136-147.e136.

DiJoseph, J. F., D. C. Armellino, E. R. Boghaert, K. Khandke, M. M. Dougher, L. Sridharan, A. Kunz, P. R. Hamann, B. Gorovits, C. Udata, J. K. Moran, A. G. Popplewell, S. Stephens, P. Frost and N. K. Damle (2004). "Antibody-targeted chemotherapy with CMC-544: a CD22-targeted immunoconjugate of calicheamicin for the treatment of B-lymphoid malignancies." Blood **103**(5): 1807-1814.

Druker, B. J., M. Talpaz, D. J. Resta, B. Peng, E. Buchdunger, J. M. Ford, N. B. Lydon, H. Kantarjian, R. Capdeville, S. Ohno-Jones and C. L. Sawyers (2001). "Efficacy and

safety of a specific inhibitor of the BCR-ABL tyrosine kinase in chronic myeloid leukemia." N Engl J Med **344**(14): 1031-1037.

Duarte, R. R. R., C. Troakes, M. Nolan, D. P. Srivastava, R. M. Murray and N. J. Bray (2016). "Genome-wide significant schizophrenia risk variation on chromosome 10q24 is associated with altered cis-regulation of BORCS7, AS3MT, and NT5C2 in the human brain." Am J Med Genet B Neuropsychiatr Genet **171**(6): 806-814.

Dumortier, A., A. Wilson, H. R. MacDonald and F. Radtke (2005). "Paradigms of notch signaling in mammals." Int J Hematol **82**(4): 277-284.

Elion, G. B. (1989). "The purine path to chemotherapy." Science **244**(4900): 41-47.

Elsaid, M. F., K. Ibrahim, N. Chalhoub, A. Elsotouhy, N. El Mudehki and A. Abdel Aleem (2017). "NT5C2 novel splicing variant expands the phenotypic spectrum of Spastic Paraplegia (SPG45): case report of a new member of thin corpus callosum SPG-Subgroup." BMC Med Genet **18**(1): 33.

Emadi, A., R. J. Jones and R. A. Brodsky (2009). "Cyclophosphamide and cancer: golden anniversary." Nat Rev Clin Oncol **6**(11): 638-647.

Evans, W. E., M. Horner, Y. Q. Chu, D. Kalwinsky and W. M. Roberts (1991). "Altered mercaptopurine metabolism, toxic effects, and dosage requirement in a thiopurine methyltransferase-deficient child with acute lymphocytic leukemia." J Pediatr **119**(6): 985-989.

Evensen, N. A., P. P. Madhusoodhan, J. Meyer, J. Saliba, A. Chowdhury, D. J. Araten, J. Nersting, T. Bhatla, T. L. Vincent, D. Teachey, S. P. Hunger, J. Yang, K. Schmiegelow and W. L. Carroll (2018). "MSH6 haploinsufficiency at relapse contributes to the development of thiopurine resistance in pediatric B-lymphoblastic leukemia." Haematologica **103**(5): 830-839.

Faham, M., J. Zheng, M. Moorhead, V. E. Carlton, P. Stow, E. Coustan-Smith, C. H. Pui and D. Campana (2012). "Deep-sequencing approach for minimal residual disease detection in acute lymphoblastic leukemia." Blood **120**(26): 5173-5180.

Familiades, J., M. Bousquet, M. Lafage-Pochitaloff, M. C. Bene, K. Beldjord, J. De Vos, N. Dastugue, E. Coyaud, S. Struski, C. Quelen, N. Prade-Houdellier, S. Dobbelstein, J. M. Cayuela, J. Soulier, N. Grardel, C. Preudhomme, H. Cave, O. Blanchet, V. Lheritier, A. Delannoy, Y. Chalandon, N. Ifrah, A. Pigneux, P. Brousset, E. A. Macintyre, F. Huguet, H. Dombret, C. Broccardo and E. Delabesse (2009). "PAX5 mutations occur frequently in adult B-cell progenitor acute lymphoblastic leukemia and PAX5 haploinsufficiency is associated with BCR-ABL1 and TCF3-PBX1 fusion genes: a GRAALL study." Leukemia **23**(11): 1989-1998.

Farber, S. and L. K. Diamond (1948). "Temporary remissions in acute leukemia in children produced by folic acid antagonist, 4-aminopteroyl-glutamic acid." N Engl J Med **238**(23): 787-793.

Ferrando, A. A., D. S. Neuberg, R. K. Dodge, E. Paietta, R. A. Larson, P. H. Wiernik, J. M. Rowe, M. A. Caligiuri, C. D. Bloomfield and A. T. Look (2004). "Prognostic

importance of TLX1 (HOX11) oncogene expression in adults with T-cell acute lymphoblastic leukaemia." Lancet **363**(9408): 535-536.

Ferrando, A. A., D. S. Neuberg, J. Staunton, M. L. Loh, C. Huard, S. C. Raimondi, F. G. Behm, C. H. Pui, J. R. Downing, D. G. Gilliland, E. S. Lander, T. R. Golub and A. T. Look (2002). "Gene expression signatures define novel oncogenic pathways in T cell acute lymphoblastic leukemia." Cancer Cell **1**(1): 75-87.

Fischer, M., M. Schwieger, S. Horn, B. Niebuhr, A. Ford, S. Roscher, U. Bergholz, M. Greaves, J. Lohler and C. Stocking (2005). "Defining the oncogenic function of the TEL/AML1 (ETV6/RUNX1) fusion protein in a mouse model." Oncogene **24**(51): 7579-7591.

Frei, E., 3rd, M. Karon, R. H. Levin, E. J. Freireich, R. J. Taylor, J. Hananian, O. Selawry, J. F. Holland, B. Hoogstraten, I. J. Wolman, E. Abir, A. Sawitsky, S. Lee, S. D. Mills, E. O. Burgert, Jr., C. L. Spurr, R. B. Patterson, F. G. Ebaugh, G. W. James, 3rd and J. H. Moon (1965). "The effectiveness of combinations of antileukemic agents in inducing and maintaining remission in children with acute leukemia." Blood **26**(5): 642-656.

Fry, T. J., N. N. Shah, R. J. Orentas, M. Stetler-Stevenson, C. M. Yuan, S. Ramakrishna, P. Wolters, S. Martin, C. Delbrook, B. Yates, H. Shalabi, T. J. Fountaine, J. F. Shern, R. G. Majzner, D. F. Stroncek, M. Sabatino, Y. Feng, D. S. Dimitrov, L. Zhang, S. Nguyen, H. Qin, B. Dropulic, D. W. Lee and C. L. Mackall (2018). "CD22-targeted CAR T cells induce remission in B-ALL that is naive or resistant to CD19-targeted CAR immunotherapy." Nat Med **24**(1): 20-28.

Gallier, F., P. Lallemand, M. Meurillon, L. P. Jordheim, C. Dumontet, C. Perigaud, C. Lionne, S. Peyrottes and L. Chaloin (2011). "Structural insights into the inhibition of cytosolic 5'-nucleotidase II (cN-II) by ribonucleoside 5'-monophosphate analogues." PLoS Comput Biol **7**(12): e1002295.

Galmarini, C. M., E. Cros, X. Thomas, L. Jordheim and C. Dumontet (2005). "The prognostic value of cN-II and cN-III enzymes in adult acute myeloid leukemia." Haematologica **90**(12): 1699-1701.

Gardner, R., D. Wu, S. Cherian, M. Fang, L. A. Hanafi, O. Finney, H. Smithers, M. C. Jensen, S. R. Riddell, D. G. Maloney and C. J. Turtle (2016). "Acquisition of a CD19-negative myeloid phenotype allows immune escape of MLL-rearranged B-ALL from CD19 CAR-T-cell therapy." Blood **127**(20): 2406-2410.

Gaulton, A., A. Hersey, M. Nowotka, A. P. Bento, J. Chambers, D. Mendez, P. Mutowo, F. Atkinson, L. J. Bellis, E. Cibrian-Uhalte, M. Davies, N. Dedman, A. Karlsson, M. P. Magarinos, J. P. Overington, G. Papadatos, I. Smit and A. R. Leach (2017). "The ChEMBL database in 2017." Nucleic Acids Res **45**(D1): D945-d954.

Gaynon, P. S., A. L. Angiolillo, W. L. Carroll, J. B. Nachman, M. E. Trigg, H. N. Sather, S. P. Hunger and M. Devidas (2010). "Long-term results of the children's cancer group studies for childhood acute lymphoblastic leukemia 1983-2002: a Children's Oncology Group Report." Leukemia **24**(2): 285-297.

Gerby, B., E. Clappier, F. Armstrong, C. Deswarte, J. Calvo, S. Poglio, J. Soulier, N. Boissel, T. Leblanc, A. Baruchel, J. Landman-Parker, P. H. Romeo, P. Ballerini and F. Pflumio (2011). "Expression of CD34 and CD7 on human T-cell acute lymphoblastic leukemia discriminates functionally heterogeneous cell populations." Leukemia **25**(8): 1249-1258.

Gidding, C. E., S. J. Kellie, W. A. Kamps and S. S. de Graaf (1999). "Vincristine revisited." Crit Rev Oncol Hematol **29**(3): 267-287.

Gokbuget, N., H. Dombret, M. Bonifacio, A. Reichle, C. Graux, C. Faul, H. Diedrich, M. S. Topp, M. Bruggemann, H. A. Horst, V. Havelange, J. Stieglmaier, H. Wessels, V. Haddad, J. E. Benjamin, G. Zugmaier, D. Nagorsen and R. C. Bargou (2018). "Blinatumomab for minimal residual disease in adults with B-cell precursor acute lymphoblastic leukemia." Blood **131**(14): 1522-1531.

Greaves, M. F., G. Janossy, J. Peto and H. Kay (1981). "Immunologically defined subclasses of acute lymphoblastic leukaemia in children: their relationship to presentation features and prognosis." Br J Haematol **48**(2): 179-197.

Gribbon, P. and A. Sewing (2005). "High-throughput drug discovery: what can we expect from HTS?" Drug Discov Today **10**(1): 17-22.

Hajduk, P. J. and J. Greer (2007). "A decade of fragment-based drug design: strategic advances and lessons learned." Nat Rev Drug Discov **6**(3): 211-219.

Hanna, R., G. L. Ong and M. J. Mattes (1996). "Processing of antibodies bound to B-cell lymphomas and other hematological malignancies." Cancer Res **56**(13): 3062-3068.

Harrison, C. J. (2009). "Cytogenetics of paediatric and adolescent acute lymphoblastic leukaemia." Br J Haematol **144**(2): 147-156.

Harrison, C. J., A. V. Moorman, C. Schwab, A. J. Carroll, E. A. Raetz, M. Devidas, S. Strehl, K. Nebral, J. Harbott, A. Teigler-Schlegel, M. Zimmerman, N. Dastuge, A. Baruchel, J. Soulier, M. F. Auclerc, A. Attarbaschi, G. Mann, B. Stark, G. Cazzaniga, L. Chilton, P. Vandenberghe, E. Forestier, I. Haltrich, S. C. Raimondi, M. Parihar, J. P. Bourquin, J. Tchinda, C. Haferlach, A. Vora, S. P. Hunger, N. A. Heerema and O. A. Haas (2014). "An international study of intrachromosomal amplification of chromosome 21 (iAMP21): cytogenetic characterization and outcome." Leukemia **28**(5): 1015-1021.

Hartford, C., E. Vasquez, M. Schwab, M. J. Edick, J. E. Rehg, G. Grosveld, C. H. Pui, W. E. Evans and M. V. Relling (2007). "Differential effects of targeted disruption of thiopurine methyltransferase on mercaptopurine and thioguanine pharmacodynamics." Cancer Res **67**(10): 4965-4972.

Harvey, R. C., C. G. Mullighan, X. Wang, K. K. Dobbin, G. S. Davidson, E. J. Bedrick, I. M. Chen, S. R. Atlas, H. Kang, K. Ar, C. S. Wilson, W. Wharton, M. Murphy, M. Devidas, A. J. Carroll, M. J. Borowitz, W. P. Bowman, J. R. Downing, M. Relling, J. Yang, D. Bhojwani, W. L. Carroll, B. Camitta, G. H. Reaman, M. Smith, S. P. Hunger and C. L. Willman (2010). "Identification of novel cluster groups in pediatric high-risk B-precursor acute lymphoblastic leukemia with gene expression profiling: correlation with genome-

wide DNA copy number alterations, clinical characteristics, and outcome." Blood **116**(23): 4874-4884.

Hatano, M., C. W. Roberts, M. Minden, W. M. Crist and S. J. Korsmeyer (1991). "Deregulation of a homeobox gene, HOX11, by the t(10;14) in T cell leukemia." Science **253**(5015): 79-82.

Hauberg, M. E., M. H. Holm-Nielsen, M. Mattheisen, A. L. Askou, J. Grove, A. D. Borglum and T. J. Corydon (2016). "Schizophrenia risk variants affecting microRNA function and site-specific regulation of NT5C2 by miR-206." Eur Neuropsychopharmacol **26**(9): 1522-1526.

Hawkins, E. D., D. Duarte, O. Akinduro, R. A. Khorshed, D. Passaro, M. Nowicka, L. Straszkowski, M. K. Scott, S. Rothery, N. Ruivo, K. Foster, M. Waibel, R. W. Johnstone, S. J. Harrison, D. A. Westerman, H. Quach, J. Gribben, M. D. Robinson, L. E. Purton, D. Bonnet and C. Lo Celso (2016). "T-cell acute leukaemia exhibits dynamic interactions with bone marrow microenvironments." Nature **538**(7626): 518-522.

Hebert, J., J. M. Cayuela, J. Berkeley and F. Sigaux (1994). "Candidate tumor-suppressor genes MTS1 (p16INK4A) and MTS2 (p15INK4B) display frequent homozygous deletions in primary cells from T- but not from B-cell lineage acute lymphoblastic leukemias." Blood **84**(12): 4038-4044.

Heigwer, F., G. Kerr and M. Boutros (2014). "E-CRISP: fast CRISPR target site identification." Nat Methods **11**(2): 122-123.

Heikamp, E. B. and C. H. Pui (2018). "Next-Generation Evaluation and Treatment of Pediatric Acute Lymphoblastic Leukemia." J Pediatr.

Hnizda, A., M. Fabry, T. Moriyama, P. Pachl, M. Kugler, V. Brinsa, D. B. Ascher, W. L. Carroll, P. Novak, M. Zaliova, J. Trka, P. Rezacova, J. J. Yang and V. Veverka (2018). "Relapsed acute lymphoblastic leukemia-specific mutations in NT5C2 cluster into hotspots driving intersubunit stimulation." Leukemia.

Hnizda, A., J. Skerlova, M. Fabry, P. Pachl, M. Sinalova, L. Vrzal, P. Man, P. Novak, P. Rezacova and V. Veverka (2016). "Oligomeric interface modulation causes misregulation of purine 5 -nucleotidase in relapsed leukemia." BMC Biol **14**(1): 91.

Holmfeldt, L., L. Wei, E. Diaz-Flores, M. Walsh, J. Zhang, L. Ding, D. Payne-Turner, M. Churchman, A. Andersson, S. C. Chen, K. McCastlain, J. Becksfort, J. Ma, G. Wu, S. N. Patel, S. L. Heatley, L. A. Phillips, G. Song, J. Easton, M. Parker, X. Chen, M. Rusch, K. Boggs, B. Vadodaria, E. Hedlund, C. Drenberg, S. Baker, D. Pei, C. Cheng, R. Huether, C. Lu, R. S. Fulton, L. L. Fulton, Y. Tabib, D. J. Dooling, K. Ochoa, M. Minden, I. D. Lewis, L. B. To, P. Marlton, A. W. Roberts, G. Raca, W. Stock, G. Neale, H. G. Drexler, R. A. Dickins, D. W. Ellison, S. A. Shurtleff, C. H. Pui, R. C. Ribeiro, M. Devidas, A. J. Carroll, N. A. Heerema, B. Wood, M. J. Borowitz, J. M. Gastier-Foster, S. C. Raimondi, E. R. Mardis, R. K. Wilson, J. R. Downing, S. P. Hunger, M. L. Loh and C. G. Mullighan (2013). "The genomic landscape of hypodiploid acute lymphoblastic leukemia." Nat Genet **45**(3): 242-252.

Homminga, I., M. J. Vuerhard, A. W. Langerak, J. Buijs-Gladdines, R. Pieters and J. P. Meijerink (2012). "Characterization of a pediatric T-cell acute lymphoblastic leukemia patient with simultaneous LYL1 and LMO2 rearrangements." Haematologica **97**(2): 258-261.

Hughes, J. P., S. Rees, S. B. Kalindjian and K. L. Philpott (2011). "Principles of early drug discovery." Br J Pharmacol **162**(6): 1239-1249.

Hunger, S. P., N. Galili, A. J. Carroll, W. M. Crist, M. P. Link and M. L. Cleary (1991). "The t(1;19)(q23;p13) results in consistent fusion of E2A and PBX1 coding sequences in acute lymphoblastic leukemias." Blood **77**(4): 687-693.

Hunger, S. P. and C. G. Mullighan (2015). "Acute Lymphoblastic Leukemia in Children." N Engl J Med **373**(16): 1541-1552.

Hunsucker, S. A., B. S. Mitchell and J. Spychala (2005). "The 5'-nucleotidases as regulators of nucleotide and drug metabolism." Pharmacology & therapeutics **107**: 1-30.

Inaba, H. and C. H. Pui (2010). "Glucocorticoid use in acute lymphoblastic leukemia: comparison of prednisone and dexamethasone." Lancet Oncol **11**(11): 1096-1106.

Itoh, R., A. Mitsui and K. Tsushima (1967). "5'-nucleotidase of chicken liver." Biochim Biophys Acta **146**(1): 151-159.

Jabbour, E., H. Kantarjian, F. Ravandi, D. Thomas, X. Huang, S. Faderl, N. Pemmaraju, N. Daver, G. Garcia-Manero, K. Sasaki, J. Cortes, R. Garris, C. C. Yin, J. D. Khoury, J. Jorgensen, Z. Estrov, Z. Bohannan, M. Konopleva, T. Kadia, N. Jain, C. DiNardo, W. Wierda, V. Jeanis and S. O'Brien (2015). "Combination of hyper-CVAD with ponatinib as first-line therapy for patients with Philadelphia chromosome-positive acute lymphoblastic leukaemia: a single-centre, phase 2 study." Lancet Oncol **16**(15): 1547-1555.

Jabbour, E., C. H. Pui and H. Kantarjian (2018). "Progress and Innovations in the Management of Adult Acute Lymphoblastic Leukemia." JAMA Oncol **4**(10): 1413-1420.

Jinnah, H. A., R. L. Sabina and G. Van Den Berghe (2013). "Metabolic disorders of purine metabolism affecting the nervous system." Handb Clin Neurol **113**: 1827-1836.

Jones, C. L., T. Bhatla, R. Blum, J. Wang, S. W. Paugh, X. Wen, W. Bourgeois, D. S. Bitterman, E. A. Raetz, D. J. Morrison, D. T. Teachey, W. E. Evans, M. J. Garabedian and W. L. Carroll (2014). "Loss of TBL1XR1 disrupts glucocorticoid receptor recruitment to chromatin and results in glucocorticoid resistance in a B-lymphoblastic leukemia model." J Biol Chem **289**(30): 20502-20515.

Jordheim, L. P., Z. Marton, M. Rhimi, E. Cros-Perrial, C. Lionne, S. Peyrottes, C. Dumontet, N. Aghajari and L. Chaloin (2013). "Identification and characterization of inhibitors of cytoplasmic 5'-nucleotidase cN-II issued from virtual screening." Biochem Pharmacol **85**(4): 497-506.

Kamijo, T., J. D. Weber, G. Zambetti, F. Zindy, M. F. Roussel and C. J. Sherr (1998). "Functional and physical interactions of the ARF tumor suppressor with p53 and Mdm2." Proc Natl Acad Sci U S A **95**(14): 8292-8297.

Kampen, K. R. (2012). "The discovery and early understanding of leukemia." Leuk Res **36**(1): 6-13.

Kantarjian, H., D. Thomas, J. Jorgensen, P. Kebriaei, E. Jabbour, M. Rytting, S. York, F. Ravandi, R. Garris, M. Kwari, S. Faderl, J. Cortes, R. Champlin and S. O'Brien (2013). "Results of inotuzumab ozogamicin, a CD22 monoclonal antibody, in refractory and relapsed acute lymphocytic leukemia." Cancer **119**(15): 2728-2736.

Kantarjian, H. M., E. Vandendries and A. S. Advani (2016). "Inotuzumab Ozogamicin for Acute Lymphoblastic Leukemia." N Engl J Med **375**(21): 2100-2101.

Karran, P. (2006). "Thiopurines, DNA damage, DNA repair and therapy-related cancer." Br Med Bull **79-80**: 153-170.

Kawasaki, H., C. J. Carrera, L. D. Piro, A. Saven, T. J. Kipps and D. A. Carson (1993). "Relationship of deoxycytidine kinase and cytoplasmic 5'-nucleotidase to the chemotherapeutic efficacy of 2-chlorodeoxyadenosine." Blood **81**(3): 597-601.

Kennedy, M. A., R. Gonzalez-Sarmiento, U. R. Kees, F. Lampert, N. Dear, T. Boehm and T. H. Rabbitts (1991). "HOX11, a homeobox-containing T-cell oncogene on human chromosome 10q24." Proc Natl Acad Sci U S A **88**(20): 8900-8904.

Kleihues, P., B. Schauble, A. zur Hausen, J. Esteve and H. Ohgaki (1997). "Tumors associated with p53 germline mutations: a synopsis of 91 families." Am J Pathol **150**(1): 1-13.

Konopleva, M., S. Konoplev, W. Hu, A. Y. Zaritskey, B. V. Afanasiev and M. Andreeff (2002). "Stromal cells prevent apoptosis of AML cells by up-regulation of anti-apoptotic proteins." Leukemia **16**(9): 1713-1724.

Koonin, E. V. and R. L. Tatusov (1994). "Computer analysis of bacterial haloacid dehalogenases defines a large superfamily of hydrolases with diverse specificity. Application of an iterative approach to database search." J Mol Biol **244**(1): 125-132.

Kufe, D., D. Spriggs, E. M. Egan and D. Munroe (1984). "Relationships among Ara-CTP pools, formation of (Ara-C)DNA, and cytotoxicity of human leukemic cells." Blood **64**(1): 54-58.

Kuiper, R. P., E. F. Schoenmakers, S. V. van Reijmersdal, J. Y. Hehir-Kwa, A. G. van Kessel, F. N. van Leeuwen and P. M. Hoogerbrugge (2007). "High-resolution genomic profiling of childhood ALL reveals novel recurrent genetic lesions affecting pathways involved in lymphocyte differentiation and cell cycle progression." Leukemia **21**(6): 1258-1266.

Kunz, J. B., T. Rausch, O. R. Bandapalli, J. Eilers, P. Pechanska, S. Schuessele, Y. Assenov, A. M. Stutz, R. Kirschner-Schwabe, J. Hof, C. Eckert, A. von Stackelberg, M. Schrappe, M. Stanulla, R. Koehler, S. Avigad, S. Elitzur, R. Handgretinger, V. Benes, J. Weischenfeldt, J. O. Korbel, M. U. Muckenthaler and A. E. Kulozik (2015). "Pediatric T-cell lymphoblastic leukemia evolves into relapse by clonal selection, acquisition of mutations and promoter hypomethylation." Haematologica **100**(11): 1442-1450.

Kuster, L., R. Grausenburger, G. Fuka, U. Kaindl, G. Krapf, A. Inthal, G. Mann, M. Kauer, J. Rainer, R. Kofler, A. Hall, M. Metzler, L. H. Meyer, C. Meyer, J. Harbott, R. Marschalek, S. Strehl, O. A. Haas and R. Panzer-Grumayer (2011). "ETV6/RUNX1-positive relapses evolve from an ancestral clone and frequently acquire deletions of genes implicated in glucocorticoid signaling." Blood **117**(9): 2658-2667.

Kviklyte, S., D. Vertommen, X. Yerna, H. Andersen, X. Xu, P. Gailly, Y. M. Bohlooly, J. Oscarsson and M. H. Rider (2017). "Effects of genetic deletion of soluble 5'-nucleotidases NT5C1A and NT5C2 on AMPK activation and nucleotide levels in contracting mouse skeletal muscles." Am J Physiol Endocrinol Metab **313**(1): E48-e62.

Lachance, H., S. Wetzel, K. Kumar and H. Waldmann (2012). "Charting, navigating, and populating natural product chemical space for drug discovery." J Med Chem **55**(13): 5989-6001.

Lamb, Y. N. (2017). "Inotuzumab Ozogamicin: First Global Approval." Drugs **77**(14): 1603-1610.

Larson, R. A. (2018). "Managing CNS disease in adults with acute lymphoblastic leukemia." Leuk Lymphoma **59**(1): 3-13.

Larson, R. C., I. Lavenir, T. A. Larson, R. Baer, A. J. Warren, I. Wadman, K. Nottage and T. H. Rabbitts (1996). "Protein dimerization between Lmo2 (Rbtn2) and Tal1 alters thymocyte development and potentiates T cell tumorigenesis in transgenic mice." Embo j **15**(5): 1021-1027.

Lehmann-Che, J., C. Bally, E. Letouze, C. Berthier, H. Yuan, F. Jollivet, L. Ades, B. Cassinat, P. Hirsch, A. Pigneux, M. J. Mozziconacci, S. Kogan, P. Fenaux and H. de The (2018). "Dual origin of relapses in retinoic-acid resistant acute promyelocytic leukemia." Nat Commun **9**(1): 2047.

Li, B., H. Li, Y. Bai, R. Kirschner-Schwabe, J. J. Yang, Y. Chen, G. Lu, G. Tzoneva, X. Ma, T. Wu, W. Li, H. Lu, L. Ding, H. Liang, X. Huang, M. Yang, L. Jin, H. Kang, S. Chen, A. Du, S. Shen, J. Ding, H. Chen, J. Chen, A. von Stackelberg, L. Gu, J. Zhang, A. Ferrando, J. Tang, S. Wang and B. B. Zhou (2015). "Negative feedback-defective PRPS1 mutants drive thiopurine resistance in relapsed childhood ALL." Nat Med **21**(6): 563-571.

Li, Y., C. Schwab, S. Ryan, E. Papaemmanuil, H. M. Robinson, P. Jacobs, A. V. Moorman, S. Dyer, J. Borrow, M. Griffiths, N. A. Heerema, A. J. Carroll, P. Talley, N. Bown, N. Telford, F. M. Ross, L. Gaunt, R. J. Q. McNally, B. D. Young, P. Sinclair, V. Rand, M. R. Teixeira, O. Joseph, B. Robinson, M. Maddison, N. Dastugue, P. Vandenberghe, P. J. Stephens, J. Cheng, P. Van Loo, M. R. Stratton, P. J. Campbell and C. J. Harrison (2014). "Constitutional and somatic rearrangement of chromosome 21 in acute lymphoblastic leukaemia." Nature **508**(7494): 98-102.

Lim, J. Y., S. Bhatia, L. L. Robison and J. J. Yang (2014). "Genomics of racial and ethnic disparities in childhood acute lymphoblastic leukemia." Cancer **120**(7): 955-962.

Lipinski, C. A., F. Lombardo, B. W. Dominy and P. J. Feeney (2001). "Experimental and computational approaches to estimate solubility and permeability in drug discovery and development settings." Adv Drug Deliv Rev **46**(1-3): 3-26.

Longo-Sorbello, G. S. and J. R. Bertino (2001). "Current understanding of methotrexate pharmacology and efficacy in acute leukemias. Use of newer antifolates in clinical trials." Haematologica **86**(2): 121-127.

Ma, X., M. Edmonson, D. Yergeau, D. M. Muzny, O. A. Hampton, M. Rusch, G. Song, J. Easton, R. C. Harvey, D. A. Wheeler, J. Ma, H. Doddapaneni, B. Vadodaria, G. Wu, P. Nagahawatte, W. L. Carroll, I. M. Chen, J. M. Gastier-Foster, M. V. Relling, M. A. Smith, M. Devidas, J. M. Guidry Auvil, J. R. Downing, M. L. Loh, C. L. Willman, D. S. Gerhard, C. G. Mullighan, S. P. Hunger and J. Zhang (2015). "Rise and fall of subclones from diagnosis to relapse in pediatric B-acute lymphoblastic leukaemia." Nat Commun **6**: 6604.

Malinge, S., S. Izraeli and J. D. Crispino (2009). "Insights into the manifestations, outcomes, and mechanisms of leukemogenesis in Down syndrome." Blood **113**(12): 2619-2628.

Malinowska-Ozdowy, K., C. Frech, A. Schonegger, C. Eckert, G. Cazzaniga, M. Stanulla, U. zur Stadt, A. Mecklenbrauker, M. Schuster, D. Kneidinger, A. von Stackelberg, F. Locatelli, M. Schrappe, M. A. Horstmann, A. Attarbaschi, C. Bock, G. Mann, O. A. Haas and R. Panzer-Grumayer (2015). "KRAS and CREBBP mutations: a relapse-linked malicious liaison in childhood high hyperdiploid acute lymphoblastic leukemia." Leukemia **29**(8): 1656-1667.

Mamonkin, M., R. H. Rouce, H. Tashiro and M. K. Brenner (2015). "A T-cell-directed chimeric antigen receptor for the selective treatment of T-cell malignancies." Blood **126**(8): 983-992.

Mansour, M. R., B. J. Abraham, L. Anders, A. Berezovskaya, A. Gutierrez, A. D. Durbin, J. Etchin, L. Lawton, S. E. Sallan, L. B. Silverman, M. L. Loh, S. P. Hunger, T. Sanda, R. A. Young and A. T. Look (2014). "Oncogene regulation. An oncogenic super-enhancer formed through somatic mutation of a noncoding intergenic element." Science **346**(6215): 1373-1377.

Mar, B. G., L. B. Bullinger, K. M. McLean, P. V. Grauman, M. H. Harris, K. Stevenson, D. S. Neuberg, A. U. Sinha, S. E. Sallan, L. B. Silverman, A. L. Kung, L. Lo Nigro, B. L. Ebert and S. A. Armstrong (2014). "Mutations in epigenetic regulators including SETD2 are gained during relapse in paediatric acute lymphoblastic leukaemia." Nature communications **5**: 3469.

Marques, A. F., N. A. Teixeira, C. Gambaretto, A. Sillero and M. A. Sillero (1998). "IMP-GMP 5'-nucleotidase from rat brain: activation by polyphosphates." J Neurochem **71**(3): 1241-1250.

Marton, Z., R. Guillon, I. Krimm, Preeti, R. Rahimova, D. Egron, L. P. Jordheim, N. Aghajari, C. Dumontet, C. Perigaud, C. Lionne, S. Peyrottes and L. Chaloin (2015). "Identification of Noncompetitive Inhibitors of Cytosolic 5'-Nucleotidase II Using a Fragment-Based Approach." J Med Chem **58**(24): 9680-9696.

Maude, S. L., N. Frey, P. A. Shaw, R. Aplenc, D. M. Barrett, N. J. Bunin, A. Chew, V. E. Gonzalez, Z. Zheng, S. F. Lacey, Y. D. Mahnke, J. J. Melenhorst, S. R. Rheingold, A. Shen, D. T. Teachey, B. L. Levine, C. H. June, D. L. Porter and S. A. Grupp (2014). "Chimeric antigen receptor T cells for sustained remissions in leukemia." N Engl J Med **371**(16): 1507-1517.

Mayr, L. M. and D. Bojanic (2009). "Novel trends in high-throughput screening." Curr Opin Pharmacol **9**(5): 580-588.

McGuire, E. A., R. D. Hockett, K. M. Pollock, M. F. Bartholdi, S. J. O'Brien and S. J. Korsmeyer (1989). "The t(11;14)(p15;q11) in a T-cell acute lymphoblastic leukemia cell line activates multiple transcripts, including Ttg-1, a gene encoding a potential zinc finger protein." Mol Cell Biol **9**(5): 2124-2132.

McLeod, H. L., E. Y. Krynetski, M. V. Relling and W. E. Evans (2000). "Genetic polymorphism of thiopurine methyltransferase and its clinical relevance for childhood acute lymphoblastic leukemia." Leukemia **14**(4): 567-572.

Mellentin, J. D., S. D. Smith and M. L. Cleary (1989). "lyl-1, a novel gene altered by chromosomal translocation in T cell leukemia, codes for a protein with a helix-loop-helix DNA binding motif." Cell **58**(1): 77-83.

Meurillon, M., Z. Marton, A. Hospital, L. P. Jordheim, J. Bejaud, C. Lionne, C. Dumontet, C. Perigaud, L. Chaloin and S. Peyrottes (2014). "Structure-activity relationships of beta-hydroxyphosphonate nucleoside analogues as cytosolic 5'-nucleotidase II potential inhibitors: synthesis, in vitro evaluation and molecular modeling studies." Eur J Med Chem **77**: 18-37.

Meyer, C., J. Hofmann, T. Burmeister, D. Groger, T. S. Park, M. Emerenciano, M. Pombo de Oliveira, A. Renneville, P. Villarese, E. Macintyre, H. Cave, E. Clappier, K. Mass-Malo, J. Zuna, J. Trka, E. De Braekeleer, M. De Braekeleer, S. H. Oh, G. Tsaur, L. Fechina, V. H. van der Velden, J. J. van Dongen, E. Delabesse, R. Binato, M. L. Silva, A. Kustanovich, O. Aleinikova, M. H. Harris, T. Lund-Aho, V. Juvonen, O. Heidenreich, J. Vormoor, W. W. Choi, M. Jarosova, A. Kolenova, C. Bueno, P. Menendez, S. Wehner, C. Eckert, P. Talmant, S. Tondeur, E. Lippert, E. Launay, C. Henry, P. Ballerini, H. Lapillone, M. B. Callanan, J. M. Cayuela, C. Herbaux, G. Cazzaniga, P. M. Kakadiya, S. Bohlander, M. Ahlmann, J. R. Choi, P. Gameiro, D. S. Lee, J. Krauter, P. Cornillet-Lefebvre, G. Te Kronnie, B. W. Schafer, S. Kubetzko, C. N. Alonso, U. zur Stadt, R. Sutton, N. C. Venn, S. Izraeli, L. Trakhtenbrot, H. O. Madsen, P. Archer, J. Hancock, N. Cerveira, M. R. Teixeira, L. Lo Nigro, A. Moricke, M. Stanulla, M. Schrappe, L. Sedek, T. Szczepanski, C. M. Zwaan, E. A. Coenen, M. M. van den Heuvel-Eibrink, S. Strehl, M. Dworzak, R. Panzer-Grumayer, T. Dingermann, T. Klingebiel and R. Marschalek (2013). "The MLL recombinome of acute leukemias in 2013." Leukemia **27**(11): 2165-2176.

Meyer, J. A., J. Wang, L. E. Hogan, J. J. Yang, S. Dandekar, J. P. Patel, Z. Tang, P. Zumbo, S. Li, J. Zavadil, R. L. Levine, T. Cardozo, S. P. Hunger, E. A. Raetz, W. E. Evans, D. J. Morrison, C. E. Mason and W. L. Carroll (2013). "Relapse-specific mutations in NT5C2 in childhood acute lymphoblastic leukemia." Nat Genet **45**(3): 290-294.

Mitra, A. K., K. R. Crews, S. Pounds, X. Cao, T. Feldberg, Y. Ghodke, V. Gandhi, W. Plunkett, M. E. Dolan, C. Hartford, S. Raimondi, D. Campana, J. Downing, J. E. Rubnitz, R. C. Ribeiro and J. K. Lamba (2011). "Genetic variants in cytosolic 5'-nucleotidase II are associated with its expression and cytarabine sensitivity in HapMap cell lines and in patients with acute myeloid leukemia." J Pharmacol Exp Ther **339**(1): 9-23.

Moriyama, T., M. L. Metzger, G. Wu, R. Nishii, M. Qian, M. Devidas, W. Yang, C. Cheng, X. Cao, E. Quinn, S. Raimondi, J. M. Gastier-Foster, E. Raetz, E. Larsen, P. L. Martin, W. P. Bowman, N. Winick, Y. Komada, S. Wang, M. Edmonson, H. Xu, E. Mardis, R. Fulton, C. H. Pui, C. Mullighan, W. E. Evans, J. Zhang, S. P. Hunger, M. V. Relling, K. E. Nichols, M. L. Loh and J. J. Yang (2015). "Germline genetic variation in ETV6 and risk of childhood acute lymphoblastic leukaemia: a systematic genetic study." Lancet Oncol **16**(16): 1659-1666.

Moriyama, T., R. Nishii, V. Perez-Andreu, W. Yang, F. A. Klussmann, X. Zhao, T. N. Lin, K. Hoshitsuki, J. Nersting, K. Kihira, U. Hofmann, Y. Komada, M. Kato, R. McCorkle, L. Li, K. Koh, C. R. Najera, S. K. Kham, T. Isobe, Z. Chen, E. K. Chiew, D. Bhojwani, C. Jeffries, Y. Lu, M. Schwab, H. Inaba, C. H. Pui, M. V. Relling, A. Manabe, H. Hori, K. Schmiegelow, A. E. Yeoh, W. E. Evans and J. J. Yang (2016). "NUDT15 polymorphisms alter thiopurine metabolism and hematopoietic toxicity." Nat Genet **48**(4): 367-373.

Morrow, M., S. Horton, D. Kioussis, H. J. Brady and O. Williams (2004). "TEL-AML1 promotes development of specific hematopoietic lineages consistent with preleukemic activity." Blood **103**(10): 3890-3896.

Muller, H. J. and J. Boos (1998). "Use of L-asparaginase in childhood ALL." Crit Rev Oncol Hematol **28**(2): 97-113.

Mullighan, C. G., S. Goorha, I. Radtke, C. B. Miller, E. Coustan-Smith, J. D. Dalton, K. Girtman, S. Mathew, J. Ma, S. B. Pounds, X. Su, C. H. Pui, M. V. Relling, W. E. Evans, S. A. Shurtleff and J. R. Downing (2007). "Genome-wide analysis of genetic alterations in acute lymphoblastic leukaemia." Nature **446**(7137): 758-764.

Mullighan, C. G., L. A. Phillips, X. Su, J. Ma, C. B. Miller, S. A. Shurtleff and J. R. Downing (2008). "Genomic analysis of the clonal origins of relapsed acute lymphoblastic leukemia." Science **322**(5906): 1377-1380.

Mullighan, C. G., X. Su, J. Zhang, I. Radtke, L. A. Phillips, C. B. Miller, J. Ma, W. Liu, C. Cheng, B. A. Schulman, R. C. Harvey, I. M. Chen, R. J. Clifford, W. L. Carroll, G. Reaman, W. P. Bowman, M. Devidas, D. S. Gerhard, W. Yang, M. V. Relling, S. A. Shurtleff, D. Campana, M. J. Borowitz, C. H. Pui, M. Smith, S. P. Hunger, C. L. Willman and J. R. Downing (2009). "Deletion of IKZF1 and prognosis in acute lymphoblastic leukemia." N Engl J Med **360**(5): 470-480.

Mullighan, C. G., J. Zhang, R. C. Harvey, J. R. Collins-Underwood, B. A. Schulman, L. A. Phillips, S. K. Tasian, M. L. Loh, X. Su, W. Liu, M. Devidas, S. R. Atlas, I. M. Chen, R. J. Clifford, D. S. Gerhard, W. L. Carroll, G. H. Reaman, M. Smith, J. R. Downing, S. P. Hunger and C. L. Willman (2009). "JAK mutations in high-risk childhood acute lymphoblastic leukemia." Proc Natl Acad Sci U S A **106**(23): 9414-9418.

Mullighan, C. G., J. Zhang, L. H. Kasper, S. Lerach, D. Payne-Turner, L. A. Phillips, S. L. Heatley, L. Holmfeldt, J. R. Collins-Underwood, J. Ma, K. H. Buetow, C.-H. Pui, S. D. Baker, P. K. Brindle and J. R. Downing (2011). "CREBBP mutations in relapsed acute lymphoblastic leukaemia." Nature **471**: 235-239.

Nachman, J. B., N. A. Heerema, H. Sather, B. Camitta, E. Forestier, C. J. Harrison, N. Dastugue, M. Schrappe, C. H. Pui, G. Basso, L. B. Silverman and G. E. Janka-Schaub (2007). "Outcome of treatment in children with hypodiploid acute lymphoblastic leukemia." Blood **110**(4): 1112-1115.

Nachman, J. B., H. N. Sather, M. G. Sensel, M. E. Trigg, J. M. Cherlow, J. N. Lukens, L. Wolff, F. M. Uckun and P. S. Gaynon (1998). "Augmented post-induction therapy for children with high-risk acute lymphoblastic leukemia and a slow response to initial therapy." N Engl J Med **338**(23): 1663-1671.

Nagar, B., O. Hantschel, M. A. Young, K. Scheffzek, D. Veach, W. Bornmann, B. Clarkson, G. Superti-Furga and J. Kuriyan (2003). "Structural basis for the autoinhibition of c-Abl tyrosine kinase." Cell **112**(6): 859-871.

Nguyen, K., M. Devidas, S. C. Cheng, M. La, E. A. Raetz, W. L. Carroll, N. J. Winick, S. P. Hunger, P. S. Gaynon and M. L. Loh (2008). "Factors influencing survival after relapse from acute lymphoblastic leukemia: a Children's Oncology Group study." Leukemia **22**(12): 2142-2150.

Novarino, G., A. G. Fenstermaker, M. S. Zaki, M. Hofree, J. L. Silhavy, A. D. Heiberg, M. Abdellateef, B. Rosti, E. Scott, L. Mansour, A. Masri, H. Kayserili, J. Y. Al-Aama, G. M. Abdel-Salam, A. Karminejad, M. Kara, B. Kara, B. Bozorgmehri, T. Ben-Omran, F. Mojahedi, I. G. Mahmoud, N. Bouslam, A. Bouhouche, A. Benomar, S. Hanein, L. Raymond, S. Forlani, M. Mascaro, L. Selim, N. Shehata, N. Al-Allawi, P. S. Bindu, M. Azam, M. Gunel, A. Caglayan, K. Bilguvar, A. Tolun, M. Y. Issa, J. Schroth, E. G. Spencer, R. O. Rosti, N. Akizu, K. K. Vaux, A. Johansen, A. A. Koh, H. Megahed, A. Durr, A. Brice, G. Stevanin, S. B. Gabriel, T. Ideker and J. G. Gleeson (2014). "Exome sequencing links corticospinal motor neuron disease to common neurodegenerative disorders." Science **343**(6170): 506-511.

O'Leary, M. C., X. Lu, Y. Huang, X. Lin, I. Mahmood, D. Przepiorka, D. Gavin, S. Lee, K. Liu, B. George, W. Bryan, M. R. Theoret and R. Pazdur (2018). "FDA Approval Summary: Tisagenlecleucel for Treatment of Patients with Relapsed or Refractory B-Cell Precursor Acute Lymphoblastic Leukemia." Clin Cancer Res.

O'Neil, J., J. Grim, P. Strack, S. Rao, D. Tibbitts, C. Winter, J. Hardwick, M. Welcker, J. P. Meijerink, R. Pieters, G. Draetta, R. Sears, B. E. Clurman and A. T. Look (2007). "FBW7 mutations in leukemic cells mediate NOTCH pathway activation and resistance to gamma-secretase inhibitors." J Exp Med **204**(8): 1813-1824.

Oshima, K., H. Khiabanian, A. C. da Silva-Almeida, G. Tzoneva, F. Abate, A. Ambesi-Impiombato, M. Sanchez-Martin, Z. Carpenter, A. Penson, A. Perez-Garcia, C. Eckert, C. Nicolas, M. Balbin, M. L. Sulis, M. Kato, K. Koh, M. Paganin, G. Basso, J. M. Gastier-Foster, M. Devidas, M. L. Loh, R. Kirschner-Schwabe, T. Palomero, R. Rabadan and A. A. Ferrando (2016). "Mutational landscape, clonal evolution patterns, and role of RAS

mutations in relapsed acute lymphoblastic leukemia." Proc Natl Acad Sci U S A **113**(40): 11306-11311.

Palomero, T., K. C. Barnes, P. J. Real, J. L. Glade Bender, M. L. Sulis, V. V. Murty, A. I. Colovai, M. Balbin and A. A. Ferrando (2006). "CUTLL1, a novel human T-cell lymphoma cell line with t(7;9) rearrangement, aberrant NOTCH1 activation and high sensitivity to gamma-secretase inhibitors." Leukemia **20**(7): 1279-1287.

Palomero, T., W. K. Lim, D. T. Odom, M. L. Sulis, P. J. Real, A. Margolin, K. C. Barnes, J. O'Neil, D. Neuberg, A. P. Weng, J. C. Aster, F. Sigaux, J. Soulier, A. T. Look, R. A. Young, A. Califano and A. A. Ferrando (2006). "NOTCH1 directly regulates c-MYC and activates a feed-forward-loop transcriptional network promoting leukemic cell growth." Proc Natl Acad Sci U S A **103**(48): 18261-18266.

Patlak, M. (2002). "Targeting leukemia: from bench to bedside." Faseb j **16**(3): 273.

Paul, S., H. Kantarjian and E. J. Jabbour (2016). "Adult Acute Lymphoblastic Leukemia." Mayo Clin Proc **91**(11): 1645-1666.

Perez-Andreu, V., K. G. Roberts, R. C. Harvey, W. Yang, C. Cheng, D. Pei, H. Xu, J. Gastier-Foster, S. E, J. Y. Lim, I. M. Chen, Y. Fan, M. Devidas, M. J. Borowitz, C. Smith, G. Neale, E. G. Burchard, D. G. Torgerson, F. A. Klussmann, C. R. Villagran, N. J. Winick, B. M. Camitta, E. Raetz, B. Wood, F. Yue, W. L. Carroll, E. Larsen, W. P. Bowman, M. L. Loh, M. Dean, D. Bhojwani, C. H. Pui, W. E. Evans, M. V. Relling, S. P. Hunger, C. L. Willman, C. G. Mullighan and J. J. Yang (2013). "Inherited GATA3 variants are associated with Ph-like childhood acute lymphoblastic leukemia and risk of relapse." Nat Genet **45**(12): 1494-1498.

Pesi, R., V. Micheli, G. Jacomelli, L. Peruzzi, M. Camici, M. Garcia-Gil, S. Allegrini and M. G. Tozzi (2000). "Cytosolic 5'-nucleotidase hyperactivity in erythrocytes of Lesch-Nyhan syndrome patients." Neuroreport **11**(9): 1827-1831.

Pesi, R., M. Turriani, S. Allegrini, C. Scolozzi, M. Camici, P. L. Ipata and M. G. Tozzi (1994). "The bifunctional cytosolic 5'-nucleotidase: regulation of the phosphotransferase and nucleotidase activities." Arch Biochem Biophys **312**(1): 75-80.

Piccaluga, P. P., M. Arpinati, A. Candoni, C. Laterza, S. Paolini, A. Gazzola, E. Sabattini, G. Visani and S. A. Pileri (2011). "Surface antigens analysis reveals significant expression of candidate targets for immunotherapy in adult acute lymphoid leukemia." Leuk Lymphoma **52**(2): 325-327.

Pierro, J., L. E. Hogan, T. Bhatla and W. L. Carroll (2017). "New targeted therapies for relapsed pediatric acute lymphoblastic leukemia." Expert Rev Anticancer Ther **17**(8): 725-736.

Pinto, R. M., J. Canales, M. A. Gunther Sillero and A. Sillero (1986). "Diadenosine tetraphosphate activates cytosol 5'-nucleotidase." Biochem Biophys Res Commun **138**(1): 261-267.

Pui, C. H. and W. E. Evans (2006). "Treatment of acute lymphoblastic leukemia." N Engl J Med **354**(2): 166-178.

Pui, C. H. and S. C. Howard (2008). "Current management and challenges of malignant disease in the CNS in paediatric leukaemia." Lancet Oncol **9**(3): 257-268.

Pui, C. H., K. G. Roberts, J. J. Yang and C. G. Mullighan (2017). "Philadelphia Chromosome-like Acute Lymphoblastic Leukemia." Clin Lymphoma Myeloma Leuk **17**(8): 464-470.

Pui, C. H., J. J. Yang, S. P. Hunger, R. Pieters, M. Schrappe, A. Biondi, A. Vora, A. Baruchel, L. B. Silverman, K. Schmiegelow, G. Escherich, K. Horibe, Y. C. Benoit, S. Izraeli, A. E. Yeoh, D. C. Liang, J. R. Downing, W. E. Evans, M. V. Relling and C. G. Mullighan (2015). "Childhood Acute Lymphoblastic Leukemia: Progress Through Collaboration." J Clin Oncol **33**(27): 2938-2948.

Radtke, F., A. Wilson, G. Stark, M. Bauer, J. van Meerwijk, H. R. MacDonald and M. Aguet (1999). "Deficient T cell fate specification in mice with an induced inactivation of Notch1." Immunity **10**(5): 547-558.

Raetz, E. A. and T. Bhatla (2012). "Where do we stand in the treatment of relapsed acute lymphoblastic leukemia?" Hematology Am Soc Hematol Educ Program **2012**: 129-136.

Ravandi, F., S. M. O'Brien, J. E. Cortes, D. M. Thomas, R. Garris, S. Faderl, J. A. Burger, M. E. Rytting, A. Ferrajoli, W. G. Wierda, S. Verstovsek, R. Champlin, P. Kebriaei, D. A. McCue, X. Huang, E. Jabbour, G. Garcia-Manero, Z. Estrov and H. M. Kantarjian (2015). "Long-term follow-up of a phase 2 study of chemotherapy plus dasatinib for the initial treatment of patients with Philadelphia chromosome-positive acute lymphoblastic leukemia." Cancer **121**(23): 4158-4164.

Relling, M. V., M. L. Hancock, J. M. Boyett, C. H. Pui and W. E. Evans (1999). "Prognostic importance of 6-mercaptopurine dose intensity in acute lymphoblastic leukemia." Blood **93**(9): 2817-2823.

Richter-Pechanska, P., J. B. Kunz, J. Hof, M. Zimmermann, T. Rausch, O. R. Bandapalli, E. Orlova, G. Scapinello, J. C. Sagi, M. Stanulla, M. Schrappe, G. Cario, R. Kirschner-Schwabe, C. Eckert, V. Benes, J. O. Korbel, M. U. Muckenthaler and A. E. Kulozik (2017). "Identification of a genetically defined ultra-high-risk group in relapsed pediatric T-lymphoblastic leukemia." Blood Cancer J **7**(2): e523.

Ries LAG, S. M., Gurney JG, Linet M, Tamra T, Young JL, Bunin GR (eds) (Bethesda, MD, 1999.). Cancer Incidence and Survival among Children and Adolescents: United States SEER Program 1975-1995, National Cancer Institute, SEER Program. .

Roberts, K. G., Y. Li, D. Payne-Turner, R. C. Harvey, Y. L. Yang, D. Pei, K. McCastlain, L. Ding, C. Lu, G. Song, J. Ma, J. Becksfort, M. Rusch, S. C. Chen, J. Easton, J. Cheng, K. Boggs, N. Santiago-Morales, I. Iacobucci, R. S. Fulton, J. Wen, M. Valentine, C. Cheng, S. W. Paugh, M. Devidas, I. M. Chen, S. Reshmi, A. Smith, E. Hedlund, P. Gupta, P. Nagahawatte, G. Wu, X. Chen, D. Yergeau, B. Vadodaria, H. Mulder, N. J. Winick, E. C. Larsen, W. L. Carroll, N. A. Heerema, A. J. Carroll, G. Grayson, S. K. Tasian, A. S. Moore, F. Keller, M. Frei-Jones, J. A. Whitlock, E. A. Raetz, D. L. White, T. P. Hughes, J. M. Guidry Auvil, M. A. Smith, G. Marcucci, C. D. Bloomfield, K. Mrozek, J. Kohlschmidt, W. Stock, S. M. Kornblau, M. Konopleva, E. Paietta, C. H. Pui, S. Jeha, M.

V. Relling, W. E. Evans, D. S. Gerhard, J. M. Gastier-Foster, E. Mardis, R. K. Wilson, M. L. Loh, J. R. Downing, S. P. Hunger, C. L. Willman, J. Zhang and C. G. Mullighan (2014). "Targetable kinase-activating lesions in Ph-like acute lymphoblastic leukemia." N Engl J Med **371**(11): 1005-1015.

Roberts, K. G., R. D. Morin, J. Zhang, M. Hirst, Y. Zhao, X. Su, S. C. Chen, D. Payne-Turner, M. L. Churchman, R. C. Harvey, X. Chen, C. Kasap, C. Yan, J. Becksfort, R. P. Finney, D. T. Teachey, S. L. Maude, K. Tse, R. Moore, S. Jones, K. Mungall, I. Birol, M. N. Edmonson, Y. Hu, K. E. Buetow, I. M. Chen, W. L. Carroll, L. Wei, J. Ma, M. Kleppe, R. L. Levine, G. Garcia-Manero, E. Larsen, N. P. Shah, M. Devidas, G. Reaman, M. Smith, S. W. Paugh, W. E. Evans, S. A. Grupp, S. Jeha, C. H. Pui, D. S. Gerhard, J. R. Downing, C. L. Willman, M. Loh, S. P. Hunger, M. A. Marra and C. G. Mullighan (2012). "Genetic alterations activating kinase and cytokine receptor signaling in high-risk acute lymphoblastic leukemia." Cancer Cell **22**(2): 153-166.

Royer-Pokora, B., U. Loos and W. D. Ludwig (1991). "TTG-2, a new gene encoding a cysteine-rich protein with the LIM motif, is overexpressed in acute T-cell leukaemia with the t(11;14)(p13;q11)." Oncogene **6**(10): 1887-1893.

Sabatino, M., J. Hu, M. Sommariva, S. Gautam, V. Fellowes, J. D. Hocker, S. Dougherty, H. Qin, C. A. Klebanoff, T. J. Fry, R. E. Gress, J. N. Kochenderfer, D. F. Stroncek, Y. Ji and L. Gattinoni (2016). "Generation of clinical-grade CD19-specific CAR-modified CD8+ memory stem cells for the treatment of human B-cell malignancies." Blood **128**(4): 519-528.

Sasaki, K., E. J. Jabbour, F. Ravandi, N. J. Short, D. A. Thomas, G. Garcia-Manero, N. G. Daver, T. M. Kadia, M. Y. Konopleva, N. Jain, G. C. Issa, V. Jeanis, H. G. Moore, R. S. Garris, N. Pemmaraju, J. E. Cortes, S. M. O'Brien and H. M. Kantarjian (2016). "Hyper-CVAD plus ponatinib versus hyper-CVAD plus dasatinib as frontline therapy for patients with Philadelphia chromosome-positive acute lymphoblastic leukemia: A propensity score analysis." Cancer **122**(23): 3650-3656.

Schenone, M., V. Dancik, B. K. Wagner and P. A. Clemons (2013). "Target identification and mechanism of action in chemical biology and drug discovery." Nat Chem Biol **9**(4): 232-240.

Schmiegelow, K., E. Forestier, M. Hellebostad, M. Heyman, J. Kristinsson, S. Soderhall and M. Taskinen (2010). "Long-term results of NOPHO ALL-92 and ALL-2000 studies of childhood acute lymphoblastic leukemia." Leukemia **24**(2): 345-354.

Schneider, D., Y. Xiong, D. Wu, V. Nlle, S. Schmitz, W. Haso, A. Kaiser, B. Dropulic and R. J. Orentas (2017). "A tandem CD19/CD20 CAR lentiviral vector drives on-target and off-target antigen modulation in leukemia cell lines." J Immunother Cancer **5**: 42.

Schneider, G. (2010). "Virtual screening: an endless staircase?" Nat Rev Drug Discov **9**(4): 273-276.

Schrappe, M., M. G. Valsecchi, C. R. Bartram, A. Schrauder, R. Panzer-Grumayer, A. Moricke, R. Parasole, M. Zimmermann, M. Dworzak, B. Buldini, A. Reiter, G. Basso, T. Klingebiel, C. Messina, R. Ratei, G. Cazzaniga, R. Koehler, F. Locatelli, B. W. Schafer, M. Arico, K. Welte, J. J. van Dongen, H. Gadner, A. Biondi and V. Conter (2011). "Late

MRD response determines relapse risk overall and in subsets of childhood T-cell ALL: results of the AIEOP-BFM-ALL 2000 study." Blood **118**(8): 2077-2084.

Shah, N. N., M. S. Stevenson, C. M. Yuan, K. Richards, C. Delbrook, R. J. Kreitman, I. Pastan and A. S. Wayne (2015). "Characterization of CD22 expression in acute lymphoblastic leukemia." Pediatr Blood Cancer **62**(6): 964-969.

Shah, N. P., C. Tran, F. Y. Lee, P. Chen, D. Norris and C. L. Sawyers (2004). "Overriding imatinib resistance with a novel ABL kinase inhibitor." Science **305**(5682): 399-401.

Shah, S., K. A. Schrader, E. Waanders, A. E. Timms, J. Vijai, C. Miething, J. Wechsler, J. Yang, J. Hayes, R. J. Klein, J. Zhang, L. Wei, G. Wu, M. Rusch, P. Nagahawatte, J. Ma, S. C. Chen, G. Song, J. Cheng, P. Meyers, D. Bhojwani, S. Jhanwar, P. Maslak, M. Fleisher, J. Littman, L. Offit, R. Rau-Murthy, M. H. Fleischut, M. Corines, R. Murali, X. Gao, C. Manschreck, T. Kitzing, V. V. Murty, S. Raimondi, R. P. Kuiper, A. Simons, J. D. Schiffman, K. Onel, S. E. Plon, D. Wheeler, D. Ritter, D. S. Ziegler, K. Tucker, R. Sutton, G. Chenevix-Trench, J. Li, D. G. Huntsman, S. Hansford, J. Senz, T. Walsh, M. Lee, C. N. Hahn, K. Roberts, M. C. King, S. M. Lo, R. L. Levine, A. Viale, N. D. Socci, K. L. Nathanson, H. S. Scott, M. Daly, S. M. Lipkin, S. W. Lowe, J. R. Downing, D. Altshuler, J. T. Sandlund, M. S. Horwitz, C. G. Mullighan and K. Offit (2013). "A recurrent germline PAX5 mutation confers susceptibility to pre-B cell acute lymphoblastic leukemia." Nat Genet **45**(10): 1226-1231.

Shalem, O., N. E. Sanjana, E. Hartenian, X. Shi, D. A. Scott, T. S. Mikkelsen, D. Heckl, B. L. Ebert, D. E. Root, J. G. Doench and F. Zhang (2014). "Genome-scale CRISPR-Cas9 knockout screening in human cells." Science **343**(6166): 84-87.

Shoichet, B. K. (2004). "Virtual screening of chemical libraries." Nature **432**(7019): 862-865.

Siegel, D. A., S. J. Henley, J. Li, L. A. Pollack, E. A. Van Dyne and A. White (2017). "Rates and Trends of Pediatric Acute Lymphoblastic Leukemia - United States, 2001-2014." MMWR Morb Mortal Wkly Rep **66**(36): 950-954.

Siegel, R. L., K. D. Miller and A. Jemal (2018). "Cancer statistics, 2018." CA Cancer J Clin **68**(1): 7-30.

Smith, M., D. Arthur, B. Camitta, A. J. Carroll, W. Crist, P. Gaynon, R. Gelber, N. Heerema, E. L. Korn, M. Link, S. Murphy, C. H. Pui, J. Pullen, G. Reamon, S. E. Sallan, H. Sather, J. Shuster, R. Simon, M. Trigg, D. Tubergen, F. Uckun and R. Ungerleider (1996). "Uniform approach to risk classification and treatment assignment for children with acute lymphoblastic leukemia." J Clin Oncol **14**(1): 18-24.

Spychala, J., V. Chen, J. Oka and B. S. Mitchell (1999). "ATP and phosphate reciprocally affect subunit association of human recombinant High Km 5'-nucleotidase. Role for the C-terminal polyglutamic acid tract in subunit association and catalytic activity." Eur J Biochem **259**(3): 851-858.

Spychala, J., V. Madrid-Marina and I. H. Fox (1988). "High Km soluble 5'-nucleotidase from human placenta. Properties and allosteric regulation by IMP and ATP." J Biol Chem **263**(35): 18759-18765.

Stieglitz, E. and M. L. Loh (2013). "Genetic predispositions to childhood leukemia." Ther Adv Hematol **4**(4): 270-290.

Stock, W., J. L. Johnson, R. M. Stone, J. E. Kolitz, B. L. Powell, M. Wetzler, P. Westervelt, G. Marcucci, D. J. DeAngelo, J. W. Vardiman, D. McDonnell, K. Mrozek, C. D. Bloomfield and R. A. Larson (2013). "Dose intensification of daunorubicin and cytarabine during treatment of adult acute lymphoblastic leukemia: results of Cancer and Leukemia Group B Study 19802." Cancer **119**(1): 90-98.

Swann, P. F., T. R. Waters, D. C. Moulton, Y. Z. Xu, Q. Zheng, M. Edwards and R. Mace (1996). "Role of postreplicative DNA mismatch repair in the cytotoxic action of thioguanine." Science **273**(5278): 1109-1111.

Swinney, D. C. and J. Anthony (2011). "How were new medicines discovered?" Nat Rev Drug Discov **10**(7): 507-519.

Tacar, O., P. Sriamornsak and C. R. Dass (2013). "Doxorubicin: an update on anticancer molecular action, toxicity and novel drug delivery systems." J Pharm Pharmacol **65**(2): 157-170.

Tasian, S. K. and S. P. Hunger (2017). "Genomic characterization of paediatric acute lymphoblastic leukaemia: an opportunity for precision medicine therapeutics." Br J Haematol **176**(6): 867-882.

Tay, B. S., R. M. Lilley, A. W. Murray and M. R. Atkinson (1969). "Inhibition of phosphoribosyl pyrophosphate amidotransferase from Ehrlich ascites-tumour cells by thiopurine nucleotides." Biochem Pharmacol **18**(4): 936-938.

Terwilliger, T. and M. Abdul-Hay (2017). "Acute lymphoblastic leukemia: a comprehensive review and 2017 update." Blood Cancer J **7**(6): e577.

Thomas, D. A., S. O'Brien, S. Faderl, G. Garcia-Manero, A. Ferrajoli, W. Wierda, F. Ravandi, S. Verstovsek, J. L. Jorgensen, C. Bueso-Ramos, M. Andreeff, S. Pierce, R. Garris, M. J. Keating, J. Cortes and H. M. Kantarjian (2010). "Chemoimmunotherapy with a modified hyper-CVAD and rituximab regimen improves outcome in de novo Philadelphia chromosome-negative precursor B-lineage acute lymphoblastic leukemia." J Clin Oncol **28**(24): 3880-3889.

Thompson, B. J., S. Buonamici, M. L. Sulis, T. Palomero, T. Vilimas, G. Basso, A. Ferrando and I. Aifantis (2007). "The SCFFBW7 ubiquitin ligase complex as a tumor suppressor in T cell leukemia." J Exp Med **204**(8): 1825-1835.

Tozzi, M. G., M. Camici, R. Pesi, S. Allegrini, F. Sgarrella and P. L. Ipata (1991). "Nucleoside phosphotransferase activity of human colon carcinoma cytosolic 5'-nucleotidase." Arch Biochem Biophys **291**(2): 212-217.

Tubergen, D. G., G. S. Gilchrist, R. T. O'Brien, P. F. Coccia, H. N. Sather, M. J. Waskerwitz and G. D. Hammond (1993). "Improved outcome with delayed intensification for children with acute lymphoblastic leukemia and intermediate presenting features: a Childrens Cancer Group phase III trial." J Clin Oncol **11**(3): 527-537.

Tzoneva, G., C. L. Dieck, K. Oshima, A. Ambesi-Impiombato, M. Sanchez-Martin, C. J. Madubata, H. Khiabanian, J. Yu, E. Waanders, I. Iacobucci, M. L. Sulis, M. Kato, K. Koh, M. Paganin, G. Basso, J. M. Gastier-Foster, M. L. Loh, R. Kirschner-Schwabe, C. G. Mullighan, R. Rabadan and A. A. Ferrando (2018). "Clonal evolution mechanisms in NT5C2 mutant-relapsed acute lymphoblastic leukaemia." Nature **553**(7689): 511-514.

Tzoneva, G., A. Perez-Garcia, Z. Carpenter, H. Khiabanian, V. Tosello, M. Allegretta, E. Paietta, J. Racevskis, J. M. Rowe, M. S. Tallman, M. Paganin, G. Basso, J. Hof, R. Kirschner-Schwabe, T. Palomero, R. Rabadan and A. Ferrando (2013). "Activating mutations in the NT5C2 nucleotidase gene drive chemotherapy resistance in relapsed ALL." Nature medicine **19**: 368-371.

Van Vlierberghe, P., A. Ambesi-Impiombato, A. Perez-Garcia, J. E. Haydu, I. Rigo, M. Hadler, V. Tosello, G. Della Gatta, E. Paietta, J. Racevskis, P. H. Wiernik, S. M. Luger, J. M. Rowe, M. Rue and A. A. Ferrando (2011). "ETV6 mutations in early immature human T cell leukemias." J Exp Med **208**(13): 2571-2579.

Vardiman, J. W., J. Thiele, D. A. Arber, R. D. Brunning, M. J. Borowitz, A. Porwit, N. L. Harris, M. M. Le Beau, E. Hellstrom-Lindberg, A. Tefferi and C. D. Bloomfield (2009). "The 2008 revision of the World Health Organization (WHO) classification of myeloid neoplasms and acute leukemia: rationale and important changes." Blood **114**(5): 937-951.

Vartanian, A., I. Prudovsky, H. Suzuki, I. Dal Pra and L. Kisselev (1997). "Opposite effects of cell differentiation and apoptosis on Ap3A/Ap4A ratio in human cell cultures." FEBS Lett **415**(2): 160-162.

Wallden, K. and P. Nordlund (2011). "Structural basis for the allosteric regulation and substrate recognition of human cytosolic 5'-nucleotidase II." J Mol Biol **408**(4): 684-696.

Wallden, K., P. Stenmark, T. Nyman, S. Flodin, S. Graslund, P. Loppnau, V. Bianchi and P. Nordlund (2007). "Crystal structure of human cytosolic 5'-nucleotidase II: insights into allosteric regulation and substrate recognition." J Biol Chem **282**(24): 17828-17836.

Wang, H., H. Yang, C. S. Shivalila, M. M. Dawlaty, A. W. Cheng, F. Zhang and R. Jaenisch (2013). "One-step generation of mice carrying mutations in multiple genes by CRISPR/Cas-mediated genome engineering." Cell **153**(4): 910-918.

Wang, J., S. N. Jani-Sait, E. A. Escalon, A. J. Carroll, P. J. de Jong, I. R. Kirsch and P. D. Aplan (2000). "The t(14;21)(q11.2;q22) chromosomal translocation associated with T-cell acute lymphoblastic leukemia activates the BHLHB1 gene." Proc Natl Acad Sci U S A **97**(7): 3497-3502.

Wang, Y., S. H. Bryant, T. Cheng, J. Wang, A. Gindulyte, B. A. Shoemaker, P. A. Thiessen, S. He and J. Zhang (2017). "PubChem BioAssay: 2017 update." Nucleic Acids Res **45**(D1): D955-d963.

Ward, E., C. DeSantis, A. Robbins, B. Kohler and A. Jemal (2014). "Childhood and adolescent cancer statistics, 2014." CA Cancer J Clin **64**(2): 83-103.

Wassmann, B., H. Pfeifer, N. Goekbuget, D. W. Beelen, J. Beck, M. Stelljes, M. Bornhauser, A. Reichle, J. Perz, R. Haas, A. Ganser, M. Schmid, L. Kanz, G. Lenz, M. Kaufmann, A. Binckebanck, P. Bruck, R. Reutzel, H. Gschaidmeier, S. Schwartz, D. Hoelzer and O. G. Ottmann (2006). "Alternating versus concurrent schedules of imatinib and chemotherapy as front-line therapy for Philadelphia-positive acute lymphoblastic leukemia (Ph+ ALL)." Blood **108**(5): 1469-1477.

Waters, T. R. and P. F. Swann (1997). "Cytotoxic mechanism of 6-thioguanine: hMutSalpha, the human mismatch binding heterodimer, binds to DNA containing S6-methylthioguanine." Biochemistry **36**(9): 2501-2506.

Weng, A. P., A. A. Ferrando, W. Lee, J. P. t. Morris, L. B. Silverman, C. Sanchez-Irizarry, S. C. Blacklow, A. T. Look and J. C. Aster (2004). "Activating mutations of NOTCH1 in human T cell acute lymphoblastic leukemia." Science **306**(5694): 269-271.

Weng, A. P., J. M. Millholland, Y. Yashiro-Ohtani, M. L. Arcangeli, A. Lau, C. Wai, C. Del Bianco, C. G. Rodriguez, H. Sai, J. Tobias, Y. Li, M. S. Wolfe, C. Shachaf, D. Felsher, S. C. Blacklow, W. S. Pear and J. C. Aster (2006). "c-Myc is an important direct target of Notch1 in T-cell acute lymphoblastic leukemia/lymphoma." Genes Dev **20**(15): 2096-2109.

Wofford, M. M., S. D. Smith, J. J. Shuster, W. Johnson, G. R. Buchanan, M. D. Wharam, A. K. Ritchey, D. Rosen, M. E. Haggard, B. L. Golembe and et al. (1992). "Treatment of occult or late overt testicular relapse in children with acute lymphoblastic leukemia: a Pediatric Oncology Group study." J Clin Oncol **10**(4): 624-630.

Wolfer, A., A. Wilson, M. Nemir, H. R. MacDonald and F. Radtke (2002). "Inactivation of Notch1 impairs VDJbeta rearrangement and allows pre-TCR-independent survival of early alpha beta Lineage Thymocytes." Immunity **16**(6): 869-879.

Worku, Y. and A. C. Newby (1982). "Nucleoside exchange catalysed by the cytoplasmic 5'-nucleotidase." Biochem J **205**(3): 503-510.

Wu, D., A. Sherwood, J. R. Fromm, S. S. Winter, K. P. Dunsmore, M. L. Loh, H. A. Greisman, D. E. Sabath, B. L. Wood and H. Robins (2012). "High-throughput sequencing detects minimal residual disease in acute T lymphoblastic leukemia." Sci Transl Med **4**(134): 134ra163.

Xia, Y., L. Brown, C. Y. Yang, J. T. Tsan, M. J. Siciliano, R. Espinosa, 3rd, M. M. Le Beau and R. J. Baer (1991). "TAL2, a helix-loop-helix gene activated by the (7;9)(q34;q32) translocation in human T-cell leukemia." Proc Natl Acad Sci U S A **88**(24): 11416-11420.

Xu, H., C. Cheng, M. Devidas, D. Pei, Y. Fan, W. Yang, G. Neale, P. Scheet, E. G. Burchard, D. G. Torgerson, C. Eng, M. Dean, F. Antillon, N. J. Winick, P. L. Martin, C. L. Willman, B. M. Camitta, G. H. Reaman, W. L. Carroll, M. Loh, W. E. Evans, C. H. Pui, S. P. Hunger, M. V. Relling and J. J. Yang (2012). "ARID5B genetic polymorphisms

contribute to racial disparities in the incidence and treatment outcome of childhood acute lymphoblastic leukemia." J Clin Oncol **30**(7): 751-757.

Yang, J. J., D. Bhojwani, W. Yang, X. Cai, G. Stocco, K. Crews, J. Wang, D. Morrison, M. Devidas, S. P. Hunger, C. L. Willman, E. A. Raetz, C. H. Pui, W. E. Evans, M. V. Relling and W. L. Carroll (2008). "Genome-wide copy number profiling reveals molecular evolution from diagnosis to relapse in childhood acute lymphoblastic leukemia." Blood **112**(10): 4178-4183.

Zein, N., A. M. Sinha, W. J. McGahren and G. A. Ellestad (1988). "Calicheamicin gamma 1I: an antitumor antibiotic that cleaves double-stranded DNA site specifically." Science **240**(4856): 1198-1201.

Zhang, J., L. Ding, L. Holmfeldt, G. Wu, S. L. Heatley, D. Payne-Turner, J. Easton, X. Chen, J. Wang, M. Rusch, C. Lu, S. C. Chen, L. Wei, J. R. Collins-Underwood, J. Ma, K. G. Roberts, S. B. Pounds, A. Ulyanov, J. Becksfort, P. Gupta, R. Huether, R. W. Kriwacki, M. Parker, D. J. McGoldrick, D. Zhao, D. Alford, S. Espy, K. C. Bobba, G. Song, D. Pei, C. Cheng, S. Roberts, M. I. Barbato, D. Campana, E. Coustan-Smith, S. A. Shurtleff, S. C. Raimondi, M. Kleppe, J. Cools, K. A. Shimano, M. L. Hermiston, S. Doulatov, K. Eppert, E. Laurenti, F. Notta, J. E. Dick, G. Basso, S. P. Hunger, M. L. Loh, M. Devidas, B. Wood, S. Winter, K. P. Dunsmore, R. S. Fulton, L. L. Fulton, X. Hong, C. C. Harris, D. J. Dooling, K. Ochoa, K. J. Johnson, J. C. Obenauer, W. E. Evans, C. H. Pui, C. W. Naeve, T. J. Ley, E. R. Mardis, R. K. Wilson, J. R. Downing and C. G. Mullighan (2012). "The genetic basis of early T-cell precursor acute lymphoblastic leukaemia." Nature **481**(7380): 157-163.

Zhang, J., C. G. Mullighan, R. C. Harvey, G. Wu, X. Chen, M. Edmonson, K. H. Buetow, W. L. Carroll, I. M. Chen, M. Devidas, D. S. Gerhard, M. L. Loh, G. H. Reaman, M. V. Relling, B. M. Camitta, W. P. Bowman, M. A. Smith, C. L. Willman, J. R. Downing and S. P. Hunger (2011). "Key pathways are frequently mutated in high-risk childhood acute lymphoblastic leukemia: a report from the Children's Oncology Group." Blood **118**(11): 3080-3087.

Zhang, J. H., T. D. Chung and K. R. Oldenburg (1999). "A Simple Statistical Parameter for Use in Evaluation and Validation of High Throughput Screening Assays." J Biomol Screen **4**(2): 67-73.

Zhang, Z. and K. E. Meier (2006). "New assignments for multitasking signal transduction inhibitors." Mol Pharmacol **69**(5): 1510-1512.

Appendix

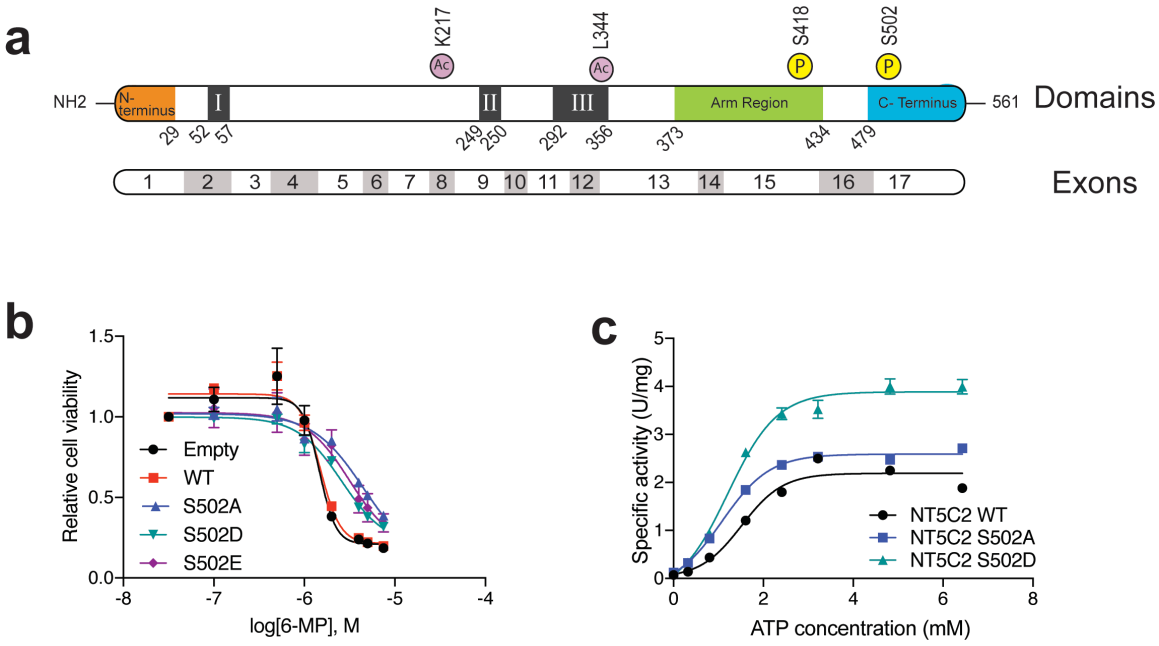

Appendix 1.1 – NT5C2 S502phosphorylation displays resistance to 6-MP and increased nucleotidase activity. (a) Post-translational modifications identified with mass spectrometry analysis of a tandem affinity pulldown from FLAG-HA NT5C2 expressing cells. (b) Cell viability assays of JURKAT T-ALL cell lines expressing NT5C2 Ser502 phospho-mimic or phospho-resistant proteins or wild type controls with increasing amounts of 6-MP. (c) *In vitro* nucleotidase activity of NT5C2 WT or NT5C2 S502D phospho-mimic or NT5C2 S502A phospho-resistant recombinant protein.